MODEL-BASED ENGINE-OUT EMISSIONS ANALYSIS FOR A GASOLINE TURBOCHARGED DIRECT INJECTION SPARK-IGNITED ENGINE IN ELEVATED HEV CRANKING SPEED

By

Amir A. Khameneian

A DISSERTATION

Submitted in partial fulfillment of the requirements for the degree of

DOCTOR OF PHILOSOPHY

In Mechanical Engineering-Engineering Mechanics

MICHIGAN TECHNOLOGICAL UNIVERSITY

2021

This dissertation has been approved in partial fulfillment of the requirements for the Degree of DOCTOR OF PHILOSOPHY in Mechanical Engineering-Engineering Mechanics.

Department of Mechanical Engineering-Engineering Mechanics

Dissertation Co-advisor: *Dr. Jeffrey D. Naber*

Dissertation Co-advisor: *Dr. Mahdi Shahbakhti*

Committee Member: *Dr. Bo Chen*

Committee Member: *Dr. David D. Wanless*

Department Chair: *Dr. William W. Predebon*

Dedication

To my father, in loving memory, my mother, and my love, Sara

who have been a constant source of support and encouragement, who taught me never to give up aspiring and working hard to achieve my dreams

Contents

List of Figures

List of Tables

Preface

The main content of this dissertation is based on two journal and peer-reviewed conference papers as the first author, two published conference papers as the second author and three journal papers under preparation and review. Publishers of these papers have granted the permissions found in Appendix C. The main contribution of the author to the overall research and body of knowledge is as follows:

- Chapter 2 comprises the materials from the below papers,

  Khameneian, Amir, Wang, Xin, Dice, Paul, Shahbakhti, Mahdi, Naber, Jeffrey D., Archer, Chad, Moilanen, Peter, Glugla, Chris, and Huberts, Garlan "Model-Based Dynamic In-Cylinder Air Charge, Residual Gas and Temperature Estimation for a GDI Spark Ignition Engine Using Cylinder, Intake and Exhaust Pressures." Proceedings of the ASME 2020 Dynamic Systems and Control Conference. Volume 2: Intelligent Transportation/Vehicles; Mechatronics; Engine/After-Treatment Systems; Modeling/Validation. Pittsburgh, Pennsylvania, USA. October 5–7, 2020. V002T26A002. ASME. https://doi.org/10.1115/DSCC2020-3280

  Khameneian, Amir, Wang, Xin, Dice, Paul, Shahbakhti, Mahdi, Naber, Jeffrey D., Archer, Chad, Moilanen, Peter, Glugla, Chris, and Huberts, Garlan.

"A Real-Time Control-Oriented Discrete Nonlinear Model Development for In-Cylinder Air Charge, Residual Gas and Temperature Prediction of a Gasoline Direct Injection Engine Using Cylinder, Intake and Exhaust Pressures." Control Engineering Practice Journal, Elsevier, CONENGPRAC-D-21-00062

These works were done with the collaboration of Ford Motor Company to develop a real-time in-cylinder air charge, residual gas, and temperature estimation model. Amir Khameneian and Xin Wang carried out the tests and data acquisition. Amir Khameneian has accomplished the analysis of the experimental data, modeling, validation, and writing this section. These papers were peer-reviewed by the 2020 ASME Dynamic Systems and Control Conference and Control Engineering Practice Journal.

- Chapter 3 comprises the materials from the papers mentioned below, which are under review,

  Khameneian, Amir, Dice, Paul, Duncan, Joel, Shahbakhti, Mahdi, Naber, Jeffrey D., Archer, Chad, Moilanen, Peter, Glugla, Chris, and Huberts, Garlan. "A Dynamic Analysis Method for Gasoline Direct Injection Engine Cold Start First Cycles Engine-Out Emissions in HEV Elevated Cranking Speed Conditions."

  Khameneian, Amir, Dice, Paul, Tuma, Nicolas, Shahbakhti, Mahdi, Naber, Jeffrey D., Archer, Chad, Moilanen, Peter, Glugla, Chris, and Huberts, Garlan. "Dynamic Individual-Cylinder Analysis of a Gasoline Direct Injection Engine Emissions for Cold Crank-Start in HEV Elevated Cranking Speed Conditions."

These works were done with the collaboration of Ford Motor Company to develop motored elevated cranking speed PCM control strategies. Amir Khameneian and Nicolas Tuma carried out the tests and data acquisition. Amir Khameneian has accomplished the analysis of the experimental data, modeling, validation, and writing this section. Behrouz Khoshbakht Irdmousa has carried out the CFD analysis for the derivation of the fuel vaporization rate.

Acknowledgments

Achieving a Ph.D. degree was quite challenging; however, more rewarding than I could have ever imagined. This important, especially the valuable experiences I have earned over the past five years, would not have been possible without my advisors, Drs. Jeffrey D. Naber and Mahdi Shahbakhti. My eternal gratitude goes to them for encouraging, guiding, and supporting me throughout the last five years. They granted me the opportunity of engaging in precious insightful discussions about our research. I am sincerely grateful to them for the time they invested in me and the wisdom they have shared. More important than scientific achievements, their display of enthusiasm and energy in the relentless pursuit of research has definitely impressed me in more ways than I can articulate.

Special thanks to Dr. Bo Chen and Dr. David D. Wanless for being on my doctoral advisory committee and providing support.

I graciously acknowledge Ford Motor Company's sponsorship of the research and technical support in preparing the test engine and experiments. A sincere acknowledgment is reserved for Garlan Huberts, Chris Glugla, Chad Archer, Peter Moilanen, and Ali Imtiaz from Ford Motor Company, whom I have spent hours discussing and fruitful commentary and critique.

I am grateful to Ford team for their valuable financial and technical support in preparation of the test engine, controllers and experiments.

I am grateful to Paul Dice, Joel Duncan, Nicolas Tuma, Tucker Alsup, William Hansley, and Alex Normand from the Advanced Power Systems Research Center (APSRC) for all their friendly assists. They helped me to build up the required background for the experimental setup and testing. In addition, I wish to thank all the faculty at Michigan Tech, especially Mechanical Engineering Department, who have assisted me with their invaluable expertise.

I would also like to thank many friends who provided comments and suggestions on my research: Drs. Xin Wang, Ehsan Ansari, Aliihsan Koca, Mustafa Aggul, Behdad Afkhami, Ali Soloukmofrad, Mohammad Alizadeh, and Azad Heidari, Zhuyong Yang, Yash Borghate, Muralidhar Nischal, Cooper Meinhart, Niranjan Miganakallu, and Behrouz Khoshbakht.

I owe a deep debt of gratitude to my father, Asadollah Khameneian, whom I promised to dedicate this dissertation before he left this world and never got to see this, to the purest love in the world, my mother, Parvin Sadrolashrafi, who is eagerly looking forward to hugging me again one more time, to my love, Sara Sadeghzadehbenam, who has always encouraged me, to the hope of our life, our lovely son, Arshia Khameneian, to my kind-hearted sister, Roghayeh Khameneian, and brother, Mehdi Khameneian.

List of Abbreviations

A	Effective Area (m^2)
AF_{stoich}	Air-to-Fuel-Ratio at Stoichiometric Conditions
C_D	Discharge Coefficient
$C_{v_{air}}$	Air Specific Heat at Constant Volume ($\frac{J}{kg.K}$)
$C_{v_{EXH}}$	Exhaust Gas Specific Heat at Constant Volume ($\frac{J}{kg.K}$)
$C_{v_{fuel}}$	Vaporized Fuel Specific Heat at Constant Volume ($\frac{J}{kg.K}$)
C_{fuel}	Liquid Fuel Specific Heat at Constant Volume ($\frac{J}{kg.K}$)
$C_{v_{H2O}}$	Air Water Vapor Specific Heat at Constant Volume ($\frac{J}{kg.K}$)
$C_{v_{res}}$	Residual Gas Specific Heat at Constant Volume ($\frac{J}{kg.K}$)
d	Disturbance Input
H_{EXH}	Fluid Enthalpy from the End of Blowdown to IVO or EVC (J)
H_{INT}	Fluid Enthalpy from IVO or EVC to BDC Compression (J)
h_{EXH}	Exhaust Stroke Convective Heat Transfer Coefficient ($\frac{W}{m^2.K}$)
h_{INT}	Intake Stroke Convective Heat Transfer Coefficient ($\frac{W}{m^2.K}$)
k_{res}	Exhaust Manifold Residual Coefficient
k_{pox}	Exhaust Manifold HC Post Oxidization Coefficient
MAP	Manifold Absolute Pressure (Pa)
m_{air}	In-Cylinder Trapped Air Mass (kg)

M_{air}	Air Molecular Weight ($\frac{kg}{kmole}$)
$m_{air_{int}}$	Mass of Inducted Air from EVC to BDC Compression (kg)
$m_{backflow_i}$	Mass of Segment Exhaust Gas Back Flow (kg)
m_{bb}	Mass of Blow by Gas (kg)
$m_{bb_{fuel}}$	Mass of Fuel Lost Through Blow by (kg)
$\dot{m}_{bb}$	Mass Flow Rate of Blow by Gas ($\frac{g}{s}$)
$m_{cyl_{out}}$	Mass of Exhaust Gas Scavenged Out of Cylinder (kg)
$m_{charge_{loss}}$	Mass of Charge Loss (kg)
$m_{evacuated_i}$	Segment Exhaust Gas Scavenged (kg)
m_{EVC}	Mass of In-Cylinder Gas at EVC (kg)
$\dot{m}_{exh}$	Exhaust Gas Mass Flow ($\frac{g}{s}$)
$\dot{m}_{exh_i}$	Segment Exhaust Gas Mass Flow ($\frac{g}{s}$)
m_{exh_i}	Mass of Segment Exhaust Gas (kg)
m_{EXH}	Mass of In-cylinder Gas at the End of Blowdown (kg)
$\dot{m}_{f_{UEGO}}$	Fuel Flow Rate Measure by UEGO Sensor ($\frac{g}{s}$)
$m_{f_{UEGO}}$	Fuel Mass Measured by UEGO Sensor (kg)
$\dot{m}_{f_{inj}}$	Injected Fuel Rate ($\frac{g}{s}$)
m_{fuel}	Injected Fuel Mass during the intake stroke (kg)
$m_{fuel_{1st}}$	Mass of First Injected Fuel during the Intake Stroke (kg)
$m_{fuel_{2nd}}$	Mass of Second Injected Fuel during the Compression Stroke (kg)
m_{fuel_b}	Mass of Fuel Contributed to Combustion (kg)

$m_{fuel_{ub}}$	Mass of Unburnt Fuel (kg)
$m_{fuel_{oil}}$	Mass of Fuel Lost to the Lubrication Oil (kg)
$m_{fuel_{res}}$	Mass of Residual Fuel (kg)
M_{fuel}	Fuel Molecular Weight ($\frac{kg}{kmole}$)
$m_{H2O_{int}}$	Mass of Inducted Air Water Vapor from EVC to BDC (kg)
m_{H2O}	In-Cylinder Trapped Air Water Vapor Mass at IVC (kg)
M_{H2O}	Air Water Vapor Molecular Weight ($\frac{kg}{kmole}$)
$m_{HC_{cyl}}$	Mass of Unburnt HC Scavenged Out of Cylinder (kg)
$m_{HC_{out}}$	Mass of Unburnt HC Scavenged Out of Exhaust Manifold (kg)
m_{IVO}	Mass of In-Cylinder Gas at IVO (kg)
$m_{man_{out}}$	Mass of Exhaust Gas Scavenged Out of Exhaust Manifold (kg)
$m_{man_{mix}}$	Mass of Mixed Exhaust Gas in Exhaust Manifold (kg)
$m_{res_{int}}$	Mass of Residual Gas Flowing back form Intake Manifold (kg)
$m_{res_{ov}}$	Mass of Overlap Residual Gas (kg)
$m_{res_{trap}}$	Mass of Trapped Residual Gas (kg)
$m_{res_{tot}}$	Mass of In-Cylinder Total Trapped Residual Gas at IVC (kg)
M_{res}	Residual Gas Molecular Weight ($\frac{kg}{kmole}$)
$m_{tot_{EVO}}$	In-Cylinder Total Trapped Mass at EVO (kg)
$m_{tot_{IVC}}$	In-Cylinder Total Trapped Mass at IVC (kg)
N	Engine Speed (RPM)
n_{poly}	Compression Stroke Polytropic Index

n_{tot}	In-Cylinder Total Trapped Mixture Molar Mass at IVC (kmole)
n_{tot_BDC}	In-Cylinder Total Trapped Mixture Molar Mass at BDC Compression (kmole)
$p_{air_{int}}$	Pressure of Inducted Air from IVO or EVC to BDC Compression (Pa)
P_{BDC}	In-Cylinder Pressure at BDC Compression (Pa)
P_{BWD}	In-Cylinder Pressure at the End of Blowdown (Pa)
p_{cyl}	Cylinder Pressure (Pa)
p_{crank}	Crankcase Pressure (Pa)
p_{down}	Downstream Pressure (Pa)
p_{exh}	Exhaust Manifold Pressure (Pa)
$P_{exh_{EVO}}$	Exhaust Manifold Pressure at EVO (Pa)
P_{EVC}	In-Cylinder Pressure at EVC (Pa)
P_{EVO}	In-Cylinder Pressure at EVO (Pa)
p_{fuel}	Injected Fuel Pressure during the intake stroke (Pa)
$p_{H2O_{int}}$	Inducted Air Water Vapor Pressure (Pa)
P_{IVO}	In-Cylinder Pressure at IVO (Pa)
P_{IVC}	In-Cylinder Pressure at IVC (Pa)
$p_{res_{int}}$	Pressure of Residual Gas Flowing back form Intake Manifold (Pa)
P_{sat}	Air Vapor Saturated Pressure (Pa)
p_{up}	Upstream Pressure (Pa)
Q_{EXH}	Heat Transfer from the End of Blowdown to IVO or EVC (J)
Q_{INT}	Heat Transfer from IVO or EVC to BDC Compression (J)

u	Control Input
U_{BDC}	Internal Energy of the Trapped Mixture at BDC (J)
U_{EVC}	Internal Energy of the In-Cylinder Gas at EVC (J)
u_{EVC}	Internal Energy of the In-Cylinder Gas at EVC in mass basis ($\frac{J}{kg}$)
$U_{fg_{fuel}}$	Internal Energy of Vaporization of Fuel (J)
$u_{fg_{fuel}}$	Internal Energy of Vaporization of Fuel in mass basis ($\frac{J}{kg}$)
U_{IVO}	Internal Energy of In-Cylinder Gas at IVO (J)
u_{IVO}	Internal Energy of In-Cylinder Gas at IVO in mass basis ($\frac{J}{kg}$)
$u_{air_{int}}$	Internal Energy of Inducted Air in mass basis ($\frac{J}{kg}$)
u_{fuel}	Internal Energy of Injected Fuel Mass in mass basis ($\frac{J}{kg}$)
$u_{H2O_{int}}$	Internal Energy of Inducted Air Water Vapor in mass basis ($\frac{J}{kg}$)
$u_{res_{int}}$	Internal Energy of Intake Manifold Flowed-back Residual Gas ($\frac{J}{kg}$)
$u_{res_{tot}}$	Internal Energy of Total Trapped Residual Gas ($\frac{J}{kg}$)
R_{exh}	Gas Constant of Exhaust Gas ($\frac{J}{kg\dot{K}}$)
R_{EXH}	Gas Constant of In-Cylinder Gas between IVO and EVC ($\frac{J}{kg\dot{K}}$)
R_{H2O}	Gas Constant of Air Water Vapor ($\frac{J}{kg\dot{K}}$)
RH	Relative Humidity (%)
R_u	Universal Gas Constant ($\frac{J}{kmole\dot{K}}$)
t	time (sec)
$T_{air_{inlet}}$	Inlet Air Temperature Before Throttle (K)
T_{amb}	Ambient Temperature (K)

T_{BDC} In-Cylinder Gas Temperature at BDC Compression (K)

T_{cyl} In-Cylinder Gas Temperature (K)

$T_{coolant}$ Engine Coolant Temperature (K)

T_{BWD} Average In-Cylinder Gas Temperature form Blowdown to IVO (K)

T_{EVC} In-Cylinder Gas Temperature at EVC (K)

T_{EVO} In-Cylinder Gas Temperature at EVO (K)

T_{exh} Exhaust Gas in Exhaust Manifold Temperature (K)

$T_{exh_{EVO}}$ Exhaust Gas in Exhaust Manifold Temperature at EVO (K)

T_{EXH} In-Cylinder Gas Temperature at the End of Blowdown (K)

T_{fuel} Fuel Temperature (K)

T_{INT} Average In-Cylinder Gas Temperature form EVC to BDC (K)

T_{IVC} In-Cylinder Gas Temperature at IVC (K)

T_{IVO} In-Cylinder Gas Temperature at IVO (K)

T_{res} Residual Gas Temperature (K)

T_{ref} Fuel Thermodynamics Reference Temperature (K)

T_{run} Inducted Gas Temperature at Intake Manifold Runner (K)

T_{up} Upstream Temperature (K)

$v_{air_{int}}$ Volume of Inducted Air from EVC to BDC in mass basis ($\frac{m^3}{kg}$)

v_{fuel} Injected Fuel Volume during the Intake Stroke in Mass Basis ($\frac{m^3}{kg}$)

$v_{H2O_{int}}$ Pressure of Inducted Air Water Vapor in mass basis ($\frac{m^3}{kg}$)

$v_{res_{int}}$ Intake Manifold Flowed-back Residual Gas Volume in mass basis ($\frac{m^3}{kg}$)

V_{BDC}	In-Cylinder Volume at BDC Compression (m^3)
V_{BWD}	In-Cylinder Volume at the End of Blowdown (m^3)
V_{EVC}	In-Cylinder Volume at EVC (m^3)
V_{EVO}	In-Cylinder Volume at EVO (m^3)
V_{IVO}	In-Cylinder Volume at IVO (m^3)
V_{IVC}	In-Cylinder Volume at IVC (m^3)
V_{man}	Exhaust Manifold Volume (m^3)
W_{EXH}	Work from the End of Blowdown to IVO or EVC (J)
W_{INT}	Work from IVO or EVC to BDC Compression (J)
x	Model State
$X_{f_{vp}}$	Vaporized Fuel Fraction
y	Output Vector
$y_{HC_{out}}$	Unburnt HC Out of Exhaust Manifold Molar Fraction (ppm)
Δt_{EXH}	Time Period from the end of Blowdown to IVO or EVC (sec)
Δt_{INT}	Time Period from IVO or EVC to BDC Compression (sec)
$\Delta\theta_{EXH}$	Duration from Blowdown to IVO in Crank Angle Degrees (CAD)
$\Delta\theta_{INT}$	Duration from EVC to BDC in Crank Angle Degrees (CAD)
Δm_{man}	Change Rate of Mass of Exhaust Manifold Content (kg)
Δm_{res}	Change Rate of Residual Gas Mass (kg)
ΔU_{EXH}	Internal Energy Change from the end of Blowdown to IVO (J)
ΔU_{INT}	Internal Energy Change from EVC to BDC Compression (J)

ΔT	Temperature Difference (K)
γ	Specific Heat Ratio of the Exhaust Gas
γ_{EVO}	Specific Heat Ratio of the In-Cylinder Gas at EVO
γ_{IVO}	Specific Heat Ratio of the In-Cylinder Gas at IVO
λ_{des}	Desired Lambda
λ_{UEGO}	UEGO Sensor Measured Lambda
ρ_{fuel}	Fuel Density ($\frac{kg}{m^3}$)
$\theta_{int_{adv}}$	Intake Valve Advance Angle (CAD)
$\theta_{exh_{ret}}$	Exhaust Valve Retard Angle (CAD)
τ_{UEGO}	UEGO Sensor Time Constant (msec)

Abstract

The in-cylinder trapped air, residual gas, and temperature are important dynamic parameters in Gasoline Direct Injection (GDI) Spark Ignition (SI) engines for fuel and combustion control. However, their real-time prediction for transient engine operations is complicated, especially when concerning variable valve timing. A dynamic cycle-by-cycle control-oriented discrete nonlinear model is proposed and developed in this thesis to estimate the in-cylinder mixture temperature and the mass of trapped air, and residual gas at the point of Intake Valve Closing (IVC). The developed model uses in-cylinder, intake and exhaust pressures as the primary inputs. The exhaust gas backflow into the cylinder is estimated using a compressible ideal gas model that is designed for engines equipped with Variable Valve Timing (VVT). The designed model is integrated into a rapid-prototype control system for real-time operation. The model's dynamic behavior is validated using an engine dynamometer transient test cycle under real-time conditions.

The cold crank-start phase significantly contributes to the engine-out total emissions during the US Federal Test Procedure (FTP). The first three engine cycles of the cold crank-start for a Gasoline Direct Injection (GDI) engine in Hybrid Electric Vehicle (HEV) elevated cranking speed is investigated at 20°C. To this end, the impact of the operating strategy on the individual-cylinder engine-out emissions is analyzed

quantitatively. For this purpose, a new dynamic method was developed to translate the engine-out emissions concentration measured at the exhaust manifold outlet to mass per cycle per cylinder. The HEV elevated cranking speed provides valve timing control, throttling, and increased fuel injection pressure from the first firings. This study concentrates on analyzing the cranking speed, spark timing, valve timing, and fuel injection strategy, and parameter effects on engine-out emissions. Design of Experiment (DOE) method is used to create a two-step multi-level fractional-factorial test plan with a minimum number of test points to evaluate the significant parameters affecting engine-out emissions during cold crank-start. The split injection parameters, including the Start of the first Injection (SOI), End of the second injection (EOI), and split ratio, in addition to the first cycle additive fuel factor, are investigated. Results show that using the high cranking speed with stabilized low intake Manifold Absolute Pressure (MAP), highly-retarded spark timing, high valve overlap, late intake first injection, 30 CAD bTDC firing EOI, and low first cycle fuel factor reduces the average fist three cycles HC emission by 94%.

Chapter 1

Introduction

1.1 In-Cylinder Parameters Estimation

Emission regulations set by the U.S. Environmental Protection Agency (EPA) and California Air Resources Board (ARB) for the Light Duty Vehicles (LDV) have progressively become more stringent over the recent decade. The combined allowed value for Nitrogen Oxides (NOx) and unburnt hydrocarbon (HC) emissions, as significant factors for smog formation, has decreased by 46% from Tier2 emission regulation beginning in MY 2017 and will see a further 65% reduction from 86 to 30 mg/mi by 2026 with Tier3 [1]. To meet the new requirements, engines have been equipped with new technologies, downsizing and turbocharging, Gasoline Direct Injection (GDI),

and VVT. Moreover, in-cylinder and exhaust pressure sensors have been utilized in several studies to develop new models to estimate individual-cylinder parameters such as in-cylinder gas temperature and residual gas. The estimated parameters are then incorporated for individual in-cylinder air charge prediction to improve Air to Fuel Ratio (AFR) control during transients. Precise AFR control in advanced engines is essential to reduce engine-out emissions to meet emission regulations. In conventional AFR control methodologies, part of the AFR control complexity relates to the transport delay from where the air-fuel mixture is prepared inside the cylinder to where an oxygen sensor senses it. Using the in-cylinder AFR control, the transport delay and the AFR excursions during dynamic conditions are reduced, resulting in more precise AFR control, especially during the transients. In addition, the estimated in-cylinder parameters are used for accurate and dynamic individual-cylinder combustion phasing control as a potential improvement for engine-out emissions reduction.

The new European Real Driving Emissions (RDE) testing requirements have been phased in from 2017. The RDE will be applied to all new cars by the beginning of 2021 to regulate vehicle emissions in real driving operations. The RDE considers higher accelerations, along with gradient, stop-and-go, or greater speeds [2]. As a result, a precise model for predicting the mass of trapped air charge and residual gas with improved dynamic behavior is required to cover broad real driving emissions. This model can significantly help to decrease the Non-Methane Organic Gases (NMOG) and NOx engine out and tailpipe emissions when coupled with catalyst temperature

and oxygen storage state control [3].

Chapter 2 of this study reviews the state-of-the-art research for air charge models for RDE conditions. It presents a new real-time model to estimate the in-cylinder trapped air charge, residual gas, and temperature in a state-of-the-art four-cylinder turbocharged GDI engine equipped with intake and exhaust VVT. The model is control-oriented, as all manipulated variables (inputs), measured intermediate variables, estimated parameters (outputs), and disturbances are formulated for engine control, model uncertainties are described, and constraints on the inputs and states are defined. The trapped air charge is calculated at Intake Valve Closed (IVC) using an event-based approach cylinder-by-cylinder. In this research, IVC is considered as the beginning of each cycle before ignition and combustion. The developed model uses the residual gas mass defined from the previous cycle that has flowed back from the exhaust and possibly into the intake. The residual gas backflow mass during the valve overlap is calculated based on the compressible ideal-gas flow using the cylinder and exhaust pressure sensors' dynamic data. The developed model is computationally efficient, not including iterative loops and complex numerical calculations, capable of being implemented in a production ECU. It is physics-based with low calibration efforts comprising 32 required calibration points in total to cover broad engine part-load speed and load conditions. In contrast, a conventional ECU requires calibrating 512 points for 24 measuring points of load, engine speed, and valve overlap every 8 points. Also, it is a dynamic model with one cycle resolution, which captures the

engine transients with less than 1.5% average relative steady-state error.

1.2 Cold Crank-Start Emissions Analysis

The Federal Test Procedure, FTP-75, is used for emission certification and fuel economy testing of light-duty vehicles in the United States. Figure 1.1 shows the US EPA Urban Dynamometer Driving Cycle for FTP-75, comprising three phases, cold start, transient and hot start. The transient cold start phase has the most significant contribution to the cumulative HC emission over the FTP-75 cycle. For instance, the cumulative tailpipe HC emission over the FTP-75 cycle for a 2010 vehicle equipped with a 3.5 liters turbocharged GDI engine and a low-temperature Three-Way Catalyst (TWC) shows that the cold-start phase is responsible for 97% of the tailpipe HC emissions [4]. More important, during the first four seconds of the cold-start phase, including the conventional low-cranking speed crank-start period, 110 mg of unburnt HC equivalent to 32% of the Tier3 limit is scavenged out of the engine [5].

Given the upcoming highly restrictive emission regulations for the combined allowed value for Nitrogen Oxides (NOx) and unburnt HC emissions, this signifies the importance of engine emission control from the cold start phase when a vehicle begins to operate. Extensive studies have been done to reduce the engine-out emissions in the FTP-75 transient and hot start phases. However, reducing the engine-out emissions

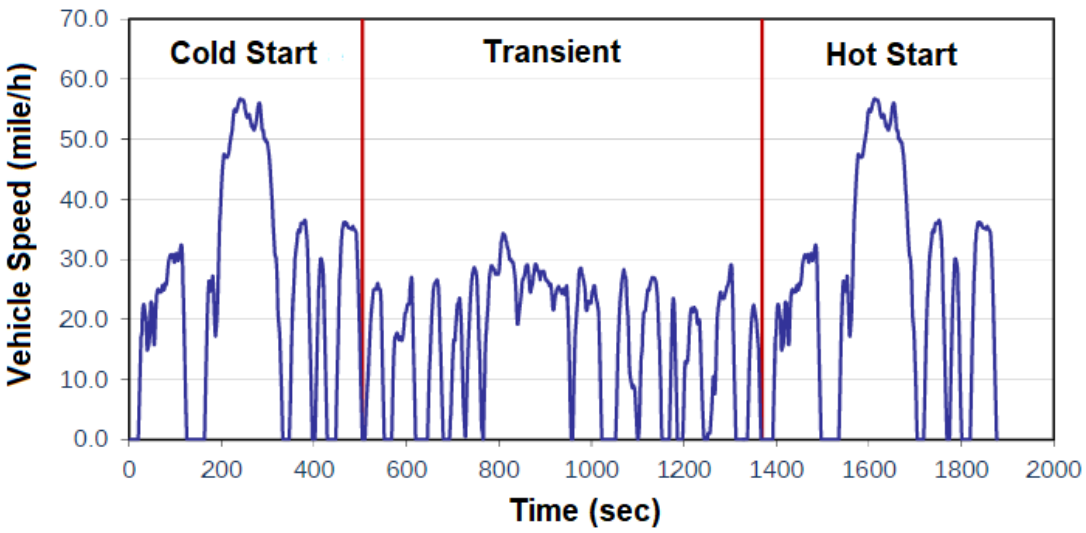

Figure 1.1: The US FTP-75 driving cycle

during the cold "crank-start" phase remains challenging, while there are multiple opportunities for improvement. For this purpose, firstly, the cold-crank-start period contribution has to be quantified precisely to analyze the cold-start emissions efficiently. This thesis aims to provide a methodology and analytical tools for engine cold crank-start dynamics and emissions analysis.

To meet the new fuel consumption requirements, new technologies, such as downsizing and turbocharging, Gasoline Direct Injection (GDI), and Variable Valve Timing (VVT), have recently been utilized broadly. For instance, GDI engines have experienced a rapid adoption in the market, increasing from 0% in 2007 to over 50% market share in 2016 in the US[6], and a foreseen market share of up to 97% by 2025[7]. In addition, many vehicle manufacturers are increasingly using Hybrid Electric Vehicles (HEV) in their near-zero-emission vehicle (ZEV) product portfolios[8] because

of specific CO2 vehicle emission reduction legislation[9].

The GDI engines have several advantages for reducing fuel consumption; however, the direct injection of the liquid fuel into the cylinder leads to emissions challenges, especially for HC during the cold-start phase. In the conventional vehicles, the cold crank-start includes the lowest temperature and lowest engine speed compared to all the other engine operating modes throughout the FTP-75 driving cycle. Therefore, considerable constraints occur on the fuel evaporation and mixture formation in conventional low cranking speed crank-start, leading to a substantial required over-fueling to guarantee an ignitable fuel-air mixture. The cold cylinder walls cause fuel film formation as one of the important reasons for increasing HC emission [10], and is further extubated due to the over-fueling requirement. Additionaly, part of the injected fuel absorbs into the oil layer and, after combustion, is desorbed back into the bulk gases as another reason for HC emission increase. Furthermore, the heat transfers away from the flame front to the cold cylinder walls increases, and the post-flame oxidization rate of the resulting emissions from combustion decreases. As a result, flame quenching distance grows, causing the increase of gaseous fuel escaping from combustion and HC emission.

Another factor of importance is that the low engine speed during cranking reduces the charge motion, resulting in poor mixture formation. As a consequence, fuel evaporation and mixture homogeneity decrease. Furthermore, the post-flame oxidization

rate decreases in low engine speed because the quality of mixing unburnt HC with the hot bulk gases reduces in the vicinity of the cold walls. Besides, the fuel evaporation decreases due to the lack of hot residual gases in the first cycle events compared to the next combustion cycles during the crank-start. A portion of the fuel injected in the first cycle that does not contribute to the combustion or scavenged out of the cylinder as unburnt HC during the exhaust stroke remains in the cylinder as residual fuel. The residual fuel contributes to the combustible mixture of the second cycle. In the cold-crank phase, higher ring-gap and lack of lubrication results in considerable blow-by rate and charge loss compared to other engine operating states [11]. As a result, a portion of the injected fuel is lost through the lubrication oil and blow-by gases into the crankcase.

In the HEVs, the engine is cranked to idle speed quickly using a powerful integrated starter and generator, or electric motor instead of the starter as an auxiliary rotation device. Therefore, the transients of the engine during the start-up are different, and there are several additional opportunities, such as VVT control, throttling, and high fuel pressure from the first firing over conventional low cranking speed vehicles for cold-start emissions improvement.

Chapter 3 presents an individual-cylinder dynamic analysis of the engine-out emissions for a GDI engine at the motored elevated HEV cranking speed during the cold crank-start initial three cycles. Firstly, the most critical parameters affecting the

engine-out emissions during the cold-crank start are specified. Then, an optimal test plan, including the test parameters levels, is derived using the DOE method. The tests are accomplished on engine-dyno with duplicating the motored elevated HEV cranking speed cold crank-start process. Finally, the experimental data are used along with the developed dynamic method for translating the emissions concentration to mass per cycle per cylinder to analyze the engine-out emissions behavior and distinguish the optimal engine operating strategy. The precise dynamic individual-cylinder cycle-by-cycle engine cold crank start analysis determines the optimal engine control inputs trajectories. The optimal control inputs trajectories can be used for predictive closed-loop AFR and combustion control during the engine cold crank-start phase to minimize the engine-out emissions.

The specific contributions of this thesis are:

1. Development of a real-time discrete non-linear cycle-by-cycle physics-based model to estimate the mass of trapped air; charge and residual gas with low calibration effort

2. A new pegging method using both intake and exhaust absolute pressures, Dual-Pressure Pegging (DPP), is introduced to compensate the thermally-induced intracycle in-cylinder pressure sensor drift for precise estimation of the gas exchange during the exhaust stroke and valve overlap;

3. Estimating the mass of exhaust gas backflows into the cylinder during valve overlap based on compressible ideal gas flow equations;

4. A new amplification technique for in-cylinder pressure transducer signal, Dual-Scale Amplification (DSA), is introduced to increase the measured in-cylinder pressure Signal-to-Noise-Ratio (SNR) during the gas exchange;

5. Integration and validation of the in-cylinder air charge, residual gas, and temperature model on the rapid-prototype engine control system for real-time operation assessment.

6. Development of a new method to quantify engine-out emissions in mass per cycle per cylinder

7. Development of an engine-dyno test methodology to duplicate the motored HEV elevated cranking speed cold crank-start process

8. Utilize DOE methods to create a two-step multi-level fractional-factorial test plan with an optimal number of test points to analyze the engine-out emissions during the cold-start first cycles

9. Analysis of the engine operating strategy, including cranking speed, spark timing, and valve timing with respect to their impact on the engine-out emissions

10. Analysis of the split injection strategy's parameters, including SOI, EOI, split ratio, and the first cycle fuel factor impact on the engine-out emissions

11. Derivation of the optimal control inputs trajectories resulting in the lowest HC and NOx emissions during the cold start first cycles

Chapter 2

In-Cylinder Air Charge, Residual Gas and Temperature Estimation

The in-cylinder trapped air, residual gas, and temperature directly impact Spark Ignition (SI) engine operation and control. However, estimation of these variables dynamically is difficult. This chapter proposes a dynamic cycle-by-cycle model for estimation of the in-cylinder mixture temperature at different events such as Intake Valve Closed (IVC) and the mass of trapped air and residual gas. In-cylinder, intake, and exhaust pressure traces are the primary inputs to the model. The mass of trapped residual gas is affected by valve overlap increase due to the exhaust gas backflow. Of importance to engines with Variable Valve Timing (VVT), the compressible ideal-gas flow correlations are applied to predict the exhaust gas backflow into the cylinder.

2.1 Introduction

Precise estimation of the in-cylinder air charge is vital for engine control. Engine torque, AFR, and combustion phasing control depend on the estimated air charge and residual gas concentration. The conventional and in-cylinder pressure-based methods have already been investigated for air charge estimation. In the conventional methods, intake Manifold Absolute Pressure (MAP) and Mass Air Flow (MAF) sensors have been utilized; however, this results in several issues, and obstacles [12]. The MAF sensor is an appropriate device to measure the engine's total air consumption in steady-state conditions. However, its measured data for transient conditions can not be used unless the filling and emptying dynamics of the intake manifold are modeled and integrated into real-time observers [13, 14, 15, 16, 17]. The intake manifold dynamic model needs MAP sensor data and Volumetric Efficiency (VE). The VE has been traditionally specified using look-up tables that require significant calibration efforts, especially for the engines with VVT [18]. Speed-density is another conventional method for air charge estimation using intake manifold temperature, MAP sensors, and VE data. The speed-density method has a lower cost and proper transient performance, but still requires considerable calibration efforts [19]. Several studies have been done to reduce VE calibration efforts, such as using Artificial Neural Network (ANN) [20, 21, 22] or a parametric model [23, 24]. The ANN model had a problem with the points outside the training region and could not be easily implemented

in mass-production engine controllers. The parametric models included several calibrated parameters requiring extensive engine test datasets to be calibrated offline and required adaptive corrections. In another study, researchers developed a model for fresh air charge and residual gas fraction estimation for a turbocharged VVT engine using engine speed, intake manifold pressure, and VVT actuator positions [25]. This model also needed significant calibration efforts, and compressible-flow-based correlations used for residual gas fraction estimation were not validated. As a source of error, in all conventional methods, the total air consumed by the engine was calculated, and the trapped air in all cylinders was assumed to be equal.

The cylinder pressure-based method was first introduced in the 1990s to overcome conventional methods' drawbacks. Table 2.1 shows the summary of cylinder pressure-based air charge and residual gas estimation models from the literature review and this work.

In one research paper, the temperature of air and fuel mixture at the beginning of compression stroke was adapted by a Kalman filter to improve the transient response of the model [26]. This research was done on a Multi-Port Fuel Injection (MPFI) engine without VVT, using the in-compressible flow-based method developed by Fox et al. [27] for residual gas fraction calculation. The Fox model uses incompressible flow with the average pressure difference between the exhaust and intake to estimate

Scholars	M. Mladek	G.Colin	J. Worm	S. Wang	A.Yazdani	A.Thomasson	This Work
Engine	MPFI Dual-position IVT	MPFI VVT	MPFI VVT	MPFI VVT	GDI VVT	Diesel VVT	GDI VVT
Estimated In-Cylinder Parameters	1. Air charge 2. Residual gas	Air charge	Air charge	Residual gas	1.Air mass 2.Residual gas	1.Air charge 2.Residual gas	1.Air charge 2.Residual gas 3.Temperature
Input Parameters	1.Cyl. Pressure 2.MAP 3.Exh. Pressure 4.Inlet air temp. 5. Spark timing	1.Cyl. Pressure 2.MAP 3.Exh. Pressure 4.Exh. temp.	Cyl. pressure	1.Cyl. pressure 2.MAP 3.Exh. Pressure	1.Cyl. Pressure 2.MAP 3.Inlet air temp. 4.Rel. humidity	1.Cyl. Pressure 2.MAP 3. Exh. Pressure	1.Cyl. Pressure 2.MAP 3.Exh. Pressure 4.Inlet air temp. 5.Rel. humidity
Model	1.Offline initial condition 2.Online iterative	Online	Offline	Real-time Control-oriented	Cycle-by-cycle Event-based Online	Offline Iterative	Cycle-by-cycle Event-based Real-time Control-oriented
Residual gas estimation	Iteration using spark timing	incompressible flow based	NA	incompressible flow based	incompressible flow based	Compressible flow based	Compressible flow based
Computation duration / sampling rate	IVC to 50% mass burned position/ 0.2CAD	IVC to IGN / 1CAD	IVC to IGN	IVO to EVC	Entire cycle / 0.5CAD	IVC to EVO	Entire cycle / 0.5CAD
Assumptions	Ideal gas law Fixed stoich. AFR	Ideal gas law First law	Ideal gas law Mass conservation	Ideal gas law	Ideal gas law Mass conservation	Ideal gas law First law	Ideal gas law First law Mass conservation
Calibration effort	NA	moderate	moderate	modearte	high	low	low
Steady-state validation	1000 to 5000RPM zero to full load	2 engine speed 2 load	1000 & 5000RPM Different EGR rate and cam pahse	1000 to 4500RPM MAP:0.3 to 0.9bar Different cam phasing	1000 to 2500RPM IMEP: 2.5 to 9bar Different cam phasing, AFR and CA50	600 to 1450RPM 50 to 2500Nm Different cam phasing	1500 to 4500RPM 2.5 to 7.5bar IMEP Different cam phasing, AFR and CA50 GT-Power TPA-based
Transient validation	NA	NA	4800 RPM/intake valve transitions	1000 to 3500 and 3500 to 1000RPM with valve timing transitions	1400 to 1600RPM 2 to 6bar IMEP (High overshoots during transitions)	Not included	1000 to 4500RPM 0.5 to 10bar IMEP (Good overshoot, rising and settling times)

Table 2.1
Summary of cylinder pressure-based air charge and residual gas estimation models compared to the study in this work

residuals for the overlap period. The dynamic behavior of Hart's model was also validated using the hot-film air mass meter data. In another research, it was assumed a fixed stoichiometric air/fuel ratio, and air charge calculations were done from Intake Valve Closed (IVC) to 50% mass burned position for every cycle [28]. This research was also accomplished on an MPFI engine with double-position variable inlet valve timing. In this research, an iterative approach was used for residual gas fraction estimation, and spark timing was considered as an input for the burn rate estimation. In one study, a model-based control strategy for estimation of the air mass was introduced to control the Exhaust Gas Recirculation (EGR), and AFR [29]. This study also used a high computational iterative method. In other studies, cylinder pressure

difference was used as Delta-P to estimate cyclic trapped fresh air charge in the cylinder [30, 31]. In these works, the in-compressible flow-based FOX model was used for residual fraction calculation, and the designed model was not suitable for the engine with cam phaser and EGR. One algorithm considered a duration between the IVC and ignition at every cycle and predicted the fresh air mass based on total in-cylinder trapped mass [32]. In this algorithm, the in-compressible flow-based correlation was used for residual fraction estimation. The proposed algorithm was sensitive to the cylinder pressure offset, and the model was not evaluated and verified for transient conditions.

In recent works on air charge and residual fraction estimation, presented by Yazdani et al. [33] and Thomasson et al. [34], Yazdani et al. proposed a cycle-by-cycle cylinder pressure-based air charge and residual gas estimation model. This model also used the incompressible flow-based Fox model as a base for estimating the mass of residual gas. Also, the transient response of the model showed significant overshoot during engine dynamic conditions. Thomasson et al. used compressible flow correlations to predict the mass of residual gas mass; however, the model was not assessed and validated for transient conditions. Shu Wang et al. [35] developed a model for estimation of the mass of residual gas for SI engines. Wang's model was control-oriented, but it also assumed the gas flow as an in-compressible flow and needed a significant amount of calibration. In addition, Cavina et al. [36] designed a static residual fraction estimator for a GDI engine based on the compressible flow-based Fox

model. Guardiola et al. [37] developed a model for cylinder charge and composition estimation for a Reactivity Controlled Compression Ignition (RCCI) engine in which in-cylinder pressure resonance with a closed-loop intake manifold observer was used. Shaver et al. [38] proposed a compressible flow-based dynamic model to estimate the residual gas effect on Homogeneous Charge Compression Ignition (HCCI) engines with Variable Valve Actuation (VVA). Most of the methods discussed above were not thoroughly validated in both steady-state and transient conditions using data from a high-fidelity engine simulation model or experimental data.

The research in this chapter aims to develop a computationally efficient, physics-based model to be implemented in the engine Electronic Control Unit (ECU) for a real-time estimate of the mass of trapped air charge and residual gas in-cylinder gas temperature with minimum calibration effort. This goal is fulfilled by designing a discrete and dynamic Multi-Input-Multi-Output (MIMO) cycle-by-cycle, event-based model, which uses in-cylinder, intake, and exhaust pressures data to estimate the outputs. The specific contributions of this work are:

1. Development of a discrete cycle-by-cycle physics-based model to estimate the mass of trapped air; charge and residual gas with low calibration effort

2. Validation of the model in steady-state and transient conditions using experimental data;

3. A new pegging method using both intake and exhaust absolute pressures, Dual-Pressure Pegging (DPP), is introduced to compensate the thermally-induced intracycle in-cylinder pressure sensor drift for precise estimation of the gas exchange during the exhaust stroke and valve overlap;

4. Gas exchange dynamics are considered using high-resolution crank-angle based cylinder pressure, intake and exhaust manifold pressures;

5. Estimating the mass of exhaust gas backflows into the cylinder during valve overlap based on compressible ideal gas flow equations;

6. A new amplification technique for in-cylinder pressure transducer signal, Dual-Scale Amplification (DSA), is introduced to increase the measured in-cylinder pressure Signal-to-Noise-Ratio (SNR) during the gas exchange;

7. Integration and validation of the model on the rapid-prototype engine control system for real-time operation assessment.

2.2 Experimental Setup

A Ford 2.0L Ecoboost turbocharged in-line 4-cylinder GDI engine was utilized for this study. The engine was equipped with two intake and two exhaust valves per cylinder. Intake and exhaust valve timings were adjusted using an oil-driven dual-independent valve phasing system. A summary of the engine technical specification

is presented in Table 2.2. A Bosch production ECU read the engine sensors and commanded the actuators to control the engine. All parameters of the Bosch production ECU were accessible through ATI Vision® software. The Bosch ECU connects with Delphi Cylinder Pressure Development Controller (CPDC) via a CAN interface. The designed real-time model in Simulink/Stateflow environment was programmed inside the CPDC and tested and validated while synchronized with the engine production ECU.

Figure 2.1 represents a schematic of the test engine experimental setup. A 450 hp Alternating Current (AC) dynamometer controlled the engine speed and load to run under desired steady-state or transient operating conditions. Two independent external cooling systems were used to adjust the engine coolant and inlet air temperatures to the desired operating values. Inlet air temperature was regulated by controlling the coolant temperature of the turbocharger after-cooler. Using these external cooling

Compression Ratio	9.3:1
Bore	87.5 mm
Stroke	83.1 mm
Connecting Rod Length	155.9 mm
Wrist-Pin Offset	0.6 mm
Base Intake Valve Open (IVO)	11° ATDC
Base Intake Valve Close (IVC)	247° ATDC
Base Exhaust Valve Open (EVO)	-216° ATDC
Base Exhaust Valve Close (EVC)	8° ATDC
Firing Order	1-3-4-2

Table 2.2
Engine technical specification

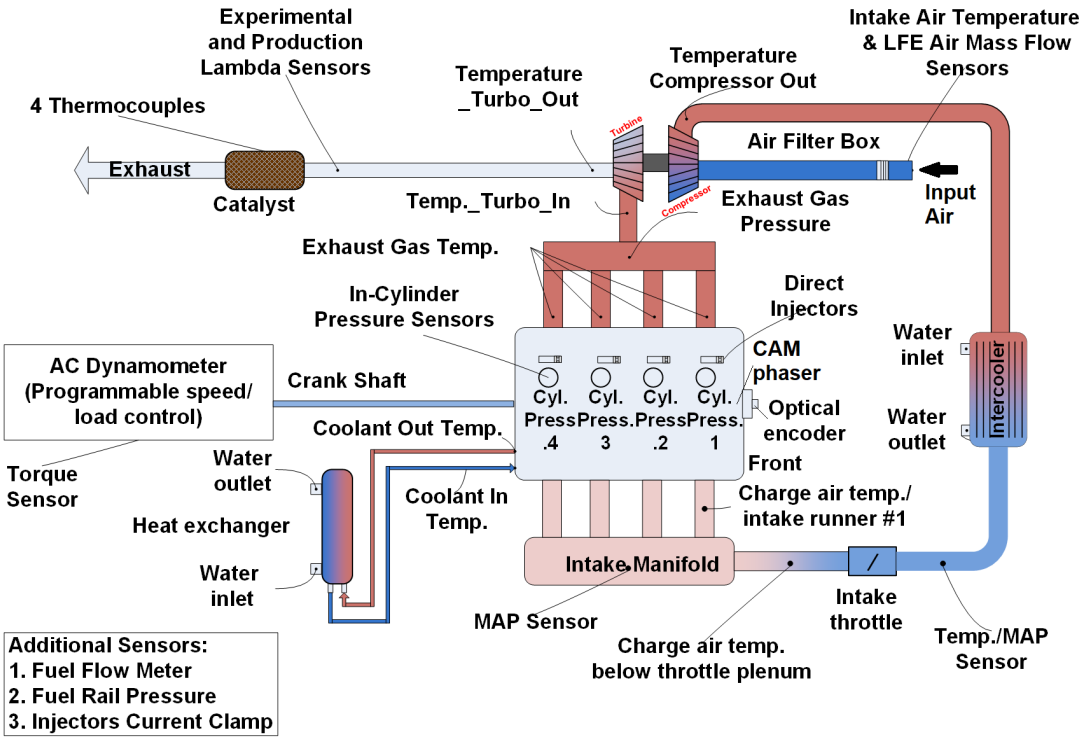

Figure 2.1: Schematic of the engine experimental setup

systems, the engine coolant and inlet air temperatures were adjusted to the engine normal operating values, 85^{o}C and 40^{o}C, respectively, while the dynamic cycle was accomplished.

Kistler 6125A pressure transducers were used to measure the cylinder pressures with an accuracy of 2%. An OMEGA pressure sensor was used to measure the dynamic pressure in the intake manifold with an accuracy of 0.25%. A fast response piezoresistive Kulite pressure sensor was used to measure the dynamic pressure in the exhaust manifold with a measurement bandwidth of 150 kHz and an accuracy of 1.5%. The temperature drift of the Kulite exhaust pressure sensor was compensated using an

OMEGA pressure sensor with a measurement bandwidth of 1 kHz. The OMEGA pressure sensor was mounted using a pipe with a length of about 90 cm to maintain a distance from the engine, not affected by the engine heat. It measured the exhaust pressure at the same location, shown in figure 2.1, as the Kulite sensor measured. An AD Combustion Analysis System (CAS) with 16-channels was used for crank angle-resolved data acquisition. Cylinder and exhaust pressure data were recorded by CAS with a sampling resolution of 0.5 CAD. High-resolution measured cylinder and exhaust pressure data captured gas exchange dynamics during the valve overlap. K-type thermocouples were used to measure inlet air and exhaust gas temperatures in the intake and exhaust ports.

The air and fuel mass flows were measured by a laminar mass flow-meter and a Coriolis flow-meter, respectively. The fuel used for the experiments is E10 gasoline with an AKI of 87. An 80I-110S Fluke AC/DC Clamp-On Current Probe was used to measure the injection pulse of the fuel injection in all cylinders. CAS with 0.5 CAD resolution recorded the injection pulse and fuel rail pressure traces. The injection pulse trace was used to extract the actual injection pulse width. A wideband UEGO sensor was also used along with the production sensor with an accuracy of 1% around lambda 1. The output of the wideband UEGO sensor was monitored using an ETAS lambda-meter and recorded by CAS.

The output of the cylinder pressure transducer needs to be referenced to an absolute

pressure, which is used for pegging. Referencing the cylinder pressure transducer output to MAP at the Bottom Dead Center (BDC) before compression is the most common pegging method [39]. However, the MAP-based pegging procedure does not consider thermally-induced intracycle and inter-cycle sensor drift caused by thermal gradients in the sensor [40]. The cylinder pressure data is the key input for estimating the trapped air charge and residual gas, especially for calculating the exhaust gas backflow during the valve overlap. Therefore, the intracycle thermal drift of the cylinder pressure sensor output should be compensated. For this purpose, a new method for Dual-Pressure Pegging is introduced in this study for cylinder pressure data pegging using both MAP and exhaust pressure data. In the DPP method, the cylinder pressure transducer output is pegged in the middle of the exhaust stroke, between 300 to 303 CAD, in addition to BDC before compression. The middle of the exhaust stroke is the point where the blowdown phase is complete, and the cylinder and exhaust pressures come to near equilibration. Figure 2.2 shows the difference between the MAP-based and DPP-based pegged cylinder pressure traces. The pressure range related to the intake and exhaust strokes is highlighted. The DPP pegging entirely compensated the cylinder pressure deviation from exhaust pressure in the MAP-pegged cylinder pressure caused by the intracycle thermal drift. As a result, cylinder pressure matches the exhaust pressure from the end of blowdown up to where intake valves open with less than 1% error.

The entire range of measurement of the cylinder pressure transducer is from 0 to 100

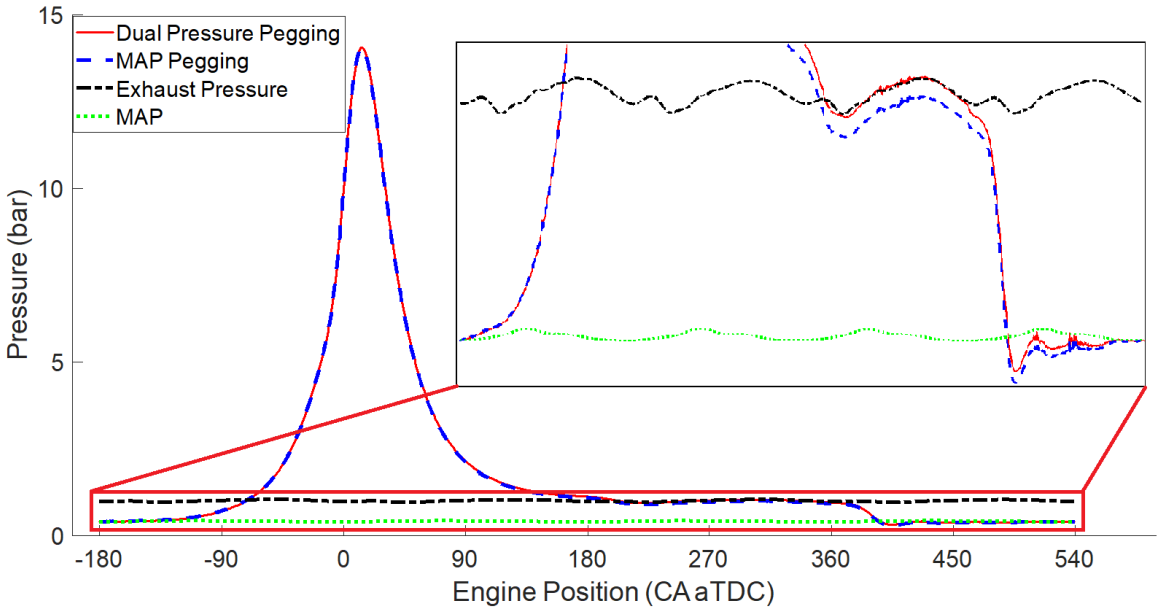

Figure 2.2: MAP and dual-pressure pegged cylinder pressure traces

bar, which is converted to 0 to 5V at the output of the main scale amplifier. Therefore, a wide region of the measured cylinder pressure in each cycle has a low SNR. This region includes the entire intake and exhaust strokes and a part of compression and expansion strokes. In this region, the cylinder pressure is between 0 to 3 bar. Even small SNR cylinder pressure during intake and exhaust strokes will propagate to a significant error to the entire designed model implemented in the CPDC. The new DSA technique is introduced to solve this problem and improve the designed model outputs' precision.

Figure 2.3 shows how the DSA technique is implemented to prepare high-precision cylinder pressure data for the CPDC. In the DSA technique, a differential amplifier is used in addition to the main scale amplifier. The new differential amplifier amplifies

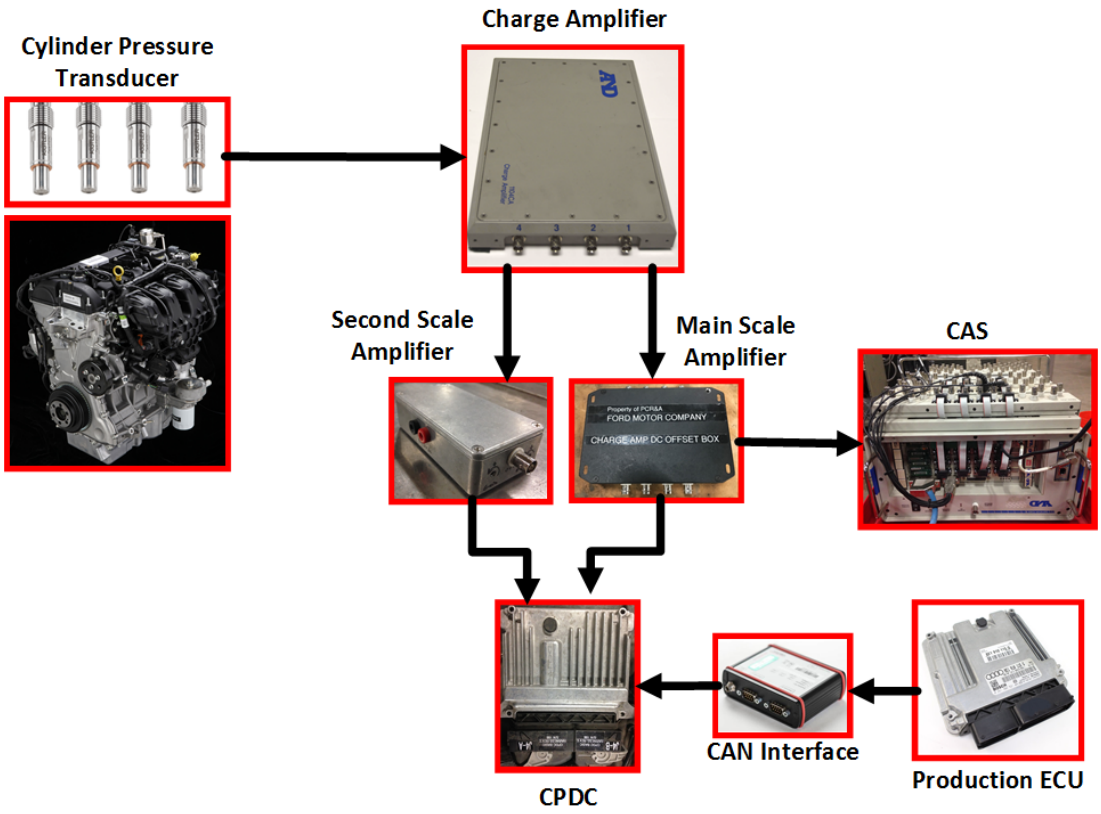

Figure 2.3: Dual-scale technique implementation on CPDC

the cylinder pressure signal from the charge amplifier output and crops out part of the data related to the high cylinder pressure zone over 3 bar. As a result, the signal range from 5 to 25 V is clipped, and the 0 to 5 V range is mapped for the cylinder pressure data in the range of 0 to 3 bar. The embedded software of the CPDC was developed so that each cylinder had two-cylinder pressure inputs, one for the range of 0 to 100bar and the second for the range of 0 to 3 bar. The cylinder pressure inputs to the designed model during the intake and exhaust strokes, including IVC, compression BDC, IVO, EVC, and EVO, were produced using second cylinder pressure input with high resolution.

2.3 Physical Model Development

In the newly developed real-time nonlinear MIMO model, individual-cylinder pressure trace in every cycle is used event-based to estimate the mass of in-cylinder trapped fresh air and residual gas. In addition, the temperature of the in-cylinder trapped mixture at IVC and exhaust gas at the end of blowdown are also predicted, which can be used as inputs to combustion phasing and catalyst thermal models, respectively. Figure 2.4 shows a block diagram of how the model operates event-by-event throughout a cycle for a single cylinder, including inputs and outputs.

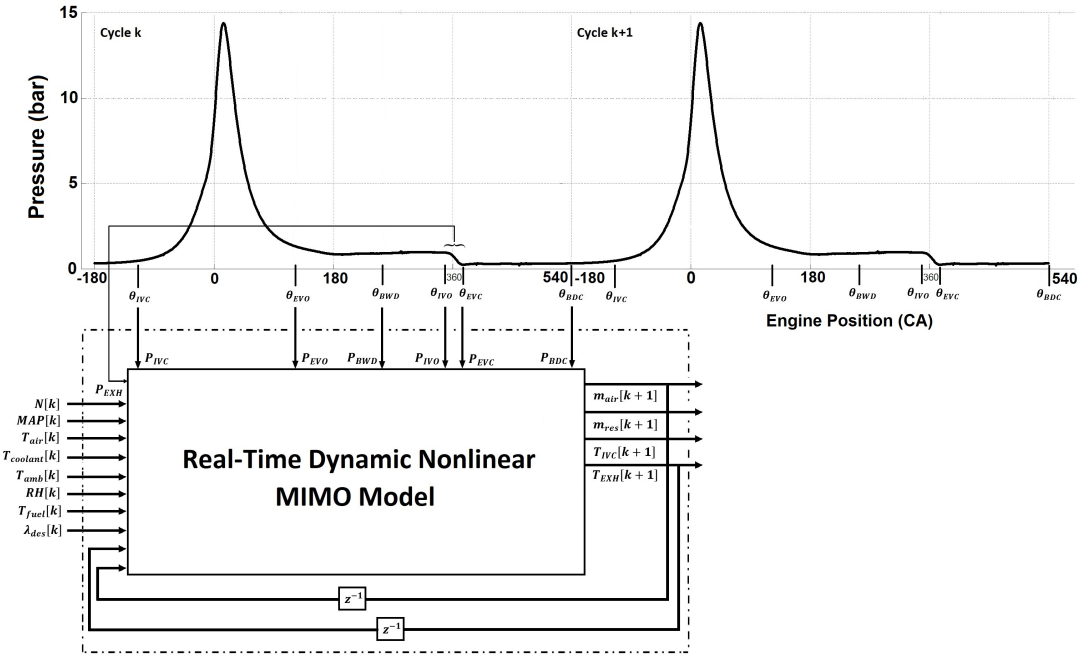

Figure 2.4: A block diagram representation of the cycle-by-cycle event-based performance of the model including inputs and outputs for a single cylinder

The model comprises several calculations based on thermodynamic laws and compressible ideal gas flow correlations. Every cylinder's cycle starts at the IVC and ends at the next cycle IVC. Figure 2.5 shows the physical laws and relationships used in the developed model throughout one cycle on a P-V diagram. The model is divided into two major sub-models, (i) residual gas and (ii) air charge.

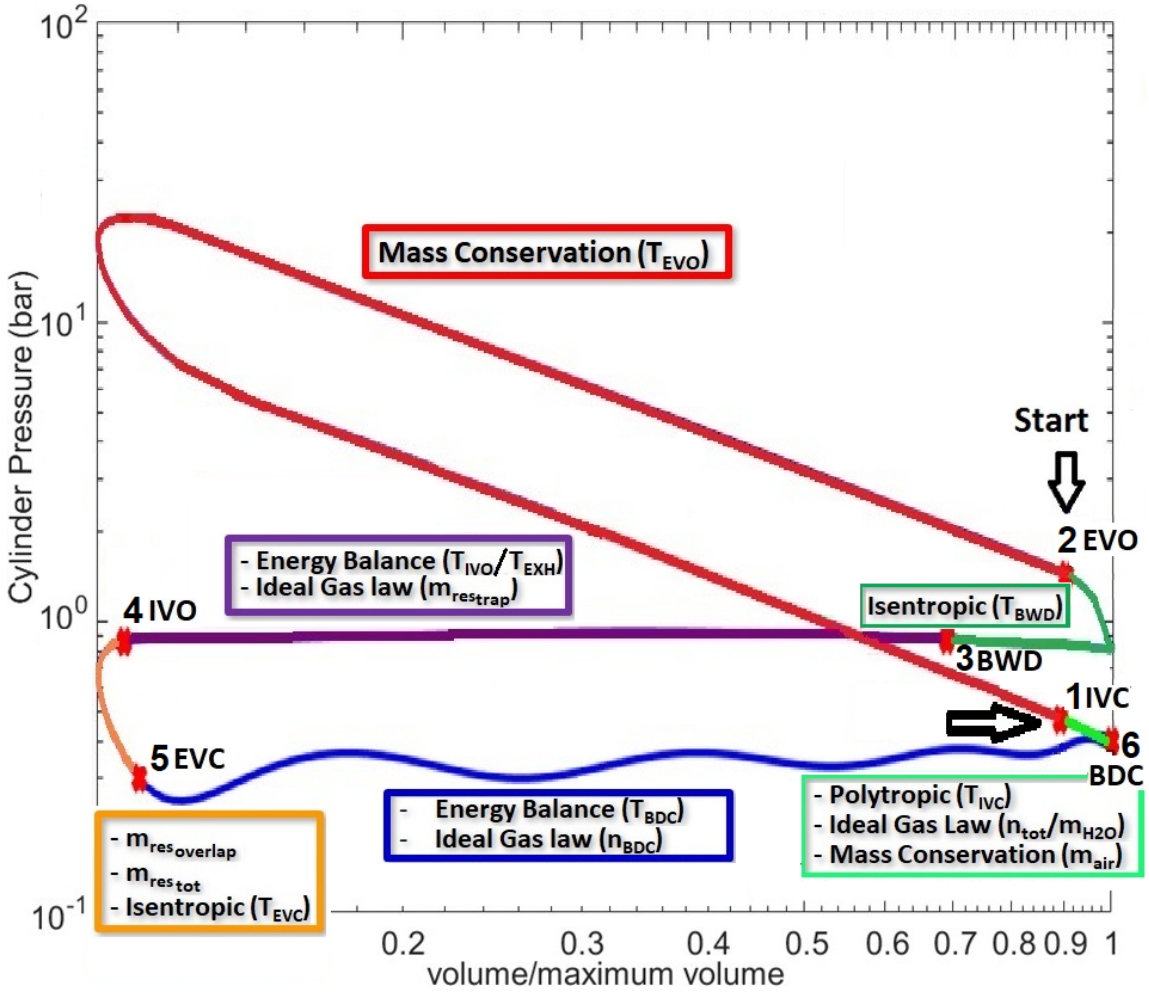

Figure 2.5: A P-V diagram including all physical laws and relationships that are used for calculation of the air charge and residual gas masses during one cycle

2.3.1 Residual Gas Sub-Model

In this study, residual gas is the in-cylinder burnt gas trapped at IVC from the previous engine cycle. The residual unburnt fuel from the previous engine cycle is assumed to be negligible for a warm engine. The mass of the total residual gas contributed in the cylinder trapped mixture at IVC is equal to the mass of in-cylinder trapped gas at EVC when there is negative overlap.

$$m_{res_{tot}}[k] = m_{EVC}[k] \tag{2.1}$$

From EVC to IVO, the combustion chamber is a closed system, and trapped residual gas remains constant. After IVO, a portion of the trapped residual gas that flows back into the intake manifold is assumed entirely sucked back into the cylinder during the intake stroke. The total residual gas contributed in the cylinder trapped mixture at IVC is composed of two portions in the positive overlap. The first portion is the exhaust gas that remains in the cylinder during the exhaust stroke and is trapped in the cylinder at IVO,

$$m_{res_{trap}}[k] = m_{IVO}[k] \tag{2.2}$$

m_{EVC} and m_{IVO} are estimated in the air charge sub-model. The second portion is the exhaust gas that flows back from the exhaust manifold into the cylinder during the valve overlap from IVO to EVC. Both exhaust and intake valves are open

simultaneously during the valve overlap, and the exhaust gas is exchanged between the exhaust manifold, cylinder, and intake manifold based on pressure differences. However, it is assumed that a portion of the exhaust gas, which flows into the intake manifold runner during the valve overlap, is completely sucked back into the cylinder during the intake stroke of the same cycle. Thus, the mass of the exhaust gas that flows back into the cylinder is a function of engine speed, in-cylinder and exhaust manifold pressures and temperatures, intake and exhaust valve timings, and exhaust valves characteristics, including profile discharge coefficient and effective area. In this study, the exhaust gas mass flow across the exhaust valves during the valve overlap is calculated using the correlation for compressible ideal gas flow for sub-critical flow as following,

$$\dot{m}_{exh}[k] = \frac{C_D A \cdot p_{up}[k]}{\sqrt{R_{exh} T_{up}[k]}} \cdot \left(\frac{P_{down}[k]}{P_{up}[k]}\right)^{\frac{1}{\gamma}} \cdot \left\{\frac{2\gamma}{\gamma - 1}\left[1 - \left(\frac{P_{down}[k]}{P_{up}[k]}\right)^{\frac{\gamma-1}{\gamma}}\right]\right\}^{\frac{1}{2}} \tag{2.3}$$

where, p_{up} and T_{up} are upstream pressure and temperature, p_{down} is the downstream pressure, A is the effective area of the engine exhaust valve, N is engine speed and R_{exh} is the gas constant of the exhaust gas, which is assumed constant and equal to $277 \frac{J}{kg.K}$, C_D is the Discharge Coefficient that is determined experimentally in the flow test bench, and γ is assumed constant and equal to 1.3 [11]. If the exhaust gas flow across the exhaust valve is choked, downstream to upstream pressure ratio, $\frac{P_{down}}{P_{up}}$ is less than or equal to the critical pressure ratio, 0.546, for $\gamma = 1.3$, and the exhaust

gas mass flow is calculated as following [11],

$$\dot{m}_{exh}[k] = \frac{C_D A \cdot p_{up[k]}}{\sqrt{R_{exh} T_{up}[k]}} \cdot \gamma^{\frac{1}{2}} \cdot \left(\frac{2}{\gamma+1}\right)^{\frac{\gamma+1}{2(\gamma-1)}} \tag{2.4}$$

After IVO, exhaust gas evacuation from the cylinder into the exhaust manifold can continue for a short duration until cylinder pressure is higher than exhaust pressure. Then, in Equation (3) or (4), upstream pressure is cylinder pressure, $p_{up} = p_{cyl}$, and downstream pressure is exhaust manifold pressure, $p_{down} = p_{exh}$. In addition, the temperature of the in-cylinder gas flowing out of the cylinder during valve overlap is the average of the in-cylinder gas temperature at IVO and EVC,

$$T_{up}[k] = T_{res}[k] = \frac{T_{IVO}[k] + T_{EVC}[k]}{2} \tag{2.5}$$

The in-cylinder gas temperature at IVO, T_{IVO}, and at EVC, T_{EVC}, are calculated in the air charge sub-model. As soon as the cylinder pressure decreases less than exhaust pressure, exhaust gas backflow into the cylinder begins. Then, Equation (3) or (4) are used assuming $p_{up} = p_{exh}$, $p_{down} = p_{cyl}$ and $T_{up} = T_{exh}$. T_{exh} is the temperature of the exhaust gas in the exhaust manifold runner from the exhaust temperature model. Due to the cylinder and exhaust pressures' highly dynamic behavior during valve overlap, the valve overlap period is divided into several segments. Each segment is determined as a period in which p_{cyl} is continuously greater than p_{exh} or vice versa. Thus, the mass of exhaust gas crossing the exhaust valve is calculated with 0.5 CAD

resolution using dynamic cylinder and exhaust pressures data for each subsection as following,

$$m_{exh_i}[k] = \frac{1}{12N[k]} \cdot \int_{\theta_i}^{\theta_{i+1}} \dot{m}_{exh_i}[k] \cdot dt \tag{2.6}$$

where m_{exh_i} is the mass of exhaust gas flows in each segment, and θ_i and θ_{i+1} define the beginning and end of each segment. If the exhaust gas flows back into the cylinder, $m_{exh_i} = m_{backflow_i}$ and if the exhaust gas is evacuated out of the cylinder, $m_{exh_j} = m_{evacuated_j}$. Then, the portion of the residual gas which is added during the valve overlap is estimated,

$$m_{res_{ov}}[k] = \sum_{i=1}^{n} m_{backflow_i}[k] - \sum_{j=1}^{m} m_{evacuated_j[k]} \tag{2.7}$$

The mass of total residual gas that remains inside the cylinder at IVC for combustion in the next engine cycle is the sum of the trapped and overlap parts,

$$m_{res_{tot}}[k] = m_{res_{trap}}[k] + m_{res_{ov}}[k] \tag{2.8}$$

2.3.2 Air Charge Sub-Model

The trapped fresh air mass is estimated as one of the in-cylinder total trapped mixture components at IVC. To estimate the trapped air mass at IVC, six calculation steps in different events are accomplished throughout a cycle, as shown in Figure 2.5.

Step 1: IVC to EVO

From IVC to EVO, both intake and exhaust valves are closed, and control volume, including the combustion chamber, is assumed to be a closed system neglecting the blow-by. The effect of gas composition change due to combustion is also ignored. Therefore, the in-cylinder gas temperature at EVO, T_{EVO}, is derived using ideal gas and mass conservation laws,

$$T_{EVO}\,[k] = \frac{P_{EVO}\,[k] \cdot V_{EVO}\,[k]}{R_u \cdot n_{tot}\,[k-1]} \tag{2.9}$$

where, R_u is the universal gas constant equal to 8314.5 $\frac{J}{kmole.K}$, n_{tot} is the number of moles of the total trapped mass at IVC from the previous cycle, P_{EVO} and V_{EVO} are cylinder pressure and volume at EVO, respectively.

Step 2: EVO to End of Blowdown(BWD)

Isentropic blowdown process is assumed after the exhaust valve opens, during which a rapid decrease of cylinder pressure occurs. The end of the blowdown point is considered a fixed engine position at 260 CAD, where cylinder pressure and exhaust manifold pressure come to be nearly equal. Thus, the in-cylinder gas temperature at blowdown, which is considered as in-cylinder exhaust gas temperature, T_{EXH}, is

calculated using an isentropic expansion equation,

$$T_{EXH}\left[k\right] = T_{EVO}\left[k\right]\left(\frac{P_{BWD}\left[k\right]}{P_{EVO}\left[k\right]}\right)^{\left(\frac{\gamma_{EVO}-1}{\gamma_{EVO}}\right)} \tag{2.10}$$

where, γ_{EVO} is assumed to be constantly equal to 1.29, which is the specific heat ratio of the exhaust gas at the temperature of 1200 K [11] and P_{BWD} is the cylinder pressure at the end of blowdown. The mass of in-cylinder trapped exhaust gas after the isentropic blowdown process is calculated as below,

$$m_{EXH}[k] = \frac{P_{BWD}[k] \cdot V_{BWD}[k]}{R_{exh} \cdot T_{EXH}[k]} \tag{2.11}$$

where V_{BWD} is cylinder volume at the end of blowdown.

Step 3: End of Blowdown(BWD) to IVO or EVC

The sequence of step 3 is from the end of blowdown to IVO if there is a positive overlap or from the end of blowdown to EVC if there is a negative overlap. From the end of blowdown to IVO or EVC, the control volume is an open system where cylinder pressure is almost constant. As a result, the energy balance equation is used,

$$-Q_{EXH}[k] + W_{EXH}[k] - H_{EXH}[k] = \Delta U_{EXH}[k] \tag{2.12}$$

where, Q_{EXH}, W_{EXH}, H_{EXH} are energy transfer by heat, work, and mass, respectively, and ΔU_{EXH} is internal energy change from the end of blowdown to IVO or EVC in the combustion chamber. Q_{EXH} is calculated as convective heat transfer from the in-cylinder exhaust gas to the cylinder wall, assuming cylinder wall temperature is the same as engine coolant temperature.

$$Q_{EXH}[k] = h_{EXH} A \cdot (T_{BWD}[k] - T_{coolant}[k]) \cdot \Delta t_{EXH}[k] \tag{2.13}$$

where h_{EXH} is convective heat transfer coefficient, A is the effective surface area, and T_{BWD} and $T_{coolant}$ are average in-cylinder exhaust gas temperature from the end of blowdown to IVO or EVC and engine coolant temperature, respectively. T_{BWD} is calculated as below,

$$T_{BWD}[k] = \frac{T_{EXH}[k] + T_{IVO/EVC}[k]}{2} \tag{2.14}$$

Δt_{EXH} is the time duration from the end of blowdown to IVO or EVC in seconds which is calculated using engine speed as below,

$$\Delta t_{EXH}[k] = \frac{\Delta \theta_{EXH}[k]}{6N[k]} \tag{2.15}$$

where $\Delta \theta_{EXH}$ is the duration from the end of blowdown to IVO or EVC in crank angle degrees. In Equation (12), W_{EXH} is negligible, assuming to have constant pressure from the end of blowdown to IVO or EVC. Also, H_{EXH} can be neglected because most of the in-cylinder exhaust gas is evacuated from EVO to the end of blowdown,

and in-cylinder and exhaust pressures come to nearly equal. Therefore, the mass of in-cylinder gas is assumed to be constant from the end of blowdown to IVO or EVC equal to m_{exh}. The change of internal energy can be calculated using average specific heat at constant volume of exhaust gas, $C_{p_{EXH}}$, as following,

$$\Delta U_{EXH}[k] = m_{EXH}[k] \cdot C_{v_{EXH}} \cdot \big(T_{IVO/EVC}[k] - T_{EXH}[k]\big) \tag{2.16}$$

where, $C_{v_{EXH}}$ is assumed to be constantly equal to $840\frac{J}{kg.K}$, for the temperature of 1000 K [11]. Thus, from a combination of the equations (11) to (16), the in-cylinder gas temperature at IVO or EVC is achieved,

$$T_{IVO/EVC}[k] = \frac{\left(\frac{6N[k]m_{EXH}[k]C_{v_{EXH}}}{h_{EXH}[k]A\Delta\theta_{EXH}[k]} - 0.5\right) T_{EXH}[k] + T_{coolant}[k]}{\frac{6N[k]m_{EXH}[k]C_{v_{EXH}}}{h_{EXH}[k]A\Delta\theta_{EXH}[k]} + 0.5} \tag{2.17}$$

$h_{EXH}A$ is the first calibration parameter of the model. The mass of in-cylinder trapped exhaust gas at IVO or EVC is calculated as following,

$$m_{IVO}[k] = \frac{P_{IVO}[k] \cdot V_{IVO}[k]}{R_{EXH} \cdot T_{IVO}[k]} \tag{2.18}$$

Where, P_{IVO} and V_{IVO} are cylinder pressure and volume at IVO.

$$m_{EVC}[k] = \frac{P_{EVC}[k] \cdot V_{EVC}[k]}{R_{EXH} \cdot T_{EVC}[k]} \tag{2.19}$$

Where, P_{EVC} and V_{EVC} are cylinder pressure and volume at EVC.

Step 4: IVO to EVC or EVC to IVO

In the case of positive overlap, the temperature of the in-cylinder gas at EVC is calculated using T_{IVO} from step 3 and the isentropic expansion equation,

$$T_{EVC}\,[k] = T_{IVO}[k] \cdot (\frac{P_{EVC}\,[k]}{P_{IVO}\,[k]})^{(\frac{\gamma_{IVO}-1}{\gamma_{IVO}})} \tag{2.20}$$

For negative overlap, the temperature of the in-cylinder gas at IVO is calculated using T_{EVC} from step 3 and isentropic expansion equation,

$$T_{IVO}\,[k] = T_{EVC}[k] \cdot (\frac{P_{IVO}\,[k]}{P_{EVC}\,[k]})^{(\frac{\gamma_{IVO}-1}{\gamma_{IVO}})} \tag{2.21}$$

where, γ_{IVO} is assumed 1.305, which is the specific heat ratio of the exhaust gas at 900 K[11].

Step 5: IVO or EVC to Compression Bottom Dead Center (BDC)

From IVO or EVC to compression BDC, air induction and direct fuel injection into the cylinder occur. The First Law of Thermodynamics for the combustion chamber assuming as an open system is,

$$Q_{INT}[k] - W_{INT}[k] + H_{INT}[k] = \Delta U_{INT}[k] \tag{2.22}$$

where, Q_{INT}, W_{INT}, H_{INT} are energy transfer by heat, work, and mass, respectively,

and ΔU_{INT} is internal energy change during intake stroke in the cylinder. Q_{INT} is calculated as convective heat transfer from in-cylinder mixture to the cylinder wall or vice versa, assuming cylinder wall temperature is the same as engine coolant temperature,

$$Q_{INT}[k] = h_{INT}[k]A \cdot (T_{INT}[k] - T_{coolant}[k]) \cdot \Delta t_{INT}[k] \tag{2.23}$$

where, h_{INT} is convective heat transfer coefficient and Δt_{INT} is the time duration from IVO or EVC to compression BDC which is calculated using engine speed,

$$\Delta t_{INT}[k] = \frac{\Delta \theta_{INT}[k]}{6N[k]} \tag{2.24}$$

Where, $\Delta \theta_{INT}$ is the duration between IVO or EVC to compression BDC in crank angle degrees. T_{INT} is the average in-cylinder mixture temperature at IVO or EVC and compression BDC,

$$T_{INT}[k] = \frac{T_{IVO/EVC}[k] + T_{BDC}[k]}{2} \tag{2.25}$$

where, T_{BDC} is the temperature of the in-cylinder trapped mixture at BDC compression. $h_{EXH}A$ is the second calibration parameter of the model. In equation (22), W_{INT} is the work produced by cylinder assuming cylinder pressure is constant while

cylinder volume is increasing,

$$W_{INT}[k] = \left(\frac{P_{IVO/EVC}[k] + P_{BDC}[k]}{2}\right) \cdot \left(V_{BDC}[k] - V_{IVO/EVC}[k]\right) \tag{2.26}$$

Where, P_{BDC} and V_{BDC} are cylinder pressure and volume at BDC compression, respectively. H_{INT} is the input enthalpy into the cylinder through air induction and fuel injection. Decomposing the input enthalpy of the different inducted gases and injected fuel to the internal energy and flow work,

$$\begin{aligned} H_{INT}[k] &= m_{air_{int}}[k]\left(u_{air_{int}} + p_{air_{int}} v_{air_{int}}\right) \\ &+ m_{H2O_{int}}[k]\left(u_{H2O_{int}} + p_{H2O_{int}} v_{H2O_{int}}\right) \\ &+ m_{res_{int}}[k]\left(u_{res_{int}} + p_{res_{int}} v_{res_{int}}\right) + m_{fuel}[k]\left(u_{fuel} + p_{fuel} v_{fuel}\right) \end{aligned} \tag{2.27}$$

where, $m_{air_{int}}$ and $m_{H2O_{int}}$ are the masses of inducted dry air and air water vapor into the cylinder from IVO or EVC to compression BDC. $m_{res_{int}}$ is the mass of a portion of the residual gas that flows into the intake manifold runner during valve overlap and is assumed to be completely inducted back into the cylinder during the intake stroke. m_{fuel} is the mass of injected fuel into the cylinder during the intake stroke

and calculated using the previous cycle estimated trapped air mass,

$$m_{fuel}\left[k\right] = \frac{^{m_{air}[k-1]}}{\lambda_{des}\left[k\right] \cdot AF_{stoich}} \tag{2.28}$$

where, λ_{des} is the desired lambda value, AF_{stoich} is the stoichiometric air-to-fuel ratio for E10 fuel and assumed constant and equal to 14.07 $\frac{kg(air)}{kg(fuel)}$. The liquid fuel is injected directly into the warm cylinder during intake stroke is mostly vaporized. Therefore, the change of internal energy from IVO or EVC to compression BDC is composed of two major parts, the injected fuel internal energy of vaporization and the difference of internal energy between two thermodynamic states,

$$\Delta U_{INT}[k] = U_{BDC}[k] - U_{IVO/EVC}[k] + U_{fg_{fuel}}[k] \tag{2.29}$$

where, $U_{IVO/EVC}$ and U_{BDC} are internal energy of in-cylinder contents at IVO or EVC and compression BDC, respectively. The internal energy of the in-cylinder mixture at compression BDC is estimated as below,

$$\begin{aligned} U_{BDC}\left[k\right] = m_{air_{int}}\left[k\right] \cdot u_{air_{int}} + m_{H2O_{int}}\left[k\right] \cdot u_{H2O_{int}} + m_{fuel}\left[k\right] \cdot u_{fuel} \\ + m_{res_{tot}}\left[k\right] \cdot u_{res_{tot}} \end{aligned} \tag{2.30}$$

where, $m_{res_{tot}}$ is the mass of total residual gas in the cylinder at compression BDC as input from the residual gas sub-model. Depending on having positive or negative valve overlap, exhaust gas in the cylinder at IVO or EVC is the trapped residual gas at IVO or EVC, respectively. Then, the internal energy of the in-cylinder gas at IVO or EVC is calculated,

$$U_{IVO/EVC}\,[k] = m_{IVO/EVC}[k] \cdot u_{IVO/EVC} \tag{2.31}$$

The injected fuel internal energy of vaporization, $U_{fg_{fuel}}$, is calculated assuming 90% of the total injected fuel is vaporized during the intake stroke in the engine normal operating condition,

$$U_{fg_{fuel}}[k] = 0.9 * m_{fuel}[k] \cdot u_{fg_{fuel}} \tag{2.32}$$

where, $u_{fg_{fuel}}$ is the internal energy of vaporization of the fuel on a unit mass basis assumed to be constant and equal to 349.8 $\frac{kJ}{Kg.K}$ at the average in-cylinder temperature during the intake stroke, 500 K. In equation (27), the pv fluid work of the cylinder

inlet mixture components can be combined and calculated as below,

$$p_{air_{int}} v_{air_{int}} + p_{H2O_{int}} v_{H2O_{int}} + p_{res_{int}} v_{res_{int}} = MAP[k] \cdot \big(V_{BDC}[k] - V_{IVO/EVC}[k]\big) \tag{2.33}$$

From the combination of the equations (22) to (33) and expressing the change of internal energies using temperature difference and average specific heat at constant volume,

$$\begin{aligned} Q_{INT}[k] - W_{INT}[k] + MAP[k] \cdot (V_{BDC}[k] - V_{EVC}[k]) + p_{fuel} \frac{m_{fuel}[k]}{\rho_{fuel}} - \\ U_{fg_{fuel}}[k] = \left(m_{air_{int}}[k] C_{v_{air}} + m_{H2O_{int}}[k] C_{v_{H2O}}\right) \left(T_{BDC}[k] - T_{run}[k]\right) + \\ m_{fuel}[k] C_{v_{fuel}} \left(T_{BDC}[k] - T_{fuel}[k]\right) + \\ m_{res_{tot}}[k] C_{v_{res}} \big(T_{BDC}[k] - T_{IVO/EVC}[k]\big) \end{aligned} \tag{2.34}$$

where, ρ_{fuel} is the density of the E10 fuel assumed to be constantly equal to 757.4 $\frac{kg}{m^3}$, p_{fuel} is the fuel pressure in the fuel rail, upstream of the injector, which is measured by a production pressure sensor, T_{run} is the inducted air temperature in the intake

manifold runner, which is modeled as a function of the boosted air temperature measured by a production sensor before throttle, $T_{air_{inlet}}$,

$$T_{run}[k] = T_{air_{inlet}}[k] + \Delta T \tag{2.35}$$

T_{fuel} is the fuel temperature in the fuel rail, which is assumed to be constant and equal to 323K, $C_{v_{air}}$, $C_{v_{fuel}}$, $C_{v_{H2O}}$ and $C_{v_{res}}$ are the average specific heat at constant volume of dry air, fuel, air water vapor and residual gas, respectively. No condensation or water injection occurs to the air from the ambient to the cylinder. Thus, air water vapor mass inside the cylinder at compression BDC, $m_{H2O_{int}}$, is achieved using ideal gas law and T_{BDC},

$$m_{H2O_{int}}[k] = \frac{(RH[k] \cdot P_{sat}[k]) \cdot V_{BDC}[k]}{R_{H2O} \cdot T_{BDC}[k]} \tag{2.36}$$

where, RH is ambient relative humidity, $P_{sat}[k]$ is air vapor saturated pressure at the ambient temperature, and R_{H2O} is the air water vapor gas constant, assuming a constant equal to 461.5 $\frac{J}{kgK}$ [11]. The trapped dry air at compression BDC is calculated as below,

$$m_{air_{int}}[k] = \left(n_{tot_{BDC}}[k] - \frac{m_{H2O_{int}}[k]}{M_{H2O}} - \frac{m_{res_{tot}}[k]}{M_{res}} - \frac{m_{fuel}[k]}{M_{fuel}} \right) \cdot M_{air} \tag{2.37}$$

where, M_{H2O}, M_{res}, M_{fuel} and M_{air} are molar masses of the air water vapor, residual gas, fuel and dry air are assumed constantly equal to be 18.02, 30.5, 100.1 and 28.97 $\frac{kg}{kmol}$, respectively. $n_{tot_{BDC}}$ is the number of moles of the total trapped mixture at compression BDC,

$$n_{tot_{BDC}}[k] = \frac{P_{BDC}[k] \cdot V_{BDC}[k]}{R_u \cdot T_{BDC}[k]} \tag{2.38}$$

From the combination of equations (34) to (38), a second-degree equation as a function of T_{BDC} is derived. Solving this equation, the temperature of the total trapped mixture at compression BDC is estimated.

Step 6: Compression BDC to IVC

In-cylinder mixture temperature at IVC, T_{IVC}, is estimated using the polytropic equation,

$$T_{IVC}[k] = T_{BDC}[k] \cdot \left(\frac{P_{IVC}[k]}{P_{BDC}[k]} \right)^{\left(\frac{n_{poly}[k]-1}{n_{poly}[k]} \right)} \tag{2.39}$$

where, P_{IVC} is in-cylinder pressure at IVC, and n_{poly} is the polytropic index in the compression stroke. The polytropic index is calculated between -60 to -120 CAD after IVC. Then, using T_{IVC} and ideal gas law, the number of moles of the total trapped mass at IVC, n_{tot}, is calculated,

$$n_{tot}[k] = \frac{P_{IVC}[k] \cdot V_{IVC}[k]}{R_u \cdot T_{IVC}[k]} \tag{2.40}$$

Where, V_{IVC} is the in-cylinder volume at IVC. In-cylinder trapped mass at IVC is

a composition of the fresh air, including air and water vapor, fuel, and residual gas. Air water vapor is calculated again at IVC using T_{IVC} and V_{IVC} in the equation (36). The mass of in-cylinder trapped dry air, m_{air}, is estimated as below,

$$m_{air}[k] = \left(n_{tot}[k] - \frac{m_{H2O}[k]}{M_{H2O}} - \frac{m_{res_{tot}}[k]}{M_{res}} - \frac{m_{fuel}[k]}{M_{fuel}} \right) \cdot M_{air} \tag{2.41}$$

2.3.3 Nonlinear Control-Oriented MIMO In-Cylinder Air Charge, Residual Gas and Temperature Model

A combination of the equations in Residual Gas and Air Charge sub-models creates a control-oriented nonlinear discrete MIMO state-space model,

$$\begin{aligned} x[k+1] &= f\left(x[k], u[k], d[k]\right) \\ y[k] &= h\left(x[k], u[k], d[k]\right) \end{aligned} \tag{2.42}$$

where, x[k] is model state, u[k] is intermediate control input, d[k] is disturbance input, and y[k] is the output vectors.

$$x[k] = \begin{bmatrix} T_{EXH}[k] \\ m_{air}[k] \end{bmatrix} \quad , \quad u[k] = \begin{bmatrix} N[k] \\ p_{cyl}[k] \\ \theta_{int_{adv}}[k] \\ \theta_{exh_{ret}}[k] \\ p_{exh}[k] \\ MAP[k] \\ T_{run}[k] \\ T_{coolant}[k] \\ \lambda_{des}[k] \\ T_{fuel}[k] \\ p_{fuel}[k] \end{bmatrix} \quad , \quad d[k] = \begin{bmatrix} RH[k] \\ T_{amb}[k] \end{bmatrix} \quad , \quad y[k] = \begin{bmatrix} T_{IVC}[k] \\ m_{air}[k] \\ m_{res}[k] \\ T_{EXH}[k] \end{bmatrix} \tag{2.43}$$

where, $\Theta_{int_{adv}}$, $\Theta_{exh_{ret}}$ are the intake and exhaust valves timing, respectively, and are used with cylinder pressure trace to produce cylinder pressure and volume in different events during an entire cycle. The ambient air relative humidity and temperature are considered as disturbances in the d vector. The state-space realization includes two states, T_{EXH} and m_{air}, which are presented as nonlinear functions of states and inputs. The inputs included in u_k are, in fact, intermediate control variables. Intermediate control variables can be described as functions of independent control

inputs, including throttle position, valve timing, injected fuel amount, and timing. The outputs of the model all can be demonstrated as nonlinear functions of the states and inputs as well,

$$\begin{aligned} T_{EXH}[k+1] &= f_1\left(T_{EXH}[k], m_{air}[k], u[k], d[k]\right) \\ m_{air}[k+1] &= f_2\left(T_{EXH}[k], m_{air}[k], u[k], d[k]\right) \\ T_{IVC}[k] &= f_3\left(T_{EXH}[k], m_{air}[k], u[k], d[k]\right) \\ m_{res}[k] &= f_4\left(T_{EXH}[k], u[k], d[k]\right) \end{aligned} \tag{2.44}$$

2.4 Model Calibration and Validation

The model described in section 4 includes two key calibration parameters, $h_{EXH}A$ and $h_{INT}A$, the convective heat transfer coefficients during exhaust and intake strokes multiplied by the effective surface area. The calibration parameters were implemented in the form of look-up tables. The selection of appropriate inputs and breakpoints of the inputs for the look-up tables were made using experimental data for a wide range of the engine normal part-load operating conditions. The two-level full-factorial Design of Experiments (DOE) method was used to determine the test plan for the

experimental data. DOE techniques help determine concurrently the individual and interactive effects of all factors that can influence the outputs of the developed model. Using DOE, a complete insight of interaction between design elements is achieved, facilitating a robust design. Using the DOE method, sensitive areas in the model that could cause problems are recognized and resolved.

The factors affecting the designed model outputs are engine speed and load (IMEP), intake and exhaust valve timing, combustion phasing (CA50), and Lambda. Table 2.3 represents the two-level DOE test plan, including low and high levels of all defined factors covering the experimental engine part-load operating conditions. The DOE test plan comprises 64 tests in total. During the DOE tests, every factor was tested on the experimental engine at its low and high levels while all other factors were fixed. Between every two DOE tests, the engine was run until the inlet air and exhaust gas temperatures were stabilized at the new test point.

A set of data was recorded for every test point as soon as all engine parameters, especially inlet air temperature, were steady. The DOE test points, including simultaneous intake valve advance and exhaust valve retard, -30 and 30 CAD respectively,

Table 2.3
DOE test plan for the designed model calibration

Factors	Engine Speed (RPM)		IMEP (kPa)		Intake Advance (°CA)		Exhaust Retard (°CA)		CA50 (°CA)		Lambda	
Levels	Low	High	Low	High	Low	High	Low	High	Low	High	Low	High
Value	1500	3500	250	750	-30	0	0	30	8	18	0.9	1
Points	2		2		2		2		2		2	

caused very high overlap, 60 CAD. Very high overlap led to unstable engine operation and high COV of IMEP. Therefore, the DOE test points comprising very high overlap were replaced with -20 and 10 CAD intake advance and exhaust retard, respectively. As a result, all DOE test points included a similar overlap duration equal to 27 CAD considering -3 CAD of overlap with cams at pinned positions in which the engine was operating stably.

Crank angle-resolved experimental data including engine position, speed, MAP, cylinder and exhaust pressures, and cycle-averaged data comprising valve timing, inlet air and exhaust gas temperatures, Lambda, ambient temperature, and humidity, as well as air and fuel mass meters data, were recorded for each test. This data was used to define the values of the calibration parameters for each engine DOE test point.

Direct measurement of residual fraction in the cylinder for calibration and validation of the designed model is possible [27]. However, residual fraction measurement is complex and has several limitations and associated uncertainties and errors. For instance, charge non-uniformity and cycle-to-cycle fluctuations result in variation of the measured hydrocarbon concentration and subsequent error on residual fraction measurement [41]. A well-accepted approach to residual fraction determination is the GT-Power TPA method [42]. The GT-Power TPA method analyzes the steady-state experimental data to determine the quantities such as residual gas fraction and cylinder temperature, which are difficult to measure directly. As a result, the calibration

of the designed model comprises two major steps. The first step is determining the residual fraction and cylinder temperature validation values using the GT-Power TPA model. The second step is to calibrate the designed model using the air and fuel mass meter data and GT-Power TPA model validation values, including the trapped air and residual masses and in-cylinder gas temperature at IVC and the end of blowdown.

2.4.1 GT-Power TPA-based Validation

The GT-Power TPA mode offers a simulation-based method to analyze steady-state experimental data to determine the quantities such as residual gas fraction and cylinder temperature, which are arduous to be measured directly. For this purpose, a single-cylinder GT-Power model of the experimental engine was built. The model was parameterized using the experimental engine geometry specification, including the combustion chamber and components at the cylinder inlet and outlet. In addition, the experimental engine valve profiles shown in Figure 2.6 and Coefficient of Discharge (CD) characteristic curves represented in Figure 2.7 (a) and (b) were set in the model. Furthermore, the injectors and fuel specifications were also adjusted in the GT-Power model based on experimental engine data.

For each steady-state DOE test point, the GT-Power model was fed by the 300 cycle-averaged intake manifold, in-cylinder, and exhaust pressure traces, as well as engine

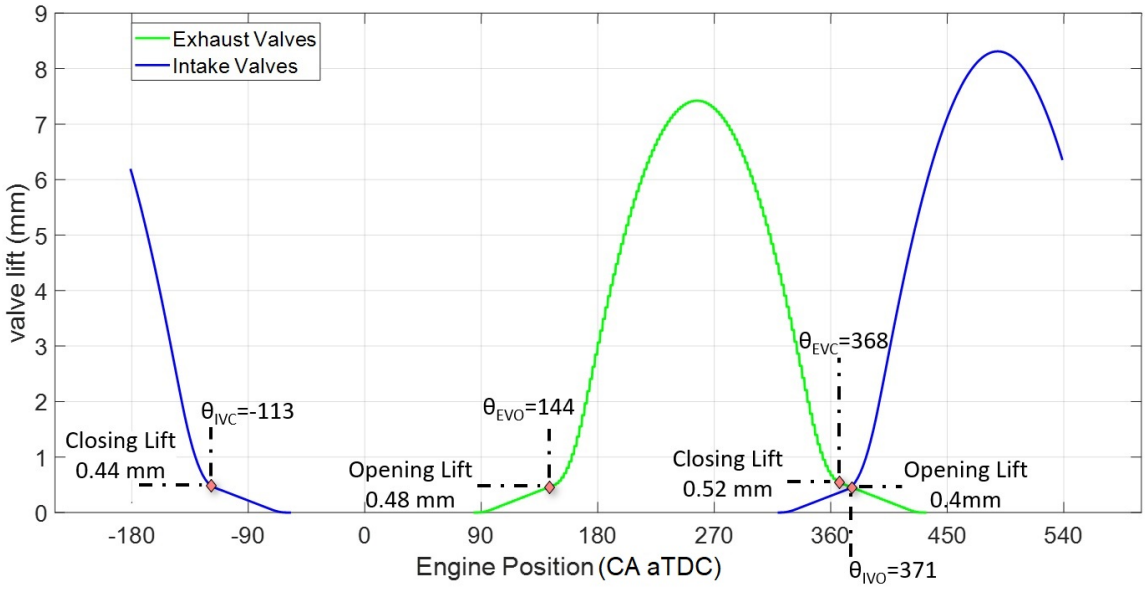

Figure 2.6: The experimental engine valves profile

speed, intake and exhaust valves timings, Lambda, inlet air, exhaust and ambient temperatures, and relative humidity. Then, the Overall Convection Multiplier of the engine cylinder heat transfer was fine-tuned such that the GT-Power simulated cylinder pressure trace coincided with the experimental data throughout the cycle at the different strokes and peak pressure with less than 1% error. Figure 2.8 shows how measured experimental and GT-Power simulated cylinder pressure traces match one another for one of the DOE test points.

The simulated values of IMEP and trapped air mass at IVC matched with the experimental data from CAS and mass flow meter with a relative error less than 2%. The identical procedure was accomplished for all DOE test points using the GT-power model to derive residual fraction, cylinder mixture temperature at IVC, and

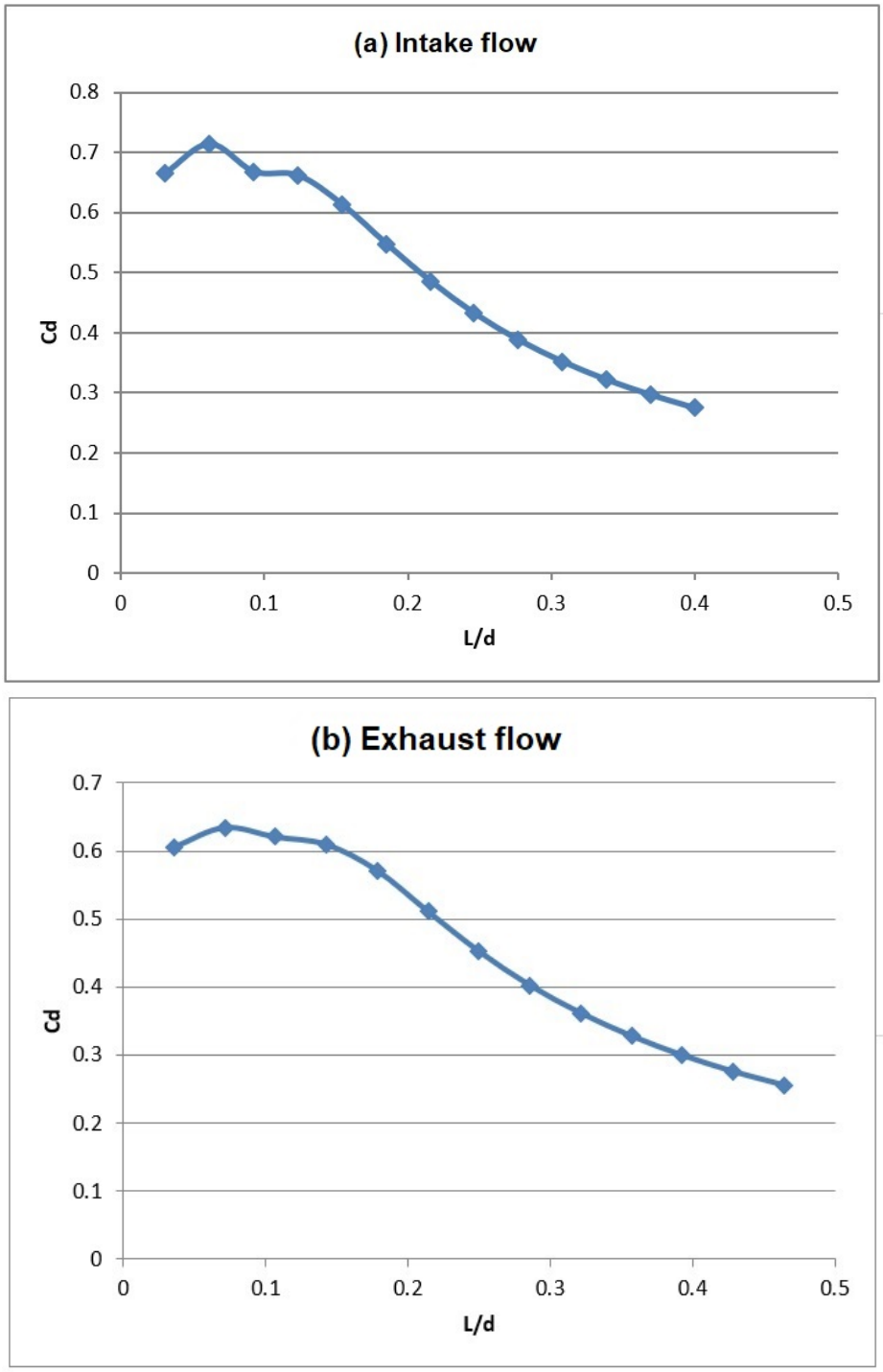

Figure 2.7: Experimental engine valves Coefficient of Discharge characteristic curves

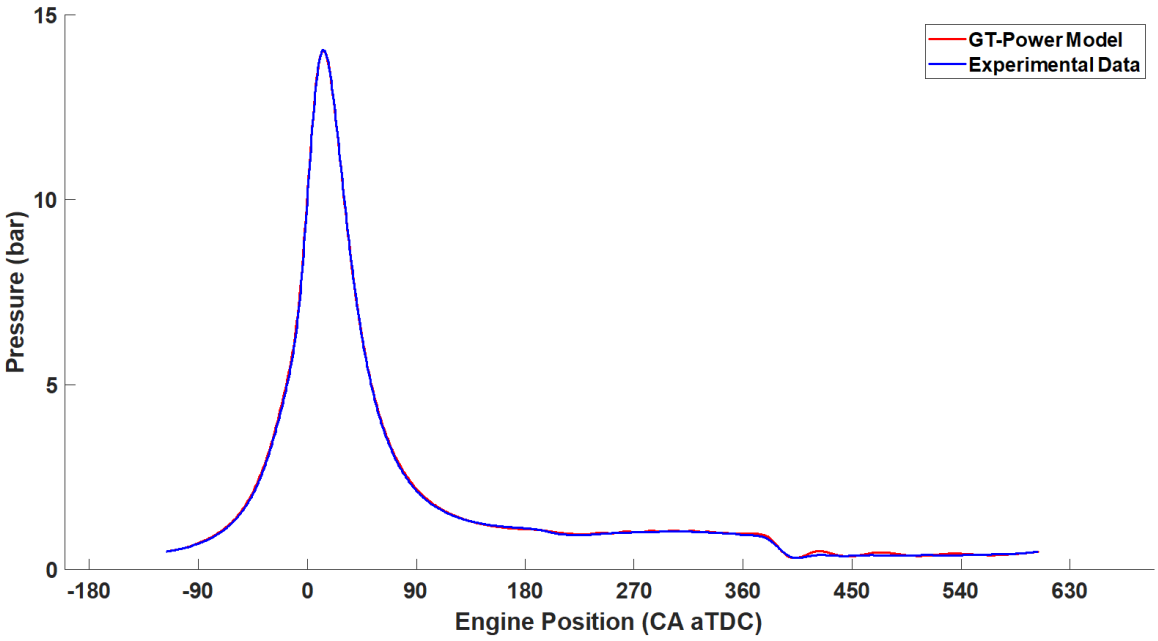

Figure 2.8: Experimental and GT-Power simulated cylinder pressure traces for the DOE test point (N=1500RPM, IMEP=250kPa, Intake Advance=0 °CA, Exhaust Retard=30 °CA, CA50=8 CA aTDC and Lambda=1)

average exhaust gas temperature during the exhaust stroke. Figure 2.9 depicts the simulated in-cylinder temperature profile, including in-cylinder gas temperature at different events, as well as trapped air mass and residual fraction from the GT-Power model for one of the DOE test points.

The estimated parameters from the GT-power model and the related DOE factors were analyzed using Minitab to define the most prevailing factors. As a result, the lowest possible calibration efforts with acceptable precision for the developed model were identified. The Pareto charts that assist in visualizing all factors' main and interaction effects to the estimated parameters are shown in Figures 2.10, 2.11, and 2.12 for significance level, α, of 0.05. The red vertical dash lines are the reference

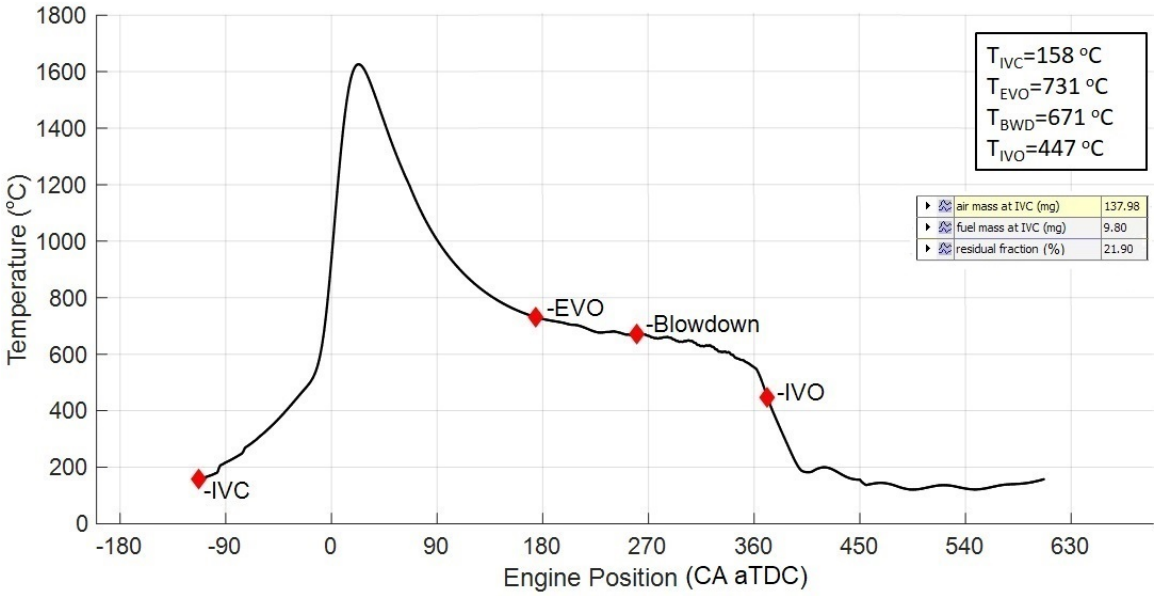

Figure 2.9: GT-Power simulated results including in-cylinder gas temperature, trapped air, fuel and residual gas masses at IVC for the similar DOE test point in Fig. 9

lines for statistical significance depends on the significance level. Bars that cross the reference line are statistically significant. For instance, in figure 2.10 for trapped air mass, the bars representing factors B, A, and AB cross the reference line at 4.5. These factors are statistically significant at the 0.05 level with the model terms. To summarize, Pareto charts show the IMEP and engine speed are dominant factors for trapped air mass at IVC, and IMEP, valves timing, and engine speed have the most contribution to the residual fraction and temperature at IVC. Therefore, the IMEP, engine speed, and valves timing were selected as inputs for the calibration look-up tables of the designed model, including two low and high levels for each, resulting in 16 calibration points in total.

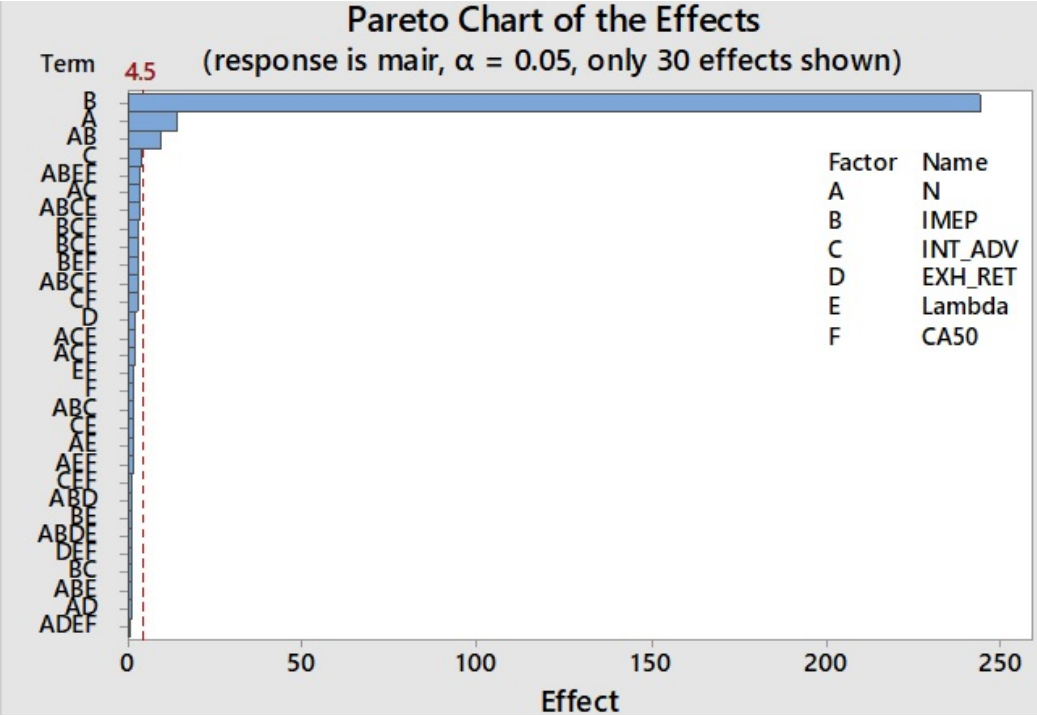

Figure 2.10: Pareto charts of the model outputs for air mass

2.4.2 MIMO Model Calibration

The developed model was parameterized with the engine specifications, including valve profile and Coefficient of Discharge used for the GT-Power model, and was fed with similar inputs. Then, the simulated results from the GT-Power model for residual fraction, in-cylinder mixture temperature at IVC, and the average exhaust gas temperature during the exhaust stroke, as shown in figure 2.9, were used for calibration and validation of the developed model.

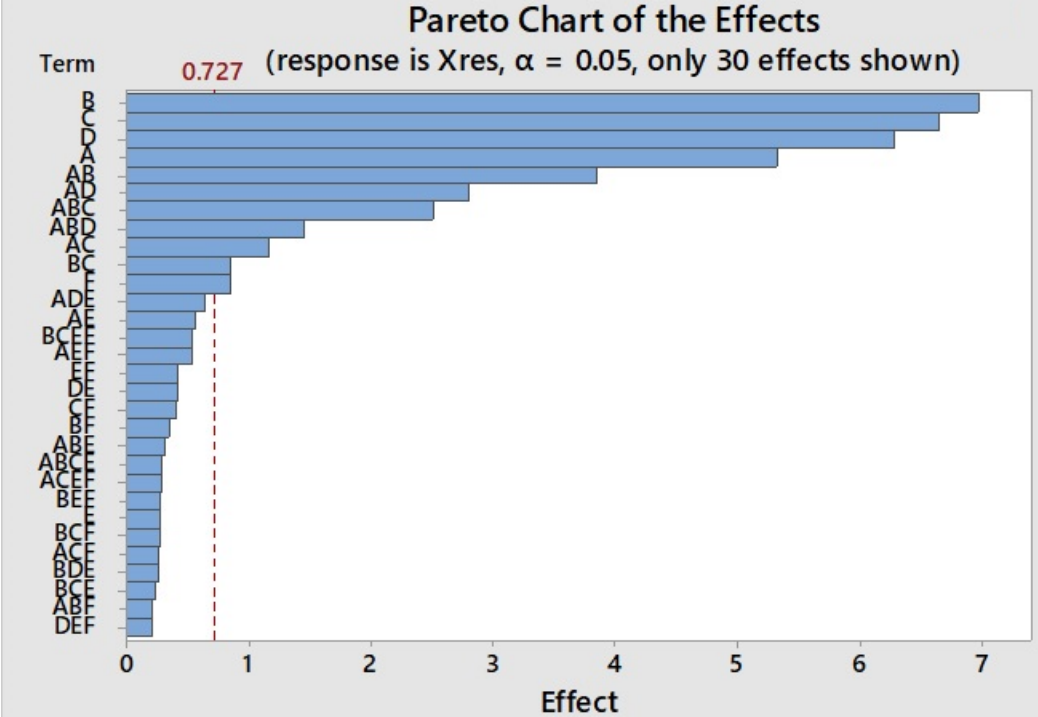

Figure 2.11: Pareto charts of the model outputs for residual fraction

As discussed above, the designed model includes two calibration parameters, convective heat transfer coefficients of heat transfer multiplied by effective area, $h_{INT}A$ and $h_{EXH}A$, in the exhaust and intake strokes. The calibration parameter, $h_{EXH}A$, primarily affects the mass of the trapped residual gas at IVO, and average cylinder exhaust gas temperature, whereas $h_{INT}A$ has the prevailing effect on the trapped air mass and cylinder mixture temperature at IVC. However, $h_{INT}A$ and $h_{EXH}A$ have an interactive effect on intermediate variables and outputs of the model. Therefore, a step-by-step calibration procedure was derived for calibration of the model as follows,

1. It is assumed the heat transfer during the exhaust stroke is negligible, and in-cylinder gas temperature is constant from the end of blowdown to IVO or EVC

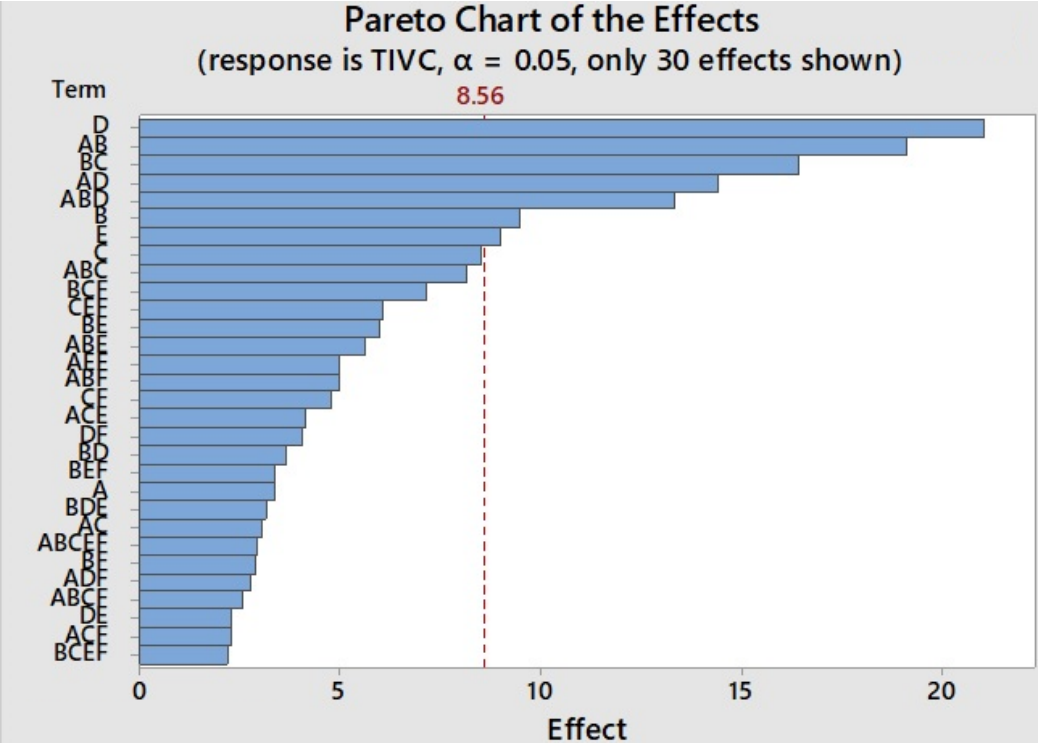

Figure 2.12: Pareto charts of the model outputs for temperature at IVC

($h_{EXH}A = 0$).

2. $h_{int}A$ is calibrated to have the model estimated air mass equal to the steady-state experimental data from the air mass meter.

3. $h_{exh}A$ is calibrated to increase the heat transfer during the exhaust stroke. As a result, the exhaust gas temperature decreases, and the mass of trapped residual gas increases. $h_{exh}A$ is calibrated to have the estimated residual fraction and exhaust gas temperature from the developed model equal to the simulated values from the GT-Power model with a defined acceptance margin.

4. $h_{int}A$ is fine-tuned concurrently with $h_{exh}A$ change to preserve the estimated

air mass equal to the experimental data.

Figure 2.13 represents the step-by-step calibration procedure flowchart. This calibration procedure was used to define the calibration parameters, $h_{INT}A$ and $h_{EXH}A$, for the 16 points from the DOE.

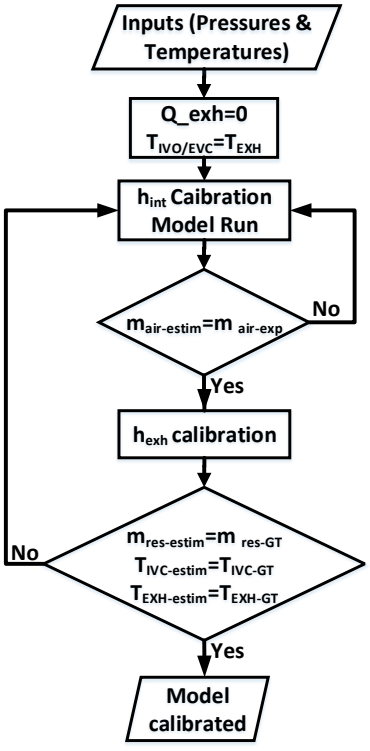

Figure 2.13: Developed model calibration procedure

2.4.3 MIMO Model Steady-State Validation

Having $h_{INT}A$ and $h_{EXH}A$ calibration parameters for different engine speeds and loads and valve timings, the heat transfers during intake and exhaust strokes were calculated, and their trends were examined and compared to expectations. Figures 2.14 and 2.15 represent the heat transfers during intake and exhaust strokes in different engine speeds and IMEPs, respectively, as well as various valve timings. Figure 2.14 shows the heat transfers during the intake, and exhaust strokes decrease while the engine speed increases at the same load, as their duration reduces. In addition, engine volumetric efficiency decreases and results in in-cylinder total trapped mass and enthalpy decrease. Here, the experimental data from the air mass meter also demonstrates total engine air consumption decrease when engine speed increases, verifying the volumetric efficiency reduction. Figure 2.15 highlights the increase in heat transfer for both intake and exhaust strokes resulting from in-cylinder trapped mass and enthalpy increase while engine load increases at constant engine speed.

On the other hand, valve overlap via exhaust valve retard leads to increased heat transfer for the intake and exhaust strokes. An increase in intake stroke heat transfer growth ensues from increasing residual fraction and in-cylinder trapped mixture temperature. In addition, the EVO retard leads to more expansion, a shorter blowdown phase, and less exhaust gas scavenging out of the cylinder. As a result, the

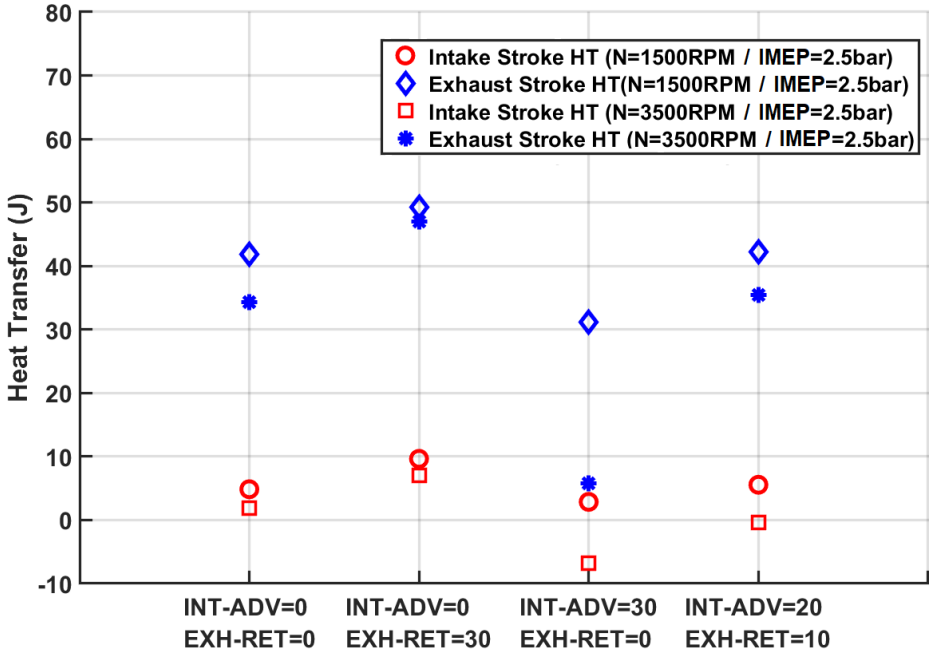

Figure 2.14: Heat transfers during intake and exhaust strokes at constant engine load

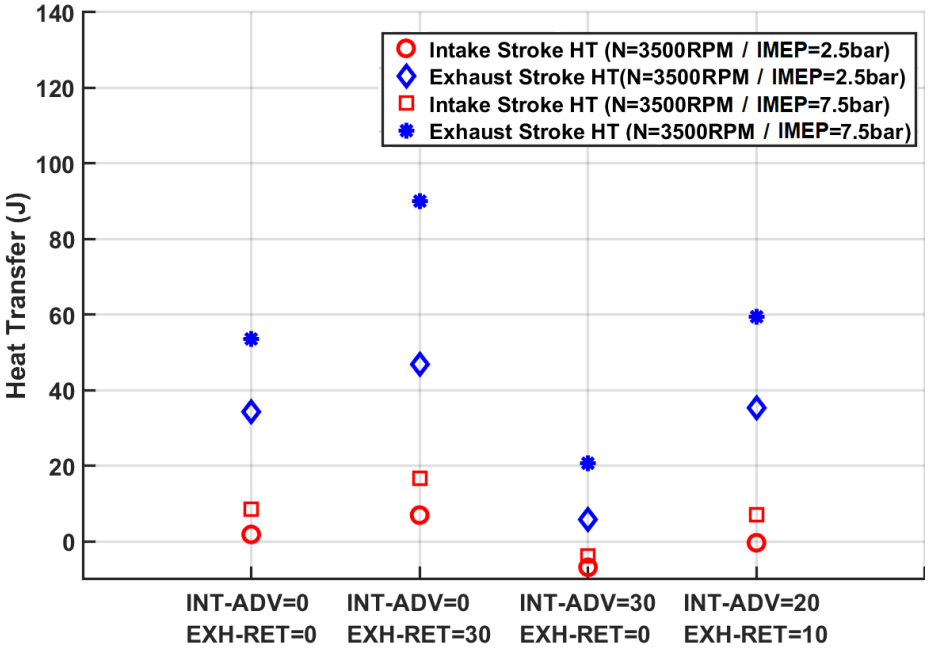

Figure 2.15: Heat transfers during intake and exhaust strokes at constant engine speed

enthalpy of the in-cylinder exhaust gas flow and heat transfer during exhaust stroke increases. Additionally, as the in-cylinder gas temperature at each event, shown in Figure 2.5 P-V diagram, depends on the temperature from prior events, increasing or decreasing the trapped mixture temperature, T_{IVC}, causes respectively, the decrease or increase of the subsequent in-cylinder exhaust gas temperature, T_{EXH}, and heat transfer during exhaust stroke as well.

Contrary to the exhaust valve retard, increased valve overlap via intake valve advance causes the intake and exhaust stroke heat transfer to decrease. Intake valve advance leads to opening the valves before TDC-Intake during the exhaust stroke while the piston is going up and intake manifold pressure is considerably lower than in-cylinder pressure. As a result, a higher amount of exhaust gases flow back into the intake manifold runner compared to the exhaust retard condition. Consequently, the residual gas is cooled down inside the intake manifold runner before it is sucked back into the cylinder during the intake stroke, resulting in the in-cylinder mixture temperature and heat transfer decrease during the intake stroke.

The trapped air mass estimated by the GT-Power model and designed model, as well as the experimental data from the LFE air mass meter, are presented in Figure 2.16. The calibrated GT-Power model and MIMO model estimate trapped air mass with less than 1.8% relative error compared to the measured LFE air mass meter experimental data. Figures 2.17 and 2.18 show the estimated residual fraction and

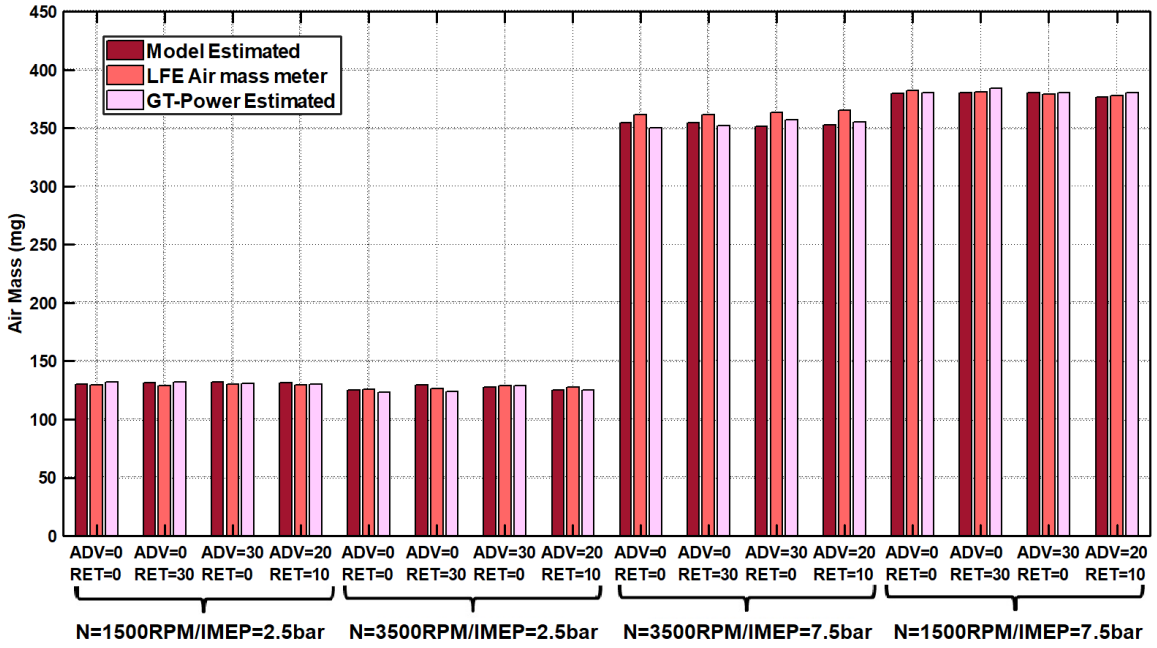

Figure 2.16: Comparison of GT-Power TPA and developed model results for in-cylinder trapped air mass

in-cylinder mixture temperature at IVC from the calibrated GT-Power and designed models. The MIMO model estimates the residual fraction and T_{IVC} within 2.1% and 1.8% in comparison to the GT-Power model results, respectively. The average of the relative error for 16 DOE test points for air mass, residual fraction, and T_{IVC} is 1.5%.

Estimated residual fraction and in-cylinder mixture temperature at IVC from the calibrated and validated designed model based on the GT-Power model simulated results and LFE air mass meter experimental data are represented for 16 DOE test points in Figures 2.19 and 2.20. The residual fraction depends significantly on engine load (IMEP), valve overlap, and engine speed, as is expected. Reduction of IMEP and engine speed and increasing valve overlap cause residual fraction to rise as expected. Figure 2.20 shows the in-cylinder mixture temperature decreases when the engine

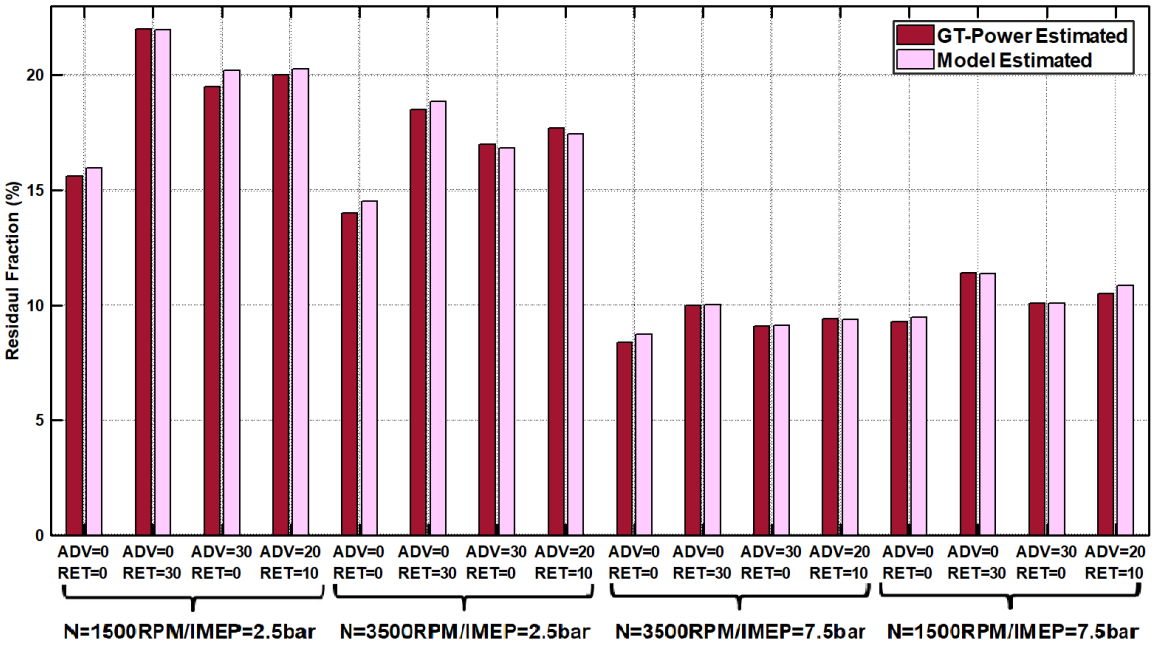

Figure 2.17: Comparison of GT-Power TPA and developed model results for Residual fraction

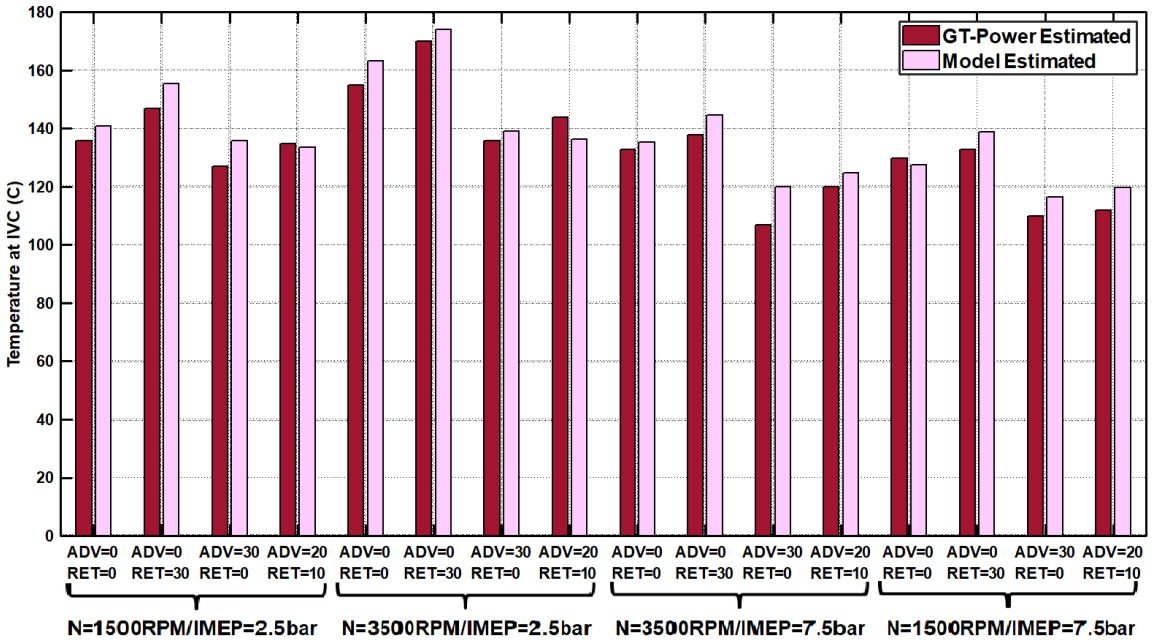

Figure 2.18: Comparison of GT-Power TPA and developed model results for in-cylinder gas temperature at IVC

load increases caused by a significant increase in the mass of trapped fresh air charge in the cylinder relative to residual gas. In addition, when engine speed increases, the duration of the intake stroke decreases, and heat transfer from the in-cylinder mixture to the cylinder wall reduces. Consequently, the in-cylinder mixture temperature at IVC increases while engine speed rises. Also, higher valve overlap at the same engine speed and load results in a higher residual fraction and higher in-cylinder mixture temperature. In Figure 2.20, intake valve advance leads to earlier intake valve open and lower cylinder pressure, resulting in a lower in-cylinder mixture temperature at IVC.

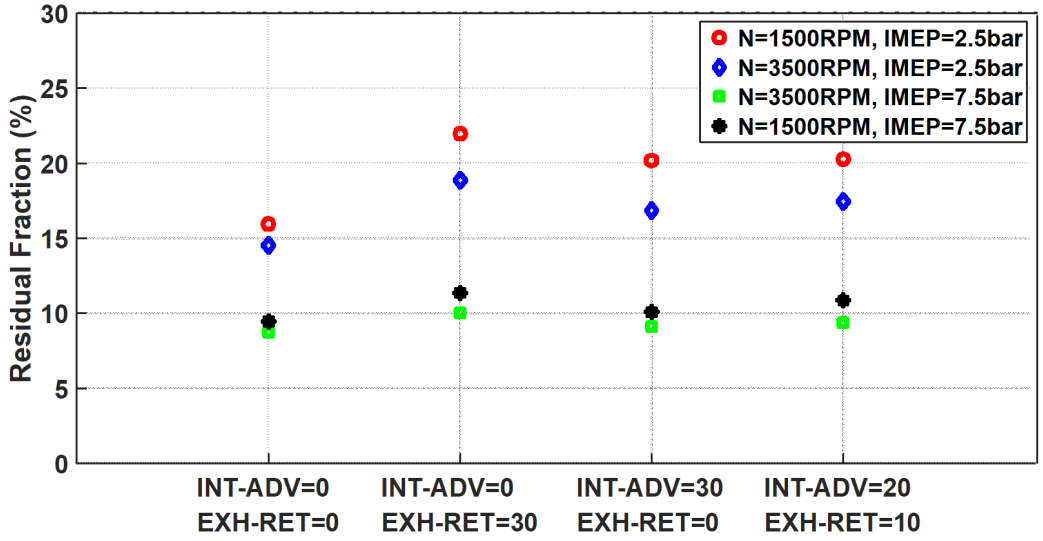

Figure 2.19: Designed model results for Residual fraction

Calibration parameters, $h_{int}A$ and $h_{exh}A$, for 16 selected DOE test points, including low and high engine speed, IMEP, and valve timing, were inserted in two 4-dimensional look-up tables using linear interpolation. The look-up tables were utilized to generate the parameters while the MIMO model was run in a transient cycle to validate the model's dynamic behavior.

2.4.4 MIMO Model Dynamic Behavior Validation

The in-cylinder air charge, residual gas, and temperature model were run and validated first offline as a Matlab code using transient experimental data. Then, the model was implemented on the CPDC rapid-prototyping ECU in Simulink/Stateflow and was run and validated in real-time in parallel to the engine production ECU via

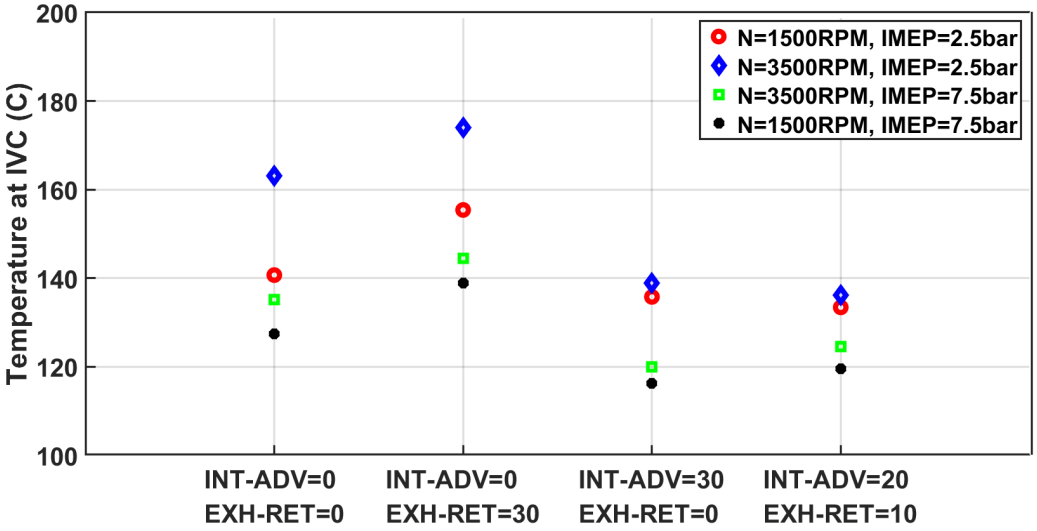

Figure 2.20: Designed model results for in-cylinder mixture temperature at IVC

CAN communication as shown in Figure 3 on the engine dynamometer.

2.4.4.1 Offline Dynamic Validation

The in-cylinder air charge, residual gas, and temperature model calibrated using GT-Power TPA results was implemented as a Matlab code and validated first in offline conditions. The model Matlab code is included in Appendix A. Then, a randomly generated transient vehicle driving cycle was applied as a reference to analyze and verify the MIMO model dynamic behavior. The driving cycle captured various tip-in/tip-out events over varied speed/load conditions. The dynamometer controller was programmed with the relevant speed/torque profile to simulate the transient driving cycle. The dynamometer reproduced the transient behavior of the engine from the test vehicle by adjusting the dyno speed, torque, and pedal position. Bosch PCM controlled the engine, and all data from production sensors and test bench instrumentation sensors were recorded throughout 1250 cycles of the dynamic cycle. The acceleration and deceleration rate of speed and torque applied by the dynamometer for the simulated driving cycle are shown in Table 2.4[43]. The scatter plot in Figure 2.21 depicts the engine operating conditions covered during the 1250 cycle test. Red dots represent the engine speed/load operating points used for offline validation of the model[44]. The blue dots show the 16 calibration points selected based on DOE analysis[45].

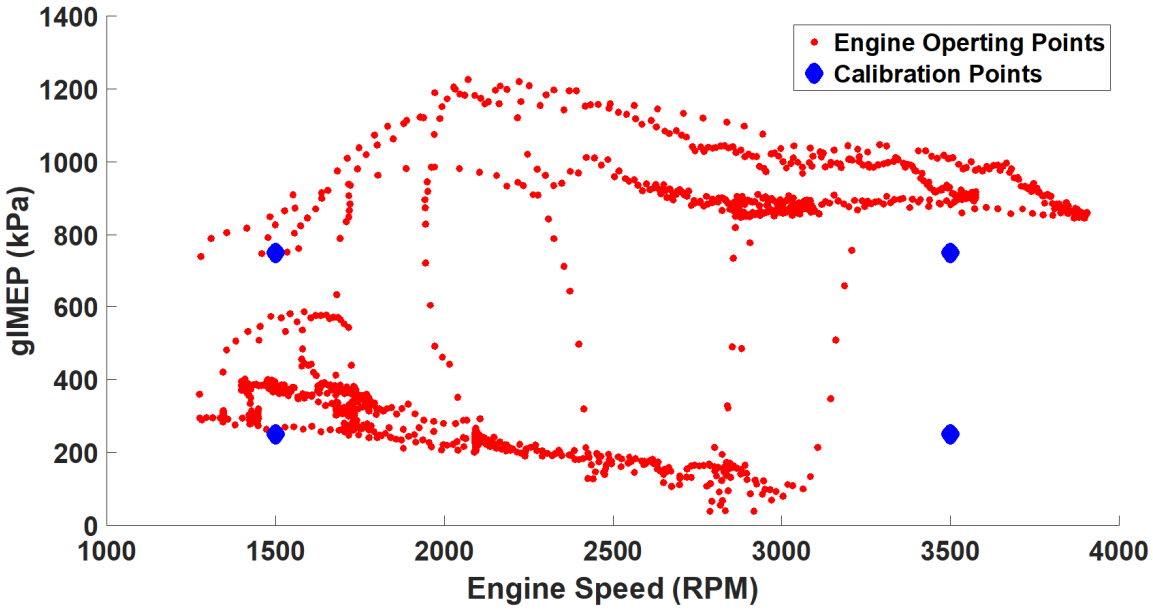

Figure 2.21: Engine operating condition scattering during transient cycle

Air and fuel mass meters are located at a distance from the engine and are not appropriate to be used as references for validation of the model estimated trapped air during transitions. Thus, the air mass in the exhaust gas is calculated using the experimental data measured by the exhaust gas oxygen (UEGO) sensor. Then, the gas transport delay from the engine cylinder to the UEGO sensor is estimated. For this purpose, the measured injection pulse width and fuel rail pressure with the injector fuel delivery calibrations were used to calculate the flow rate of the injected

Maximum speed		Maximum load	
acceleration (rpm/sec)	deceleration (rpm/sec)	acceleration (bar/sec)	deceleration (bar/sec)
1370	-1150	33	-63

Table 2.4
Transient test acceleration and deceleration specification

fuel mass, $\dot{m}_{f_{inj}}$. The test engine injector's fuel delivery characteristic curves in mg per injection based on injection pulse width in msec and fuel rail pressure in psi have been shown in Figure 2.22.

As the representative of the gas transport transient behavior, fuel transport dynamics from when it is injected directly into the cylinder to when an experimental lambda sensor measures its effect is modeled for a wide range of engine speed and load as following,

$$\frac{\dot{m}_{f_{UEGO}}(s)}{\dot{m}_{f_{inj}}(s)} = \frac{1}{1+\tau_{UEGO}s} \cdot e^{-s\Delta T} \tag{2.45}$$

Where, $\dot{m}_{f_{UEGO}}$ is the flow rate of the fuel mass measured by the UEGO sensor,

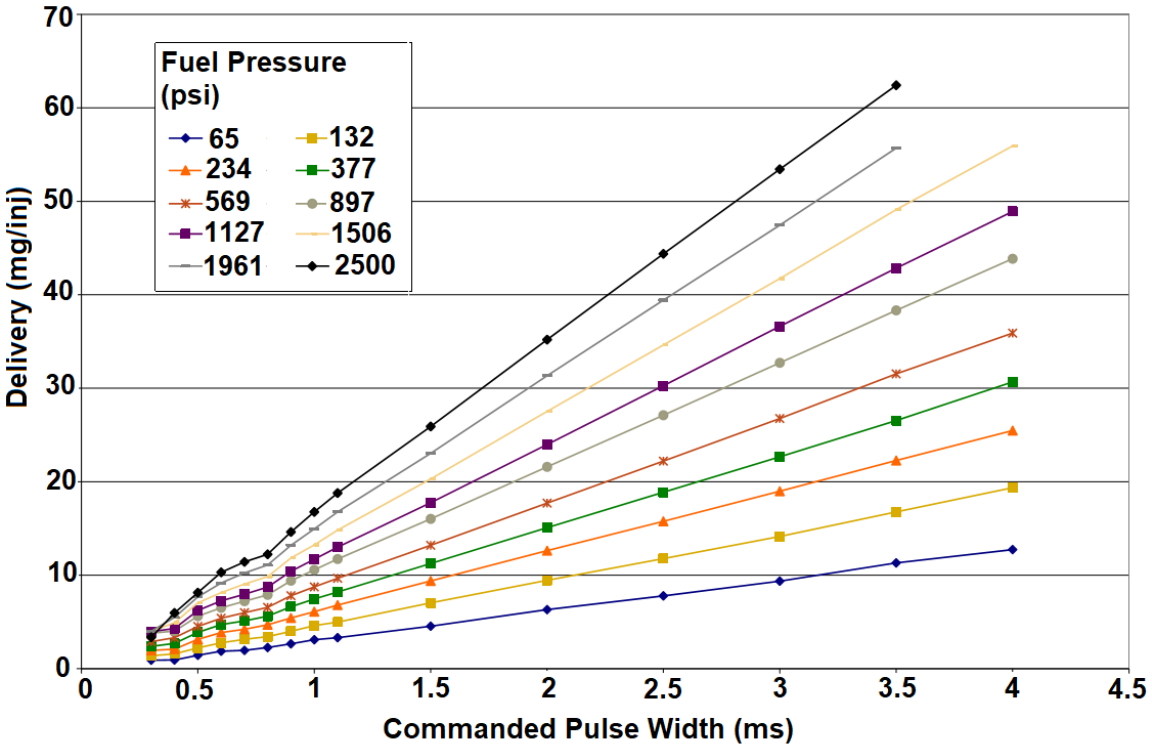

Figure 2.22: Injector fuel delivery characteristic curves

$_{UEGO}$ is the time constant of the sensor from its specification sheet and ΔT is the period between the moment of fuel injection into the cylinder and the moment of AFR measurement by the UEGO sensor. ΔT was measured in different engine speeds and loads by commanding lambda value to be changed from stoichiometric condition to both rich and lean conditions[46]. The transport-delay compensated lambda value resulting from the fuel transport dynamics model is used to produce the experimental reference dynamic air charge as followed

$$m_{air_{ref}} = \lambda_{UEGO} \cdot AF_{stoich} \cdot m_{f_{UEGO}} \tag{2.46}$$

Figure 2.23 depicts the inputs and outputs of the designed discrete cycle-based in-cylinder air charge, residual gas, and temperature model during the dynamic cycle. The spark timing, controlled by the production PCM to the optimum value throughout the transient cycle, is also shown in figure 2.23. After any acceleration or deceleration, the model output for air charge settled in a new steady-state level with less than 2% error. However, a 2% steady-state error results from the 16 point calibration for the entire range of the engine part-load operating condition[45]. Other vital outputs comprising the mass of trapped and overlap backflow residual gas and in-cylinder gas temperatures at IVC and after blowdown are also depicted in Figure 2.23. Dynamic behavior of the in-cylinder trapped mixture temperature at IVC during transitions is interesting as it is an essential input for combustion phasing estimation[43]. Similarly, in-cylinder exhaust gas temperature at the end of the blowdown should have proper

dynamic behavior as it is propagated to the engine-out exhaust gas temperature estimation that is used in the catalyst warm-up model[45].

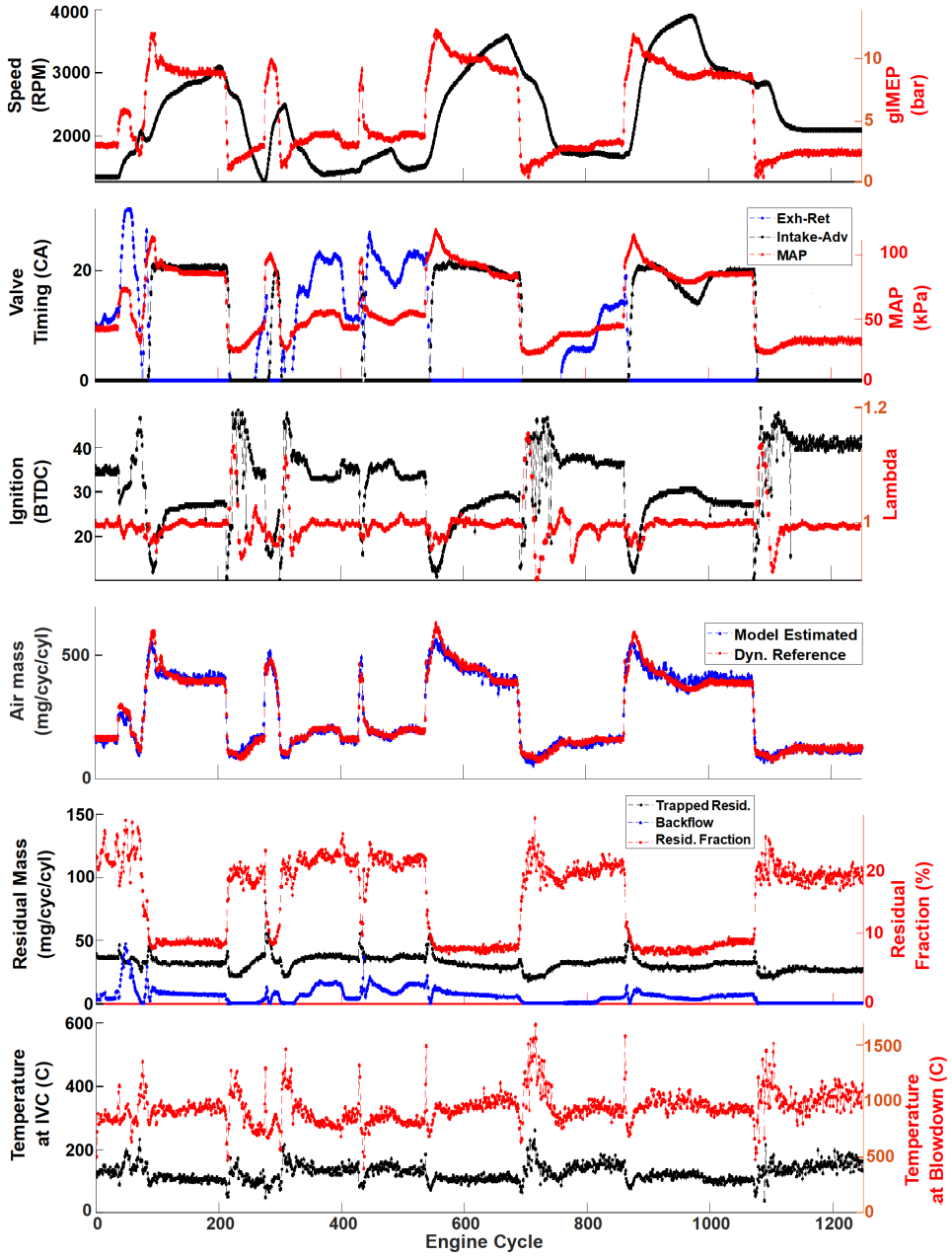

Figure 2.23: The offline MIMO model validated outputs in a transient driving cycle

To scrutinize the MIMO model dynamic behavior during transitions, one of the tip-in and tip-out transitions shown in Figure 2.24 is zoomed in and analyzed in detail. Figure 2.24 shows a tip-in between cycles 70 and 90 in which about 900 and 80 kPa increase in the IMEP and MAP occurs, respectively. In addition, the exhaust valve timing experiences 27 CAD retard from the parking position and settles back to the parking position again at the end of the transition. The intake valve remains in the parking position until cycle 86 and then advances for 12 CAD. As it is seen in Figure 2.24, the model estimated trapped air charge at IVC increases from 100 mg to 530 mg following the experimental reference dynamic air charge cycle-by-cycle without delay. Furthermore, the estimated trapped air pursues the dynamic of the model's inputs during acceleration and does not show any extra overshoot. The residual fraction also decreases by about 12% due to the trapped air charge increase, while the valve overlap is approximately the same at the beginning and end of the transition.

Figure 2.25 shows a tip-out between cycles 680 and 700 in which about 800 and 60 kPa decrease in the IMEP and MAP occurs, respectively. In addition, the intake valve timing changes from 20 CAD advance to the parking position while the exhaust valve remains entirely at the parking position. As it is seen in Figure 2.25, the model estimated trapped air charge at IVC decreases from 405 mg to 95 mg following the experimental reference dynamic air charge cycle-by-cycle without delay. The estimated trapped air follows the dynamic of the model's inputs during deceleration and does not show any extra overshoot. The residual fraction also increases by about

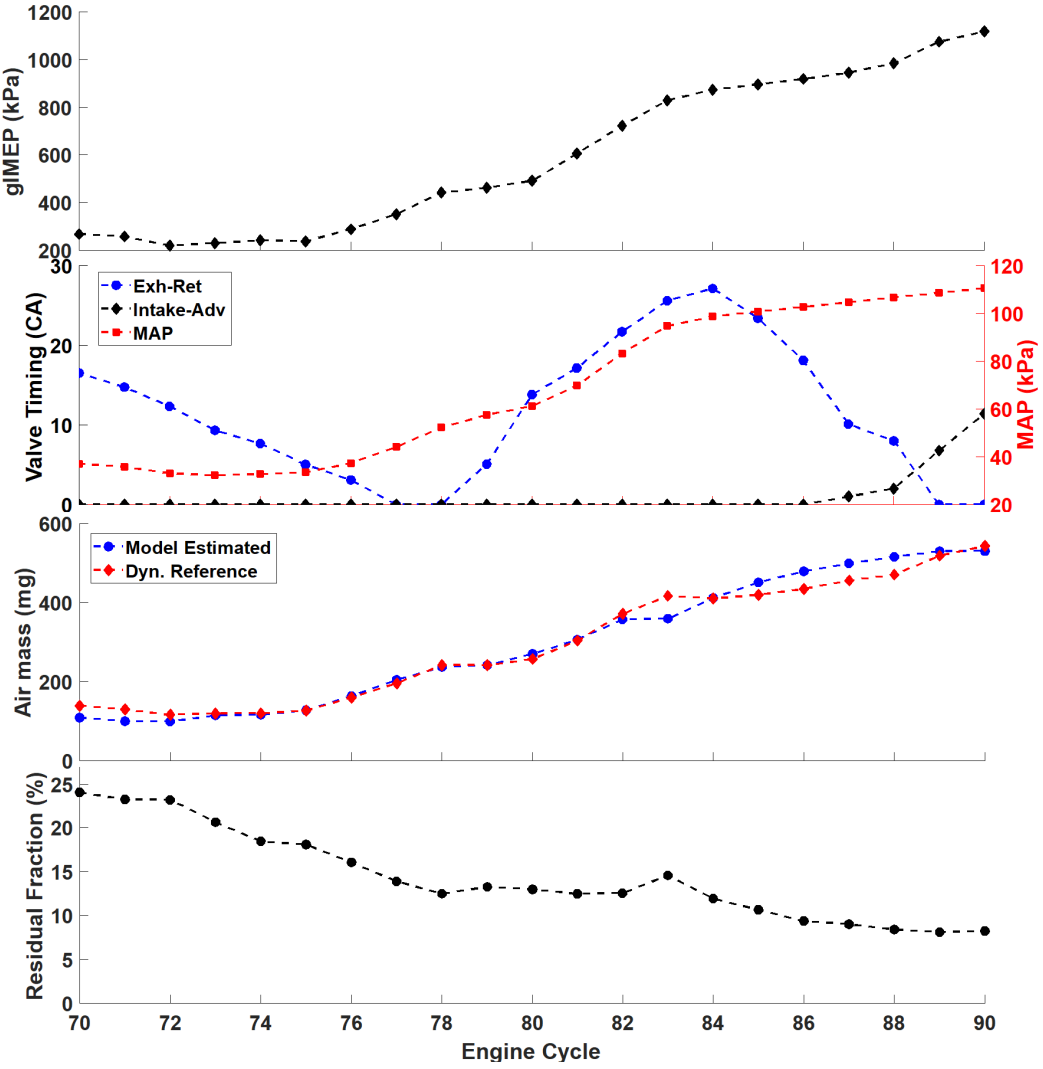

Figure 2.24: The offline MIMO model validated outputs during a tip-in transition

10% due to a 310 mg trapped air charge decrease while the valve overlap decreases for about 20 CAD.

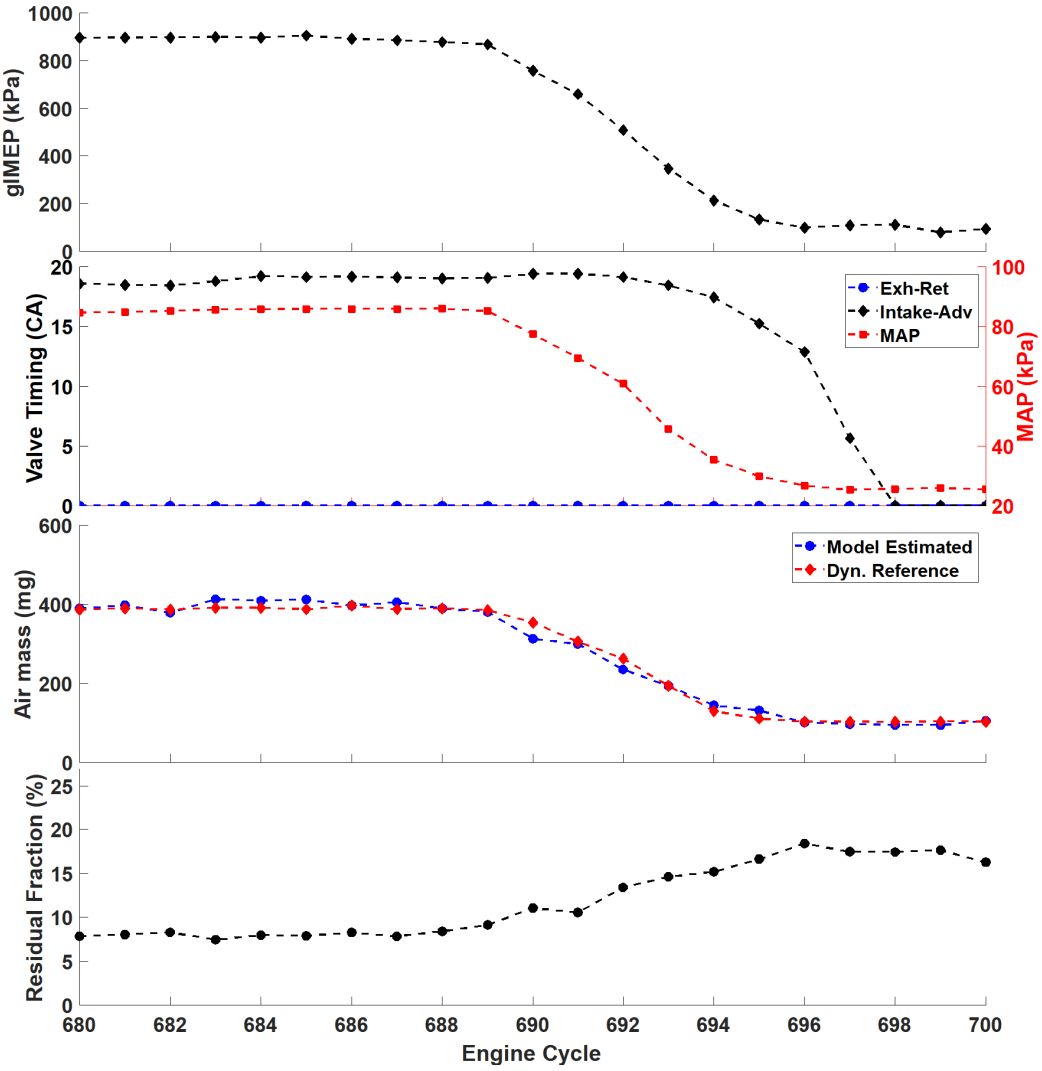

Figure 2.25: The offline MIMO model validated outputs during a tip-out transition

2.4.4.2 Real-Time Implementation and Validation

The model was implemented on the CPDC rapid-prototyping ECU in Simulink/Stateflow and was run and validated in real-time in parallel to the engine production ECU via CAN communication as previously shown in Figure 2.3 on the engine

dynamometer. The Simulink/Stateflow model is included in Appendix B. The calibration parameters comprising convective heat transfer coefficients of heat transfer during intake and exhaust strokes were added to the real-time model as two look-up tables. The look-up tables included real-time cycle-based engine speed, IMEP, and intake and exhaust valves timing as inputs.

The dynamic behavior of the implemented real-time model on CPDC was assessed and validated in a 1350 cycles transient cycle on the engine dynamometer. Bosch PCM controlled the engine with CPDC being operated in parallel. Figure 2.26 shows inputs and outputs of the real-time model on CPDC recorded by ATI-Vision software during the cycle. The dynamics of the inputs, including valve timing, Lambda, and in-cylinder pressure in different events, are seen in Figure 2.26. Figure 2.26 also depicts that in the steady-state regions, the real-time estimated air mass follows the experimental LFE air mass meter data with less than 2% error. Figure 2.27 shows the real-time model estimated air charge against the LFE air mass meter data per cycle and cylinder. The average error is 1.45 mg throughout the transient cycle steady-state regions, and the standard deviation of error is 4.2 mg. The real-time dynamic behavior of the estimated trapped residual gas, the mass of exhaust gas flowing back into the cylinder during valve overlap, residual fraction, and in-cylinder gas temperature at IVC and after blowdown are also depicted in Figure 2.26. Similarly, the estimated residual gas and in-cylinder temperature parameters' dynamics do not include overshoot.

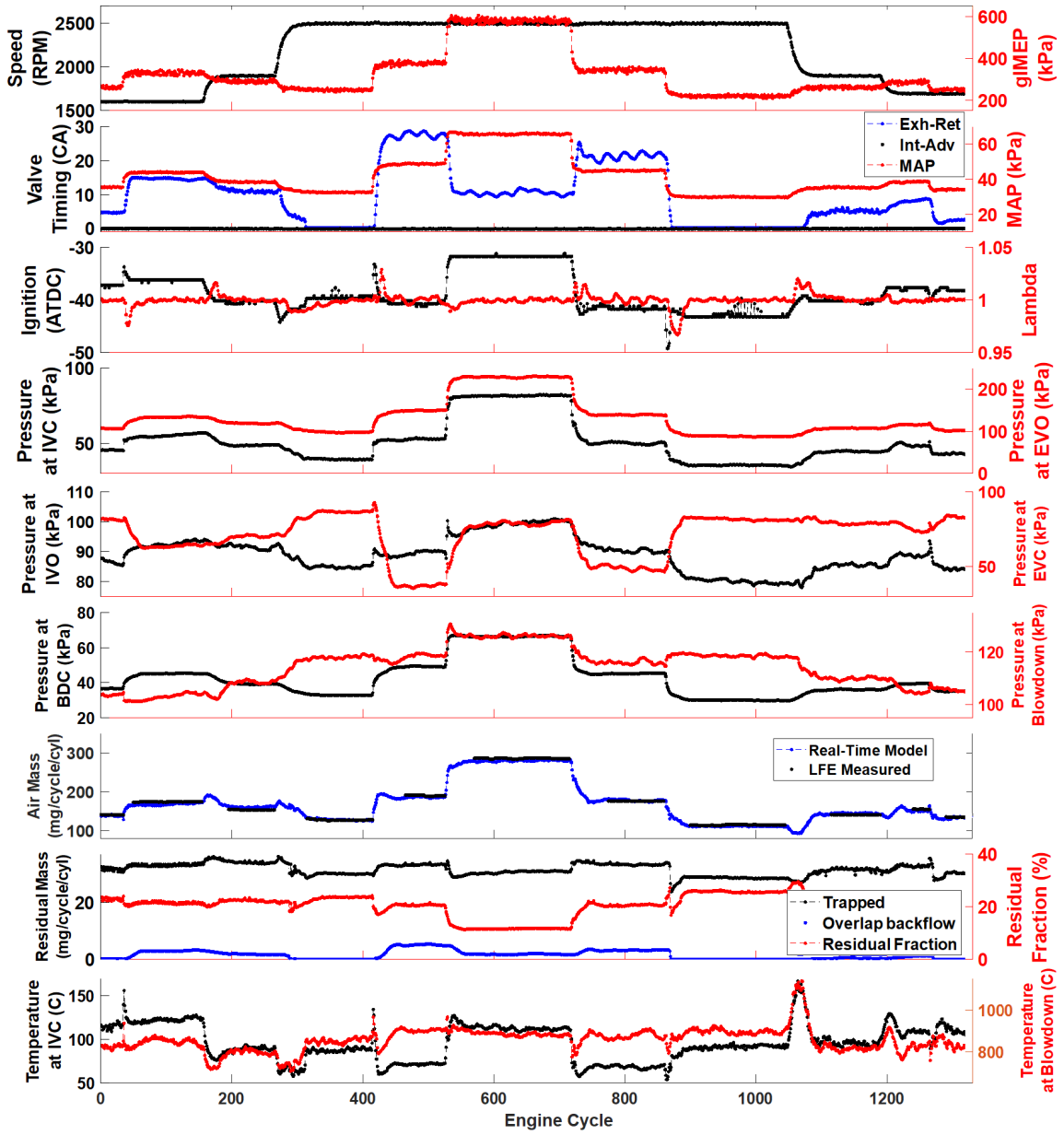

Figure 2.26: The experimental validation of real-time model in a transient driving cycle

To analyze the real-time model dynamic behavior during transitions, one of the tip-in and tip-out transitions shown in Figure 2.26 is zoomed in and assessed in detail. Figure 2.28 shows a tip-in between cycles 520 and 540, including the IMEP and

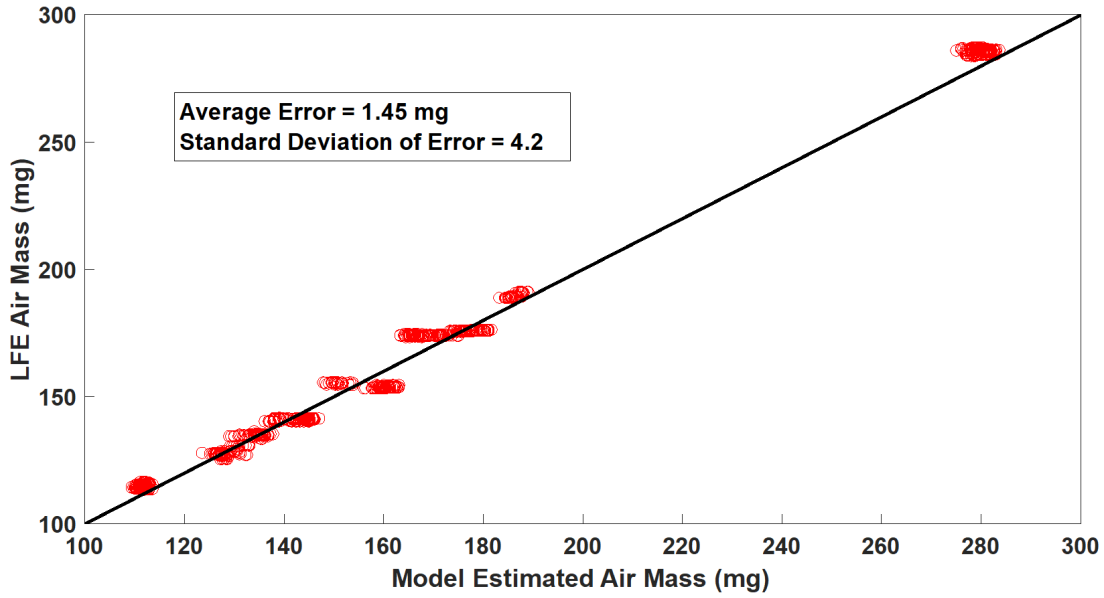

Figure 2.27: The real-time model estimated air charge against the LFE air mass meter data per cycle and cylinder

MAP dynamics while engine load increases. The exhaust valve timing is changed from 28 to 11 CAD retarded while the intake valve remains in the parking position. The dynamics of the in-cylinder pressure at IVC and EVO are also seen in Figure 2.28. The model estimated trapped air charge at IVC follows the input dynamics, especially the in-cylinder pressure dynamics, cycle-by-cycle during the acceleration. The residual fraction also decreases by about 9% due to a 17 CAD decrease of valve overlap while the trapped air charge increases about 80mg.

Figure 2.29 shows a tip-out between cycle 710 and 730 in which about 255 and 21 kPa decrease in the IMEP and MAP occurs, respectively. The exhaust valve timing is retarded 16 CAD while the intake valve remains in the parking position. The model estimated trapped air charge at IVC follows the input dynamics, especially the

in-cylinder pressure dynamics, cycle-by-cycle during the deceleration. The residual fraction also increases by about 7% due to a 15 CAD increase of valve overlap while the trapped air charge decreases about 80 mg.

2.4.5 MIMO Model Sensitivity Analysis

The designed model included several assumptions. The sensitivity of the model outputs to the considered assumptions is analyzed for the range of engine part load conditions in this section.

Gas Composition Change from IVC to EVO

The ideal gas and mass conservation laws were used in the developed model for calculation of the T_{EVO} from T_{IVC}, assuming gas composition does not change from IVC to EVO for simplification. In reality, the gas composition is changed from a mixture including unburned air and fuel and burned residual gas at IVC to mostly burned gas at IVO in the engine's normal operating condition. Uncertainty analysis shows that this assumption causes less than 0.5% relative error in the trapped air charge and residual gas estimation.

Constant End of Blowdown Position

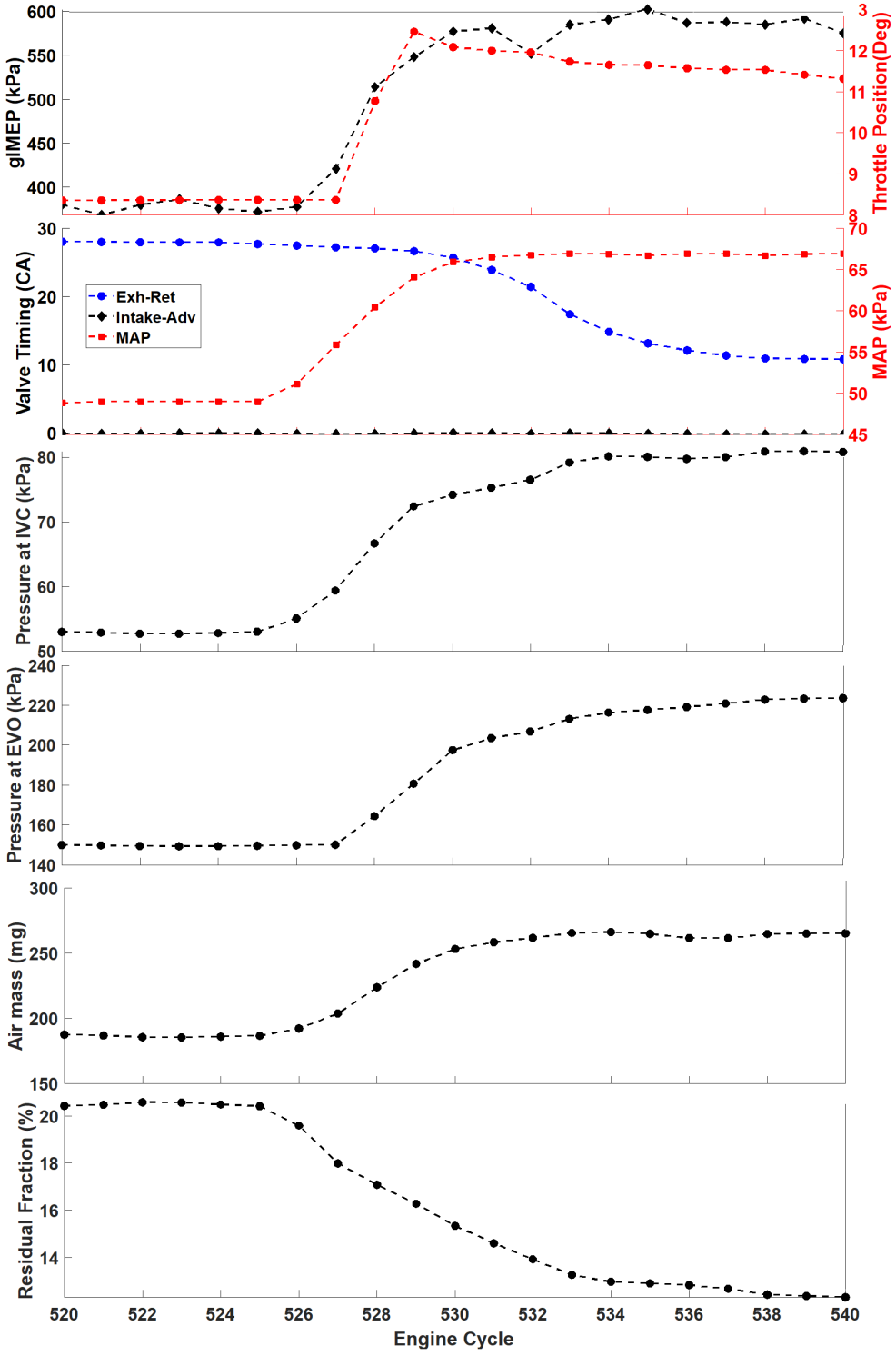

Figure 2.28: Zoomed-in view of Figure 2.26. The real-time model validated outputs during a tip-in transition

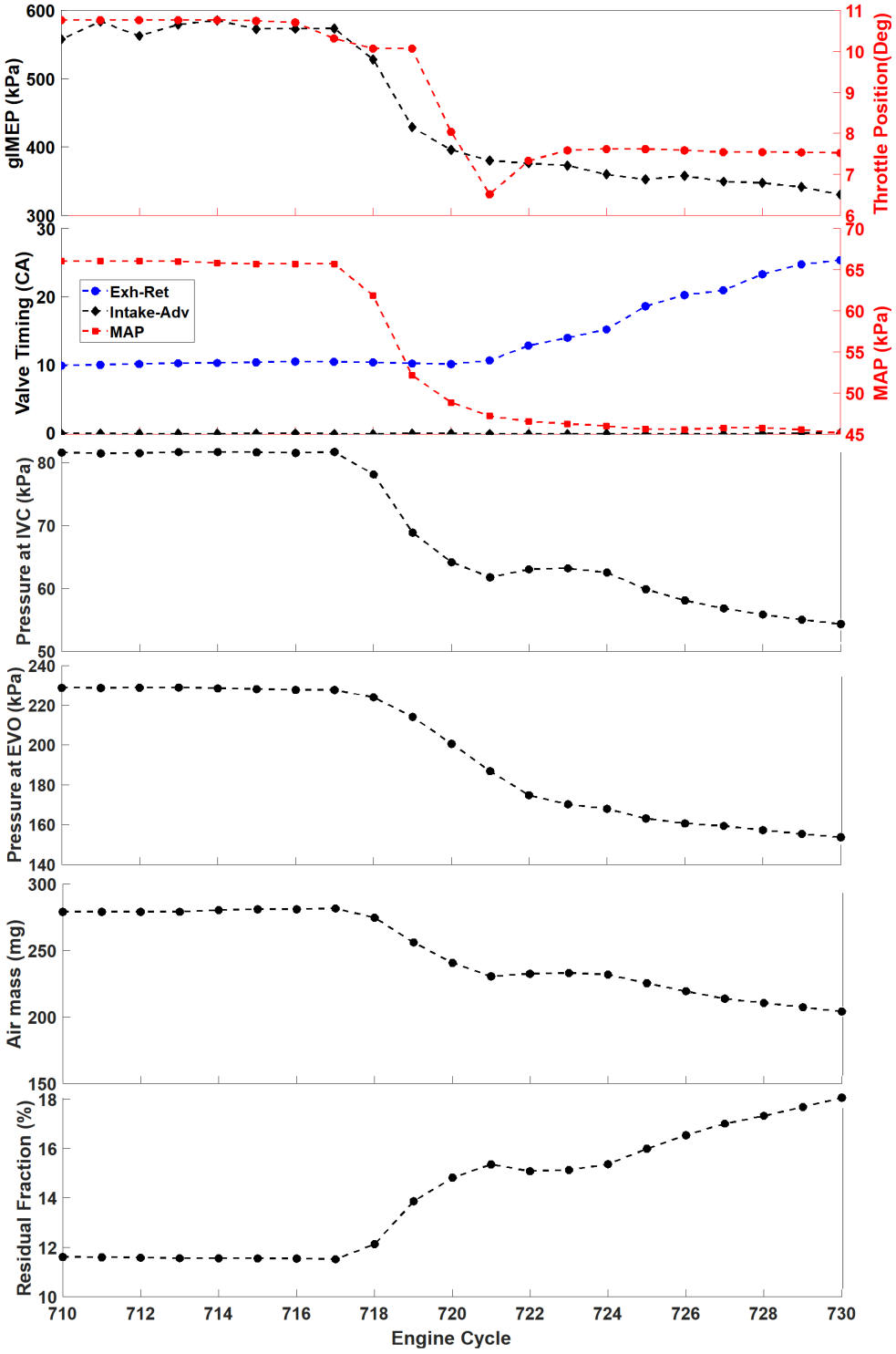

Figure 2.29: Zoomed-in view of Figure 2.26. The real-time model validated outputs during a tip-out transition

The designed model used 260 CAD as a constant engine position for the end of blowdown. In reality, the end of blowdown changes with engine speed and load and cam phasing. Uncertainty analysis shows that 20 ^{o}CA change of the end of blowdown position from 250 to 270 ^{o}CA results less than 0.15% change in the trapped air charge and residual gas estimation. The position of the end of blowdown impacted the calculation of T_{IVO} or T_{EVC} using the energy balance equation used from the end of blowdown to IVO or EVC. Therefore, the uncertainty resulted from the variation of the end of blowdown position is compensated by the calibration parameter, $h_{EXH}A$.

Constant Specific Heat Ratios

The developed model used a constant specific heat ratio of the exhaust gas at IVO and EVO. However, the specific heat ratio of the exhaust gas changes with equivalence ratio and temperature variation[11]. For our case, equivalence ratio, and T_{EVO} and T_{IVO} change for the DOE tests were over the range of 0.9 to 1, 940 to 1380 K, and 650 to 930 K, respectively. Consequently, γ_{EVO} and γ_{IVO} could have a variation from 1.25 to 1.35[11]. This 0.1 variation in the specific heat ratios causes a 0.25% relative change in the trapped air charge and residual gas estimate.

Constant Fuel Vaporization Portion

In the model, the portion of the fuel is vaporized during the intake stroke while it is

injected into the cylinder chamber was constantly considered equal to 90%. Uncertainty analysis shows that a 5% change in the portion of vaporization of the injected fuel results in a 1% change in the trapped air charge estimate. The vaporization portion of the fuel impacts the charge cooling of the inducted gases. Therefore, the uncertainty resulting from the fuel vaporization portion is lumped into the calibration parameter, $h_{INT}A$.

2.5 Summary and Conclusion

A nonlinear discrete MIMO physics-based model was developed to estimate the mass of trapped air and residual gas and in-cylinder mixture temperature in a turbocharged VVT-GDI engine. A precise dynamic cycle-by-cycle prediction of individual-cylinder mass of trapped air and residual gas and in-cylinder mixture temperature at IVC are vital to improving fuel and combustion phasing control. The developed model used dynamic in-cylinder, intake, and exhaust pressures to estimate the required parameters and was validated through dynamic experiments and analysis. Compressible ideal gas flow correlations were used to derive the model from estimating the residual gas resulting from exhaust backflow during valve overlap.

The model was calibrated and validated using experiments developed based on a full-factorial, two-level DOE test plan, including 64 test points. The GT-Power TPA

method and experimental data from the LFE air mass meter were used to calibrate and validate the designed model in steady-state conditions with a maximum 1.5% average relative error. The optimum number of calibration points was determined using DOE analysis based on Pareto charts. As a result, 16 calibration values were defined as adequate calibration effort for each calibration parameter to have less than 2% error of the estimated parameters across all tested engine part-load operating conditions. The calibration effort of the model is significantly low, 32 points, compared to the extensive VE look-up table calibration, 512 points required in VVT-based traditional models.

The model was implemented as a built-in code in the Delphi CPDC rapid prototype engine controller for experimental assessment and validation in real-time conditions. Dynamic validation of the real-time model was accomplished using a transient cycle in real-time conditions. The estimated parameters followed the transitions cycle-by-cycle with no lag and extra overshoot and less than 2% steady-state relative error. Compared to the GT-Power TPA model, the developed model runs 2800 times faster and was easily implemented on the rapid-prototype ECU.

The model has been designed modular and can be further developed for other engine operating conditions, such as cold-start, in the future.

Chapter 3

Elevated HEV Cranking Speed Cold Start Emissions Analysis

The cold crank-start phase significantly contributes to the engine-out total emissions during the US Federal Test Procedure (FTP). The first three engine cycles of the cold crank-start for a Gasoline Direct Injection (GDI) engine in Hybrid Electric Vehicle (HEV) elevated cranking speed is investigated at 20°C. To this end, the impact of the operating strategy on the individual-cylinder engine-out emissions is analyzed quantitatively. For this purpose, a new dynamic method was developed to translate the engine-out emissions concentration measured at the exhaust manifold outlet to mass per cycle per cylinder. The HEV elevated cranking speed provides valve timing control, throttling, and increased fuel injection pressure from the first firings. This study

concentrates on analyzing the cranking speed, spark timing, valve timing, and fuel injection strategy and parameters effect on engine-out emissions. Design of Experiment (DOE) method is used to create a two-step multi-level fractional-factorial test plan with a minimum number of test points to evaluate the significant parameters affecting engine-out emissions during cold crank-start. Out of the first step DOE analysis, the optimal cranking speed, spark timing, and valve timing, which results in the lowest unburnt HydroCarbon (HC) and NOx emissions, are distinguished. Then, fixing the first step parameters at their optimal values, the second step is accomplished with the fuel injection parameters sweep. The split injection parameters, including the Start of the first Injection (SOI), End of the second injection (EOI), and split ratio, in addition to the first cycle additive fuel factor, are investigated. Results show that the high cranking speed with stabilized low MAP, highly-retarded spark timing, high valve overlap, late intake first injection, 30 CAD bTDC firing EOI, and low first cycle fuel factor reduces the HC emissions 94%.

3.1 Introduction

Several studies have already examined GDI engine operation strategy and emissions analysis during the cold crank-start phase. Table 3.1 describes the summary of the GDI engine emissions analysis from the literature and this work. In one study, Rodriguez et al. investigated the effect of the operation strategy on first cycle CO, HC,

and PM/PN emissions in a GDI engine through analyzing a single combustion event-out emissions in different Start of Injection (SOI), Fuel Enrichment Factor (FEF), spark timing, and fuel pressure [5]. In another study, the same authors evaluated the effects of the injected fuel mass, SOI, and spark timing on the initial three engine cycles-out emissions [47]. In these two studies, the valve timing was in a conventional parking position. I another work, Rodriguez et al. researched the effect of valve timing with large negative valve overlap on initial three engine cycles-out emissions at constant engine load, combustion lambda, spark timing, and injection timing in another study [48]. All three above studies were carried out for the conventional cranking speed of 280 rpm. Next, Rodriguez et al. accomplished a carbon accounting analysis in different FEF, single injection timing, spark timing, MAP, fuel pressure, and engine cranking speed to assess the amounts of fuel contribute to combustion, being evacuated as unburnt HC emissions, remaining in the combustion chamber as residual fuel, and lost as blow-by or being absorbed in the lubrication oil [49]. All the above studies were done with the engine operating in single cylinder mode, resulting in an intrinsic deviation from 4-cyl engine real dynamic behavior during cold crank-start even if the engine is externally assisted in simulating the 4-cyl engine speed transient. In addition, Rodriguez et al. have not analyzed the effect of the split injection strategy on cold crank-start emissions. More important, to convert the measured concentrations from emission analyzers to the mass, they have used the theoretical isentropic expansion of an ideal gas for the exhaust process, which imposes another

Scholars	J.Rodriguez	J.Rodriguez	Jinghu Hu	Zheng Xu	V. Kale	This Work
Mode	Crank First cycle	Crank First cycle	Crank 5 cycles	Crank Fast Idle	Crank 3 cycles	Crank 3 cycles
Cranking Speed (RPM)	Low/280	280/700/1200	Low/280	200/500/1200	Low/180	600/1100/1600
Fuel Pressure (bar)	Low/50	Low/50	50 to 125	100	4 to 30	100
Fuel Injection Strategy	Single Injection	Single Injection	Split Injection	Split Injection	Single Injection	Split Injection Intake/Compression
Analyzed Parameters	1. Fuel Pressure 2. Spark Timing 3. Valve Timing 4. FEF 5. SOI	1. Cranking Speed 2. Fuel Pressure 3. Spark Timing 4. FEF 5. SOI 6. MAP	N/A	N/A	1.AFR 2.SOI	1. Cranking Speed 2. Spark Timing 3. Valve Timing 4. Fuel Factor 5. SOI 6. EOI
Emission Estimation	1.Quasi-steady 2. Single cylinder 3. Mass flow	1.Quasi-steady 2. Single cylinder 3. Mass flow	1.Quasi-steady 2. Mass flow	1.Quasi-steady 2. Mass	N/A	1. Dynamic 2. Individual-cylinder 3. Mass
Estimated Parameters	N/A	N/A	N/A	Fuel evaporation	N/A	1. Trapped air mass 2. Residual Fraction 3. In-cylinder temp. 4. Combustion lambda 5. Residual fuel 6. Fuel evaporation 7. Blowby rate 8. Exhaust gas dynamic 9. Post-oxidized HC
Emission Measurement	1. HFR400 FFID 2. Fast NDIR500 3. Cylinder runner	1. HFR400 FFID 2. Fast NDIR500 3. Cylinder runner	1. Horiba (accumulated) 2. Engine out	1. FFID 2. Accumulated	N/A	1. HFR500 FFID 2. Fast NDIR500 3. Engine out
Combustion Classification	Negative IMEP Misfire	N/A	N/A	N/A	N/A	Pressure ratio vs IMEP Normal late-burn Misfire/Partial burn

Table 3.1
Summary of GDI engine cold crank-start emissions analysis compared to the study in this work

error in estimation.

Fan et al. studied the effect of split injection on the combustion characteristics of the first crank-cycle in constant conventional cranking speed, spark timing, fuel pressure, and valve timing in parking position [50], and analyzed HC emissions concentration for the entire cranking process without translating to mass [51]. Wiemer et al. investigated the effect of fuel quantity, injection timing, and spark timing in an engine with a stratified fuel injection strategy during the conventional speed cold crank-start-up phase and evaluated the HC emissions in concentration [52]. Xu et al. analyzed

the effect of split injection strategy on engine cranking and run-up HC emissions based on cumulative feed gas HC in concentration [53]. Hu et al. introduced a new cumulative-based technique for cycle-resolved measuring of cold start first five cycles HC and CO/CO2 emissions in the conventional cranking speed GDI engine cold start operating conditions with constant parameters [54]. Kale et al. investigated the conventional cranking speed SI engine startup trace on a single cylinder GDI engine simulating the engine's initial combustion cycles including engine speed, manifold pressure and fuel pressure [55].

Some other studies on engine-out emissions during cold crank-start were conducted for HEVs. Yu et al. investigated the transient characteristics of combustion and single-cylinder-out HC emissions concentration in different cranking speed start/stop operation initial cycles in HEV equipped with a Port-Fuel-Injected (PFI) engine [56, 57]. Li et al. analyzed effects of coolant temperature, fuel temperature, cranking speed, injection timing, and total equivalence ratio on the combustion characteristics and emissions concentration of the GDI engine first combustion cycle under stratified combustion conditions for HEV quick start process [58]. Pham et al. researched the characterization of cumulative HC and NOx emissions from blended plug-in HEVs during the high-power cold-starts in different driving cycles [59]. Kawaguchi et al. investigated cumulative HC and NOx emissions during cold-start phase of the FTP-75 driving cycle for a motored start concept in a PHEV with PFI engine [60]. All the

above studies have relied either on cycle-resolved emissions concentration or cumulative mass measurement.

This study aims to better understand the dynamic behavior of the engine-out emissions during the cold crank-start phase of a GDI engine at HEV high cranking speeds. To this end, the engine-out emissions are analyzed utilizing a new dynamic method developed to translate the emissions concentration measured with fast in-situ analyzers at the exit of the exhaust manifold to mass per cycle per cylinder. The impact of the engine operating strategy, including cranking speed, spark timing, valve timing, and fuel injection parameters on the initial three engine cycles emissions, are investigated. The specific contributions of this work are:

1. Development of a new method to quantify engine-out emissions in mass per cycle per cylinder
2. Development of an engine-dyno test methodology to duplicate the motored HEV elevated cranking speed cold crank-start process
3. Utilize DOE methods to create a two-step multi-level fractional-factorial test plan with an optimal number of test points
4. Analyse of the engine operating strategy, including cranking speed, spark timing, and valve timing with respect to their impact on the engine-out emissions
5. Analysis of the split injection strategy's parameters, including SOI, EOI, split

ratio, and the first cycle fuel factor impact on the engine-out emissions

6. Derivation of the optimal control inputs trajectories resulting in the lowest HC and NOx emissions during the cold start first cycles

3.2 Experimental Setup

3.2.0.1 Engine Setup

The experiments were accomplished using a Ford 2.0L Ecoboost turbocharged in-line 4-cylinder GDI engine with independent intake and exhaust cam phasing control. A summary of the engine technical specification is presented in Table 3.2. A Bosch production ECU read the engine sensors and commanded the actuators to control the engine. All parameters of the Bosch production ECU were accessible through ATI Vision® software.

Figure 3.1 represents a schematic of the test engine experimental setup.A 450 hp Alternating Current (AC) dynamometer controlled the engine speed or load. NI-VeriStand software was used to develop and speed/torque profile to generate and apply appropriate stimulus commands to the dynamometer to duplicate the intended HEV motored crank-start speed-torque profile. Kistler 6125A pressure transducers

Compression Ratio	9.3:1
Bore	87.5 mm
Stroke	83.1 mm
Connecting Rod Length	155.9 mm
Wrist-Pin Offset	0.6 mm
Base Intake Valve Open (IVO)	11° ATDC
Base Intake Valve Close (IVC)	247° ATDC
Base Exhaust Valve Open (EVO)	-216° ATDC
Base Exhaust Valve Close (EVC)	8° ATDC
Firing Order	1-3-4-2

Table 3.2
Engine technical specification

were used to measure the cylinder pressures with an accuracy of 2%. An OMEGA pressure sensor was used to measure the dynamic pressure in the intake manifold with an accuracy of 0.25%. A fast response piezoresistive Kulite pressure sensor was used to measure the dynamic pressure in the exhaust manifold with a measurement bandwidth of 150 kHz and an accuracy of 1.5%. An AD Combustion Analysis System (CAS) with 32-channels was used for crank angle-resolved data acquisition. Cylinder, intake and exhaust pressure data were recorded by CAS with a sampling resolution of 0.5 CAD. High-resolution measured cylinder, intake and exhaust pressure data captured gas exchange dynamics during the valve overlap and exhaust gas transients in the exhaust manifold during the exhaust stroke. The cylinder pressure data was pegged based on Dual-Pegging method using both MAP and exhaust pressure data. K-type thermocouples were used to measure inlet air and exhaust gas temperatures in the intake port and exhaust gas path.

The air and fuel mass flows were measured by a laminar flow-meter and a Coriolis

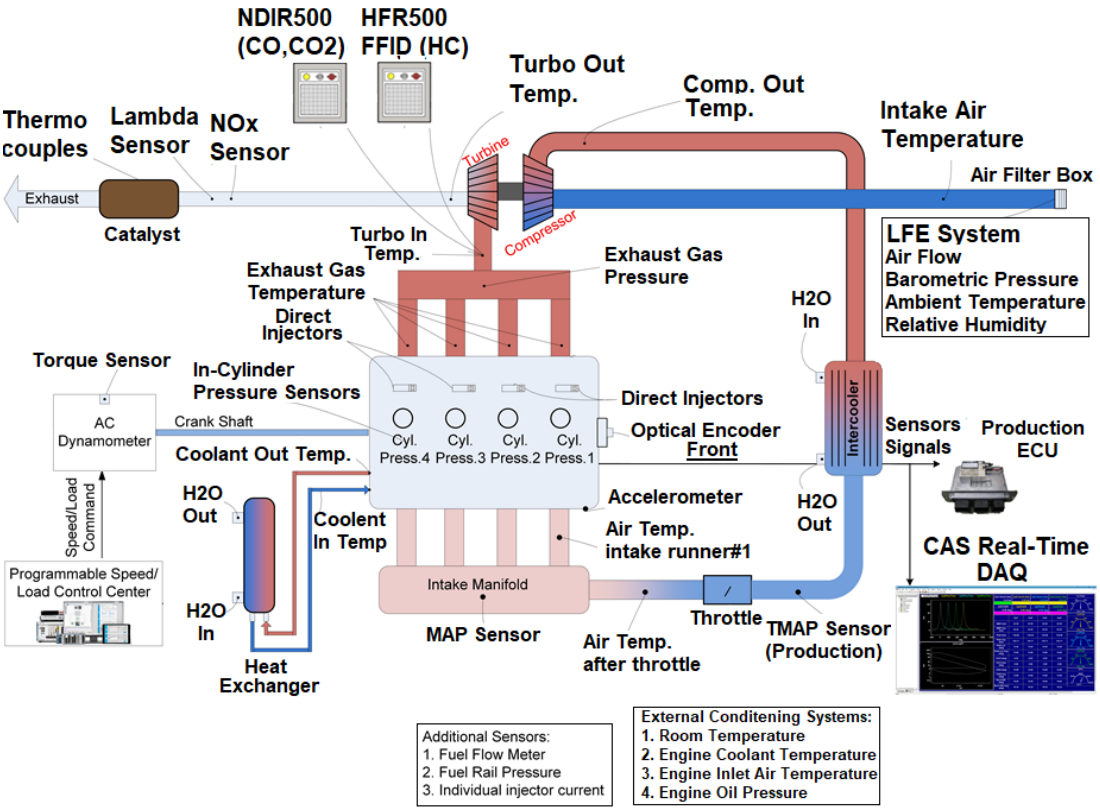

Figure 3.1: Schematic of the engine experimental setup

flow-meter, respectively. The fuel used for the experiments is E10 gasoline with an AKI of 87. An 80I-110S Fluke AC/DC Clamp-On Current Probe was used to measure the injection pulse of the fuel injection in all cylinders. CAS with 0.5 CAD resolution recorded the injection pulse and fuel rail pressure traces. The injection pulse trace was used to extract the injection pulse width to confirm the ECU commanded values. A wideband UEGO sensor was also used along with the production sensor with an accuracy of 1% around lambda 1. The output of the wideband UEGO sensor was monitored using an ETAS lambda-meter and recorded by CAS.

The fast response analyzers from Cambustion were used to measure the exhaust

composition. The HFR500 Fast Flame Ionization Detector (FFID) unit measured the HC concentration with a response time t10-90 of 1ms. The NDIR500 fast analyzer measured CO and CO2 concentrations, with a response time t10-90 of 8ms. Figure 3.2 and 3.3 represents the assembly of the emission analyzers' probes on the engine and the sampling location of the emissions at the exhaust manifold outlet. CAS with 0.5 CAD resolution recorded the emissions traces. In this study, the measured HC and CO/CO2, and GT-Power simulated NOx concentration were used for for analysis. However, the dynamic event-by-event exhaust gas mass flowing out of the exhaust manifold estimated by the developed method can be used to translate the measured NOx emission concentration to mass in future work.

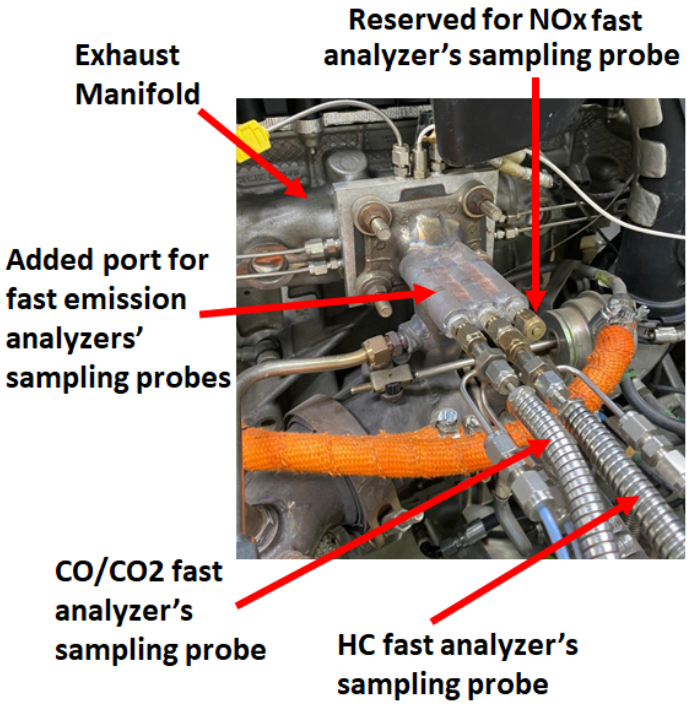

Figure 3.2: HC and CO/CO2 emission analyzers assembly on the engine exhaust manifold outlet

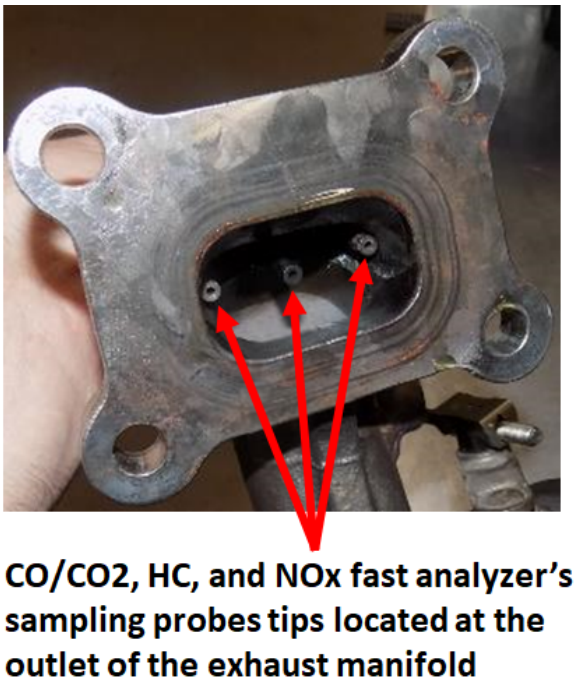

Figure 3.3: HC and CO/CO2 emission analyzers probes' tips position

3.2.0.2 Experiment Description

As seen in the experimental setup shown in Figure 3.1, the experiments for this study were carried out in multi-cylinder mode at the engine real operating conditions in the motored HEV elevated cranking speed cold crank-start phase. As a result, the real speed/torque transient of a 4-cylinder engine is analyzed during the crank-start conditions. To duplicate the HEV motored crank-start process at different cranking speeds, the dynamometer was programmed to generate the appropriate speed/torque profile. Figure 3.4 represents the dynamometer speed/torque command for motored HEV elevated cranking speed cold crank-start experiment with 1100 RPM cranking speed. A short high-speed command from the dynamometer increased the engine

speed to 1100 RPM rapidly and kept the engine motoring at 1100 RPM for 3 seconds. The three-seconds motoring phase was included in the experiment to provide adequate time to increase the oil pressure required for valve actuator activation to adjust the valve timing to the target value from the first firing. Furthermore, the MAP was reduced and stabilized, and fuel pressure was increased to the fuel pressure at the engine's targeted operating conditions, 100 bar, from the first firing. After the first firing, the dynamometer commanded engine speed equal to 1500 RPM for the transition period from 1100 RPM to 1500 RPM during the crank-start phase. Finally, a small torque ramp was applied by the dynamometer reducing the effective inertia of the driveshaft and dyno in the test cell and simulating the inertia and accessories torque in the vehicle when the engine begins to fire.

Figure 3.5 shows how the engine speed and normalized load, spark timing, and fuel pressure follows the reference HEV profiles using the appropriate dynamometer speed/torque command shown in Figure 3.4. In addition, the valve timing dynamics, including the intake advance and exhaust retard is represented in figure 3.5 (d) and (e), showing that valve timing has reached the target value before the first firing. The experiment was done at cranking speed equal to 1100 RPM, spark timing, -10, -5.2, -0.4, 4.4, 9.2, 14 CA aTDC in firing order, intake advance, 20 CAD, exhaust retard, 20 CAD, fuel factor, 1.15, split ratio, 0.5, SOI and EOI, 165 and 50 CA bTDC firing, respectively. The fuel factor is defined from the proportion of AFR from the injected fuel mass to the fuel is required for a stoichiometric AFR based on the estimated

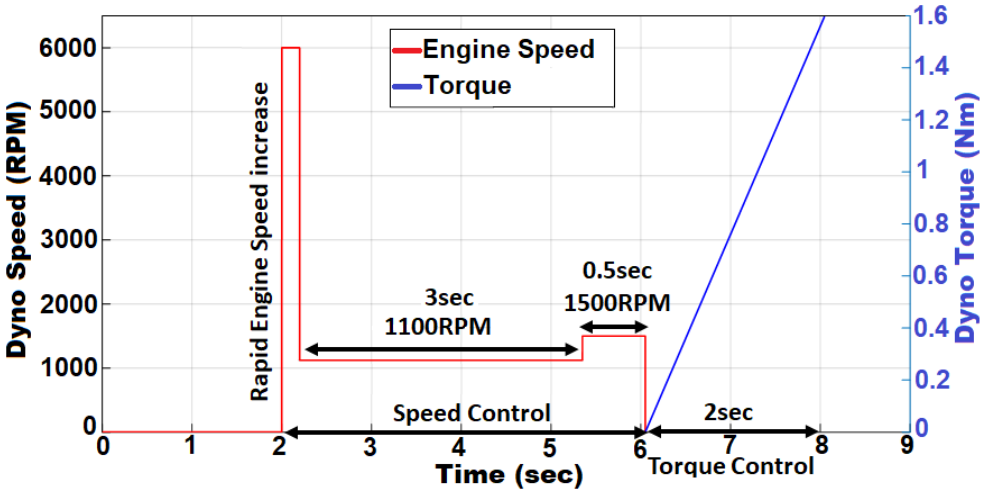

Figure 3.4: Programmable dynamometer speed/torque command for motored cold crank-start with 1100 RPM cranking speed

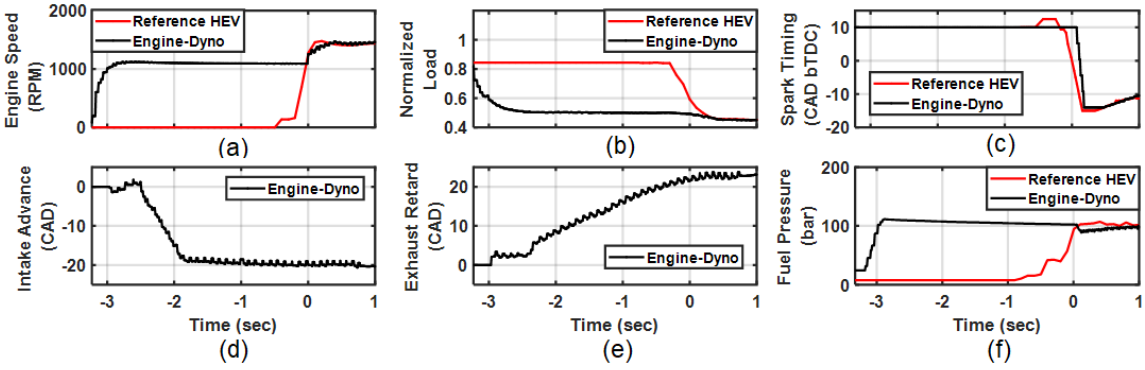

Figure 3.5: The engine speed, normalized load, spark timing, and fuel pressure profiles for the duplicated engine-dyno and reference HEV experiments besides the valve timing dynamics at the motored high cranking speed cold crank-start

trapped air mass. The fuel factor shows the amount of additional fuel injected in the first cycle to the fuel required in stoichiometric conditions.

In all experiments, the test room ambient, engine coolant, and intake air temperatures were retained at the cold-start temperature requirement of the FTP-75 driving cycle,

$20^oC \pm 1^o$. For this purpose, two independent external cooling systems were used to adjust the engine coolant and inlet air temperatures to the desired operating values. Inlet air temperature was regulated by controlling the coolant temperature of the turbocharger after-cooler. Seven cold-start tests were carried out per day, including one overnight-cooled and six forced-cooled. At the end of each test day, the engine was run in idle and part load conditions for half an hour to evaporate and exhaust the fuel contamination of the engine lubrication oil created from the cold start tests. For the overnight-cooled test, the engine was soaked for at least 12 hours from the engine running for the fuel contamination removal on the previous test day. In addition, the engine was motored for 100 cycles at 1000 RPM and Wide Open Throttle (WOT) condition after each experiment to evacuate the residual HC from the combustion chamber and exhaust path for the next test. After each cold-start test, the engine was cooled-done to 18^oC using the external cooling system, fuel pressure and PCM was reset, and the engine was naturally soaked for an hour to reach the FTP-75 requirement temperature, $20^oC \pm 1^o$.

Figure 3.6 represents the standard deviation of the measured average first cycle HC emissions of a cold-start test that has been repeated on 3 different days, seven times per day, once at the overnight-cooled conditions, and six times at the forced-cooled conditions. For the 3 overnight-cooled tests, results showed 0.13 mg standard deviation, and for the 18 forced-cooled tests, 0.11 mg standard deviation was achieved. Therefore, applying precisely similar experiment conditions from test to test has

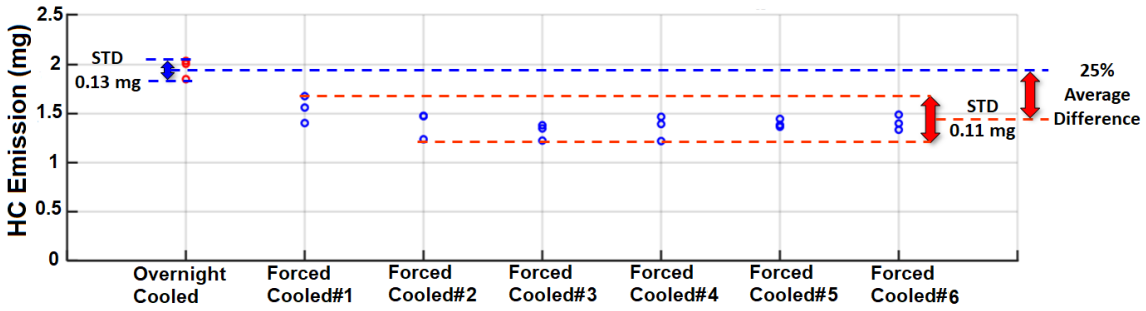

Figure 3.6: The average measured first cycle HC emissions for a test repeated in 3 different days at overnight-cooled and forced-cooled conditions for the test results reputability check

shown the results are quite repeatable. In addition, the results shown in Figure 3.6 represent a 25% deviation between the average measured HC emissions of 3 overnight-cooled tests and 18 forced-cooled tests. This amount of deviation is reasonable because no matter how careful you are, the forced-cooled test conditions can never be equal to 12-hours soaked engine test conditions. However, it was used to derive an accurate correction factor and apply it to the forced-cooled test results.

3.3 Method Development

The cold-crank-start phase is a highly dynamic condition. Therefore, each combustion event has its own unique characteristics, as shown in Figure 3.7 for a motored elevated cranking speed experiment. The experiment was done at cranking speed equal to 1100 RPM, spark timing, -10, -5.2, -0.4, 4.4, 9.2, 14 CA aTDC in firing order, intake advance, 20 CAD, exhaust retard, 20 CAD, fuel factor, 1.15, split ratio,

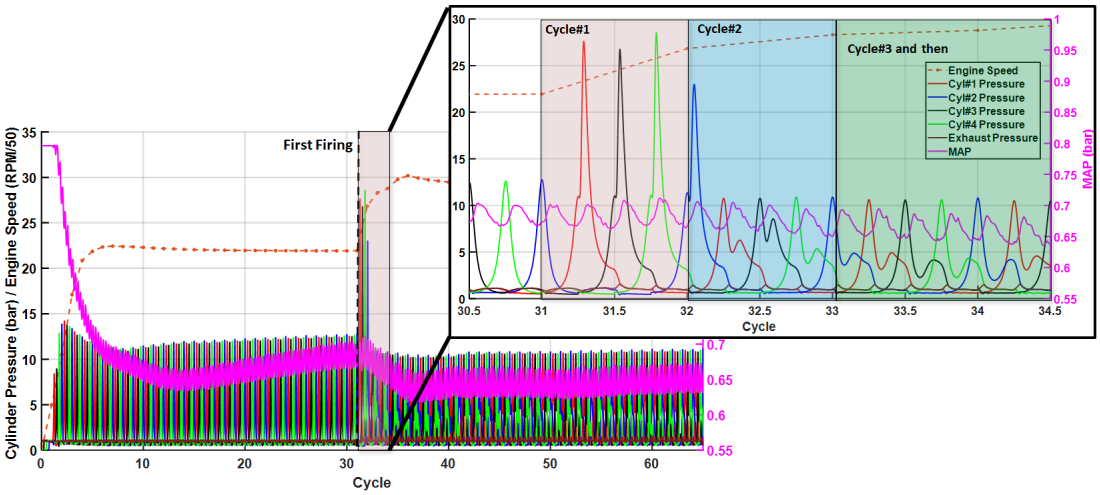

Figure 3.7: Motored cold-start experiment at cranking speed 1100 RPM with zoomed-in first three cycles

0.5, SOI and EOI, 165 and 50 CA bTDC firing, respectively. The fuel factor is defined from the proportion of AFR from the injected fuel mass to the fuel is required for a stoichiometric AFR based on the estimated trapped air mass. The fuel factor shows the amount of additional fuel injected in the first cycle to the fuel required in stoichiometric conditions.

The cold-crank-start phase includes engine speed and MAP dynamics, especially in the case of low cranking speed. During the first cycle, cylinder temperature is low and includes cold air as trapped residual gas. As a result, the pistons ring-gap is high, and there is a lack of lubrication oil, causing significant blow-by rate and charge loss, including the lost fuel. Air residual is replaced by hot burned exhaust gas from the second event, and cylinder wall temperature increases from the first cycle combustion, resulting in high in-cylinder temperature transients. As a result, injected fuel

evaporation behavior varies significantly from the first cycle to the next. Therefore, a considerable portion of the injected fuel in the first cycle does not evaporate before the spark to be able to contribute to the combustion, and either exhausted as unburnt HC out of the cylinder or remains inside the cylinder as residual fuel; the residual fuel contributes to the next cycle's combustible mixture.

The engine control inputs, including throttle angle, spark timing, injected fuel amount, and timing, all follow transient profiles. Furthermore, the first cycle fuel efficiency factor and consequently combustion Air-to-Fuel-Ratio (AFR) is different. Moreover, in the motored high-speed HEV crank-start, valve timing is also controlled from the first cycle. The exhaust gas dynamics inside the exhaust manifold are also added, considering the air inside the exhaust manifold is replaced by the burnt exhaust gas event-by-event during the first cycle. Finally, the exhausted unburnt HC is post oxidized, especially for the highly-retarded spark timing late-burn combustion. As a result, a dynamic method is used for the individual-cylinder translation of the engine-out emissions concentration to mass during the cold-start first three cycles, considering all the above-mentioned transients. Figure 3.8 represents a block diagram of the method, including the top-level Inputs/outputs. The in-cylinder parameters are estimated dynamically using the GT-Power Three Pressure Analysis (TPA) as outlined below and detailed the previous studies' developed in-cylinder air charge, residual gas, and temperature model[43, 44, 45, 61] adapted for motored cold-start first cycles.

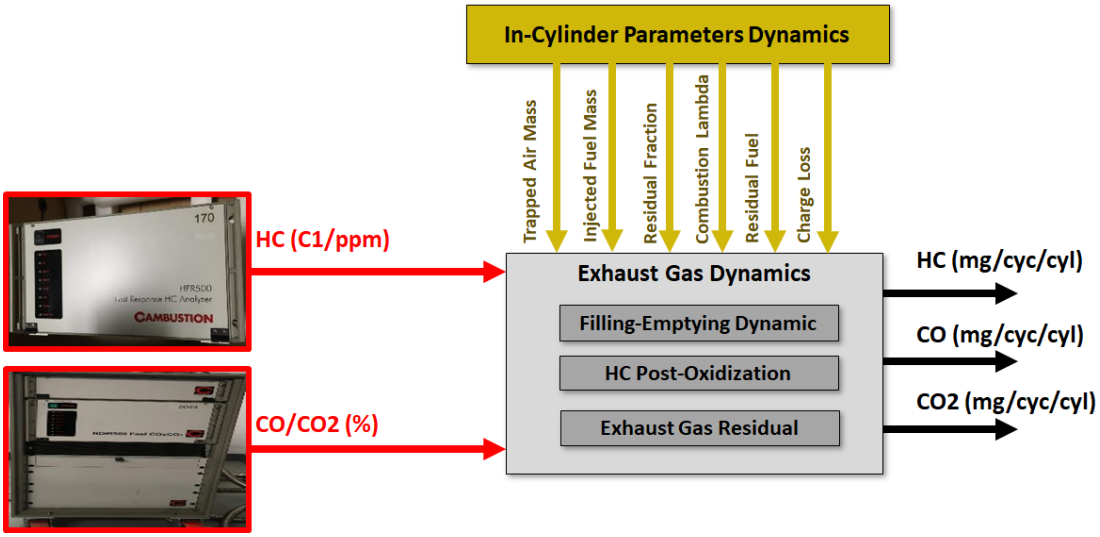

Figure 3.8: Dynamic engine-out emissions concentration translation to mass per cycle per cylinder top-level Inputs/outputs

This section introduces a new dynamic method for the individual-cylinder translation of the engine-out emissions during cold-start first three cycles, considering all the dynamics mentioned above. The method consists of GT-Power TPA model development, the previous studies' developed in-cylinder air charge, residual gas and temperature model[43, 44, 45, 61] adaptation for motored cold-start first cycles, fuel vaporization CFD analysis in different split injection strategies, and exhaust gas dynamics inside the exhaust manifold.

3.3.1 GT-Power TPA Simulation

Direct measurement of the in-cylinder parameters such as gas temperature, trapped air mass, residual fraction, and combustion AFR is arduous. For instance, measurement of the residual fraction is possible[27], but complex and has several limitations and associated uncertainties and errors. For example, charge non-uniformity and cycle-to-cycle fluctuations result in variation of the measured hydrocarbon concentration and subsequent error on residual fraction measurement [41]. A well-accepted approach to determine in-cylinder parameters is the GT-Power Three Pressure Analysis (TPA) method [42]. The GT-Power TPA method analyzes the experimental data focusing on the cylinder, intake, and exhaust pressure traces, to determine the quantities such as residual gas fraction and cylinder temperature, which are difficult to measure directly.

Figure 3.9 shows the GT-Power TPA model adapted for the cold start first cycle. The model consists of three distinct parts. The main part is a single-cylinder model parameterized using the test engine specification. The second part is the split injection model that provides split ratio, first and second injection timings—the third part defines motoring cycles before the first firing. Figure 3.9 also represents the individual-cylinder dynamic cylinder, intake, and exhaust pressure traces as the main inputs to the GT-Power TPA model. The GT-Power model is fed by synchronized engine

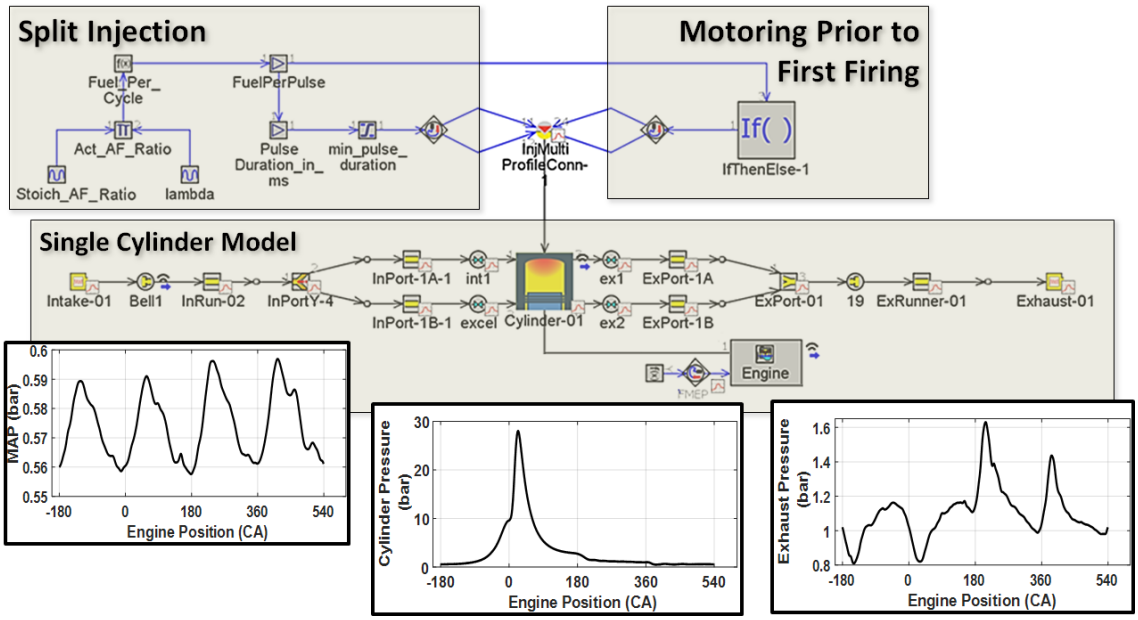

Figure 3.9: Adapted GT-Power TPA model for cold-start first cycle

speed, spark timing, intake and exhaust valves timings, inlet air, exhaust, ambient temperatures, and relative humidity for each firing event. For the first cycle, intake components and inlet air initial temperature are considered to be the same as ambient temperature. Also, the initial exhaust gas is set to be air, and exhaust gas and exhaust path components temperatures are adjusted to the ambient temperature. In addition, leak path equivalent diameter and crankcase pressure and temperature are inputs for the blow-by rate estimation. The leak path equivalent diameter calculation method will be explained later in this paper. Crankcase pressure and temperature are assumed to be constantly equal to 96 kPa and ambient temperature, respectively. Another important input to the model is the fuel vaporization profile. The fuel vaporization profile is derived using CDF analysis and explained later in this paper.

After initializing the model for one event, e.g., first firing of a high-cranking speed cold-start test at cylinder 1, the model is calibrated to coincide the GT-Power simulated cylinder pressure trace with experimental cylinder pressure trace at peak pressures and during different strokes with less than 1% error. Also, the trapped air mass and IMEP calculated by GT-power must match the experimental air mass measured by air mass meter and IMEP calculated by CAS with less than 2% difference. Engine speed, MAP, and engine inlet air mass flow are stabilized after three-second motoring in motored high cranking speed cold start conditions, as is shown in Figure 3.10. Therefore, the measured engine inlet air mass flow can be appropriately used for GT-Power TPA estimated trapped air mass validation with adequate precision.

The GT-Power model calibration procedure comprised three parameters that require adjustment: effective compression ratio, combustion lambda, and cylinder overall

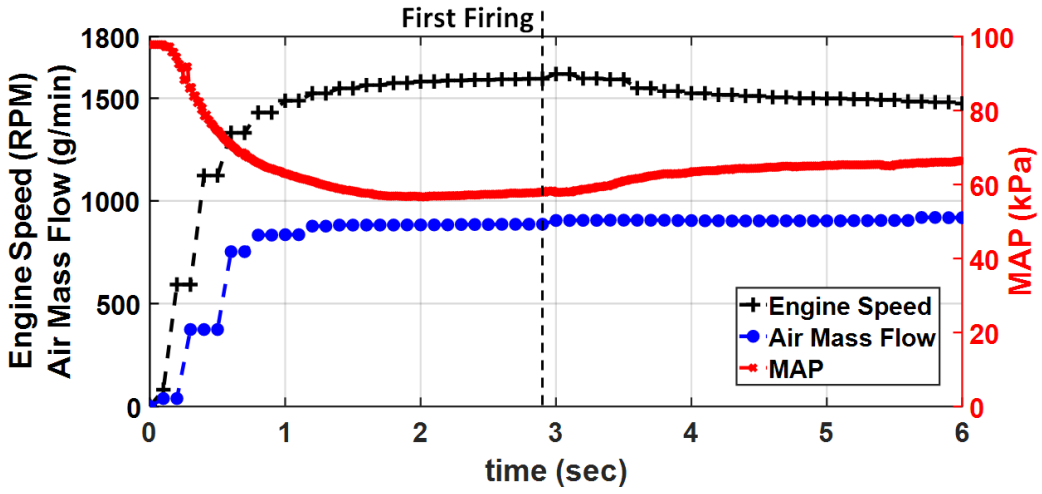

Figure 3.10: Engine Speed, MAP, and engine inlet air flow dynamics during high cranking speed cold-start

convective heat transfer multiplier. These three parameters are not independent and have interactive effects on simulated cylinder pressure trace. However, each parameter effect on the cylinder pressure trace is clearly distinguished. The effective compression ratio has a dominant effect on pressure profile during compression and peak pressures, including compression and firing peak pressures. The effective compression ratio effect on compression peak pressure is clearly recognizable in late-burn cases. The combustion lambda and overall convective heat transfer multiplier affect cylinder pressure at the firing peak pressure and expansion stroke. However, the combustion lambda has a prevailing effect on the firing peak pressure, and the overall convective heat transfer multiplier impacts the cylinder pressure during expansion. The GT-power model is calibrated and run cylinder-by-cylinder for the first three cycles. The results, including the in-cylinder temperature, the mass of trapped air and residual gas at IVC, and blow-by gas mass, are used for adapted air charge model calibration. The exhaust gas temperature in the exhaust manifold is utilized to estimate the exhaust gas dynamics inside the exhaust manifold. The equivalent combusted fuel mass is used for individual-cylinder engine-out emissions concentration to mass translation.

3.3.2 Cold Start Adapted In-Cylinder Air Charge, Residual Gas, and Temperature Model

In this study, the designed in-cylinder air charge, residual gas, and temperature estimation model[45] is developed to be used for motoring and cold crank-start operating conditions. The air charge model is an event-based model in which different physics and thermodynamics-based equations are utilized between different events to estimate the temperature and mass of the in-cylinder trapped gas, as shown in Figure 3.11. The model comprises two calibration parameters, convective heat transfer coefficients of heat transfer multiplied by effective area, $h_{INT}A$ and $h_{EXH}A$, in the exhaust and intake strokes. The model was developed for the engine part-load operating conditions but is modular and can be modified and extended easily for other engine operating states. In the following, the model adaptation for motoring and cold crank-start conditions will be explained.

3.3.2.1 Motoring

Each experiment starts with the motoring of the engine by the dynamometer for three seconds. The engine coolant and inlet air temperature are assumed equal to ambient temperature at the beginning of the motoring phase. Therefore, the model begins

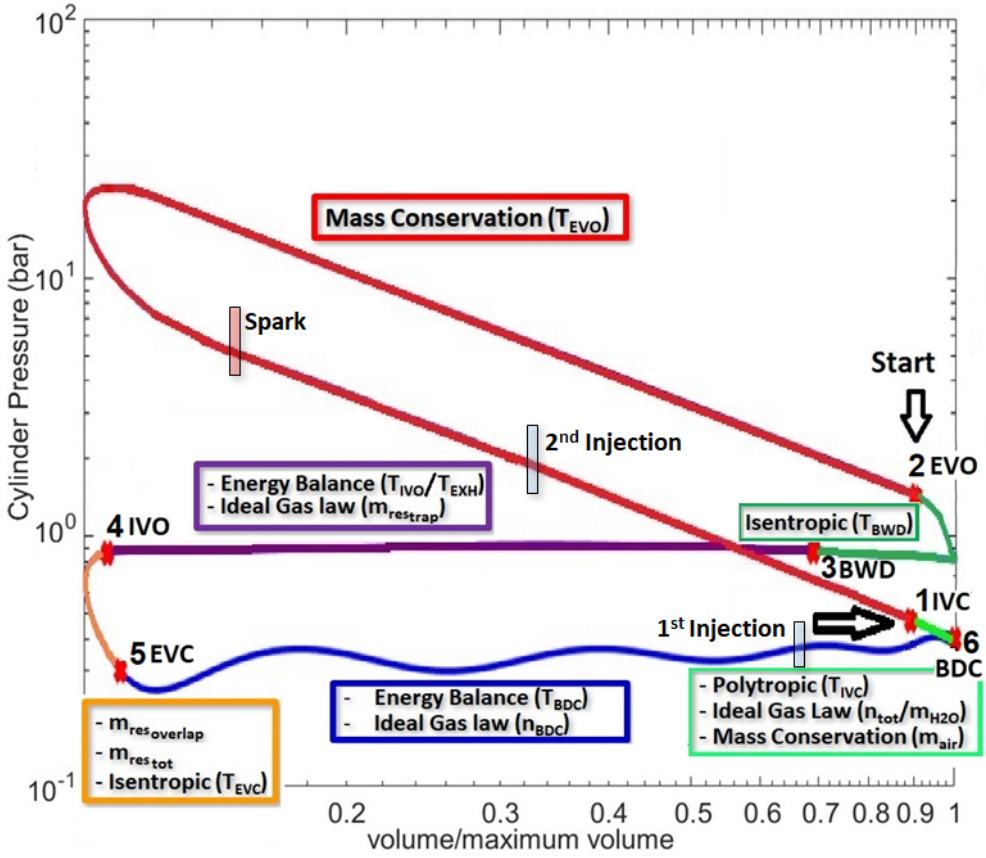

Figure 3.11: A P-V diagram including all physical laws and relationships that are used for calculation of the air charge and residual gas masses during one cycle

to estimate the in-cylinder parameters from the first motoring cycle, assuming the initial temperature of the in-cylinder mixture at BDC compression is equal to ambient temperature. The Polytropic, mass conservation, and isentropic expansion equations are similarly used to estimate the in-cylinder gas temperature at IVC, EVO, and the end of blowdown. From the end of blowdown to IVO or EVC, depending on having positive or negative valve overlap, the cylinder content is only air, contrary to the firing conditions where the cylinder includes exhaust gas. Therefore, convective heat transfer from the in-cylinder gas, which is only air, to the cylinder walls is assumed

to be negligible, and $h_{exh}A = 0$. As a result, the air charge model is simplified for motoring conditions to have just one calibration parameter, and the in-cylinder gas temperature remains constant from the end of blowdown to IVO or EVC,

$$T_{IVO/EVC}[k] = T_{EXH}[k] \tag{3.1}$$

From the IVO to EVC or EVC to IVO, the isentropic expansion equation is likewise used. From IVO or EVC to BDC compression, there is air induction into the cylinder without fuel injection during the intake stroke. Therefore, the first law of thermodynamics is simplified by eliminating the fuel injection effects, including flow work, change of internal energy resulting from the injected fuel mass, and internal energy of vaporization. The model is calibrated in two levels of motoring speeds, IMEPs, and valve timings, for motoring conditions using just the convective heat transfer coefficient of heat transfer multiplied by effective area for intake stroke, $h_{INT}A$.

3.3.2.2 Cold Crank-Start

After the last motoring cycle, the cold crank-start phase starts with the first firing cylinder. The in-cylinder air charge, residual gas, and temperature estimation at IVC for first firing events are launched with the air residual gas from the last motoring cycle and estimated in-cylinder gas temperature at BDC compression. While there

is split intake/compression injection at the cold start first cycles, the first injection occurs during the last motoring cycle intake stroke. In the warm engine operating conditions, it is assumed that all injected fuel into the cylinder is nearly vaporized before BDC compression in the presence of hot residual exhaust gas. For the cold crank-start, especially at the first cycle in which residual gas is cold fresh air from the last motoring cycle, the small fraction of the liquid fuel injected into the cylinder during the intake stroke succeeds to be vaporized before BDC compression. The vaporized fuel fraction, $X_{f_{vap}}$, is derived from the CFD analysis as a function of cylinder temperature and pressure during the intake stroke and used for calculation of the internal energy of vaporization of the vaporized fuel,

$$U_{fg_{fuel}}[k] = X_{f_{vap}}(P_{BDC}, T_{BDC}) * m_{fuel_{1st}}[k] \cdot u_{fg_{fuel}}(P_{BDC}, T_{BDC}) \qquad (3.2)$$

Where $m_{fuel_{1st}}$ is the injected fuel mass during the first injection at intake stroke, and $u_{fg_{fuel}}$ is the internal energy of vaporization of the fuel on a unit mass basis as a function of cylinder pressure and temperature. In addition, as it was explained before, a considerable amount of the injected fuel during the first cycle, which is not contributed to the combustion in the same cycle, remains in the cylinder as residual fuel. The major part of the residual fuel is assumed to be vaporized due to the heat from the combustion at the same cycle. Therefore, the residual gas inside the cylinder from the first cycle to the second cycle at IVO consists of exhaust gas and gaseous

residual fuel. As a result, the first law of thermodynamics was used from IVO or EVC to BDC compression, is extended for cold crank-start conditions as below,

$$\begin{aligned} Q_{INT}[k] - W_{INT}[k] + MAP[k] \cdot (V_{BDC}[k] - V_{EVC}[k]) + p_{fuel}\frac{m_{fuel}[k]}{\rho_{fuel}} - \\ U_{fg_{fuel}}[k] = (m_{air_{int}}[k]C_{v_{air}} + m_{H2O_{int}}[k]C_{v_{H2O}})\,(T_{BDC}[k] - T_{run}[k]) + \\ (1 - X_{f_{vap}}(P_{BDC}, T_{BDC})) * m_{fuel_{1st}}[k]C_{fuel}\,(T_{BDC}[k] - T_{fuel}[k]) + \\ X_{f_{vap}}(P_{BDC}, T_{BDC}) * m_{fuel_{1st}}[k]C_{v_{fuel}}\,(T_{BDC}[k] - T_{ref}) + \\ m_{fuel_{res}}[k]C_{v_{fuel}}\left(T_{BDC}[k] - T_{IVO/EVC}[k]\right) + \\ m_{res_{tot}}[k]C_{v_{res}}\left(T_{BDC}[k] - T_{IVO/EVC}[k]\right) \end{aligned} \tag{3.3}$$

Where, $m_{fuel_{res}}$ is the residual fuel remaining unburnt in the cylinder and contributes to the next cycle combustion, T_{ref} is the reference temperature constantly equal to 273.15 K, and C_{fuel} is the average specific heat of liquid fuel assume to be equal to 2140 $\frac{J}{kg\bar{K}}$[11]. In addition, the mass conservation from IVC to EVO must be included the charge loss through blow-by and the second injection mass,

$$m_{tot_{EVO}}[k] = m_{tot_{IVC}}[k] + m_{fuel_{2nd}}[k] - m_{bb}[k] \tag{3.4}$$

Where, $m_{tot_{IVC}}$ and $m_{tot_{EVO}}$ are the total in-cylinder trapped mass at IVC and EVO, $m_{fuel_{2nd}}$ is the mass of fuel injected at the second injection during the compression stroke, and m_{bb} is the mass of the in-cylinder trapped charge is lost through blow-by.

3.3.3 Charge loss

As it was mentioned in section 4.1, GT-Power TPA estimates the charge loss through blow-by. However, the GT-Power TPA model needs the leak path equivalent diameter to estimate the blow-by gas mass. The leak path equivalent diameter, C_DA, is calculated here as the average blow-by leakage path between the combustion chamber and the engine crankcase from when cylinder pressure increases over the crankcase pressure after IVC up to EVO. For this purpose, the compressible ideal gas flow for sub-critical flow equations[11] are used as follows,

$$C_DA = \frac{\dot{m}_{bb} \cdot \sqrt{RT_{cyl}}}{p_{cyl} \cdot \left(\frac{P_{crank}}{P_{cyl}}\right)^{\frac{1}{\gamma}} \cdot \left\{\frac{2\gamma}{\gamma-1}\left[1-\left(\frac{P_{crank}}{P_{cyl}}\right)^{\frac{\gamma-1}{\gamma}}\right]\right\}^{\frac{1}{2}}} \tag{3.5}$$

Where, p_{cyl} and T_{cyl} are cylinder pressure and temperature, p_{crank} is the crankcase pressure, R is the gas constant, $\dot{m}_{bb}$ is the blow-by mass flow is determined experimentally during the engine motoring at test bench , and γ is assumed constant and equal to 1.4[11]. If the blow-by flow from the combustion chamber to the crankcase

is choked; The crankcase to cylinder pressure ratio, $\frac{P_{crank}}{P_{cyl}}$ is less than or equal to the critical pressure ratio, 0.528, for $\gamma = 1.4$, the leak path equivalent diameter is calculated as following[11],

$$C_D A = \frac{\dot{m}_{bb} \cdot \sqrt{R T_{cyl}}}{p_{cyl} \cdot \gamma^{\frac{1}{2}} \left(\frac{2}{\gamma+1}\right)^{\frac{\gamma+1}{2(\gamma-1)}}} \tag{3.6}$$

The calculated leak path equivalent diameter, $C_D A$, is given as an input to the GT-Power TPA model to estimate the mass of the individual-cylinder blow-by gas, m_{bb}.

3.3.4 CFD Fuel Evaporation Analysis

This research utilizes a CFD model to compute the fuel evaporation rate for the GDI engine with fuel, modeled as iso-octane. The engine geometry is developed by CATIA software and validated based on the compression ratio. The developed model is used to define the fluid dynamic boundaries at CONVERGE CFD software. The RNG k- model is applied to model the mean flow characteristics for the turbulent flow conditions. The developed CFD model uses the Reynolds-Average Navier- Stokes to compute the fluid dynamics and the O'Rourke model to simulate turbulent dispersion.

The GDI fuel injection process is molded by developing a 6-hole injector nozzle model spraying iso-octane at a 15-degree cone angle. Kelvin- Helmholtz and Rayleigh-Taylor

models are used to model injected fuel breakup and parcel formation. Generated parcels are assumed to be evenly distributed through the injection cone. Drag force on fuel droplets is modeled by using a spherical drop drag approach. Finally, the fuel and wall interaction is considered to be rebound and slide mode. The developed model is used to investigate fuel evaporation rate at various intake initial conditions by using the Frossling model. The computed evaporation rates from the CFD model are represented by the evaporation rate formula used to update the GT-Power model. Figure 3.12 shows the CFD model structure and the iso-octane fuel droplets pattern inside the combustion chamber after direct injection. The injected iso-octane evaporates and creates a stratified mixture inside the combustion chamber. Figure 3.13 presents the distribution of the evaporated iso-octane mass fraction at 180 degrees after the start of injection.

The evaporated iso-octane mass is used to compute the rate of evaporation. Figure 3.14 represents the results obtained from the CFD analysis for the injected fuel evaporation profile, while 17.3 mg of fuel is injected into the cylinder with the temperature of 340 K and different pressures during the intake stroke. Figure 3.15 shows the fuel evaporation profile for 17.3 mg of fuel injected late at intake stroke with a cylinder pressure of 50 kPa and different temperatures. The computed fuel evaporation profiles from the CFD model are used as inputs to the GT-Power TPA and air charge model. The SOI coincides with 0 in Figures 3.14 and 3.15, and the injection pulse width is 15 CAD equal to 1.5 msec in 1600 RPMengine speed.

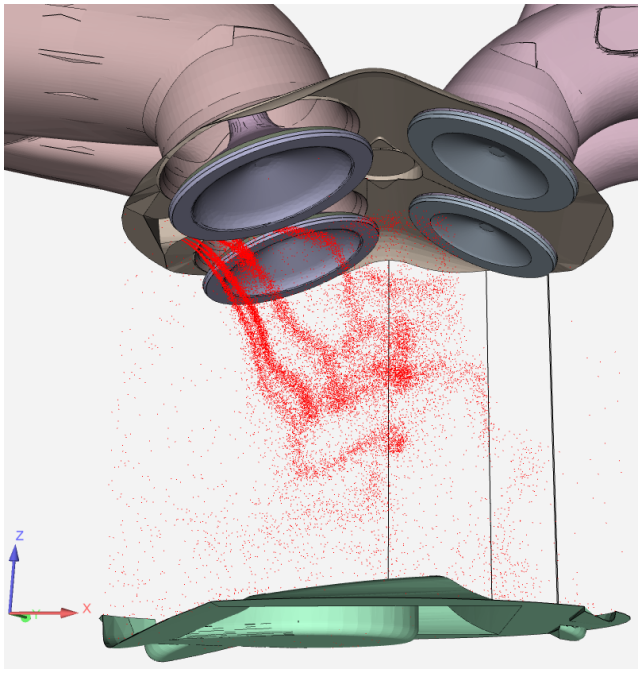

Figure 3.12: CFD analysis for evaporated fuel fraction profile derivation for cold-start first cycles, the model structure

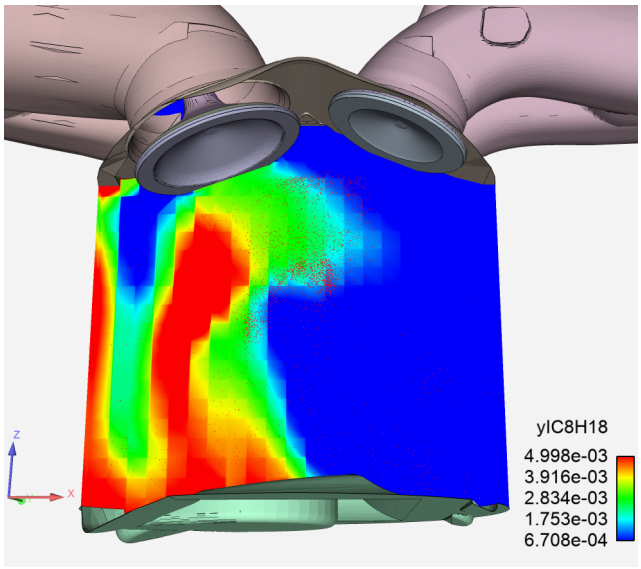

Figure 3.13: CFD analysis for evaporated fuel fraction profile derivation for cold-start first cycles, fuel droplets pattern

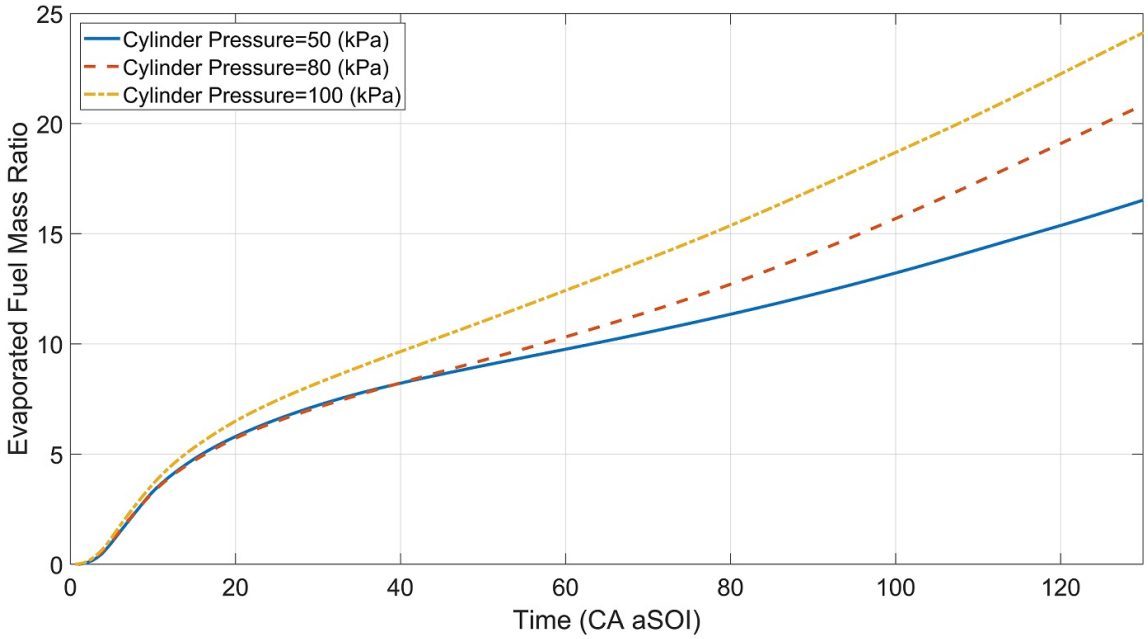

Figure 3.14: Evaporated fuel fraction profile from the CFD analysis for injected fuel quantity of 17.3 mg, and temperature, 340 K, in different cylinder pressures

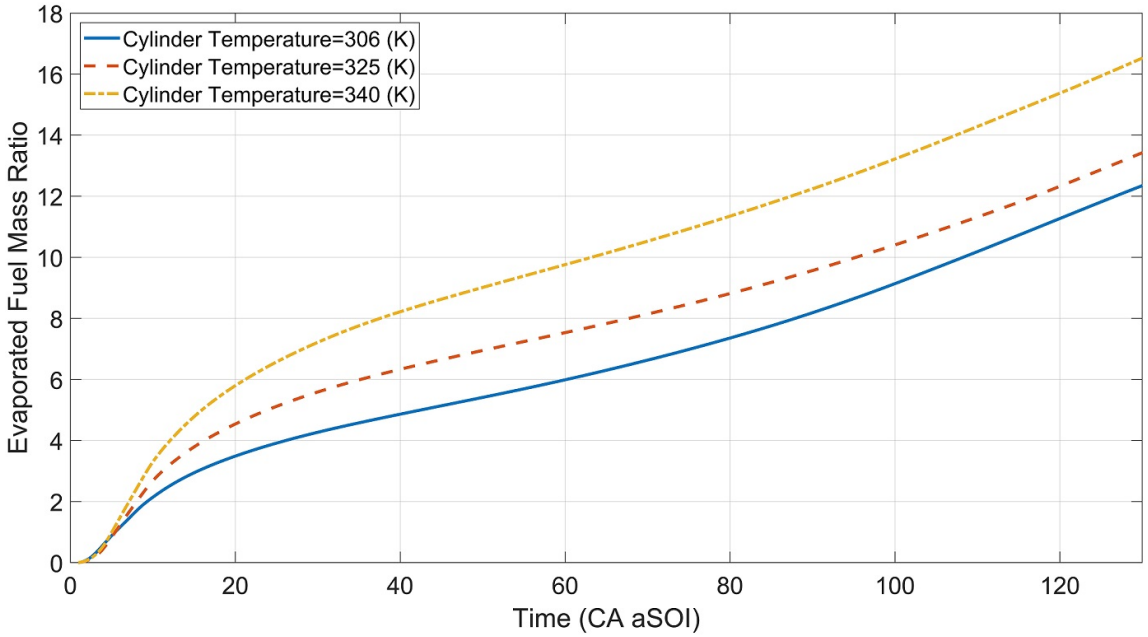

Figure 3.15: Evaporated fuel fraction profile from the CFD analysis for injected fuel quantity of 17.3 mg, and pressure, 50 kPa, in different cylinder temperatures

3.3.5 Exhaust Gas Dynamics

The test engine includes a 0.46 liter integrated water-cooled exhaust manifold. Figure 3.16 shows a sectioned 3D model of the exhaust manifold, including the categorized detail volume of each cylinder's exhaust path in liter. Exhaust gas from the cylinder output to the exhaust manifold outlet, where FFID and NDIR measure the emissions, shown in Figure 3.16 for cylinder one as an example, experiences different dynamics during the cold-crank-start phase.

Figure 3.17 represents the exhaust gas dynamics passing from the motoring phase to the cold crank-start stage based on the measured exhaust manifold pressure data.

Firstly, during the motoring cycle exhaust manifold is filled with cold air, and after

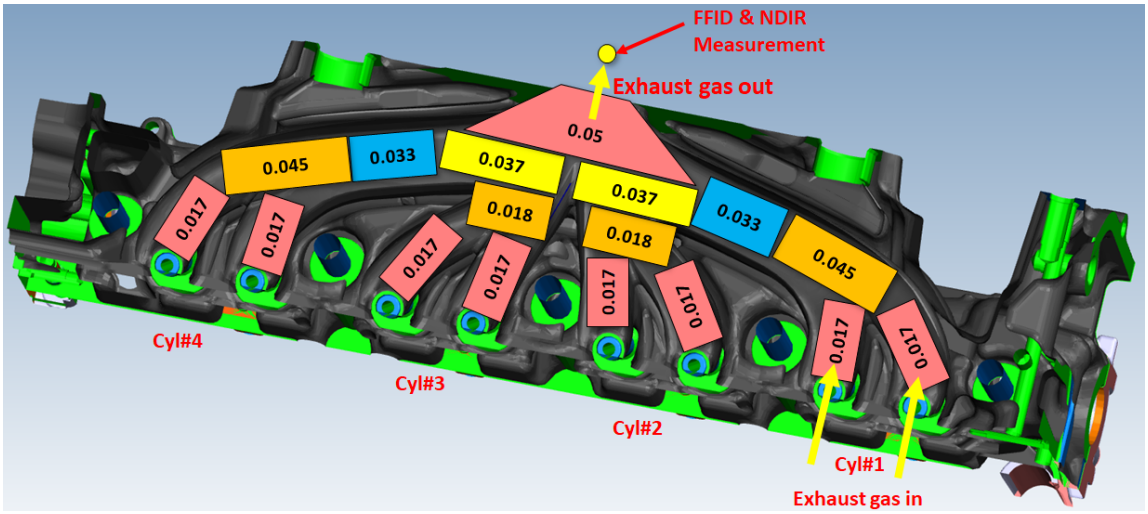

Figure 3.16: The test engine exhaust manifold sectioned 3D model

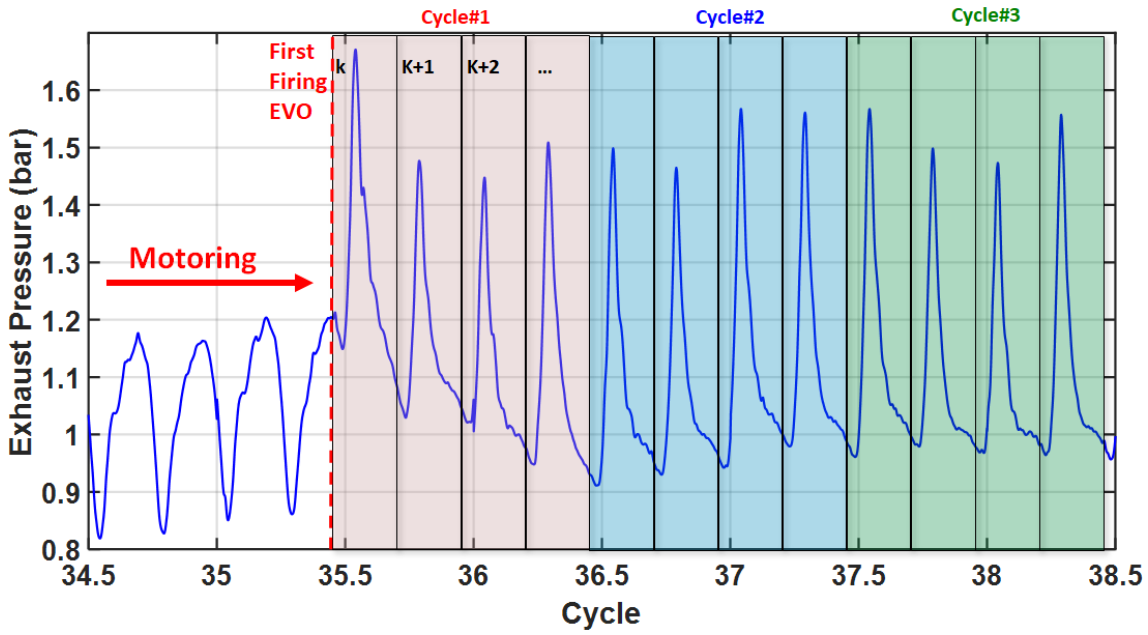

Figure 3.17: Exhaust manifold pressure dynamic from motoring to cold crank-start and fast-idle

the EVO of the first firing event, the air is replaced by hot burnt exhaust gas event-by-event. Therefore, the mass of the exhaust gas trapped inside the exhaust manifold between two consecutive events' EVO dynamically changes during the cold crank-start phase until the engine reaches the steady-state fast-idle conditions. The rate of the change of exhaust manifold content mass between two consecutive firing events' EVO is calculated as follows,

$$\Delta m_{man}[k] = \frac{P_{exh_{EVO}}[k] \cdot V_{man}}{R_{exh} \cdot T_{exh_{EVO}}[k]} - \frac{P_{exh_{EVO}}[k-1] \cdot V_{man}}{R_{exh} \cdot T_{exh_{EVO}}[k-1]} \tag{3.7}$$

Where, k is the event number, V_{man} is the exhaust manifold volume, R_{exh} is the gas

constant of the exhaust gas constantly equal to $277\frac{J}{kg.K}$, and $P_{exh_{EVO}}$ and $T_{exh_{EVO}}$ are the exhaust manifold pressure and temperature at EVO. Air charge model calibrated using the GT-Power TPA simulated results estimate the $T_{exh_{EVO}}$. Then, the correlation between the mass of exhaust gas enters into the exhaust manifold from the cylinder, $m_{cyl_{out}}$ to the mass of exhaust gas is exhausted out of the exhaust manifold, m_{manout} is calculated,

$$m_{cyl_{out}}[k] = m_{man_{out}}[k] + \Delta m_{man}[k] \tag{3.8}$$

In addition, it is assumed that the exhaust gas flowing out the exhaust manifold is a mix of the exhaust gas that has remained inside the exhaust manifold from the previous events, $m_{man_{mix}}$ and the exhaust gas entering into the exhaust manifold from the current event, $m_{cyl_{out}}$,

$$m_{man_{out}}[k] = m_{man_{mix}}[k-1] + m_{cyl_{out}}[k] \tag{3.9}$$

In other words, a portion of the exhaust gas entering into the exhaust manifold from the current event, equal to $m_{man_{mix}}$, remains inside the exhaust manifold as a residual to the next event. Therefore, the exhaust manifold residual coefficient is defined as below,

$$k_{res}[k] = \frac{m_{man_{mix}}[k-1]}{m_{cyl_{out}}[k]} \tag{3.10}$$

The exhaust manifold residual coefficient was derived experimentally for different engine speeds and loads cylinder-by-cylinder. For this purpose, the engine speed and load range were determined 750 to 1600 RPM and 1 to 8 bar, respectively, based on the cranking speed and MAP variation limits during cold crank-start tests. Then, the engine is run in the steady-state conditions at the defined cold crank-start speeds and loads with the PCM's commanded injection amount for stoichiometric conditions. The injected fuel amount is changed manually to 75% of the stoichiometric condition cylinder-by-cylinder. It is assumed if any exhaust gas from the previous events is not mixed with the exhaust gas coming out of the event with 25% less injected fuel amount, the measured CO2 value should decrease the same amount. Therefore, the difference between the measured average CO2 with 25% reduced fuel injection amount and 25% decreased CO2 from the stoichiometric conditions shows how many percent exhaust gas was mixed from the previous events to the current event scavenged exhaust gas. Figure 3.18 shows the experimental result of the above-mentioned test at 1600 RPM engine speed and 59 kPa MAP for cylinder 1. As it is seen, the measured CO2 mass shows a decrease from 197.1 mg to 175.3 mg, whereas a 25% decrease in CO2 mass would result in 147.8 mg. As a result, 27.5 mg exhaust gas equal to 16% of the total exhaust gas should be flowed out of the exhaust manifold from the current event belonged to the previous events and was mixed with the exhaust gas scavenged from cylinder 1. The above-mentioned method was repeated for all cylinders in different engine speeds and loads defined above.

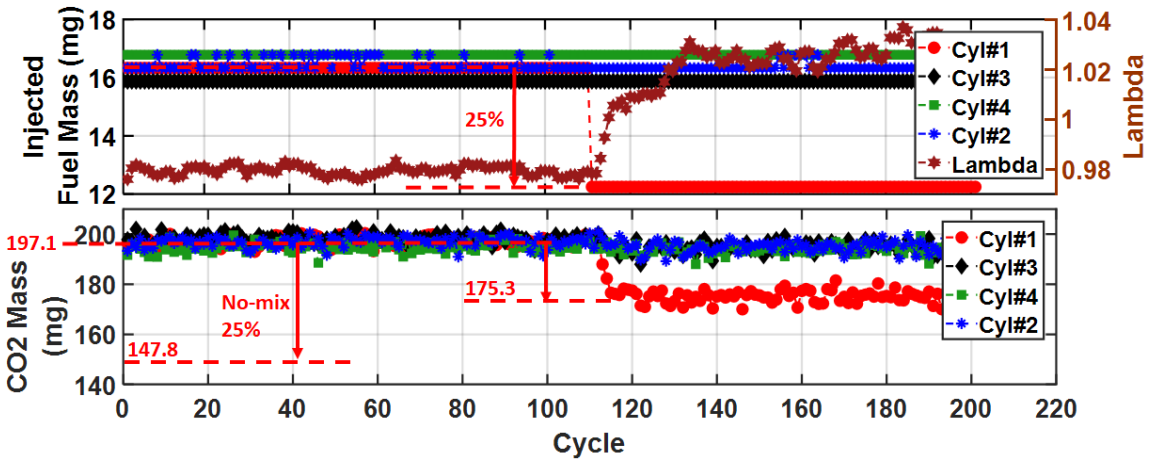

Figure 3.18: The steady-state test for determination of the exhaust manifold residual coefficient at 1600 RPM engine speed and 59 kPa MAP for cylinder 1.

Another important phenomenon for the exhaust gas in the exhaust manifold, especially in highly late-burn conditions, is the unburnt HC post oxidization. The post oxidization dynamics is more significant and requires more investigation when partial burn or misfire occur. For the normal combustion, the post oxidization coefficient, k_{pox} is assumed to be constant and defined experimentally. The uncertainty the post oxidization coefficient change can impose on the precision of the engine-out emissions translation will be analyzed later in this study.

3.3.6 Emissions Concentration Translation

This section represents how the GT-Power TPA, adapted air charge model, charge loss, and exhaust gas dynamics outputs are combined to translate the engine-out

emissions concentration to mass per cycle per cylinder. From the mass conservation and considering the cylinder combustion chamber as the control volume, the mass of gas exhausted out of the cylinder is estimated event-based as the following,

$$m_{cyl_{out}}[k] = m_{air}[k] + m_{fuel_{inj}}[k] - m_{charge_{loss}}[k] - m_{fuel_{res}}[k] - \Delta m_{res}[k] \qquad (3.11)$$

Where, m_{air} is the trapped air mass at IVC, and Δm_{res} is the cycle-by-cycle change rate of the residual gas mass during the cold crank-start estimated by the air charge model, and $m_{fuel_{inj}}$ is the total injected fuel into the cylinder calculated from the measured injection pulse width. $_{res}$ does not change cycle-by-cycle substantially and Δm_{res} tends to zero after the cold start first cycles pass, and the engine enters to the fast idle steady-state conditions, while the engine speed, MAP, and cam phasing remain constant.

The charge loss is the sum of the in-cylinder gas loss through the blow-by, m_{bb}, and liquid fuel is absorbed into the oil, $m_{fuel_{oil}}$,

$$m_{charge_{loss}}[k] = m_{bb}[k] + m_{fuel_{oil}}[k] \qquad (3.12)$$

The total injected fuel into the cylinder in the current cycle can be divided into the fuel, which is contributed to the combustion in the same cycle and burnt, m_{fuel_b}, and

the fuel remains unburnt, $m_{fuel_{ub}}$,

$$m_{fuel_{inj}}[k] = m_{fuel_b}[k] + m_{fuel_{ub}}[k] \tag{3.13}$$

The GT-Power TPA model estimates the mass of burnt fuel. The unburnt fuel either remains inside the cylinder as residual fuel, or is lost through blow-by gas, $m_{bb_{fuel}}$, or absorbs to the oil, or is exhausted out of the cylinder as unburnt hydrocarbon, $m_{HC_{cyl}}$,

$$m_{fuel_{ub}}[k] = m_{fuel_{res}}[k] + m_{bb_{fuel}}[k] + m_{fuel_{oil}}[k] + m_{HC_{cyl}}[k] \tag{3.14}$$

The exhaust manifold is considered the control volume, including HC post oxidization and mixed residual exhaust gas effects. Therefore, the unburnt hydrocarbon flowing out of the exhaust manifold from the current cylinder event EVO to the next cylinder event EVO, $m_{HC_{out}}$, is correlated to the unburnt hydrocarbon evacuated out of the cylinder as following,

$$m_{HC_{out}}[k] = m_{HC_{cyl}}[k] - k_{pox}[k]m_{HC_{cyl}}[k] - k_{res}[k]m_{HC_{cyl}}[k] \tag{3.15}$$

The molar mass of the unburnet HC flowing out of the exhaust manifold measured

by FFID, $y_{HC_{out}}$ is converted to mass as following,

$$m_{HC_{out}}[k] = y_{HC_{out}}[k] \cdot \frac{M_{fuel}}{M_{exh}} \cdot m_{man_{out}}[k] \tag{3.16}$$

Where, M_{fuel} and M_{exh} are the molar masses of the fuel and exhaust gas. M_{fuel} is considered equal to 100.1 for E10 fuel. The exhaust gas is assumed to be a complete burnt gas, neglecting the share of the unburnt HC. Therefore, M_{exh} is considered equal to 29 $\frac{kg}{kmol}$ [11]. From the combination of the equations (8) and (11) to (16), and assuming the mass of vaporized fuel is lost through the blow-by is negligible, the mass of exhaust gas flowing out of the exhaust manifold from the current cylinder event EVO to the next cylinder event EVO is determined by,

$$m_{man_{out}}[k] = \frac{m_{air}[k] + m_{fuel_b}[k] - m_{bb}[k] - \Delta m_{res}[k] - \frac{y_{HC_{out}}[k]\frac{M_{fuel}}{M_{exh}}\Delta m_{man}[k]}{1-k_{pox}-k_{res}}}{1 - \frac{y_{HC_{out}}[k]\frac{M_{fuel}}{M_{exh}}}{1-k_{pox}-k_{res}}} - \Delta m_{man}[k] \tag{3.17}$$

The mass of the residual fuel from the first cycle to the next cycle is an input required for the air charge model. Residual fuel is estimated as below,

$$m_{fuel_{res}}[k] = m_{fuel_{inj}}[k] - m_{fuel_b}[k] - m_{HC_{cyl}}[k] - m_{bb_{fuel}}[k] - m_{fuel_{oil}}[k] \tag{3.18}$$

Here, the total lost fuel through the blow-by gas and absorption to the oil at the first cycle is assumed to be constantly 20% of the total injected fuel [49]. This will be discussed and validated based on the equivalent combusted fuel mass estimated by GT-Power TPA and the translated experimental unburnt HC data in the method validation section. Moreover, the residual fuel mass does not directly influence the emissions translation and is used as an input to the air charge model. The uncertainty that the lost fuel fraction can impose on the engine-out emissions translation through variation of the residual fuel mass will be analyzed later in this section.

Figure 3.19 shows the concept block diagram of the method is used for the emissions concentration dynamic translation to mass per cycle per cylinder, including the different components' interrelations. The cylinder, intake, and exhaust pressure traces are the primary inputs to the method. Besides, the total injected fuel mass is calculated using the measured injection pulse width. The method consists of five major components: the GT-Power TPA, adapted air charge and residual gas model, CFD analysis, fueling, and individual-cylinder engine-out emissions. The GT-Power TPA estimates the in-cylinder gas temperature and trapped air and residual gas masses for calibration and validation of the adapted air charge model. In addition, the GT-Power TPA calculates the equivalent combusted fuel and blow-by gas masses, which are used as inputs to fueling and adapted air charge, respectively. The CFD analysis estimates the vaporized fuel fraction based on in-cylinder pressure and temperature and total injected fuel mass and delivers it to the air charge model. The fueling

component calculates the unburnt fuel mass from the total injected fuel mass and equivalent combusted fuel mass from the GT-Power TPA. Then, the unburnt fuel is decomposed to the lost fuel, residual fuel, and unburnt HC scavenged out of the cylinder. Finally, the individual cylinder engine-out emissions component considers the exhaust manifold dynamics to translate the engine-out emissions to mass per cycle per cylinder using the estimated variables from other components.

exhaust gas dynamic

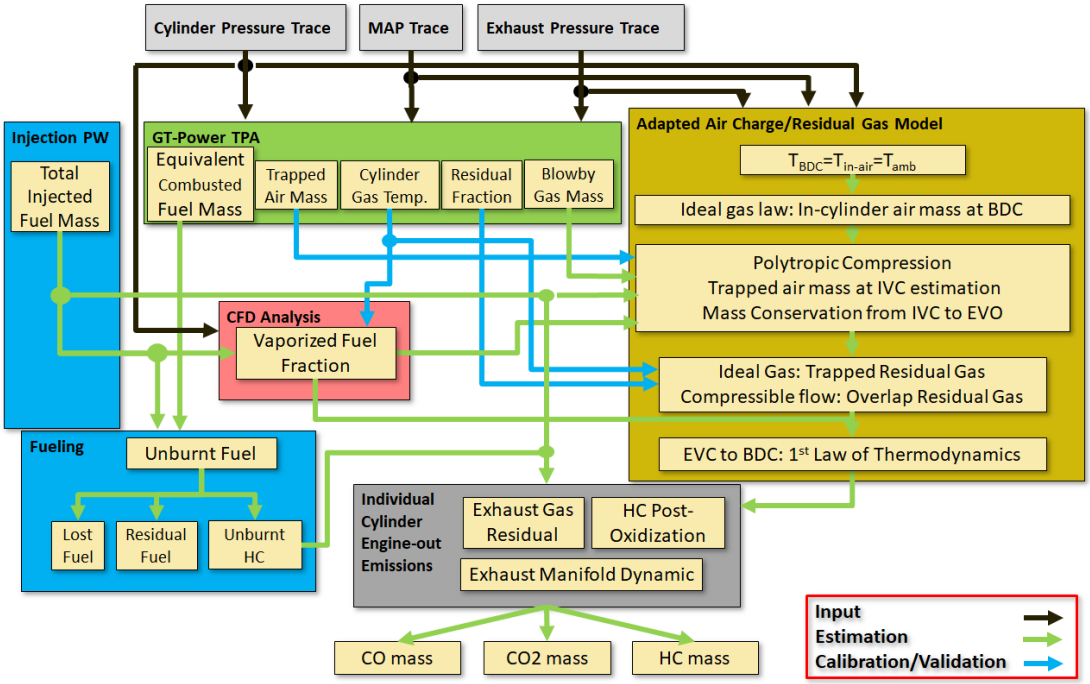

Figure 3.19: Concept block diagram of the method for dynamic translation of the emissions concentration to mass per cycle per cylinder

3.4 Validation and Results

3.4.1 Calibration and Validation

The first step in using the method from section 3.3 for dynamic translation of the measured engine-out emissions concentration to mass per cycle per cylinder was calibration and running the GT-Power model for each experiment cylinder-by-cylinder. The results from the GT-Power TPA, including the mass of in-cylinder trapped air, residual gas, and the burnt gas temperature during the exhaust stroke, were used to calibrate the air charge model. In addition, the mass of blow-by gas and equivalent combusted fuel from the GT-Power TPA were given as inputs to the air charge model and emissions concentration translation part. Figure 3.20 represents the cylinder pressure traces coincidence for the first firing of the experiment shown in Figure 3.7 after the GT-Power model calibration. The table in Figure 3.20 includes the simulated results of the calibrated GT-Power model. The GT-Power TPA results showed that the calibrated GT-Power model estimated the IMEP and trapped air mass with 1.7% and 1.8% errors, respectively. One reason for the 1.8% error in the estimation of the trapped air charge is cylinder-to-cylinder air induction variation. The residual gas, which consists of air for the first cycle, was predicted 85.7 mg, resulting in a 24% residual fraction for 40 CAD valve overlap. To produce 7.16 bar IMEP, GT-Power

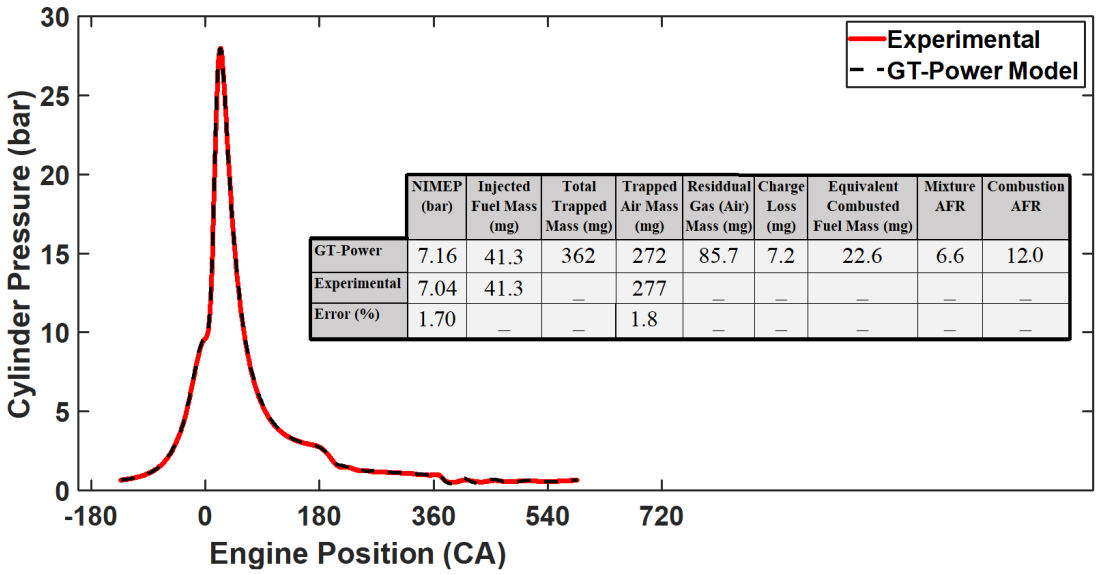

	NIMEP (bar)	Injected Fuel Mass (mg)	Total Trapped Mass (mg)	Trapped Air Mass (mg)	Residdual Gas (Air) Mass (mg)	Charge Loss (mg)	Equivalent Combusted Fuel Mass (mg)	Mixture AFR	Combustion AFR
GT-Power	7.16	41.3	362	272	85.7	7.2	22.6	6.6	12.0
Experimental	7.04	41.3	_	277	_	_	_	_	_
Error (%)	1.70	_	_	1.8	_	_	_	_	_

Figure 3.20: Calibrated GT-Power model for the engine conditions given in Figure 3.7 with results

TPA showed that 22.6 mg of the 41.3 mg total injected fuel was contributed to the combustion. Therefore, the mixture and combustion AFRs were 12 and 6.6, respectively. The combustion AFR was calculated as the proportion of trapped air mass to the equivalent combusted fuel mass, and mixture lambda was the proportion of the trapped air mass to the total injected fuel mass. Finally, the GT-Power TPA model estimated about 2% of the total trapped mass, equal to 7.2 mg, was lost through blow-by. The GT-Power TPA model used the leak path equivalent diameter equal to 0.88 mm, calculated by the charge loss part, as input for estimating the mass of blow-by gas.

Here, both fuel injections occurred during the compression stroke. Therefore, these injections were considered in the IVC to EVO mass conservation calculation in the air

charge model. For the cases that the first injection happens late in the intake stroke, for example, at 205 CAD before TDC firing for 1.5 msec equal to 15 CAD, and at the cylinder pressure 46 kPa and temperature 345 K, only 6% of the fuel is vaporized before BDC compression based on the CFD analysis results that discussed in section 3.3.4. The vaporized fuel fraction, here 6%, was given as an input to the air charge model energy balance calculation from EVC to BDC compression. The exhaust gas dynamics calculations showed the exhaust gas flowing out of the exhaust manifold consisted of 15.7% mixed from the previous events and 84.3% of the exhaust gas evacuated out of the current cylinder event. Therefore, the exhaust manifold residual coefficient of 15.7% was used for 1600 RPM cranking speed and 7 bar IMEP.

The developed method was calibrated and used to translate the engine-out emissions concentration into the mass per cycle per cylinder in 48 different cold start tests, which will be determined later based on DOE analysis method. As mentioned before, the engine speed, MAP, and engine inlet air mass flow are in the steady-state conditions after three-sec motoring in motored high cranking speed cold start conditions, as shown in Figure 3.10. Therefore, the measured engine inlet air mass flow can be appropriately used for GT-Power TPA estimated trapped air mass validation with adequate precision. Figure 3.21 shows the calibrated GT-Power TPA and adapted air charge model individual-cylinder estimated trapped air mass against the LFE air mass meter experimental data for the cold start first cycle of the 36 tests of the first step of DOE tests, which will be defined later in DOE analysis section. The average

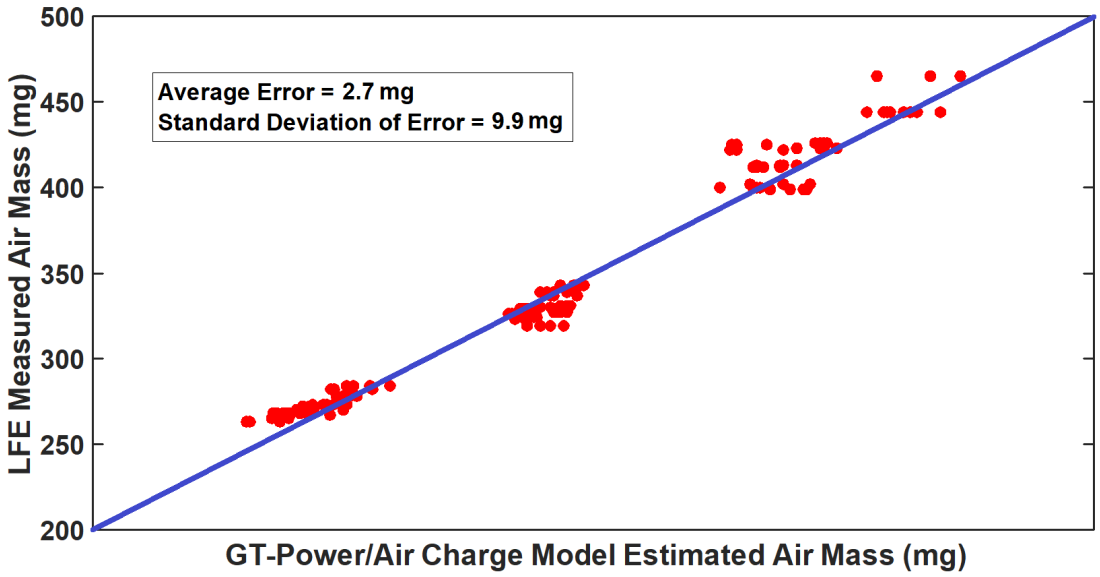

Figure 3.21: The GT-Power TPA and adapted air charge model estimated air mass versus the LFE air mass meter data for the cold start first cycle

error and standard deviation of error are 2.7 and 9.9 mg, respectively.

Figure 3.22 shows the calibrated GT-Power TPA model individual-cylinder estimated IMEP against the CAS calculated IMEP based on the experimental cylinder pressure trace for the cold start first three cycles of the 36 experiments. The average error and standard deviation of error are 0.06 and 0.05 bar, respectively. Figures 3.21 and 3.22 show that the GT-Power TPA model was calibrated precisely enough for the first three cycles of 36 experiments. Therefore, other estimated parameters from the calibrated GT-Power TPA, such as residual fraction and equivalent combusted fuel mass, can be used with adequate precision in the developed method to translate the engine-out emissions concentration to mass per cycle per cylinder.

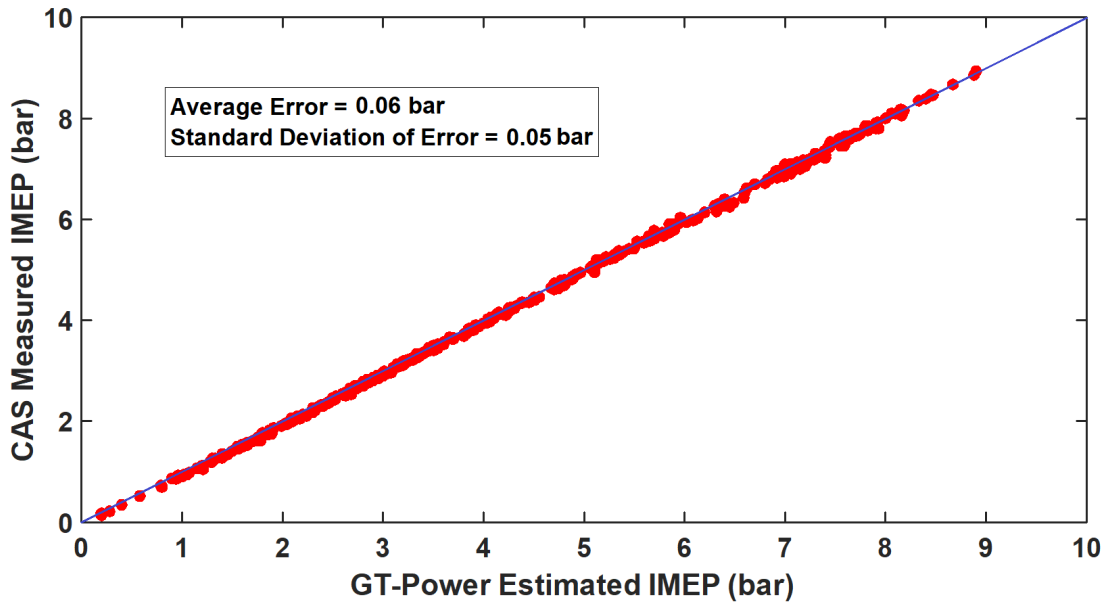

Figure 3.22: The GT-Power TPA estimated IMEP versus CAS measured IMEP for the cold start first three cycles

3.4.2 DOE Analysis

Design of Experiments (DOE) techniques help determine concurrently the individual and interactive effects of factors that can influence the outputs of the developed model. Using DOE, an insight of interaction between design elements is achieved, facilitating a robust design. In this study, a two-step multi-level fractional-factorial DOE method was used to prepare a test plan for the experimental data. The main objective of the test plan was to analyze the impact of the most important factors on the engine-out emissions during the cold crank-start conditions with a minimum number of test points.

Table 3.3 describes a list of essential factors that could influence the engine-out emissions during the cold crank-start phase in two rows. The upper row represents the engine and throttle position, engine speed, spark, and valve timing. The lower row depicts the fuel injection parameters. Then, the effect of each factor on the engine-out emissions during the cold crank-start was analyzed. This analysis was based on the results of the works already carried out and represented in the literature and experimental data from the tests accomplished in this study. The DOE factors investigation results showed that the number of motoring cycles before the first firing and first firing cylinder does not significantly influence the engine-out emissions during the cold crank-start conditions.

The throttle position profile and the AFR of the second cycle and on were controlled by the production PCM based on the calibration. The PCM was calibrated that the engine followed the elevated HEV cranking speed crank-start profile. The fuel pressure increased to the normal engine operating value of 100 bar from the first firing due to the motoring, was considered the optimal value for the DOE tests. One intake injection and one compression injection with a split ratio equal to 0.5 were used for the split injection strategy based on the PCM software functions and calibration. Finally, cranking speed, spark timing, valve timing, first cycle fuel factor, and SOI and EOI in the split injection strategy were chosen as the most dominant factors affecting the engine-out emissions during the cold crank-start phase, shown in bold in Table 3.3.

Table 3.3
Factors affecting the engine-out emissions during the cold crank-start conditions

Motoring Cycles (Delay to First Firing)	Engine Position (First Firing Cylinder)	**Engine Cranking Speed**	Throttle Position (MAP)	**Spark Timing**	**Valve Timing**	
					Intake Advance	**Exhaust Retard**
Fuel Injection			**Split Injection Strategy**			
Fuel Pressure	**First Cycle Fuel Factor**	Cycle 2nd and on AFR	Number of intake injections	Number of compression injections	**SOI intake**	**EOI Compression**	**Split Ratio**

Next, the selected factors' levels were determined, comprising the low, medium, and high levels. The factors' low and high levels were defined experimentally, considering the stability limit of the engine. As a result, three levels were considered for the cranking speed, including 600 RPM as the closest point to the conventional cranking speed, mid-point equal to 1100 RPM, and 1600 RPM as the elevated HEV cranking speeds. The spark timing levels were defined -10, 0, and 14 CAD aTDC to capture advanced, retarded, and highly-retarded spark timing effects on the engine-out emissions. The valve timing levels comprised intake advance and exhaust retard. The intake valve levels included 0 and 20 CAD advance. Also, 0 and 20 CAD were assigned for the exhaust valve retard. These points covered 40 CAD highly overlap, 0CAD parking position, and 20 CAD moderate overlap conditions. This provided analysis of no valve overlap, 40 CAD high valve overlap, and 20 CAD intake advance and exhaust retard independent effects on the engine-out emissions. The number of tests decreased from 432 tests to 48 tests using the two-step method DOE, while all the essential parameters effects on the engine-out cold crank-start emissions were evaluated. The first step included the cranking speed, spark timing, and valve timing sweep while the fuel injection parameters were under the control of the PCM. The

injection fuel amount at the first cycle, the second cycle, and on AFR, the first and second fuel injection timings and split ratio were kept constant by PCM. Then, the optimal cranking speed, spark timing, and valve timing resulting in the minimum HC emissions were determined. Table 3.4 describes the first step of DOE tests, including 36 tests.

What is shown in Table 3.4 for the spark timing levels are, in fact, the initial value of the spark timing for the first firing events. Figure 3.23 represents the complete profile of the ignition timing for the first three cycles of the cold start dynamic tests. As seen, for highly retarded spark timing, the spark timing is constantly equal to 14 CAD aTDC from the first firing to the end of the third cycle. For two other spark timings, including 0 and -10 CAD aTDC, the spark timing remains at the initial value during the first 7 events. It tends gradually to 14 CAD aTDC highly retarded catalyst warm-up phase target value from the end of the third cycle.

At the second step of the DOE tests, the fuel injection parameters were swept while cranking speed, spark timing, and valve timing was kept constant at their optimal values from the first step of DOE tests. Two levels were considered for the first

Table 3.4
Cold crank-start first cycles emissions DOE tests carried out in step 1

Factors	Cranking Speed (RPM)			Spark Timing (CAD aTDC)			Intake Advance (CAD)		Exhaust Retard (CAD)	
Levels	Low	Medium	High	Low	Medium	High	Low	High	Low	High
Quantity	600	1100	1600	-10	0	14	-20	0	0	20
Points	3			3			2		2	

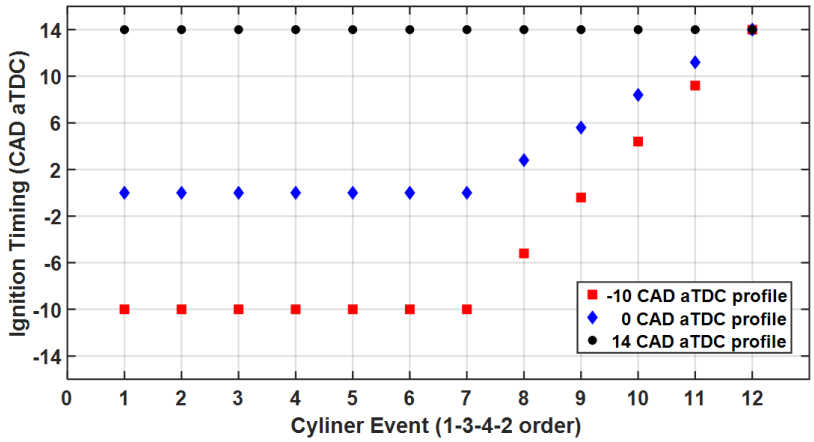

Figure 3.23: The cold start first cycles experiments' ignition timing profiles

cycle fuel factor, 1.15 and 1.45, in addition to the high fuel factor for high cranking speed, 1.65, that were applied and analyzed during the first step of the DOE tests based on the PCM conventional calibration. This helped to understand the effects of the low and moderate fuel factor on the engine-out emissions, comparing with the conventional high fuel factor results from the first step of the DOE tests. The levels of the SOI of the first injection were defined as 205 and 145 CAD bTDC firing. These two levels, along with the 165 CAD bTDC firing as SOI applied automatically by PCM during the first step of the DOE tests, helped investigate the effects of the SOI on the engine-out emissions for late intake and early and middle of compression first injection. The literature review and experimental data from the previous works at the conventional cranking speed utilizing split injection strategy showed the EOI of the second injection had a significant effect on the engine-out emissions during the cold crank-start conditions. An optimally selected EOI could create a local rich mixture before the spark, improving the combustion. Therefore, three different levels were

Table 3.5
Cold crank-start first cycles emissions DOE tests carried out in step 2

Factors	Start Factor		Split Ratio	SOI (CAD bTDC Firing)		EOI (CAD bTDC Firing)		
Levels	Low	High	Medium	Low	High	Low	Medium	High
Quantity	1.15	1.45	0.5	145	205	0	30	60
Points	2		1	2		3		

defined for EOI, including 60, 30, and 0 CAD bTDC, to investigate its effects on the engine-out emissions for far, near, and adjacent to spark conditions. Table 3.5 lists the second step of DOE tests, including 12 tests. Finally, a two-step fractional-factorial multi-level DOE test plan was derived to conduct the required experiments for a complete analysis of the engine-out emissions during the cold start first cycles. The DOE test plan totally comprised 48 tests, including 12 tests from the first step and 36 tests at the second step, 12 tests. Each selected factor was tested on the experimental engine at its defined levels during the DOE tests while all other factors were kept constant.

3.4.3 Results and Discussion

The developed method in section 3.3 was used to translate the engine-out emissions concentration to mass per cycle per cylinder for the accomplished 48 tests. Figure 3.24 represents the engine speed and MAP dynamics during the cold crank-start phase in different cranking speeds to better understand the effect of the engine transient

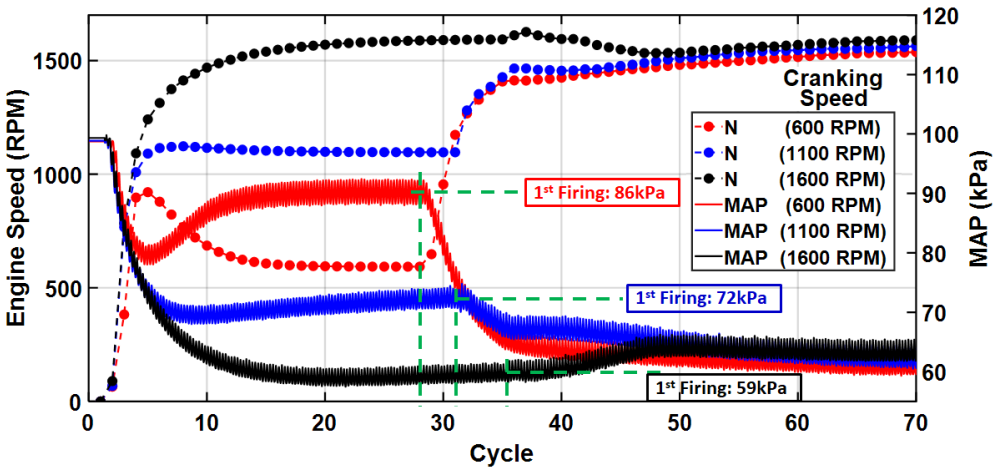

Figure 3.24: Engine speed and MAP dynamics during the motored cold crank-start

behavior on the developed method results. Based on the PCM software and calibration, especially the throttling, the MAP at the first firing is higher at lower cranking speeds and tends to similar value after three to five cycles. Therefore, for 600 and 1100 RPM, there are MAP dynamics during the cold-start first cycles, whereas for 1600 RPM, the MAP has already been stabilized at the low target fast-idle value.

Figure 3.25 represents the engine operating conditions and developed method important intermediate variables and output parameters for cold crank-start first three cycles. All plots include 12 consecutive events, showing the results from sweeping of the cranking speed, intake valve advance (Int-Adv), and exhaust valve retard (Exh-Ret) at constant spark timing, 0 CAD aTDC, and fuel injection parameters. Figure 3.25 (a), (b) and (c) show how IMEP, trapped air mass, and mixture lambda change event-by-event from the first firing. The mixture lambda was calculated based on the total injected fuel mass and trapped air mass. Higher MAP in lower cranking

speeds in the first cycle resulted in higher trapped air mass and higher IMEP at approximately similar injected fuel mass. Therefore, the mixture lambda was richer for higher cranking speeds due to the reduced trapped air mass.

Generally, the trapped air mass at the first cycle was significantly higher than the next cycles due to air as residual gas from the last motoring cycle to the first firing cycle. After the first cycle, the trapped air mass decreased gradually for 600 and 1100 RPM cranking speeds pursuing the MAP dynamics. For 1600 RPM, the MAP has already been stabilized in a lower fast-idle target value, which results in a trapped air mass sudden decrease, as it is seen in Figure 3.25 (b). Figure 3.25 (e) depicts that the first cycle fuel factor (FF) is higher in higher cranking speeds due to the lower trapped air mass with similar commanded injected fuel mass. The mixture lambda for cycle 2 and on is richer for higher cranking speeds due to lower trapped air mass and the PCM fast-idle open-loop lambda control strategy, as shown in Figure 3.25 (c). The combustion lambda was derived using the AFR calculated from the trapped air mass, and the fuel mass contributed to the combustion. Figure 3.25 (d) shows that the combustion lambda is closer to stoichiometric conditions for high cranking speed. The combustion lambda shows a leaner combusted mixture for lower cranking speeds. The estimated mass of the residual gas was lower for the higher cranking speed, as shown in Figure 3.25 (f). The mass of the exhaust gas flowing out of the exhaust manifold reduced event-by-event as the cold air already filled in the exhaust manifold during the motoring cycles was gradually replaced by hot burnt exhaust

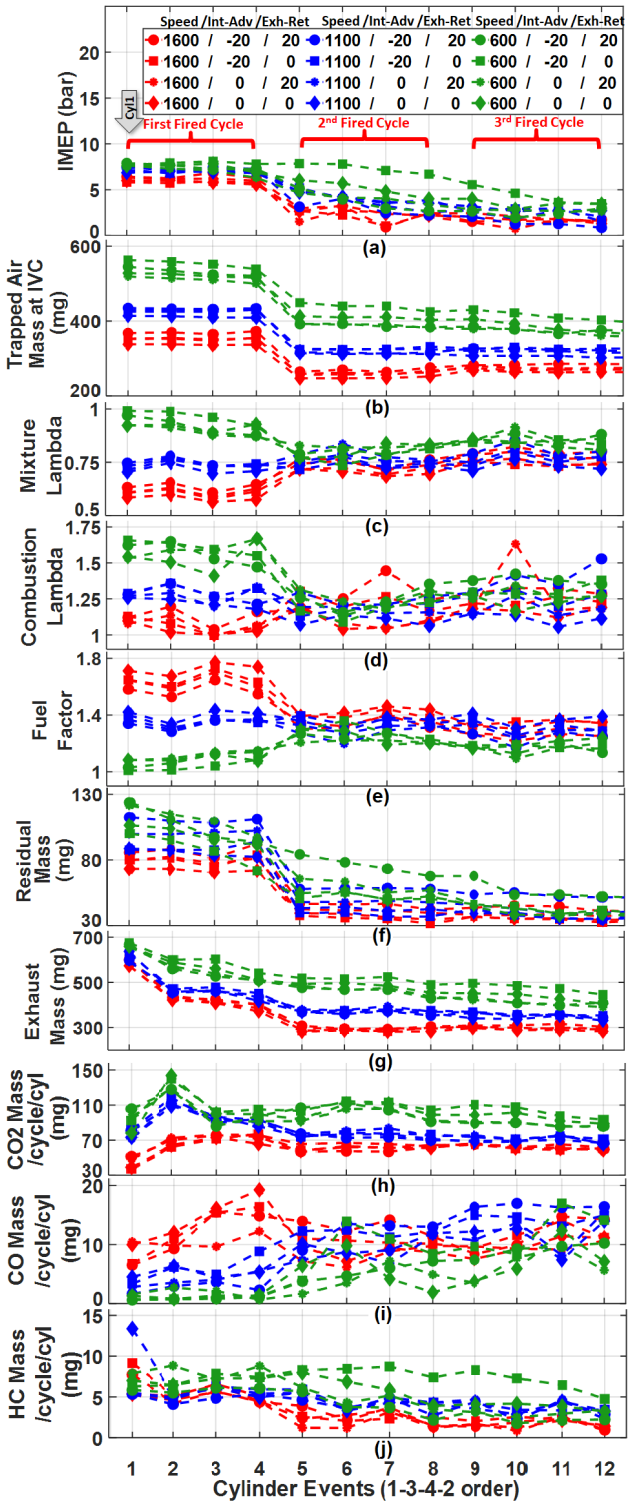

Figure 3.25: Cold start first three cycles operating conditions and engine-out emissions at constant 0 CAD aTDC spark timing

gas, as shown in figure 3.25 (g). In addition, the mass of engine-out exhaust gas was higher for lower cranking speed following the mass of trapped air, residual gas and equivalent combusted fuel dynamics.

Figure 3.25 (h), (i) and (j) show the developed method's translated individual-cylinder engine-out CO/CO2 and HC emissions. The cranking speed of 1600 RPM results in significantly lower HC emissions, especially from the second cycle and on, as shown in Figure 3.25 (j). Figure 3.25 (i) shows CO emission rises with increasing the cranking speed in the first cycle. For the second cycle and on, CO emission is slightly higher for higher cranking speeds. Despite having a similar injected fuel mass at the first cycle for different cranking speeds, CO2 emission is higher for lower cranking speeds, as shown in Figure 3.25 (h). After the first cycle, CO2 emission is lower at high cranking speed because of lower injected fuel mass.

Figure 3.26 shows the engine operating conditions and developed method output parameters for cold crank-start first three cycles, sweeping the spark timing and valve timing at constant cranking speed, 1600 RPM, and fuel injection parameters. Retarded spark timing resulted in lower IMEP, as shown in Figure 3.26 (a). Figure 3.26 (b) and (f) show that the mass of trapped air and residual gas did not change significantly while spark timing varied. The mixture lambda and combustion lambda followed the trapped air and injected fuel mass dynamics and did not vary considerably with spark timing change, except for the events with partial-burn combustion, as

shown in figure 3.26 (c) and (d). For the partial-burn events, the combustion lambda shows very lean values. Figure 3.26 (e) shows that the first cycle fuel factor is also similar for different spark timing based on the PCM calibration. The mass of exhaust gas flowing out of the exhaust manifold did not change remarkably with the spark timing variation following the dynamics of the trapped air, residual gas, and equivalent combusted fuel, as shown in Figure 3.26 (g). The exhaust gs flowing out of the exhaust manifold got equal to the exhaust gas scavenged out of the cylinder when the transition of the exhaust manifold content from the cool air to the hot burnt exhaust gas, and the engine speed and MAP changes were passed, and the engine entered to the steady-state fast idle mode.

The developed method's translated individual-cylinder engine-out CO/CO2 and HC emissions are shown in Figure 3.26 (h), (i), and (j). Retarded spark timing resulted in a lower HC emissions during the first and second cycles, as shown in Figure 3.26 (j), due to the crevice volume to total volume ratio reduction, lower pressure in the Crevice volume, more time for vaporization and mixing, and a higher post-oxidization effect. Furthermore, the mass of CO/CO2 and HC emissions did not trend with combustion lambda dynamics for the events, including partial-burn, because a significant portion of the fuel flowed out of the cylinder as unburnt HC was post-oxidized in the exhaust manifold. Figure 3.26 (i) shows that the CO emission is also lower for highly retarded spark timing conditions during the first and second cycles. This helped resolve high CO emissions in high cranking speed conditions to some extent. Figure 3.26 (i) and

(j) show that high valve overlap for highly-retarded spark timing conditions results in twofold HC and CO emissions reduction at the first and second cycles. To sum up, 1600 RPM cranking speed, 14 CAD aTDC spark timing, and 40 CAD valve overlap were found as the optimal point of the first step DOE tests with minimum HC emissions.

Figure 3.27 shows the average NOx emission emitted from the engine during the first three cycles for the first step of DOE tests. The NOx emission was estimated using the Extended-Zeldovich model in GT-Power TPA. The results show that NOx emission is significantly lower for highly-retarded spark timing due to the low cylinder peak pressure resulting in lower peak temperature.

The second step of the DOE tests was carried out at the optimal cranking speed, spark timing, and valve timing concluded from the first step. Figure 3.28 represents results from 5 tests out of the second step 12 DOE tests giving the lowest HC emissions for the cold-start first three cycles. Reduced fuel factor to 1.15, late intake first injection at 205 CAD bTDC firing, and 60 CAD bTDC firing EOI of the second injection resulted in the lowest HC emissions for the first cycle. This is because the engine speed has already been increased to 1600 RPM during the motoring phase. As a result, the conventional engine run-up phase, including the rapid speed increase from 280 RPM to 1250 RPM, which requires high fuel injection for guaranteeing the start quality, does not exist in the HEV elevated cranking speed cold crank-start conditions.

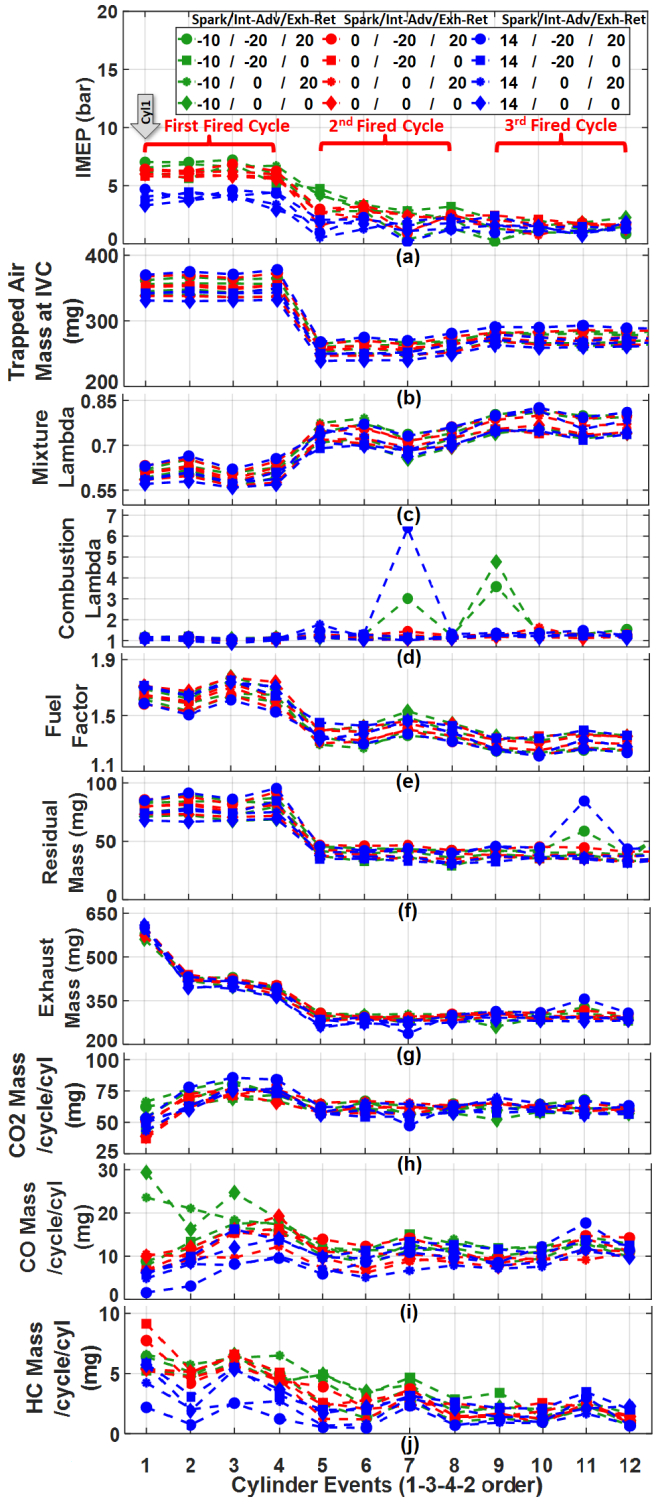

Figure 3.26: Cold start first three cycles operating conditions and engine-out emissions at constant 1600 RPM cranking speed

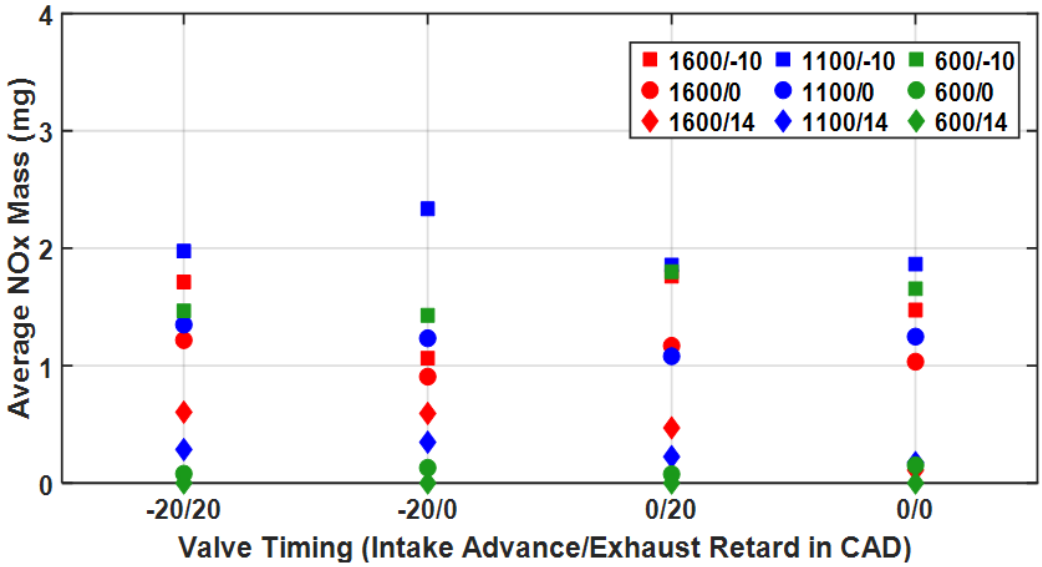

Figure 3.27: The first three cycles average NOx emission mass for the first step of the DOE tests

However, this test point shows higher HC emissions for the second and third cycles than the experiment with moderate fuel factor, 1.45, late intake first injection at 205 CAD bTDC firing, and 30 CAD bTDC firing EOI. This can be due to the leaner combusted mixture at the second and third cycles because of the low first cycle fuel factor and decreased residual fuel from the first cycle to the next cycles.

Figure 3.29 represents the first, second, and third cycles and entire three cycles accumulated HC emissions trend for the entire DOE tests, including arrows showing the HC emissions change trend versus cranking speed, spark timing and valve timing. The results showed the HC emissions reduction trend with the cranking speed increase, except for the test points, including partial-burn or misfire events, as highlighted with vertical green arrows on the Figure 3.29. In Figure 3.29, the horizontal

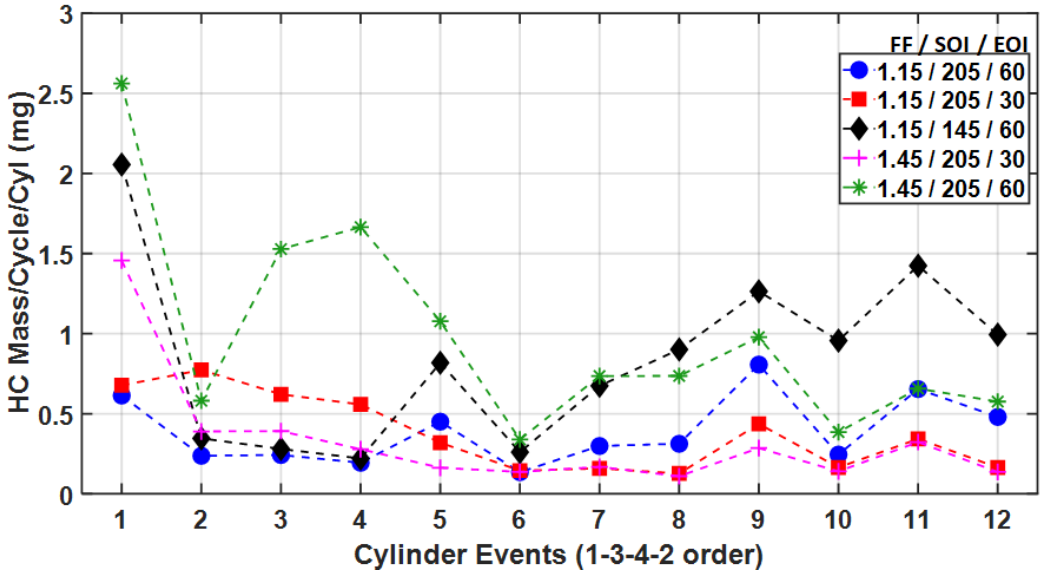

Figure 3.28: The best results for the HC emissions in the second step of the DOE tests

brown Arrows show the HC emissions trend based on the valve timing change. For the first cycle, the HC emissions trend versus valve timing demonstrated that no overlap condition results in slightly lower HC emissions at low cranking speed. However, with increasing the cranking speed, the high overlap condition gives a better result. High valve overlap led to additional trapped air mass and a very lean mixture due to high MAP and air as residual gas in the first cycle for low cranking speed. However, increasing the cranking speed was accompanying by MAP reduction resulting in lower trapped air mass. Therefore, the high overlap benefited high cranking speed conditions to increase the trapped air mass and prevent excessive rich mixture with the same amount of injected fuel. The HC emissions trend versus valve timing clearly showed the high valve overlap conditions for the second and third cycles resulted in lower HC emissions for all cranking speeds. The high valve overlap led to higher hot

residual exhaust gas at cycles two and three, improving the fuel vaporization rate and mixture preparation quality. The optimal points from the first step of DOE tests and for the first cycle and total three cycles highlighted with a red box at the legend of the Figure 3.29. As a result, the optimal point with minimum total first three cycles HC emissions from the first part of the DOE tests belonged to high cranking speed and high overlap conditions.

The optimal point from the first step of the DOE tests was indicated, and the test results with the lowest HC emissions from the second part of the DOE tests have been zoomed in for better analysis in Figure 3.29. The zoomed-in plot depicts that the low fuel factor, 1.15, with late intake first injection at 205 CAD bTDC firing, and EOI at 60 CAD bTDC firing gave the minimum HC emissions result for the first cycle. For the second and third cycles, the lowest HC emissions was achieved with a moderate fuel factor of the first cycle equal to 1.45. Increasing the fuel factor in the first cycle from 1.15 to 1.45 resulted in higher residual fuel from the first cycle to the next cycle. As a result, higher residual fuel mostly vaporized during the first cycle expansion stroke helped improve the second and third cycles' air-fuel mixture and combustion.

For the EOI in the first cycle, 60 CAD bTDC firing resulted in two times lower HC emissions comparing to 30 CAD bTDC firing. The first cycle comprises the lowest in-cylinder trapped mixture temperature due to the lack of hot residual exhaust gas

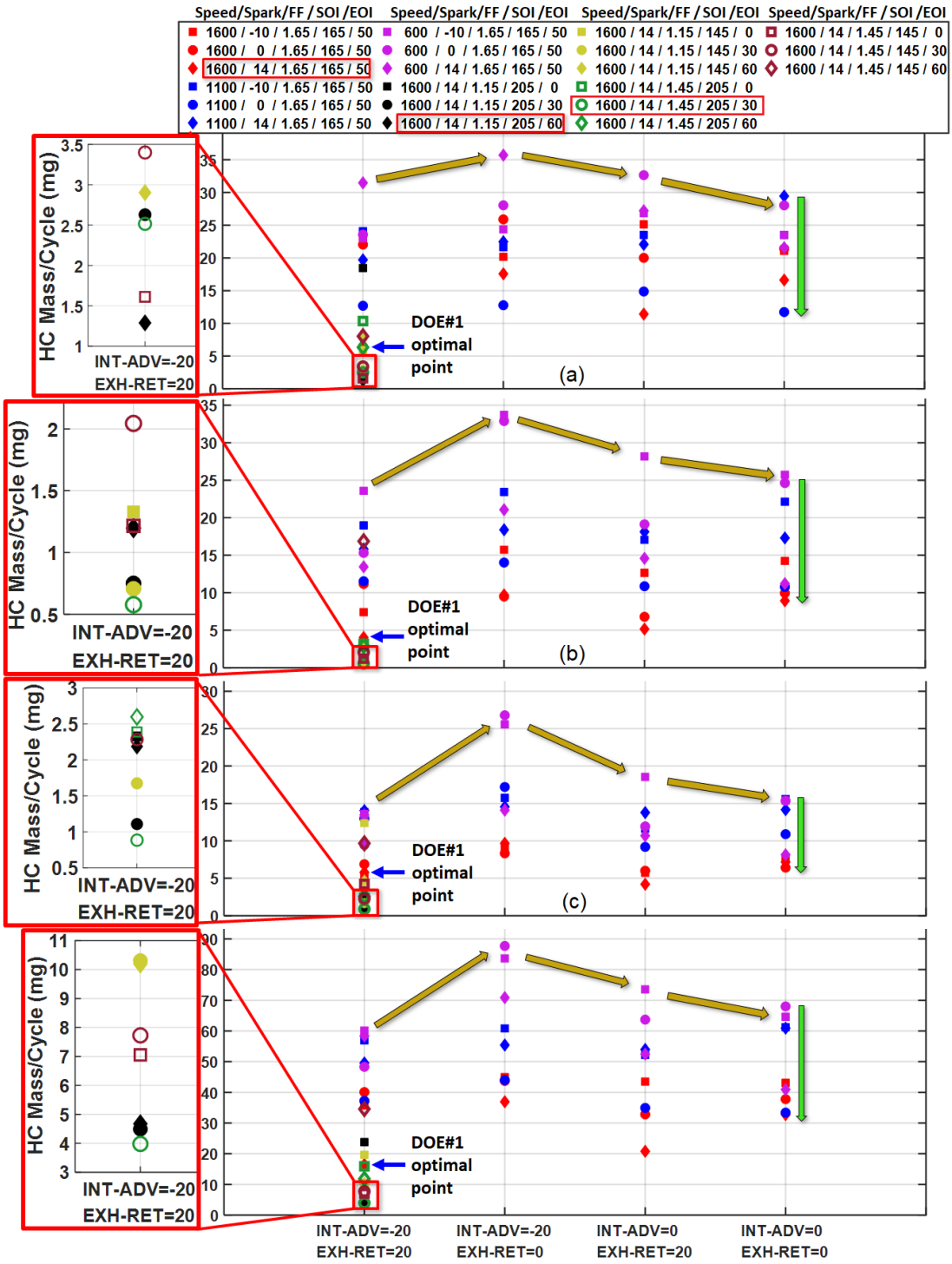

Figure 3.29: HC emissions trend from the DOE tests, (a) first cycle, (b) second cycle, (c) third cycle, (d) total first 3 cycles.

before the spark occurs. From the second cycle and on the air residual is replaced by the hot exhaust residual gas and in-cylinder gas temperature increases. As a result, the fuel vaporization rate in the first cycle is reasonably lower compared to the subsequent cycles. Therefore, the second injected fuel close to the spark needed more time to be vaporized and make a local rich area near the spark plug in the first cycle compared to the second and third cycles. A closer second injection to the spark in the first cycle did not give the fuel adequate time to vaporize and even might lead to spark wetting. Consequently, decreasing the time between the end of the second injection and spark in the first cycle showed an exponential increase in the HC emissions, 93% increase while EOI changed from 60 to 0 CAD bTDC firing. For the second and third cycles, the cylinder temperature at compression stroke is considerably higher due to the presence of the hot residual exhaust gas from the previous cycle. Thus, the fuel evaporation rate is higher than the first cycle, resulting in reduced HC emissions for 30 CAD bTDC firing EOI.

Tables 3.6, 3.7, and 3.8 describes the first, second, and third cycles accumulated HC emissions values for the second part of the DOE tests, respectively. Table 3.9 represents the accumulated HC emissions values resulted from the second part of the DOE tests for entire first three cycles. The moderate first cycle fuel factor equal to 1.45, late intake first injection at 205 CAD bTDC firing, 30 CAD bTDC firing EOI give the minimum engine-out HC emissions for high cranking speed, highly retarded spark timing, and high valve overlap cold crank-start first 3 cycles.

Table 3.6
HC emissions results from the DOE tests for the first cycle in mg

Fuel Factor	EOI (CAD bTDC) / SOI (CAD bTDC)	0	30	60
1.15	205	18.5	2.6	**1.3**
	145	5.9	7.9	2.9
1.45	205	10.4	**2.5**	6.3
	145	**1.6**	3.4	8.0

Table 3.7
HC emissions results from the DOE tests for the second cycle in mg

Fuel Factor	EOI (CAD bTDC) / SOI (CAD bTDC)	0	30	60
1.15	205	3.0	**0.8**	1.2
	145	1.3	**0.7**	2.7
1.45	205	3.2	**0.6**	2.9
	145	1.2	2.1	16.9

Table 3.8
HC emissions results from the DOE tests for the third cycle in mg

Fuel Factor	EOI (CAD bTDC) / SOI (CAD bTDC)	0	30	60
1.15	205	2.3	**1.1**	2.2
	145	12.4	**1.7**	4.6
1.45	205	2.4	**0.9**	2.6
	145	4.2	2.3	9.7

Table 3.10 demonstrates the comparison of the HC emissions from this point as the optimal point to the baseline point. The baseline was considered the point with low cranking speed, advanced spark timing, no overlap, and fuel injection parameters based on the PCM calibration. The fuel injection parameters were 1.05 as fuel factor,

Table 3.9
HC emissions results from the DOE tests for the first three cycles

Fuel Factor	EOI (CAD bTDC) / SOI (CAD bTDC)	0	30	60
1.15	205	23.8	4.5	**4.7**
	145	19.6	10.3	10.2
1.45	205	16.0	**4.0**	11.8
	145	7.0	7.8	34.6

compression/compression fuel injection strategy, including 165 and 50 CAD bTDC firing as SOI and EOI. *As it is seen, a significant reduction, by 94%, of the engine-out HC emissions was achieved from the baseline to the optimal high cranking speed cold crank-start conditions.*

Another important analysis for the cold start first cycle is the injected fuel path analysis. Figure 3.30 shows the injected fuel path analysis results for two different DOE test points with the same injected fuel amount. Figure 3.30 (a) depicts the fuel path for high cranking speed, highly retarded spark timing, and high overlap

Table 3.10
HC emissions reduction at the optimal point of the high cranking speed conditions compared to the baseline

	Cycle	Cranking Speed (RPM)	Valve Overlap (CAD)	Spark Timing (CAD aTDC)	Fuel Factor	SOI (CAD bTDC)	EOI (CAD bTDC)	SR	HC (mg)	HC Reduction (%)
Baseline	1st	600	0	-10	1.05	165	50	0.5	23.5	
	2nd	600	0	-10 to -0.4	1.05	165	50	0.5	25.7	
	3rd	600	0	4.4 to 14	1.05	165	50	0.5	15.4	
	Total	600	0	-10 to 14	1.05	165	50	0.5	64.6	
Optimal Point	1st	1600	40	14	1.45	205	30	0.5	2.5	89
	2nd	1600	40	14	1.45	205	30	0.5	0.6	97
	3rd	1600	40	14	1.45	205	30	0.5	0.9	94
	Total	1600	40	14	1.45	205	30	0.5	4.0	94

conditions, whereas Figure 3.30 (b) is related to low cranking speed, advanced spark timing, and no overlap conditions as the baseline point. Equivalent combusted fuel mass is higher for the test with advanced spark timing equal to 64% against 54% for the highly retarded conditions. Unburnt HC scavenged out of the cylinder is lower, 5.7 mg, for lower cranking speed against 8.9 mg for high cranking speed. However, the unburnt HC flowing out of the exhaust manifold is lower, 2.2 mg, for the high cranking speed against 4.8 mg for the low cranking speed due to the higher post-oxidization effect. For the test with 14 CAD aTDC spark timing, 75% of the unburnt HC scavenged out of the cylinder was post oxidized, whereas, for -10 CAD aTDC spark timing, only 15.8% of the unburnt HC was post-oxidized. This shows the significance of the post oxidization effect in unburnt HC emissions reduction at the exhaust manifold outlet and catalyst inlet for highly retarded spark timing conditions. Furthermore, about 20% of the fuel was lost through the blow-by gas and absorption into the lubrication oil for both cases. The mass of fuel lost through blow-by was higher because of higher cylinder peak pressure for the low cranking speed case. The residual fuel was higher for the high cranking speed test, 6%, against 2.2% for the low cranking speed test, because the fuel factor was considerably lower in the low cranking speed case.

3.4.4 Sensitivity Analysis

This section analyzes the sensitivity of the developed method's outputs to the estimated parameters and assumptions for cold start first three cycles. Table 3.7 details the percent relative change in the average estimated engine-out emissions if different parameters are calculated with a 10% deviation.

The predicted trapped air mass has the most dominant effect on the engine-out emissions concentration translation accuracy using the designed method. A 10% deviation in the trapped air mass estimation can result in an 8% change in the average first three cycles engine-out emissions calculation. To minimize the trapped air charge estimation uncertainty, the air charge model was calibrated to estimate the trapped

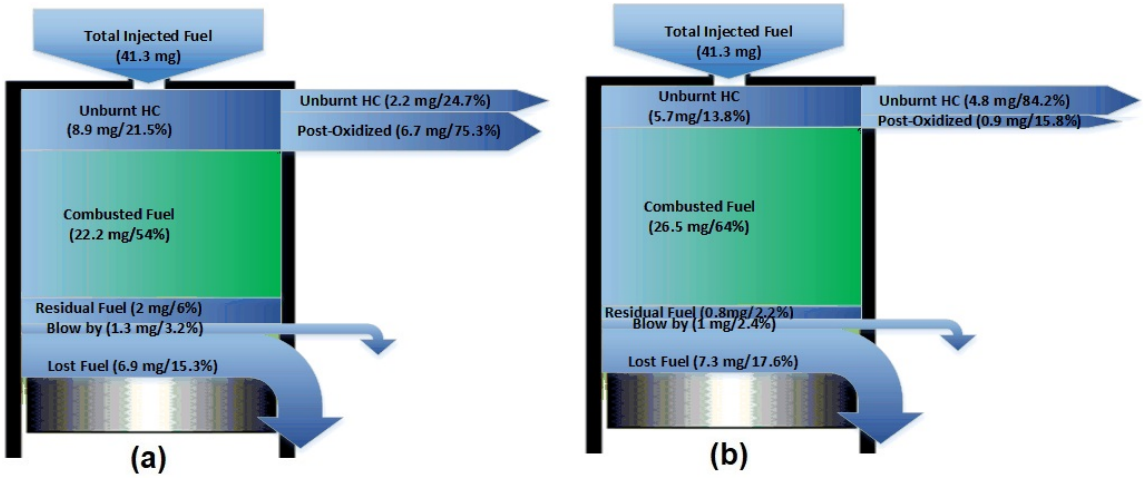

Figure 3.30: Cold start first cycle fuel path analysis (a) 1600 RPM cranking speed, 14 CAD aTDC spark timing, 40 CAD valve overlap, 1.65 fuel factor (b) 600 RPM cranking speed, -10 CAD aTDC spark timing, 0 CAD valve overlap, 1.15 fuel factor.

Table 3.11
Sensitivity of the average engine-out emissions during the cold-start first 3 cycles to the developed method parameters

10% Change of	Trapped Air Mass	Residual Gas Mass	Equivalent Combusted Fuel Mass	Blow-by Gas Mass	HC Post-Oxidization Coefficient	Exhaust Manifold Residual Coefficient	Lost Fuel Fraction
Average First 3 Cycles Engine-Out Emissions (%)	8	0.4	0.5	0.2	0.2	0.4	0.4

air mass with a maximum 1% deviation from the GT-Power TPA simulated results and 2.7 mg average error against the experimental air mass meter data. Another parameter estimated by the air charge model is the mass of residual gas, which causes a 0.4% relative difference in engine-out emissions estimation if it changes by 10%.

The mass of equivalent combusted fuel and blow-by gas estimated by GT-Power TPA propagates 0.5% and 0.2% relative change in average engine-out emissions concentration translation for cold start first three cycles if they vary 10%. The HC post-oxidization coefficient, k_{pox}, assumed to be constant, results in a 0.2% relative difference in the average estimated engine-out emissions if calibrated with a 10% deviation from the assumed value. The exhaust manifold residual coefficient was a calibration parameter based on engine speed and load. The uncertainty analysis shows 10% variation in the calibration of the exhaust manifold residual coefficient can lead to a 0.4% relative change in the average engine-out emissions translation. Finally, a 10% difference in the first cycle lost fuel fraction calibration causes a 0.4% relative change in the estimated average engine-out emissions.

3.5 Summary and Conclusions

Engine-out emissions from a GDI engine were dynamically analyzed at the elevated HEV high cranking speed conditions using a new translation method of the emissions concentration to mass per cycle per cylinder. For this purpose, the motored HEV cold crank-start speed/load profile was duplicated under engine-dyno conditions using a programmable dynamometer. A DOE testing and analysis was carried out to derive an efficient test plan with the minimum number of tests. A two-step fractional-factorial multi-level DOE test plan, including cranking speed, spark timing, valve timing, first cycle fuel factor, SOI of the first injection, and EOI of the second injection with 48 test points in total was conducted. Using the prepared DOE test plan, the cold start experiments were accomplished in a fully-conditioned test room based on the FTP-75 driving cycle cold start phase requirements.

The experimental data were used with the calibrated translation method to analyze the engine dynamics and output emissions during the cold start first three cycles. The first step of DOE tests showed that 1600 RPM cranking speed with 14 CAD aTDC highly retarded spark timing and 40 CAD high valve overlap leads to the lowest HC emissions, while fuel injection parameters were under the PCM control. In the second step, fuel injection parameters were swept while the cranking speed, spark timing, and valve timing were kept at optimal values from the first part of the DOE tests.

From the second step of the DOE tests, it was concluded that a moderate first cycle fuel factor equal to 1.45, late intake first injection at 205 CAD bTDC firing, and 30 CAD bTDC firing EOI in high cranking speed, highly retarded spark timing, and high valve overlap conditions reduce the engine-out HC emissions by 94% compared to the baseline conditions.

Chapter 4

Conclusion and Future Work

4.1 Summary and Conclusion

This study comprised two parts: (i) the development of a real-time model for in-cylinder temperature, air charge, and residual gas estimation, and (ii) dynamic analysis of the engine-out emissions during the cold crank-start at elevated HEV cranking speed. The summary and conclusion from this thesis are provided in the following.

4.1.1 Air Charge, Residual Gas and Temperature Model

A dynamic physics-based model for estimating the mass of trapped air and residual gas, and in-cylinder mixture temperature in a turbocharged VVT-GDI engine was proposed. Precise and dynamic cycle-by-cycle prediction of the mass of trapped air and residual gas, and in-cylinder mixture temperature at IVC aid to improve fuel and combustion phasing control. Amelioration of injected fuel mass and precise control of combustion phasing especially during transients are two main targets for reducing fuel consumption and engine-out emissions. The developed model estimated the parameters using in-cylinder, intake and exhaust pressure traces and was validated through dynamic experiments and analysis. The portion of the residual gas resulting from exhaust backflow during valve overlap was predicted based on compressible ideal gas flow correlations.

A full-factorial, two-level DOE test plan including 64 test points was developed for the experiments required for the designed model calibration and validation. The GT-Power TPA method and experimental data from LFE air mass meter were used to calibrate and validate the designed model at steady-state conditions. Then, DOE analysis using Pareto charts was undertaken to find the optimum number of calibration points. DOE analysis results represented engine speed, IMEP, and intake and exhaust valve timings as important factors. Thus, 16 calibration points were

determined as adequate calibration effort for each calibration parameter. Dynamic validation of the developed model was accomplished using a transient driving cycle. The estimated parameters followed the transitions cycle-by-cycle with no lag and overshoot and had less than 1.5% relative steady-state error.

4.1.2 Engine-Out Cold Crank-Start Emissions Analysis

Dynamic estimation of the engine-out emissions in mass per cycle per cylinder is required to analyze different engine operating conditions and control inputs effects on the engine-out emissions during the cold start first cycles. Therefore, in this study,

- A new dynamic method was developed for individual-cylinder translation of the engine-out emissions concentration to mass in a turbocharged VVT-GDI engine.
- The developed method used GT-Power TPA with crank-angle resolved cylinder, intake, and exhaust pressures as primary inputs to estimate the in-cylinder trapped air charge, residual gas, and temperature during the cold start first three cycles.
- The air charge model designed in the previous work was modified and enhanced for the engine motoring and cold crank-start states and calibrated using the simulated results from the GT-Power TPA.

- The portion of the injected fuel contributed to combustion and the mass of blow-by gas were two important parameters predicted by GT-Power TPA.

- The injected fuel vaporization profile under different cylinder pressure and temperature conditions was derived using CFD analysis and applied in the analysis.

- The leak path equivalent diameter for blow-by gas was calculated using the cylinder pressure data.

- The developed method integrated the exhaust gas dynamics inside the exhaust manifold to the adapted air charge model and GT-Power TPA estimated parameters to translate the experimental fast emission analyzers data in concentration to the mass per cycle per cylinder.

- The sensitivity analysis on the developed method's outputs concerning the estimated parameters and assumptions variations showed the trapped air mass is the dominant factor affecting the calculated engine out emissions on a mass basis.

The method was calibrated and validated using the IMEP data calculated by CAS based on the measured cylinder pressure trace and experimental air mass meter data from 48 cold start tests, sweeping cranking speed, spark timing, and valve timing. The results showed that the mass of trapped air charge as the most important parameter in translating the emissions concentration to mass was estimated with the average

error equal to 2.7 mg. Furthermore, the simulated IMEP from the GT-Power TPA showed significantly low average error against the CAS experimental data, equal to 0.06 bar, representing high precision of the equivalent combusted fuel estimation by GT-power TPA.

The experimental data were used with the calibrated translation method to analyze the engine dynamics and output emissions during the cold start first three cycles. The first step of DOE tests showed that 1600RPM cranking speed with 14 CAD aTDC highly retarded spark timing and 40 CAD high valve overlap leads to the lowest HC emissions, while fuel injection parameters were under the PCM control. At the second step, fuel injection parameters were swept while the cranking speed, spark timing, and valve timing was kept at optimal values from the first part of the DOE tests. The second step of the DOE tests represented that applying a moderate first cycle fuel factor equal to 1.45, late intake first injection at 205 CAD bTDC firing, and 60 CAD bTDC firing EOI in high cranking speed, highly retarded spark timing, and high valve overlap conditions reduce the engine-out HC emissions by 94% compared to the baseline conditions. The low cranking speed, advanced spark timing, no valve overlap with compression/compression injection strategy, including 1.05 as the first cycle fuel factor, 165 CAD bTDC as SOI of the first injection, and 50 CAD bTDC firing as EOI the second injection had been specified as the baseline conditions.

4.2 Suggestions for Future Works

Extension to this work, some future actions are introduced for air charge, residual gas and temperature model, and engine-out cold crank-start emissions modeling and control in the following.

4.2.1 Air Charge, Residual Gas and Temperature Model

The real-time in-cylinder air charge, residual gas, and temperature model were developed and calibrated for the engine part-load conditions. However, the model was designed event-based and modular, consisting of an entire engine cycle physics and thermodynamics. As a result, the model can be easily extended to be used for other engine states; As was extended and used for motoring and cold crank-start states in chapter 2.

As future work, the model can be developed to be used for all engine states, including full load, idle, fuel cut-off, etc. In addition, the in-cylinder emissions measurement method using fast emission analyzers can be used as an experimental reliable approach for the dynamic validation of the estimated residual gas fraction by the air charge

developed model. Furthermore, the developed model can be used for the individual-cylinder cycle-by-cycle AFR and combustion control.

4.2.2 Engine-Out Cold Crank-Start Emissions Analysis

For the engine-out emissions modeling and optimization during the engine cold crank-start and fast-idle phases, the results from the engine-out emissions analysis in Chapter 3 can be used and extended for enigne modeling, optimization, and control applications as the following,

1. A complete real-time control-oriented model can be developed for the dynamic individual-cylinder engine-out emissions estimation during the cold crank-start phase by modeling the fuel evaporation rate, equivalent combusted fuel fraction, blow by gas mass, and residual fuel mass based on different control inputs and integrated into the adapted air charge model.

2. The control-oriented cold crank-start emissions model can be merged to a catalyst thermal model to derive an integrated engine cold-start model. An adaptive optimal control method can then be designed based on the control-oriented cold-start model using the optimal control inputs trajectories from the engine-out emissions analysis results from Chapter 3.

3. An adaptive optimal controller can be designed to optimize the catalyst light-off time and minimize the engine-out emissions during the cold start phase simultaneously.

References

[1] The US Environmental Protection Agency (EPA). *Control of Air Pollution From Motor Vehicles: Tier 3 Motor Vehicle Emission and Fuel Standards*. 2014.

[2] International Council On Clean Transportation. *Real-Driving Emissions Test Procedure For Exhaust Gas Pollutant Emissions Of Cars And Light Commercial Vehicles In Europe*. 2017.

[3] Jin Woo Choung, Soo Min Lee, Sung Jae Kim, Dong Hoon Lee, and Kiyoung Kwon. Smart engine control strategy for the fuel efficiency improvement via understanding the unique behavior of twc. Technical report, SAE paper 2019-01-1406, 2019.

[4] By Hai-Ying Chen and Hsiao-Lan Russell Chang. Development of low temperature three-way catalysts for future fuel efficient vehicles. *Johnson Matthey Technology Review*, 59(1):64–67, 2015.

[5] J Felipe Rodriguez and Wai K Cheng. Effect of operation strategy on first cycle

co, hc, and pm/pn emissions in a gdi engine. *SAE International Journal of Engines*, 8(3):1098–1106, 2015.

[6] Stacy C Davis, Susan E Williams, Robert G Boundy, and Sheila Moore. 2015 vehicle technologies market report. Technical report, Oak Ridge National Lab.(ORNL), Oak Ridge, TN (United States), 2016.

[7] Hui He and Anup Bandivadekar. Passenger car fuel-efficiency standards in china and the us: stringency and technology. 2020–2025. *International Council on Clean Transportation*, 2013.

[8] Alternative Fuels Advanced Vehicles Data Center (AFCD). Us hybrid-electric vehicle sales; 2010. Technical report, http://www.afdc.energy.gov/afdc/data/vehicles.html, 2010.

[9] National Research Council. *Cost, effectiveness, and deployment of fuel economy technologies for light-duty vehicles*. National Academies Press, 2015.

[10] Vincent S Costanzo and John B Heywood. Effect of in-cylinder liquid fuel films on engine-out unburned hydrocarbon emissions for an si engine. Technical report, SAE Paper 2012-01-1712, 2012.

[11] J. B. Heywood. *Internal Combustion Engine Fundamentals*. 1988.

[12] Zhe Wang, Qilun Zhu, and Robert Prucka. A review of spark-ignition engine air charge estimation methods. *SAE paper 2016-01-0620, 2016*.

[13] Alexander Stotsky and Ilya Kolmanovsky. Application of input estimation techniques to charge estimation and control in automotive engines. *Control Engineering Practice*, 10(12):1371–1383, 2002.

[14] Ilya Kolmanovsky, Irina Sivergina, and Jing Sun. Simultaneous input and parameter estimation with input observers and set-membership parameter bounding: theory and an automotive application. *International Journal of Adaptive Control and Signal Processing*, 20(5):225–246, 2006.

[15] Thomas Leroy, Jonathan Chauvin, Guénaël Le Solliec, and Gilles Corde. Air path estimation for a turbocharged si engine with variable valve timing. In *Proc. of the American Control Conference*, pages 5088–5093, 2007.

[16] Per Andersson and Lars Eriksson. Cylinder air charge estimator in turbocharged si-engines. *SAE paper, 2004-01-1366*.

[17] Osvaldo Barbarisi, G Alessandro, and G Luigi. An extended kalman observer for the in-cylinder air mass flow estimation. In *Proceedings of MECA02 International Workshop on Diagnostics in Automotive Engines and Vehicles, Oct., Fisciano SA*, pages 1–14, 2002.

[18] Stephen Magner, Mrdjan Jankovic, and Stephen Cooper. Methods to reduce air-charge characterization data for high degree of freedom engines. *SAE paper 2004-01-0903, 2004*.

[19] Mrdjan Jankovic and Steve W Magner. Air-charge estimation and prediction in spark ignition internal combustion engines. In *American Control Conference, 1999. Proceedings of the 1999*, volume 1, pages 217–221. IEEE, 1999.

[20] Gerard W Malaczynski, Martin Mueller, Jeffrey Pfeiffer, David Cabush, and Kevin Hoyer. Replacing volumetric efficiency calibration look-up tables with artificial neural network-based algorithm for variable valve actuation. *SAE paper 2010-01-0158, 2010*.

[21] Bin Wu, Zoran Filipi, Dennis N Assanis, Denise M Kramer, Gregory L Ohl, Michael J Prucka, and Eugene DiValentin. Using artificial neural networks for representing the air flow rate through a 2.4 liter vvt engine. *SAE paper 2004-01-3054, 2004*.

[22] Jamil El Hadef, Guillaume Colin, Vincent Talon, and Yann Chamaillard. Neural model for real-time engine volumetric efficiency estimation.

[23] Raymond C Turin, Rong Zhang, and Man-Feng Chang. Volumetric efficiency model for variable cam-phasing and variable valve lift applications. *SAE paper 2008-01-0995, 2008*.

[24] Lyle Kocher, Ed Koeberlein, DG Van Alstine, Karla Stricker, and Greg Shaver. Physically based volumetric efficiency model for diesel engines utilizing variable intake valve actuation. *International Journal of Engine Research*, 13(2):169–184, 2012.

[25] T Leroy, G Alix, J Chauvin, A Duparchy, and F Le Berr. Modeling fresh air charge and residual gas fraction on a dual independent variable valve timing si engine. *SAE International Journal of Engines*, 1(1):627–635, 2009.

[26] Martin Hart, Michael Ziegler, and Otmar Loffeld. Adaptive estimation of cylinder air mass using the combustion pressure. *SAE paper 980791, 1998.*

[27] Jonathan W Fox, Wai K. Cheng, and John B Heywood. A model for predicting residual gas fraction in spark-ignition engines. *SAE Transactions*, pages 1538–1544, 1993.

[28] Michael Mladek and Christopher H Onder. A model for the estimation of inducted air mass and the residual gas fraction using cylinder pressure measurements. *SAE paper 2000-01-0958, 2000.*

[29] Norbert Müller and Rolf Isermann. Control of mixture composition using cylinder pressure sensors. *SAE paper 2001-01-3382, 2001.*

[30] A Akimoto, H Itoh, and H Suzuki. Development of delta p method to optimize transient a/f-behavior in mpi engine. *JSAE Review*, 10(4), 1989.

[31] Jeremy Worm. An evaluation of several methods for calculating transient trapped air mass with emphasis on the "delta p" approach. *SAE paper 2005-01-0990, 2005.*

[32] G Colin, P Giansetti, Y Chamaillard, and P Higelin. In-cylinder mass estimation using cylinder pressure. *SAE paper 2007-24-0049, 2007.*

[33] Arya Yazdani, Jeffrey Naber, Mahdi Shahbakhti, Paul Dice, Chris Glugla, Stephen Cooper, Douglas McEwan, and Garlan Huberts. Air charge and residual gas fraction estimation for a spark-ignition engine using in-cylinder pressure. *SAE paper 2017-01-0527, 2017.*

[34] Andreas Thomasson, Sepideh Nikkar, and Erik Höckerdal. Cylinder pressure based cylinder charge estimation in diesel engines with dual independent variable valve timing. *SAE paper 2018-01-0862, 2018.*

[35] Shu Wang, Robert Prucka, Michael Prucka, and Hussein Dourra. Control-oriented residual gas mass prediction for spark ignition engines. *International Journal of Engine Research*, 16(7):897–907, 2015.

[36] N. Cavina et al. Residual gas fraction estimation: Application to a GDI engine with variable valve timing and egr. *SAE transactions*, pages 1774–1782, 2004.

[37] C. Guardiola et al. Cylinder charge composition observation based on in-cylinder pressure measurement. *Measurement*, 131:559–568, 2019.

[38] Gregory M Shaver, J Christian Gerdes, Matthew J Roelle, Patrick A Caton, and Christopher F Edwards. Dynamic modeling of residual-affected homogeneous charge compression ignition engines with variable valve actuation. (2005): 374-381.

[39] Michael FJ Brunt and Christopher R Pond. Evaluation of techniques for absolute cylinder pressure correction. *SAE paper 970036, 1997*.

[40] Andrew L Randolph. Methods of processing cylinder-pressure transducer signals to maximize data accuracy. *SAE transactions*, pages 191–200, 1990.

[41] Francois Galliot, Wai K Cheng, Chun-On Cheng, Mark Sztenderowicz, John B Heywood, and Nick Collings. In-cylinder measurements of residual gas concentration in a spark ignition engine. *SAE transactions*, pages 1144–1150, 1990.

[42] Mark N Subramaniam, Henning Kleeberg, Anamitra Bhattacharyya, Nick Chomic, and Dean Tomazic. A multi-cylinder airflow & residual gas estimation tool applied to a vehicle demonstrator. Technical report, SAE Paper 2010-01-0169, 2010.

[43] Xin Wang, Amir Khameneian, Paul Dice, Bo Chen, Mahdi Shahbakhti, Jeffrey D Naber, Chad Archer, Qiuping Qu, Chris Glugla, and Garlan Huberts. Model-based combustion duration and ignition timing prediction for combustion phasing control of a spark-ignition engine using in-cylinder pressure sensors. In *International Design Engineering Technical Conferences and Computers and Information in Engineering Conference*, volume 59292, page V009T12A033. American Society of Mechanical Engineers, 2019.

[44] Xin Wang, Amir Khameneian, Paul Dice, Bo Chen, Mahdi Shahbakhti, Jeffrey D Naber, Chad Archer, Qiuping Qu, Chris Glugla, and Garlan Huberts.

Control-oriented model-based burn duration and ignition timing prediction with recursive-least-square adaptation for closed-loop combustion phasing control of a spark ignition engine. In *Dynamic systems and control conference*, volume 59155, page V002T12A004. American Society of Mechanical Engineers, 2019.

[45] Amir Khameneian, Xin Wang, Paul Dice, Mahdi Shahbakhti, Jefferey D Naber, Chad Archer, Peter Moilanen, Chris Glugla, and Garlan Huberts. Model-based dynamic in-cylinder air charge, residual gas and temperature estimation for a gdi spark ignition engine using cylinder, intake and exhaust pressures. In *Dynamic Systems and Control Conference*, volume 84287, page V002T26A002. American Society of Mechanical Engineers, 2020.

[46] M Shahbakhti, M Ghafuri, AR Aslani, A Sahraeian, SA Jazayeri, and S Azadi. A method to determine fuel transport dynamics model parameters in port fuel injected gasoline engines during cold start and warm-up conditions. *Journal of Engineering for Gas Turbines and Power*, 132(7):074504, 2010.

[47] J Felipe Rodriguez and Wai K Cheng. Cycle-by-cycle analysis of cold crank-start in a gdi engine. *SAE International Journal of Engines*, 9(2):1210–1219, 2016.

[48] J Felipe Rodriguez and Wai K Cheng. Reduction of cold-start emissions through valve timing in a gdi engine. *SAE International Journal of Engines*, 9(2):1220–1229, 2016.

[49] J Felipe Rodriguez and Wai K Cheng. Fuel carbon pathway in the first cranking cycle of a gasoline direct injection engine. *International Journal of Engine Research*, 17(6):690–701, 2016.

[50] Q Fan, J Bian, H Lu, L Li, and J Deng. Effect of the fuel injection strategy on first-cycle firing and combustion characteristics during cold start in a tsdi gasoline engine. *International Journal of Automotive Technology*, 13(4):523–531, 2012.

[51] Qianwang Fan and Liguang Li. Transient characteristics of cold start emissions from a two-stage direct injection gasoline engines employing the total stoichiometric ratio and local rich mixture start-up strategy. Technical report, SAE Paper 2012-01-1068, 2012.

[52] S Wiemer, H Kubach, and U Spicher. Investigations on the start-up process of a disi engine. *SAE Transactions*, pages 1261–1270, 2007.

[53] Zheng Xu, Jianwen Yi, Steven Wooldridge, David Reiche, Eric Curtis, and George Papaioannou. Modeling the cold start of the ford 3.5 l v6 ecoboost engine. *SAE International Journal of Engines*, 2(1):1367–1387, 2009.

[54] Jinghu Hu, Matthew Hall, Ron Matthews, Peter Moilanen, Steven Wooldridge, and Jianwen Yi. A novel technique for measuring cycle-resolved cold start

emissions applied to a gasoline turbocharged direct injection engine. *SAE International Journal of Advances and Current Practices in Mobility*, 2(2020-01-0312):2469–2478, 2020.

[55] Vaibhav S Kale. *Improving startability and reducing emissions in flexfuel spark ignition direct injection variable cam timing engine*. Ph.D. Thesis, Michigan Technological University, 2014.

[56] S Yu, G Dong, and L Li. Transient characteristics of emissions during engine start/stop operation employing a conventional gasoline engine for hev application. *International Journal of Automotive Technology*, 9(5):543–549, 2008.

[57] Shui Yu, Guangyu Dong, Yuan Gao, and Liguang Li. Transient characteristics of combustion and emissions during start up at higher cranking speed in a pfi engine for hev application. Technical report, SAE Paper 2008-01-2420, 2008.

[58] Xianjing Li and Liguang Li. A study on combustion and emission characteristics of gdi engine for hev at quick start. Technical report, SAE Paper 2014-01-2709, 2014.

[59] Allen Pham and Marko Jeftic. Characterization of gaseous emissions from blended plug-in hybrid electric vehicles during high-power cold-starts. Technical report, SAE Paper 2018-01-0428, 2018.

[60] Bungo Kawaguchi, Kazuhiro Umemoto, Seitaro Misawa, Shigemasa Hirooka, and Takashi Kawai. Ice vehicle challenge toward zero emissions: future technology

harmonization in electrified powertrain system. Technical report, SAE Paper 2019-01-2217, 2019.

[61] Amir Khameneian, Xin Wang, Paul Dice, Mahdi Shahbakhti, Jefferey D Naber, Chad Archer, Peter Moilanen, Chris Glugla, and Garlan Huberts. A real-time control-oriented discrete nonlinear model development for in-cylinder air charge, residual gas and temperature prediction of a gasoline direct injection engine using cylinder, intake and exhaust pressures. Control Engineering Practice, 2021.

[62] U EPA. Regulatory impact analysis: Final rulemaking for 2017-2025 light-duty vehicle greenhouse gas emission standards and corporate average fuel economy standards. *Regulatory Impact Analysis EPA-420-R-12-016, US Environmental Protection Agency*, 2012.

Appendix A

Air Charge, Residual Gas and Temperature Model Matlab Code

```
close all;
clc;

%% Read data from NI, ATI and CAS
    test_num = 9;

    cd 'E:\Tech Info\Test data\20180725\ATI';
    TEST_ATI = sprintf('TEST%d.xlsx', test_num);
    Data_ATI = xlsread(TEST_ATI);

    IGN_ATI = Data_ATI(38:end,6);
    N_ATI   = Data_ATI(38:end,2);
    Int_ATI = Data_ATI(38:end,49);
    Exh_ATI = Data_ATI(38:end,48);
    TC_ATI  = Data_ATI(38:end,21);
    Lam_ATI = Data_ATI(38:end,73);
    Lamdes_ATI = Data_ATI(38:end,34);
```

```
THP_ATI = Data_ATI(38:end,76);
AIR_ATI = Data_ATI(38:end,20)*453592;
Fuel_ATI = Data_ATI(38:end,65)*0.453592;
PW_ATI = Data_ATI(38:end,216);
PWSEP_ATI = Data_ATI(38:end,209);
RES_ATI = Data_ATI(38:end,107)*453592;
FRP_ATI = Data_ATI(38:end,101)*0.0689476; ↩
                % bar
MAP_ATI = Data_ATI(38:end,53);                % kPa
MCT_ATI = (Data_ATI(38:end,37)-32)/1.8; ↩
                % C

SPK_SRC = Data_ATI(38:end,7);
TRQ_SRC = Data_ATI(38:end,8);
ETC_SRC = Data_ATI(38:end,85);
FUL_SRC = Data_ATI(38:end,238);
EPS_Stat = Data_ATI(38:end,237);
IS_SRC  = Data_ATI(38:end,239);
INJ_Mode = Data_ATI(38:end,247);
ENG_Stat = Data_ATI(38:end,249);


l_N_ATI = length(N_ATI);
k=0;
Cycle_ATI(1)=0;
for k=2:l_N_ATI
Cycle_ATI(k) = (N_ATI(k,1)/40000)+Cycle_ATI(k-1);
end

k=0;
i=1;
for k=1:l_N_ATI
    if Cycle_ATI(k)>=i
        N_ATI_cycle(i)=N_ATI(k);
        IGN_ATI_cycle(i) = IGN_ATI(k);
        Int_ATI_cycle(i) = Int_ATI(k);
        Exh_ATI_cycle(i) = Exh_ATI(k);
        TC_ATI_cycle(i)  = TC_ATI(k);
        Lam_ATI_cycle(i) = Lam_ATI(k);
        Lamdes_ATI_cycle(i) = Lamdes_ATI(k);
        THP_ATI_cycle(i) = THP_ATI(k);
        AIR_ATI_cycle(i) = AIR_ATI(k);
```

```
        Fuel_ATI_cycle(i) = Fuel_ATI(k);
        PW_ATI_cycle(i) = PW_ATI(k);
        PWSEP_ATI_cycle(i) = PWSEP_ATI(k);
        RES_ATI_cycle(i) = RES_ATI(k);
        FRP_ATI_cycle(i) = FRP_ATI(k);                ↩
           % bar
        MAP_ATI_cycle(i) = MAP_ATI(k);                ↩
           % kPa
        MCT_ATI_cycle(i) = MCT_ATI(k);                ↩
           % C
        SPK_SRC_cycle(i) = SPK_SRC(k);
        TRQ_SRC_cycle(i) = TRQ_SRC(k);
        ETC_SRC_cycle(i) = ETC_SRC(k);
        FUL_SRC_cycle(i) = FUL_SRC(k);
        EPS_Stat_cycle(i) = EPS_Stat(k);
        IS_SRC_cycle(i)  = IS_SRC(k);
        INJ_Mode_cycle(i) = INJ_Mode(k);
        ENG_Stat_cycle(i) =  ENG_Stat(k);
        i=i+1;
    end
end

ATI_trigger_idx = find( IGN_ATI_cycle(1300:end) - ↩
   IGN_ATI_cycle(1300)<=-1.5, 1, 'first')+1300;

cd('E:\Tech Info\Test data\20180725\NI')

TEST_NI = sprintf('Log File_2018_7_25_%d.tdms', ↩
   test_num-1);
Data_NI = TDMS_readTDMSFile(TEST_NI);
N_NI = Data_NI.data{1,21};

NI_trigger = Data_NI.data{1,20};

NI_time_stamp = transpose(0:0.1:0.10*(length(↩
   NI_trigger)-1));

NI_trigger_idx = find(NI_trigger<=100, 1, 'first')↩
   -1;

folder_loc = 'E:\Tech Info\Test data\20180725\CAS'; ↩
        %Change as per your location
```

```
 s = num2str(test_num);                  % Converts ↩
    number to string

 basepath    = strcat(folder_loc,'\TEST',s);
 cd(basepath)                          % Goto Basepath

 foo   = load('Trace.cpdc.mat');
 CAS_sync = getfield(foo,char(fieldnames(foo)));
 clear foo;

 foo   = load('CAIGN.Cyl1.EST.mat');
 IGN_CAS = getfield(foo,char(fieldnames(foo)));
 clear foo;

 foo   = load('RPM.Timer.mat');
 N_CAS = getfield(foo,char(fieldnames(foo)));
 clear foo;

 foo   = load('Average.MAP.mat');
 MAP_avg_CAS = getfield(foo,char(fieldnames(foo)));
 clear foo;

 foo   = load('Trace.Fuel_Rail.mat');
 FRP_CAS = getfield(foo,char(fieldnames(foo)));
 clear foo;
 FRP_avg_CAS= mean(FRP_CAS);


 CAS_ATI_trigger_idx = find( IGN_CAS(1200:end) - ↩
    IGN_CAS(1200)>=5, 1, 'first')-1+1200;
 cycle_diff_CAS_ATI = ATI_trigger_idx- ↩
    CAS_ATI_trigger_idx ;
 CAS_end_idx = length(IGN_CAS);

l_N_NI = length(N_NI);
 k=0;
 Cycle_NI(1)=0;
 for k=2:l_N_NI
 Cycle_NI(k) = (N_NI(1,k)/1200)+Cycle_NI(k-1);
 end
```

```
    NI_trigger_time = NI_time_stamp(NI_trigger_idx); ↩
                %Time of trigger in NI
    NI_trigger_cycle = fix(Cycle_NI(NI_trigger_idx)); ↩
           % Trigger cycle

    resh_CPDCIn = reshape(CAS_sync,[],1);     % ↩
       reshaping in one column
    CAS_tirgger_idx = find(resh_CPDCIn>0.4, 1, 'first')↩
       -1;    % index for first trigger
    CAS_tirgger_cycle = fix(CAS_tirgger_idx/size(↩
       CAS_sync,1));  % Cycle for first trigger

    if NI_trigger_cycle>=CAS_tirgger_cycle
                cycle_diff = NI_trigger_cycle- ↩
                   CAS_tirgger_cycle;
                Cycle_NI_syncd = Cycle_NI-cycle_diff-1;
            else
                cycle_diff =  CAS_tirgger_cycle-↩
                   NI_trigger_cycle;
                Cycle_NI_syncd = Cycle_NI+cycle_diff;
    end

    CAS_sync_m = mean(CAS_sync,1);
    EGT1_NI = Data_NI.data{1,15};
    Tind_NI = Data_NI.data{1,6};
    Tturboin_NI = Data_NI.data{1,25};

N_NI_syncd =  interp1(Cycle_NI_syncd,N_NI,[1:1:size(↩
   N_CAS,2)]);
EGT1_syncd =  interp1(Cycle_NI_syncd,EGT1_NI,[1:1:size(↩
   N_CAS,2)]);
Tind_syncd = interp1(Cycle_NI_syncd,Tind_NI,[1:1:size(↩
   N_CAS,2)]);
Tturboin_syncd = interp1(Cycle_NI_syncd,Tturboin_NI↩
   ,[1:1:size(N_CAS,2)]);

%% NUMBER of CYCLES and Alignment between Data
cycle_select=1; % cycle select is the parameter used ↩
   when estimator validation is used based
% on experimental air charge from injector PW, FRP and ↩
   lambdas. In fact it is
```

```
% the parameter that syncs and aligns beginning of estiamtion between ACAP and
% experimental air charge. Here it is one because validation is based on a single value (LFE output)

foo=load('Average.Fuel_Flow.mat');
AVGFUEL001= getfield(foo,char(fieldnames(foo)));
clear foo;
[m,num_cycle]=size(AVGFUEL001(cycle_select:end)); % number of cycles obtained from each of the logged parmaters (here: fuel)


%% Calibration Parameters
        N_table = [1270 3905];
        IMEP_table = [0 1250];
        Exh_table = [0 31.5];
        Int_table = [-30 0];

      hint_table = reshape([0.95, -2.05, 8.45, -1.55, 1,1,1,1, 1.25, 0.75, 0.55, 5.05, 5.95, 6.95, 9.35, 24.65],2,2,2,2);
      hexh_table = reshape([5.5,   1.5,  5.8,   6.8,  1,1,1,1, 5.5,  8.5,  17.8,  16.5, 7.1,  14,   6.8,  29.5],2,2,2,2);

    %% Engine Geometry Parameters
Vc = 60204.97e-9;          % clearance volume (m^3)
l  = 155.87e-3;            % connecting rod length (m)
S  = 83.10e-3;             % Stroke (m)
a  = S/2;                  % crankshaft radius (m)
rc = 9.30;                 % compression ratio
B  = 87.50e-3;             % Bore (m)
R  = l/a;                  % ratio of connecting rod to crank radius
Vd = (559.9059)*1e-6-Vc; % displacement volume (m^3)
X  = 0.60e-3;              % wist_pin_offset  (m)
g      = 1.33;             % gamma for flow calculation
Dv_int = 32.5/1000;        %  intake valve inner seat diameter (m)
Dv_exh = 28/1000;          %  exhaust valve inner seat diameter (m)
```

```
% 0.5CA resolution intake and exhaust valves lift (mm)
```

```
Exh_lift = [0 0 0 0 0.00044 0.00044 0.00044 0.00044 ↩
   0.00259 0.00259 0.00259 0.00259 0.0076  0.0076  0.0076↩
     0.0076  0.01612 0.01612 0.01612 0.01612 0.02826 ↩
   0.02826 0.02826 0.02826 0.04352 0.04352 0.04352 ↩
   0.04352 0.06091 0.06091 0.06091 0.06091 0.07909 ↩
   0.07909 0.07909 0.07909 0.09732 0.09732 0.09732 ↩
   0.09732 0.11554 0.11554 0.11554 0.11554 0.13376 ↩
   0.13376 0.13376 0.13376 0.15199 0.15199 0.15199 ↩
   0.15199 0.17021 0.17021 0.17021 0.17021 0.18843 ↩
   0.18843 0.18843 0.18843 0.20665 0.20665 0.20665 ↩
   0.20665 0.22488 0.22488 0.22488 0.22488 0.2431  0.2431↩
     0.2431  0.2431  0.26132 0.26132 0.26132 0.26132 ↩
   0.27955 0.27955 0.27955 0.27955 0.29777 0.29777 ↩
   0.29777 0.29777 0.31599 0.31599 0.31599 0.31599 ↩
   0.33422 0.33422 0.33422 0.33422 0.35244 0.35244 ↩
   0.35244 0.35244 0.37066 0.37066 0.37066 0.37066 ↩
   0.38888 0.38888 0.38888 0.38888 0.40711 0.40711 ↩
   0.40711 0.40711 0.42533 0.42533 0.42533 0.42533 ↩
   0.44355 0.44355 0.44355 0.44355 0.46178 0.46178 ↩
   0.46178 0.46178 0.48  0.48  0.48  0.48  0.49928 ↩
   0.49928 0.49928 0.49928 0.52782 0.52782 0.52782 ↩
   0.52782 0.57119 0.57119 0.57119 0.57119 0.63115 ↩
   0.63115 0.63115 0.63115 0.70858 0.70858 0.70858 ↩
   0.70858 0.80395 0.80395 0.80395 0.80395 0.91748 ↩
   0.91748 0.91748 0.91748 1.04922 1.04922 1.04922 ↩
   1.04922 1.19911 1.19911 1.19911 1.19911 1.36697 ↩
   1.36697 1.36697 1.36697 1.55241 1.55241 1.55241 ↩
   1.55241 1.75458 1.75458 1.75458 1.75458 1.96845 ↩
   1.96845 1.96845 1.96845 2.18642 2.18642 2.18642 ↩
   2.18642 2.4063  2.4063  2.4063  2.4063  2.62673 ↩
   2.62673 2.62673 2.62673 2.84643 2.84643 2.84643 ↩
   2.84643 3.06408 3.06408 3.06408 3.06408 3.27878 ↩
   3.27878 3.27878 3.27878 3.4899  3.4899  3.4899  3.4899↩
     3.697 3.697 3.697 3.697 3.89974 3.89974 3.89974 ↩
   3.89974 4.09783 4.09783 4.09783 4.09783 4.29107 ↩
   4.29107 4.29107 4.29107 4.47926 4.47926 4.47926 ↩
   4.47926 4.66226 4.66226 4.66226 4.66226 4.83993 ↩
   4.83993 4.83993 4.83993 5.01216 5.01216 5.01216 ↩
   5.01216 5.17886 5.17886 5.17886 5.17886 5.33994 ↩
   5.33994 5.33994 5.33994 5.49533 5.49533 5.49533 ↩
   5.49533 5.64496 5.64496 5.64496 5.64496 5.78877 ↩
   5.78877 5.78877 5.78877 5.92672 5.92672 5.92672 ↩
   5.92672 6.05876 6.05876 6.05876 6.05876 6.18484 ↩
   6.18484 6.18484 6.18484 6.30494 6.30494 6.30494 ↩
   6.30494 6.41903 6.41903 6.41903 6.41903 6.52707 ↩
   6.52707 6.52707 6.52707 6.62904 6.62904 6.62904 ↩
   6.62904 6.72491 6.72491 6.72491 6.72491 6.81468 ↩
   6.81468 6.81468 6.81468 6.89831 6.89831 6.89831 ↩
   6.89831 6.9758  6.9758  6.9758  6.9758  7.04713 ↩
   7.04713 7.04713 7.04713 7.1123  7.1123  7.1123  7.1123↩
```

```
Int_lift = [0 0.00031 0.00216 0.00671 0.0147  0.0263  ↩
   0.04106 0.05806 0.076 0.094 0.112 0.13  0.148 0.166 ↩
   0.184 0.202 0.22  0.238 0.256 0.274 0.292 0.31  0.328 ↩
   0.346 0.364 0.382 0.4 0.41902 0.44728 0.49074 0.55129 ↩
   0.62992 0.72715 0.84326 0.97836 1.13244 1.30536 ↩
   1.49688 1.70649 1.93288 2.16859 2.40788 2.6489  ↩
   2.89035 3.13085 3.36892 3.60355 3.8341  4.06013 ↩
   4.28134 4.49748 4.70836 4.91383 5.11376 5.30806 ↩
   5.49663 5.67939 5.85629 6.02726 6.19226 6.35125 ↩
   6.50418 6.65104 6.79177 6.92638 7.05482 7.17708 ↩
   7.29315 7.403 7.50663 7.60402 7.69517 7.78006 7.85869 ↩
   7.93105 7.99713 8.05694 8.11045 8.15768 8.19862 ↩
   8.23326 8.2616  8.28365 8.2994  8.30885 8.312 8.30885 ↩
   8.2994  8.28365 8.2616  8.23326 8.19862 8.15769 ↩
   8.11047 8.05696 7.99717 7.9311  7.85877 7.78017 ↩
   7.69531 7.60421 7.50687 7.40331 7.29354 7.17757 ↩
   7.05543 6.92713 6.7927  6.65215 6.50552 6.35285 ↩
   6.19416 6.0295  5.85892 5.68246 5.5002  5.31219 ↩
   5.11853 4.91931 4.71464 4.50466 4.28953 4.06944 ↩
   3.84466 3.61549 3.38238 3.14597 2.90722 2.66754 ↩
   2.42829 2.19081 1.95707 1.73278 1.52491 1.33497 ↩
   1.16357 1.011 0.87739 0.76277 0.66701 0.58979 0.53048 ↩
   0.48795 0.46006 0.441 0.42  0.405 0.387 0.369 0.351 ↩
   0.333 0.315 0.297 0.279 0.261 0.243 0.225 0.207 0.189 ↩
   0.171 0.153 0.135 0.117 0.099 0.081 0.06301 0.04558 ↩
   0.03003 0.01746 0.00846 0.00303 0.00058 0.00001 0];

% Exhaust valve profile
Exh_Lv=1e-3*[0 1 2 3 4 5 6 7 8 9 10 11 12];
Exh_CDA=[0 0.000104724  0.000244374 0.000358699 ↩
   0.00049458  0.000633434 0.000712386 0.000739482 ↩
   0.000761232 0.000762962 0.000762477 0.000773482 ↩
   0.00079742]; %m^2


%% Engine Run-time

    c=2;
    lambda    = Lam_ATI_cycle(cycle_diff_CAS_ATI:↩
      CAS_end_idx+cycle_diff_CAS_ATI-1); ↩
                        % lambda in test
```

```
int_adv   = -Int_ATI_cycle(cycle_diff_CAS_ATI:↩
   CAS_end_idx+cycle_diff_CAS_ATI-1); ↩
                % absolute intake valve advance ↩
   value
exh_ret   =  Exh_ATI_cycle(cycle_diff_CAS_ATI:↩
   CAS_end_idx+cycle_diff_CAS_ATI-1); ↩
                % absolute exhaust valve ↩
   retardvalue
i=1;
for i=1:num_cycle
if exh_ret(i)<=0.5
    exh_ret(i)=0;
end

if int_adv(i)<=0.5
    int_adv(i)=0;
end
end
FRP_ATI   =  FRP_ATI_cycle(cycle_diff_CAS_ATI:↩
   CAS_end_idx+cycle_diff_CAS_ATI-1);
THP_ATI   =  THP_ATI_cycle(cycle_diff_CAS_ATI:↩
   CAS_end_idx+cycle_diff_CAS_ATI-1);
Overlap   = int_adv+exh_ret-3;  % valve aoverlap
rel_hum = 0.42*ones(CAS_end_idx,1);
%     rel_hum   = RH_syncd(1,idx_start_CAS:end)/100;↩
                % relative humidity
%     amb_temp  = Tamb_syncd(1,idx_start_CAS:end)↩
   +273.15;        % ambient temperature (K)
amb_temp = (((79-32)/1.8)+273.15)*ones(CAS_end_idx↩
   ,1);
T_ind_air = Tind_syncd(1,cycle_diff:end)+273.15+2; ↩
          % inducted air temperature (K)
T_co      = ((TC_ATI_cycle(cycle_diff_CAS_ATI:↩
   CAS_end_idx+cycle_diff_CAS_ATI-1)-32)/1.8)+273.15;↩
           % Coolant temperature (k)
Exh_run_temp = EGT1_syncd(1,cycle_diff:end)↩
   +273.15+2;
Turboin_temp = Tturboin_syncd(1,cycle_diff:end)↩
   +273.15+2;
RES_ATI    = RES_ATI_cycle(cycle_diff_CAS_ATI:↩
   CAS_end_idx+cycle_diff_CAS_ATI-1); ↩
                  % lambda in test
```

```
    AIR_ATI    = AIR_ATI_cycle(cycle_diff_CAS_ATI:↩
       CAS_end_idx+cycle_diff_CAS_ATI-1); ↩
                        % lambda in test
    Xres_ATI   = (RES_ATI./(RES_ATI+AIR_ATI))*100;

%% Thermodynamics parameters
% Temperature assumptions to calculate Cp and gamma
% EVO temp 1200 K
% EVC temp 700 K
% IVC temp 400 K
% IVO temp 900 K

% Moar masses and gas constants
MW_res   = 30.45;                % residual gas molar ↩
   mass (kg/kmol)
MW_air   = 28.97;                % air molar mass (kg/↩
   kmol)
MW_vapor = 18.02;                % water vapor molar ↩
   mass (kg/kmol)
R_u      = 8.31446*1000;         % universal gas ↩
   constant (J/kmol.K)
R_evo    = R_u / MW_res;         % cylinder mixture gas ↩
   constant at EVO [J/KgK]
R_vapor  = 461.5;                % water vapor gas ↩
   constant (J/kg.K)
R_air  = 287.06;                 % air gas constant (J/↩
   kg.K)

%% Specific heats From EES
Cv_7 = 768.25;
Cv_air_in = 720;                          % J/kg.K
Cv_air_7  = 860;                          %J/kg.K
Cv_air_intake = (Cv_air_in+Cv_air_7)/2; %J/kg.K

Cv_vapor_in = 1800;                              %J/kg.K
Cv_vapor_7  = 1411;                              % J/kg.K
Cv_vapor_intake = (Cv_vapor_in+Cv_vapor_7)/2; %J/kg.K

Cv_res_in = 840;                          % J/kg.K
Cv_res_7  = 730;                          %J/kg.K
Cv_res_intake = (Cv_res_in+Cv_res_7)/2;  %J/kg.K
```

```
Cv_fuel_in = 2140;                                  % J/kg.K
Cv_fuel_7  = 1660;                                  %J/kg.K
Cv_fuel_intake = (Cv_fuel_in+Cv_fuel_7)/2;          %J/kg.K

%% Humidity
temperature_table=[255.15 258.15 261.15 264.15 266.15 ↩
   269.15 272.15 275.15 277.15 280.15 283.15 286.15 ↩
   289.15 291.15 294.15 297.15 300.15 302.15 305.15 ↩
   308.15 311.15 314.15 316.15 319.15 322.15 325.15 ↩
   328.15 331.15 334.15 337.15 340.15 343.15 346.15 ↩
   349.15 352.15]; % K
p_sat_table=1e3*[0.15 0.19 0.24 0.3 0.37 0.46 0.56 0.69 ↩
   0.84 1.03 1.23 1.48 1.77 2.1 2.5 2.96 3.5 4.1 4.81 ↩
   5.62 6.56 7.62 8.78 10.14 11.68 13.42 15.75 18.16 ↩
   20.87 23.92 27.35 31.18 35.45 40.2 45.49]; % Pa

%%  FUEL SPECS
LHV_fuel           = 41.64e6;  % {J/kg} % E10
A_F_stoich         = 14.06;    % E10
C_isooctane        = 242.49;   % kJ/K.kmol % Cp and Cv ↩
   are the same (liquid)
C_ethanol          = 112.4;    % kJ/K.kmol % Cp and Cv ↩
   are the same (liquid)
MW_ethanol         = 46.07;    % kg/kmol
MW_isooctane       = 114.23;   % kg/kmol
ethanol_density    = 789;      % kg/m^3
fuel_density       = 757.4;    % kg/m^3  % E10
isooctane_density = 743.1;

ethanol_mass_fraction   = 0.1*ethanol_density/↩
   fuel_density; % calculated from volume fraction 10% of↩
    volume is ethanol 90% is isooctane
isooctane_mass_fraction = 0.9*isooctane_density/↩
   fuel_density;
MW_fuel = 1/(ethanol_mass_fraction/MW_ethanol+↩
   isooctane_mass_fraction/MW_isooctane); % g/mol % E10
ethanol_mole_fraction = ethanol_mass_fraction*MW_fuel/↩
   MW_ethanol;
isooctane_mole_fraction = isooctane_mass_fraction*↩
   MW_fuel/MW_isooctane;
```

```
%Cp_fuel=((ethanol_mole_fraction*C_ethanol+↩
   isooctane_mole_fraction*C_isooctane)/MW_fuel)*1000; % ↩
   [J/kg.K]

h_fg_fuel_piston = 306200; %  [J/kg]    {At piston ↩
   temperature (120 C)} {obtained from EES}
h_fg_fuel_ivc    = 301500; %  {J/Kg}    {assumed at IVC ↩
   temp}    {obtained from EES}
h_fg_fuel_intake           = 349.8e3; ↩
                                % enthalpy of fuel J/kg

% Fuel Injection and Combustion Properties
z = 0.9;   %  {Fuel fraction going into air after ↩
   injection}
y = 0.9;   %  {Fuel fraction vaporized before  IVC}

T_evc_fuel = 50+273.15; % [K] {saturation Temperature}


%% Loading ACAP data for each cylinder
for c=c:1:c  % c for each cylinder
    if  c==1
        foo   = load('PresTrace.Cyl1.mat');
        P_kPa = getfield(foo,char(fieldnames(foo)))*1e5;↩
            % cylinder pressure trace (Pa)
        P_kPa = P_kPa(1:end,cycle_select:end);
        clear foo;

        foo    = load('IMEP.Cyl1.mat');
        IMEP_g = getfield(foo,char(fieldnames(foo)));
        IMEP_g = IMEP_g(cycle_select:end);
        clear foo;

        foo    = load('NMEP.Cyl1.mat');
        IMEP_n = getfield(foo,char(fieldnames(foo)));
        IMEP_n = IMEP_n(cycle_select:end);
        clear foo;

        foo    = load('PMEP.Cyl1.mat');
        IMEP_p = getfield(foo,char(fieldnames(foo)));
        IMEP_p = IMEP_p(cycle_select:end);
        clear foo;
```

```
foo             = load('CAIGN.Cyl1.EST.mat');
theta_ignition = getfield(foo,char(fieldnames(↩
   foo)));
theta_ignition = theta_ignition(cycle_select:end↩
   );
clear foo;

foo = load('tqca1.mat');
CA  = getfield(foo,char(fieldnames(foo)));
clear foo;
for i=1:1:size(CA,1)
    CA(i)=CA(i)-floor((i-1)/1440)*720;
end

foo     = load('Trace.MAP.mat');
MAP_raw = getfield(foo,char(fieldnames(foo)))*1↩
   e3; % manifold pressure trace (Pa)
MAP_raw = MAP_raw(1:end,cycle_select:end);
clear foo;

foo     = load('vol1.mat');
VOL_CAS = getfield(foo,char(fieldnames(foo)))/1↩
   e9; % cylinder volume (m^3)
clear foo;

foo     = load('CA50.Cyl1.mat');
CA50 = getfield(foo,char(fieldnames(foo))); ↩
          % CA50 (CA AFTDC)
CA50 = CA50(1:end,cycle_select:end);
clear foo;

foo     = load('CA10.Cyl1.mat');
CA10 = getfield(foo,char(fieldnames(foo))); ↩
          % CA50 (CA AFTDC)
CA10 = CA10(1:end,cycle_select:end);
clear foo;

foo     = load('CA90.Cyl1.mat');
CA90 = getfield(foo,char(fieldnames(foo))); ↩
          % CA50 (CA AFTDC)
CA90 = CA90(1:end,cycle_select:end);
```

```
    clear foo;

    shift = 0;   % CA=CA-0;  CA=CA-540; or CA=CA+180↩
        % 180=-540

elseif c==2
    foo   = load('PresTrace.Cyl2.mat');
    P_kPa = getfield(foo,char(fieldnames(foo)))*1e5;↩
       % cylinder pressure trace (Pa)
    P_kPa = P_kPa(1:end,cycle_select:end);
    clear foo;

    foo    = load('IMEP.Cyl2.mat');
    IMEP_g = getfield(foo,char(fieldnames(foo)));
    IMEP_g = IMEP_g(cycle_select:end);
    clear foo;

    foo    = load('NMEP.Cyl2.mat');
    IMEP_n = getfield(foo,char(fieldnames(foo)));
    IMEP_n = IMEP_n(cycle_select:end);
    clear foo;

    foo    = load('PMEP.Cyl2.mat');
    IMEP_p = getfield(foo,char(fieldnames(foo)));
    IMEP_p = IMEP_p(cycle_select:end);
    clear foo;

    foo             = load('CAIGN.Cyl1.EST.mat');
    theta_ignition = getfield(foo,char(fieldnames(↩
      foo)));
    theta_ignition = theta_ignition(cycle_select:end↩
      );
    clear foo;

    foo = load('tqca1.mat');
    CA  = getfield(foo,char(fieldnames(foo)));
    clear foo;
    for i=1:1:size(CA,1)
        CA(i)=CA(i)-floor((i-1)/1440)*720;
    end

    foo     = load('Trace.MAP.mat');
```

```
    MAP_raw = getfield(foo,char(fieldnames(foo)))*1↩
       e3; % manifold pressure trace (Pa)
    MAP_raw = MAP_raw(1:end,cycle_select:end);
    clear foo;

    foo     = load('vol1.mat');
    VOL_CAS = getfield(foo,char(fieldnames(foo)))/1↩
       e9; % cylinder volume (m^3)
    clear foo;

    foo     = load('CA50.Cyl2.mat');
    CA50 = getfield(foo,char(fieldnames(foo))); ↩
              % CA50 (CA AFTDC)
    CA50 = CA50(1:end,cycle_select:end);
    clear foo;

    foo     = load('CA10.Cyl2.mat');
    CA10 = getfield(foo,char(fieldnames(foo))); ↩
              % CA50 (CA AFTDC)
    CA10 = CA10(1:end,cycle_select:end);
    clear foo;

    foo     = load('CA90.Cyl2.mat');
    CA90 = getfield(foo,char(fieldnames(foo))); ↩
              % CA50 (CA AFTDC)
    CA90 = CA90(1:end,cycle_select:end);
    clear foo;

    shift = 0;   % CA=CA-0;  CA=CA-540; or CA=CA+180↩
         % 180=-540

elseif c==3
    foo=load('-mat','TQ03.P01');
    P_kPa= getfield(foo,char(fieldnames(foo)));
    clear foo;
    foo=load('-mat','IMEP03.P01');
    IMEP_g= getfield(foo,char(fieldnames(foo)));
    IMEP_g=IMEP_g(cycle_select:end);
    clear foo;
    foo=load('-mat','TQENCD.P01');
    CA= getfield(foo,char(fieldnames(foo)));
    clear foo;
```

```
    foo=load('-mat','TQ_MAP.P01');
    MAP= getfield(foo,char(fieldnames(foo)));
    clear foo;
    for i=1:1:size(CA,1)
        CA(i)=CA(i)-floor((i-1)/1440)*720;
    end
    load('-mat','CVOL720.PFG');
    VOL_ACAP=CVOL720CFG/1e6; %m^3
    shift=-360;  % shift/2=-180 2 because of CA ↩
       sampling   CA=CA-180;
    foo=load('-mat','CAIGN03.P01');
    theta_ignition=getfield(foo,char(fieldnames(foo)↩
       ));
    theta_ignition=theta_ignition(cycle_select:end);
    clear foo;
elseif c==4
    foo=load('-mat','TQ04.P01');
    P_kPa= getfield(foo,char(fieldnames(foo)));
    clear foo;
    foo=load('-mat','IMEP04.P01');
    IMEP_g= getfield(foo,char(fieldnames(foo)));
    IMEP_g=IMEP_g(cycle_select:end);
    clear foo;
    foo=load('-mat','TQENCD.P01');
    CA= getfield(foo,char(fieldnames(foo)));
    clear foo;
    foo=load('-mat','TQ_MAP.P01');
    MAP= getfield(foo,char(fieldnames(foo)));
    clear foo;
    for i=1:1:size(CA,1)
        CA(i)=CA(i)-floor((i-1)/1440)*720;
    end
    load('-mat','CVOL720.PFG');
    VOL_ACAP=CVOL720CFG/1e6; %m^3
    shift=-720;  %   CA=CA-360;
    foo=load('-mat','CAIGN04.P01');
    theta_ignition=getfield(foo,char(fieldnames(foo)↩
       ));
    theta_ignition=theta_ignition(cycle_select:end);
    clear foo;
end %
```

```
 foo   = load('RPM.Timer.mat');
 N_rpm = getfield(foo,char(fieldnames(foo))); % ↩
    engine speed (rpm)
 N_rpm = N_rpm(1:end,cycle_select:end);
 clear foo;

 foo     = load('Average.MAP.mat');
 MAP_avg = getfield(foo,char(fieldnames(foo)))*1e3; ↩
    % Average manifold pressure per cycle (Pa)
 MAP_avg = MAP_avg(1:end,cycle_select:end);
 clear foo;

 foo   = load('Trace.ExhaustPressure.mat');
 p_exh = getfield(foo,char(fieldnames(foo)))*1e3;   ↩
    % Exhaust pressure trace (Pa)
 p_exh = p_exh(1:end,cycle_select:end);
 clear foo;

 foo   = load('Trace.ExhaustPressureOmega.mat');
 p_exh_omega = getfield(foo,char(fieldnames(foo)))*1↩
    e3;   % Exhaust pressure trace (Pa)
 p_exh_omega = p_exh_omega(1:end,cycle_select:end);

foo   = load('Trace.InjectorPulse.mat');
INJ_CAS = getfield(foo,char(fieldnames(foo)));
clear foo;

    %% Intake and Exhaust valves characteristics

        [bbb,aaa] = butter(3,0.1);
        [ccc,ddd] = butter(3,0.05);

        p_exh_filt = filtfilt(bbb,aaa,p_exh);   %Pa
        p_exh_omega_filt = filtfilt(bbb,aaa,↩
           p_exh_omega); %Pa

        p_exh_omega_mean = mean(p_exh_omega_filt);
        p_exh_mean = mean(p_exh_filt);
        p_drift_omega = p_exh_mean - ↩
           p_exh_omega_mean;

        k=0;
```

```
            for k=1:num_cycle

                p_exh_cor(1:1440,k) = p_exh_filt(1:end,k↩
                   )-p_drift_omega(k);

            end

            Pexh_cor = reshape(p_exh_cor,num_cycle↩
               *1440,1);

%% MAP and raw cylinder pressure filtered and pegging

    CA       = repmat(CA,num_cycle,1);              % ↩
       reshaped in array to be used in ref_press
    P_kPa    = reshape(P_kPa,num_cycle*1440,1);     % ↩
       reshaped in array to be used in ref_press
    MAP      = reshape(MAP_raw,num_cycle*1440,1); % ↩
       reshaped in array to be used in ref_press
    MAP_filt = filtfilt(ccc,ddd,MAP);               % MAP ↩
       filtering Fc=0.05 and order=3

    [pr,po]  = ref_press_dual(circshift(CA,-shift),P_kPa↩
       ,MAP_filt,Pexh_cor,-180,-177,300,303);   % MAP/↩
       Exhaust Pressure-Based Dual-Pegging

    cycle_size = floor(size(pr)/1440);           % round ↩
       down
    pr         = pr(1:cycle_size(1)*1440);

    VOL = VOL_CAS;                                  % ↩
       Cylinder volume read from CAS data in m^3
    v = VOL/max(VOL);                               % ↩
       normalized cylinder volume

    resh_pr = reshape(pr,1440,cycle_size(1));       % ↩
       reshaped cylinder pressure to CA*cycles in Pa
    mean_pr = mean(resh_pr,2);                      % mean↩
        value per 300 cylces of cylinder pressure in Pa
    mean_pr = circshift(mean_pr,shift);
    resh_pr = circshift(resh_pr,shift);

    MAP      = MAP(1:cycle_size(1)*1440);
```

```
resh_MAP = reshape(MAP,1440,cycle_size(1));    % ↩
   reshaped manifold pressure to CA*cycles in Pa
mean_MAP = mean(resh_MAP,2);                   % mean↩
    value per 300 cylces of manifold pressure in Pa
mean_MAP = circshift(mean_MAP,shift);
resh_MAP = circshift(resh_MAP,shift);
resh_pr_filt=filtfilt(bbb,aaa,resh_pr);     %Pa

%% Intake and Exhaust Cam Arrays

 theta_ivc_base = (-180+67)*ones(size(resh_pr,2),1);↩
     % array with the length of estimaton required
theta_ivc      = theta_ivc_base(1:end)-transpose(↩
   int_adv);

theta_ivo_base = (11+360)*ones(size(resh_pr,2),1);
theta_ivo      = theta_ivo_base(1:end)-transpose(↩
   int_adv);

theta_evo_base = (180-36)*ones(size(resh_pr,2),1);
theta_evo      = theta_evo_base(1:end)+transpose(↩
   exh_ret);

theta_evc_base = (360+8)*ones(size(resh_pr,2),1);
theta_evc      = theta_evc_base(1:end)+transpose(↩
   exh_ret);

theta_7        = -180*ones(size(resh_pr,2),1);      ↩
   %BDC in intake stroke
theta_bwd = 260*ones(size(resh_pr,2),1);       % ↩
   blowdown=exh

%% Polytropics Calculations
theta_1_comp = -90;                            % point↩
    1 in compression
theta_2_comp = -50;                            % point↩
    2 in compression
theta_1_exp  = 70;                             % point↩
    1 in expansion
theta_2_exp  = 110;                            % point↩
    2 in expansion
```

```
index_1_comp = find(CA>=theta_1_comp,1);
index_2_comp = find(CA>=theta_2_comp,1);
index_1_exp  = find(CA>=theta_1_exp,1);
index_2_exp  = find(CA>=theta_2_exp,1);

VOL_1_comp   = VOL_CAS(index_1_comp);        % ↩
   already changed to m^3
VOL_2_comp   = VOL_CAS(index_2_comp);
VOL_1_exp    = VOL_CAS(index_1_exp);
VOL_2_exp    = VOL_CAS(index_2_exp);

%%
for kk=1:1:size(resh_pr,2);

    [p_max_bar(kk),index_max(kk)] = max(resh_pr(:,kk↩
       ));
    theta_max(kk)                 = CA(index_max(kk)↩
       );
    p_max(kk)                     = p_max_bar(kk); ↩
                      % cylinder peak pressure (Pa)
    VOL_max(kk)                   = VOL_CAS(↩
       index_max(kk));       % cylinder volume at ↩
       peak pressure (m^3)

    index_ivc(kk) = find(CA>=theta_ivc(kk),1);
    p_ivc(kk)     = resh_pr(index_ivc(kk),kk);     %↩
        cylinder pressure at IVC (Pa)
    VOL_ivc(kk)   = VOL_CAS(index_ivc(kk)); ↩
                            % cylinder volume at IVC↩
        (m^3)

    index_evo(kk) = find(CA>=theta_evo(kk),1);
    p_evo(kk)     = resh_pr(index_evo(kk),kk);     %↩
        cylinder pressure at EVO (Pa)
    VOL_evo(kk)   = VOL_CAS(index_evo(kk)); ↩
                            % cylinder volume at IVC↩
        (m^3)

    index_evc(kk) = find(CA>=theta_evc(kk),1);
    p_evc(kk)     = resh_pr(index_evc(kk),kk);     %↩
        cylinder pressure at EVC (Pa)
```

```
VOL_evc(kk)   = VOL_CAS(index_evc(kk)); ↩
                        % cylinder volume at IVC↩
    (m^3)

index_7(kk) = find(CA>=theta_7(kk),1);
p_7(kk)     = resh_pr(index_7(kk),kk);          %↩
    cylinder pressure at BDC (Pa)
VOL_7(kk)   = VOL_CAS(index_7(kk)); ↩
                           % cylinder volume at↩
    IVC (m^3)

index_ivo(kk) = find(CA>=theta_ivo(kk),1);
p_ivo(kk)     = resh_pr(index_ivo(kk),kk);      %↩
    cylinder pressure at IVO (Pa)
VOL_ivo(kk)   = VOL_CAS(index_ivo(kk)); ↩
                        % cylinder volume at IVC↩
    (m^3)

index_ign(kk) = find(CA>=theta_ignition(kk),1);
p_ign(kk)     = resh_pr(index_ign(kk),kk);      %↩
    cylinder pressure at Ignition (Pa)
VOL_ign(kk)   = VOL_CAS(index_ign(kk)); ↩
                        % cylinder volume at IVC↩
    (Pa)

index_bwd(kk) = find(CA>=theta_bwd(kk),1);
p_bwd(kk)     = resh_pr(index_bwd(kk),kk);      %↩
    cylinder pressure at blowdown (Pa)
VOL_bwd(kk)   = VOL_CAS(index_bwd(kk)); ↩
                        % cylinder volume at ↩
   blowdown (m^3)
```

```
CRA_angle_exh(1:701,kk) = [84 84.5  85  85.5  86
    86.5  87  87.5  88  88.5  89  89.5  90  90.5
    91  91.5  92  92.5  93  93.5  94  94.5  95
  95.5  96  96.5  97  97.5  98  98.5  99  99.5
  100 100.5 101 101.5 102 102.5 103 103.5 104
  104.5 105 105.5 106 106.5 107 107.5 108 108.5
  109 109.5 110 110.5 111 111.5 112 112.5 113
  113.5 114 114.5 115 115.5 116 116.5 117 117.5
  118 118.5 119 119.5 120 120.5 121 121.5 122
  122.5 123 123.5 124 124.5 125 125.5 126 126.5
  127 127.5 128 128.5 129 129.5 130 130.5 131
  131.5 132 132.5 133 133.5 134 134.5 135 135.5
  136 136.5 137 137.5 138 138.5 139 139.5 140
  140.5 141 141.5 142 142.5 143 143.5 144 144.5
  145 145.5 146 146.5 147 147.5 148 148.5 149
  149.5 150 150.5 151 151.5 152 152.5 153 153.5
  154 154.5 155 155.5 156 156.5 157 157.5 158
  158.5 159 159.5 160 160.5 161 161.5 162 162.5
  163 163.5 164 164.5 165 165.5 166 166.5 167
  167.5 168 168.5 169 169.5 170 170.5 171 171.5
  172 172.5 173 173.5 174 174.5 175 175.5 176
  176.5 177 177.5 178 178.5 179 179.5 180 180.5
  181 181.5 182 182.5 183 183.5 184 184.5 185
  185.5 186 186.5 187 187.5 188 188.5 189 189.5
  190 190.5 191 191.5 192 192.5 193 193.5 194
  194.5 195 195.5 196 196.5 197 197.5 198 198.5
  199 199.5 200 200.5 201 201.5 202 202.5 203
  203.5 204 204.5 205 205.5 206 206.5 207 207.5
  208 208.5 209 209.5 210 210.5 211 211.5 212
  212.5 213 213.5 214 214.5 215 215.5 216 216.5
  217 217.5 218 218.5 219 219.5 220 220.5 221
  221.5 222 222.5 223 223.5 224 224.5 225 225.5
  226 226.5 227 227.5 228 228.5 229 229.5 230
  230.5 231 231.5 232 232.5 233 233.5 234 234.5
  235 235.5 236 236.5 237 237.5 238 238.5 239
  239.5 240 240.5 241 241.5 242 242.5 243 243.5
  244 244.5 245 245.5 246 246.5 247 247.5 248
  248.5 249 249.5 250 250.5 251 251.5 252 252.5
  253 253.5 254 254.5 255 255.5 256 256.5 257
  257.5 258 258.5 259 259.5 260 260.5 261 261.5
  262 262.5 263 263.5 264 264.5 265 265.5 266
  266.5 267 267.5 268 268.5 269 269.5 270 270.5
  271 271.5 272 272.5 273 273.5 274 274.5 275
  275.5 276 276.5 277 277.5 278 278.5 279 279.5
  280 280.5 281 281.5 282 282.5 283 283.5 284
  284.5 285 285.5 286 286.5 287 287.5 288 288.5
  289 289.5 290 290.5 291 291.5 292 292.5 293
  293.5 294 294.5 295 295.5 296 296.5 297 297.5
  298 298.5 299 299.5 300 300.5 301 301.5 302
  302.5 303 303.5 304 304.5 305 305.5 306 306.5
```

```
        index_pos_evo(kk) = find(CRA_angle_exh(1:701,kk)↩
           >=theta_evo(kk),1);
        index_pos_ivo(kk) = find(CRA_angle_exh(1:701,kk)↩
           >=theta_ivo(kk)-1,1);
        index_pos_evc(kk) = find(CRA_angle_exh(1:701,kk)↩
           >=theta_evc(kk),1);

        Lv_exh_ov(index_pos_ivo(kk):index_pos_evc(kk),kk↩
           ) = 1e-3*Exh_lift(index_pos_ivo(kk):↩
           index_pos_evc(kk)); % exhaust valve lift ↩
           during overlap (m)
        Lv_exh(index_pos_evo(kk):index_pos_ivo(kk),kk) =↩
            1e-3*Exh_lift(index_pos_evo(kk):index_pos_ivo↩
           (kk));    % exhaust valve lift from EVO to EVC↩
            (m)

        CDA_exh(index_pos_ivo(kk):index_pos_evc(kk),kk) ↩
             = interp1(Exh_Lv,Exh_CDA,Lv_exh_ov(↩
           index_pos_ivo(kk):index_pos_evc(kk),kk));


    end

      %% Initialization

      temp1=1e-5;    % Previous cycle Temperature at BDC
      temp2=200e-6;  % Previous cycle residual molar ↩
         mass
      temp3=1.27;   % Previous cycle polytropic ↩
         coefficient

          %% Data for Analysis
%       LFE_air = LFEair_syncd(idx_start_CAS:end)↩
   *1000*30./N_rpm(1:end);
      CAS_air=(AVGFUEL001(1:end)*30*1000./N_rpm(1:end))↩
         .*lambda(1:end)*14.07;

end

%% cycle starts from IVC
```

```
%     tic;
    for k=2:1:size(resh_pr_filt,2)-100   % Calculates ↩
       for cycles

      hA_int(k) = interpn(N_table, IMEP_table, Exh_table↩
         , Int_table, hint_table,N_rpm(k), IMEP_g(k)*100,↩
          exh_ret(k), -int_adv(k));            % (J)
      hA_exh(k) = interpn(N_table, IMEP_table, Exh_table↩
         , Int_table, hexh_table,N_rpm(k), IMEP_g(k)*100,↩
          exh_ret(k), -int_adv(k));            % (J)
      poly_comp(k-1) = temp3; ↩
                                                          ↩
         % poly_comp calculated in previous cycle
      n_tot(k-1)       = temp1; ↩
                                                          ↩
         % temperature at BDC calculated in previous ↩
         cycle (K)
      m_air(k-1)       = temp2;

        N_deg_sec(k) = N_rpm(k)*6;      % engine speed {↩
           Convert RPM to degree/s}

        T_evo(k) = (((p_evo(k)*VOL_evo(k))/(R_u*n_tot(k↩
           -1)))); % Temperature at EVO (K)
        m_evo_mg(k) = ((p_evo(k)*VOL_evo(k))/(R_evo*↩
           T_evo(k)))*1e6;  % mg
        n_evo(k)    = ((p_evo(k)*VOL_evo(k))/(R_u*T_evo(↩
           k)));         % kmol    %   {Ideal gas law}

        %%%%%%%%%%%%%%%%%%%%%%%%%%%%%%%%     EVO to End ↩
           of Blowdown(exhaust)     %%%%%%%%%%%%%%%%%%%%

        T_exh(k) = T_evo(k)*(p_bwd(k)/p_evo(k))↩
           ^((1.324-1)/1.324);  %using isentropic ↩
           blowdown (T_evo assumed to be 1200K)
        m_exh(k) = (p_bwd(k)*VOL_bwd(k))/(R_evo*T_exh(k)↩
           );

        if theta_ivo(k)-theta_evc(k) >= 0
```

```
%%%%%%%%%%%%%%%%%%%%%%%%%%%%%%%%      End of ↩
   Blowdown to EVC      ↩
   %%%%%%%%%%%%%%%%%%%%%%%%%%%%%%%%

DT_bwd(k) = (theta_evc(k)-theta_bwd(k))/↩
   N_deg_sec(k);
Conv_Coef(k) = (Cv_res_in*m_exh(k))/(hA_exh(k)*↩
   DT_bwd(k));
T_evc(k) = (((Conv_Coef(k)-0.5)*T_exh(k))+T_co(k↩
   ))/(Conv_Coef(k)+0.5);
Q_exh(k) = hA_exh(k)*(((T_exh(k)+T_evc(k))/2)-↩
   T_co(k))*DT_bwd(k);
m_evc_mg(k) = ((p_evc(k)*VOL_evc(k))/(R_evo*↩
   T_evc(k)))*1e6;  % mg

%%%%%%%%%%%%%%%%%%%%%%%%%%%%%%%%        EVC to ↩
   IVO       ↩
   %%%%%%%%%%%%%%%%%%%%%%%%%%%%%%%%%%%%%%%%%%%%%%%%

T_ivo(k)     = T_evc(k)*(p_ivo(k)/p_evc(k))↩
   ^((1.344-1)/1.344);   % using isentropic ↩
   blowdown (T_ivo assumed 900 K)
m_ivo_mg(k) = ((p_ivo(k)*VOL_ivo(k))/(R_evo*↩
   T_ivo(k)))*1e6;      % mg
m_res_trap(k) = m_evc_mg(k);

T_exh1(k)=(T_exh(k)+T_evc(k))/2;
T_exh2(k)=(T_evo(k)+T_evc(k))/2;
else

%%%%%%%%%%%%%%%%%%%%%%%%%%%%%%%%      End of ↩
   Blowdown to IVO      ↩
   %%%%%%%%%%%%%%%%%%%%%%%%%%%%%%%%

DT_bwd(k) = (theta_ivo(k)-theta_bwd(k))/↩
   N_deg_sec(k);
Conv_Coef(k) = (Cv_res_in*m_exh(k))/(hA_exh(k)*↩
   DT_bwd(k));
T_ivo(k) = (((Conv_Coef(k)-0.5)*T_exh(k))+T_co(k↩
   ))/(Conv_Coef(k)+0.5);
Q_exh(k) = hA_exh(k)*(((T_exh(k)+T_ivo(k))/2)-↩
   T_co(k))*DT_bwd(k);
```

```
        m_ivo_mg(k) = ((p_ivo(k)*VOL_ivo(k))/(R_evo*↩
           T_ivo(k)))*1e6;  % mg

        %%%%%%%%%%%%%%%%%%%%%%%%%%%%%%%%%        IVO to ↩
           EVC      ↩
           %%%%%%%%%%%%%%%%%%%%%%%%%%%%%%%%%%%%%%%%%%%%%%

        T_evc(k)    = T_ivo(k)*(p_evc(k)/p_ivo(k))↩
           ^((1.344-1)/1.344);   % using isentropic ↩
           blowdown (T_ivo assumed 900 K)
        m_evc_mg(k) = ((p_evc(k)*VOL_evc(k))/(R_evo*↩
           T_evc(k)))*1e6;     % mg
        m_res_trap(k) = m_ivo_mg(k);
        T_exh1(k)=(T_exh(k)+T_ivo(k))/2;
        T_exh2(k)=(T_evo(k)+T_ivo(k))/2;
        end
        T_ov(k) = (T_ivo(k)+T_evc(k))/2;

        %% RGF ESTIMATION

if theta_ivo(k)-theta_evc(k) < 0

            % Overlap Exhaust flow calculation
            p_exh_ov = p_exh_cor(index_ivo(k):index_evc(↩
               k)+2,k);         % Exhaust pressure during ↩
               overlap (Pa)
            p_ov  = resh_pr_filt(index_ivo(k):index_evc(↩
               k)+2,k);          % Cylinder pressure ↩
               during overlap (Pa)
            CDA_exh_ov = nonzeros(CDA_exh(1:569,k));
            CDA_exh_ov_back = CDA_exh_ov;

            p_exh_ov_m(k) = mean(p_exh_ov); ↩
                                            % Average of ↩
               exhaust pressure during overlap (Pa)
            p_ov_m (k) = mean(p_ov); ↩
                                                   % ↩
               Average of cylinder pressure during ↩
               overlap (Pa)

            co1=0;
            co2=0;
```

```
co3=0;
co4=0;
for co1=1:1:index_evc(k)-index_ivo(k)+2
p_ratio_ov = p_exh_ov(co1)/p_ov(co1);
   if p_ratio_ov <= 0.54

       int_ov21(co1,k) = CDA_exh_ov(co1).*↩
          p_ov(co1); % integral part for ↩
          choked flow from cylinder to ↩
          exhaust port

   elseif p_ratio_ov > 0.54 && p_ratio_ov < ↩
      1

        co2=co2+1;
        % integral part for subcritical flow↩
            from cylinder to exhaust port
        int_ov22(co2,k) = CDA_exh_ov(co1).*↩
           p_ov(co1).*((p_exh_ov(co1)/p_ov(↩
           co1)).^(1/g)).*(1-((p_exh_ov(co1)/↩
           p_ov(co1)).^((g-1)/g))).^0.5;

   elseif p_ratio_ov >= 1 && p_ratio_ov < ↩
      1.852

       co3=co3+1;
       % integral part for subcritical flow ↩
          from exhaust port to cylinder
       int_ov31(co3,k) = CDA_exh_ov_back(co1↩
          ).*p_exh_ov(co1).*((p_ov(co1)/↩
          p_exh_ov(co1)).^(1/g)).*(1-((p_ov(↩
          co1)/p_exh_ov(co1)).^((g-1)/g)))↩
          .^0.5;

   elseif p_ratio_ov >= 1.852
       co4=co4+1;
       int_ov32(co4,k) = CDA_exh_ov_back(co1↩
          ).*p_exh_ov(co1);

   end
end
```

```
% preparation of delta-t for integration for↩
    different areas

t_step = 0.5/N_deg_sec(k);
t_ov21(1:co1-co2-co3-co4,k) = transpose(0:↩
   t_step:t_step*(co1-co2-co3-co4-1));
t_ov22(1:co2,k) = transpose(0:t_step:t_step↩
   *(co2-1));
t_ov31(1:co3,k) = transpose(0:t_step:t_step↩
   *(co3-1));
t_ov32(1:co4,k) = transpose(0:t_step:t_step↩
   *(co4-1));

% exhaust mass flow calculation during ↩
   overlap in different directions (mg)

if co1-co2-co3-co4 > 1
    integ_ov_21(k) = trapz(t_ov21(1:end,k),↩
       int_ov21(1:end,k));
    m_exh_ov1(k) = 1e6*(1/((R_evo*T_ov(k))↩
       ^0.5)) * (g^0.5) * ((2/(g+1))^((g+1)↩
       /(2*(g-1)))) * integ_ov_21(k);
elseif co1-co2-co3-co4 <= 1
                m_exh_ov1(k)=0;
end

if co2 > 1
    integ_ov_22(k) = trapz(t_ov22(1:end,k),↩
       int_ov22(1:end,k));
    m_exh_ov2(k) = 1e6*(1/((R_evo*T_ov(k))↩
       ^0.5))*((2*g/(g-1))^0.5) * integ_ov_22↩
       (k);
elseif co2 <= 1
                m_exh_ov2(k)=0;
end

if co3 > 1
    integ_ov_31(k) = trapz(t_ov31(1:end,k),↩
       int_ov31(1:end,k));
    m_exh_ov3(k) = 1e6*(1/((R_evo*↩
       Exh_run_temp(k))^0.5))*((2*g/(g-1))↩
       ^0.5) * integ_ov_31(k);
```

```
    elseif co3 <= 1
                    m_exh_ov3(k)=0;
    end

    if co4 > 1
         integ_ov_32(k) = trapz(t_ov32(1:end,k),↩
            int_ov32(1:end,k));
         m_exh_ov4(k) = 1e6*(1/((R_evo*↩
            Exh_run_temp(k))^0.5))*(g^0.5) * ↩
            ((2/(g+1))^((g+1)/(2*(g-1)))) * ↩
            integ_ov_32(k);
    elseif co4 <= 1
                    m_exh_ov4(k)=0;
    end

    m_exh_ov(k)  = m_exh_ov4(k)+m_exh_ov3(k)-↩
       m_exh_ov1(k)-m_exh_ov2(k);  % total ↩
       exhaust mass flow (mg)

    m_res(k) = (m_ivo_mg(k)+m_exh_ov(k))*1e-6; ↩
                % total residual mass (kg)
    n_res(k) = m_res(k)/MW_res; ↩
                           % total residual molar↩
        mass (kmol)
    m_res_mg(k)  = m_res(k)*1e6; ↩
                              % total residual ↩
       mass in mg


elseif theta_ivo(k)-theta_evc(k) >= 0

   % total residual mass calculation for the ↩
      case there is no overlap part
    m_exh_ov(k) = 0;
    m_res(k) = m_ivo_mg(k)*1e-6;    % total ↩
       residual mass (kg)
    n_res(k) = m_res(k)/MW_res; % total residual↩
        molar mass (kmol)
    m_res_mg(k)  = m_res(k)*1e6;     % total ↩
       residual mass in mg
    p_exh_ov_m(k) = 0;
    p_ov_m(k) = 0;
```

```
end % flag_residual


%%%%%%%%%%%%%%%%%%%%%%%%%%%%%%%%%% EVC/IVO to ↩
   point 7 %%%%%%%%%%%%%%%%%%%%

 %%%%%%%%%%%%%%%%%%%%%%%%%%%%%%    Vapor mass ↩
    calculation at BDC %%%%%%%%%%%%%%%%%%%%

 p_sat(k)   = interp1(temperature_table,↩
    p_sat_table,amb_temp(k));                    %↩
     water vapor satuation pressure (Pa)
 p_vapor(k) = rel_hum(k)*p_sat(k); ↩
                                                   ↩
    % water vapor partial pressure (Pa)

%%%%%%%%%%%%%%%%%%%%%%%%%%%%%%%    Fuel mass ↩
   calculation %%%%%%%%%%%%%%%%%%%%

    m_fuel(k)    = m_air(k-1)./(A_F_stoich*↩
       lambda(k));  % fuel mass for next cycle (↩
       kg)
    n_fuel(k)    = m_fuel(k)/MW_fuel; ↩
                   % fuel molar mass for next ↩
       cyle (kmol)
    m_fuel_mg(k) = m_fuel(k)*1e6; ↩
                        % fuel mass in mg

   %%%%%%%%%%%%%%%%%%%%%%%%%%%%%%    Temperature ↩
      at BDC calculation %%%%%%%%%%%%%%%%%%%%

       Q_imp(k)                    = (1-z) * ↩
          m_fuel(k) * h_fg_fuel_piston; % heat ↩
          transfer due to impinged fuel {J}
       Q_charge_cooling_intake(k) = ↩
          h_fg_fuel_intake * z * y * m_fuel(k); %↩
           latent heat of fuel vaporization (J)

       W_PV_fuel(k) = FRP_ATI_cycle(k)*m_fuel(k)↩
          *1e5/fuel_density;       % intake fuel ↩
          flow work (J)
```

```
if theta_ivo(k)-theta_evc(k) >= 0

   p_intake(index_ivo(k):1440,k)  = resh_pr(↩
      index_ivo(k):1440,k);          % ↩
      Cylinder pressure during intake (Pa)
   v_intake(index_ivo(k):1440)  = VOL_CAS(↩
      index_ivo(k):1440);            % ↩
      Cylinder volume during intake (m^3)
   W_intake(k) = trapz(v_intake(index_ivo(k)↩
      :1440),p_intake(index_ivo(k):1440,k)); ↩
                % Boundary work from EVC to ↩
      BDC (J)

   MAP_intake(index_ivo(k):1440,k)  = ↩
      MAP_raw(index_ivo(k):1440,k);       % ↩
      Cylinder pressure during intake (Pa)
   W_PV_intake(k) = trapz(v_intake(index_ivo↩
      (k):1440),MAP_intake(index_ivo(k):1440,↩
      k));       % Fluid work from EVC to BDC↩
       (J)
   DT_int(k) = (540-theta_ivo(k))/N_deg_sec(↩
      k);

   a_7(k) = m_fuel(k)*Cv_fuel_intake + m_res↩
      (k)*Cv_res_intake - MW_air*↩
      Cv_air_intake*(n_res(k)+n_fuel(k))...
       -(hA_int(k)*DT_int(k)/2);
   b_7(k) = -((hA_int(k)*DT_int(k)*((T_ivo(k↩
      )/2)-T_co(k)))+Q_imp(k)-W_intake(k)-↩
      Q_charge_cooling_intake(k)+W_PV_intake(↩
      k)+...
       W_PV_fuel(k)-(MW_air*Cv_air_intake*(↩
          n_res(k)+n_fuel(k))*T_ind_air(k))-(↩
          MW_vapor*p_vapor(k)*VOL_7(k)*↩
          Cv_vapor_intake/R_u)...
       -(MW_air*Cv_air_intake*((p_7(k)-↩
          p_vapor(k))*VOL_7(k)/R_u)) + m_fuel↩
          (k)*Cv_fuel_intake*T_evc_fuel +...
       m_res(k)*Cv_res_intake*T_ivo(k));
   c_7(k) = -((MW_air*Cv_air_intake*((p_7(k)↩
      -p_vapor(k))*VOL_7(k)/R_u))...
```

```
        +(MW_vapor*p_vapor(k)*VOL_7(k)*↩
           Cv_vapor_intake/R_u))*T_ind_air(k);


    % Temperature at BDC 2nd degree equation ↩
       coefficients

    T_7(k) = (-b_7(k)+(b_7(k)^2- 4*a_7(k)*c_7↩
       (k))^0.5)/(2*a_7(k)); % cylinder ↩
       temperature at BDC (K)

    T_7_2(k) = (-b_7(k)-(b_7(k)^2- 4*a_7(k)*↩
       c_7(k))^0.5)/(2*a_7(k));

    n_tot_7(k)=((p_7(k)*VOL_7(k))/(R_u*T_7(k)↩
       ));  % kmol    %   {Ideal gas law}

    Q_int(k) = hA_int(k)*(((T_ivo(k)+T_7(k))↩
       /2)-T_co(k))*DT_int(k);
else
    p_intake(index_evc(k):1440,k)  = resh_pr(↩
       index_evc(k):1440,k);          % ↩
       Cylinder pressure during intake (Pa)
    v_intake(index_evc(k):1440)  = VOL_CAS(↩
       index_evc(k):1440);            % ↩
       Cylinder volume during intake (m^3)
    W_intake(k) = trapz(v_intake(index_evc(k)↩
       :1440),p_intake(index_evc(k):1440,k)); ↩
                % Boundary work from EVC to ↩
       BDC (J)

    MAP_intake(index_evc(k):1440,k)  = ↩
       MAP_raw(index_evc(k):1440,k);       % ↩
       Cylinder pressure during intake (Pa)
    W_PV_intake(k) = trapz(v_intake(index_evc↩
       (k):1440),MAP_intake(index_evc(k):1440,↩
       k));       % Fluid work from EVC to BDC↩
        (J)
    DT_int(k) = (540-theta_evc(k))/N_deg_sec(↩
       k);
```

```
                a_7(k) = m_fuel(k)*Cv_fuel_intake + ↩
                   m_res(k)*Cv_res_intake - MW_air*↩
                   Cv_air_intake*(n_res(k)+n_fuel(k))...
                   -(hA_int(k)*DT_int(k)/2);
               b_7(k) = -((hA_int(k)*DT_int(k)*((T_evc(k↩
                  )/2)-T_co(k)))+Q_imp(k)-W_intake(k)-↩
                  Q_charge_cooling_intake(k)+W_PV_intake(↩
                  k)+...
                   W_PV_fuel(k)-(MW_air*Cv_air_intake*(↩
                      n_res(k)+n_fuel(k))*T_ind_air(k))-(↩
                      MW_vapor*p_vapor(k)*VOL_7(k)*↩
                      Cv_vapor_intake/R_u)...
                   -(MW_air*Cv_air_intake*((p_7(k)-↩
                      p_vapor(k))*VOL_7(k)/R_u)) + m_fuel↩
                      (k)*Cv_fuel_intake*T_evc_fuel +...
                   m_res(k)*Cv_res_intake*T_evc(k));
               c_7(k) = -((MW_air*Cv_air_intake*((p_7(k)↩
                  -p_vapor(k))*VOL_7(k)/R_u))...
                   +(MW_vapor*p_vapor(k)*VOL_7(k)*↩
                      Cv_vapor_intake/R_u))*T_ind_air(k);

               % Temperature at BDC 2nd degree equation ↩
                  coefficients

               T_7(k) = (-b_7(k)+(b_7(k)^2- 4*a_7(k)*c_7↩
                  (k))^0.5)/(2*a_7(k)); % cylinder ↩
                  temperature at BDC (K)

               T_7_2(k) = (-b_7(k)-(b_7(k)^2- 4*a_7(k)*↩
                  c_7(k))^0.5)/(2*a_7(k));

               n_tot_7(k)=((p_7(k)*VOL_7(k))/(R_u*T_7(k)↩
                  )); % kmol    %   {Ideal gas law}

               Q_int(k) = hA_int(k)*(((T_evc(k)+T_7(k))↩
                  /2)-T_co(k))*DT_int(k);

           end

%%%%%%%%%%%%%%%%%%%%%%%%%%%%%%    Temperature at Intake ↩
   Valve Closed calculation (K) %%%%%%%%%%%%%%%%%%%%%%
```

```
            T_ivc(k) = T_7(k)*(p_ivc(k)/p_7(k))^((↩
               poly_comp(k-1)-1)/poly_comp(k-1));

            %%%%%%%%%%%%%%%%%%%%%%%%%%%%    Total ↩
               trapped molar Mass calculation at IVC (↩
               kmol) %%%%%%%%%%%%%%%%%%%%

            n_tot_new(k) = ((p_ivc(k)*VOL_ivc(k))/(R_u*↩
               T_ivc(k)));
            temp1=n_tot_new(k);

            %%%%%%%%%%%%%%%%%%%%%%%%%%%%    Vapor mass ↩
               calculation at IVC %%%%%%%%%%%%%%%%%%%%

            m_vapor(k) = (p_vapor(k)*VOL_ivc(k))/(↩
               R_vapor*T_ivc(k)); ↩
                                          % water vapor mass↩
                (kg)
            n_vapor(k) = m_vapor(k)/MW_vapor; ↩
                                                          ↩
               % water vapor molar mass (kmol)
%             w_vapor(k) = n_vapor(k)/n_tot(k); ↩
                                                   % vapor↩
    mole fraction

            %%%%%%%%%%%%%%%%%%%%%%%%%%%%    Air mass ↩
               calculation %%%%%%%%%%%%%%%%%%%%

                % fuel molar mass calculated based on ↩
                   previuos cycle air (kmol)
                % residual gases produced in previous ↩
                   cycle molar mass (kmol)

                n_air(k)    = n_tot_new(k)-n_res(k)-↩
                   n_vapor(k)-n_fuel(k); % air molar mass↩
                    (kmol)
                m_air_new(k)= n_air(k)*MW_air; ↩
                                          % air mass ↩
                   (kg)
                temp2       = m_air_new(k);
                w_air(k)    = n_air(k)/n_tot_new(k);
```

```
            m_air_mg(k) = m_air_new(k)*1e6; ↩
                                          % air mass ↩
               in mg

            %%%%%%%%%%%%%%%%%%%%%%%%%%    Total ↩
               trapped mass calculation at IVC (kg) ↩
               %%%%%%%%%%%%%%%%%%%%

            m_tot(k)    = m_fuel(k)+m_vapor(k)+m_air_new↩
               (k)+n_res(k)*MW_res;

            m_tot_mg(k) = m_tot(k)*1e6; ↩
                                                  % ↩
               total trapped mass in mg

             %%%%%%%%%%%%%%%%%%%%%%%%%%    Polytropic ↩
                index calculation %%%%%%%%%%%%%%%%%%%%

        p_1_comp(k)      = resh_pr(index_1_comp,k); % ↩
           pressure at point 1 for compression (Pa)
        p_2_comp(k)      = resh_pr(index_2_comp,k); % ↩
           pressure at point 2 for compression (Pa)
        poly_comp_new(k) = abs((log(p_2_comp(k))-log(↩
           p_1_comp(k)))/(log(VOL_2_comp)-log(VOL_1_comp)↩
           ));
        temp3            = poly_comp_new(k);

        X_res(k) = m_res(k)*100/(m_air_new(k)+m_res(k));
        X_res_m = mean(X_res);
        X_res_std = std(X_res);

    end  % t   cycles
zz=1250
figure
    h = subplot(4,1,1);
    set(h, 'Position', [0.1 .78 0.8 0.2]);
    hold on
    plot(N_CAS(1,1:CAS_end_idx), 'MarkerFaceColor','k','↩
       MarkerEdgeColor','k','Marker','o',...
   'LineStyle','--','color','k','MarkerSize',3);
    grid on;
    set(gca,'FontSize',14)
```

```
 ylabel({'Speed';'(RPM)'})
 yyaxis right
 plot(IMEP_g(1,1:CAS_end_idx)*100, 'MarkerFaceColor↩
    ','r','MarkerEdgeColor','r','Marker','o',...
'LineStyle','--','color','r','MarkerSize',3);
 ylabel({'gIMEP';'(kPa)'})
 xlim([0 zz])
 set(gca,'XTicklabel',[])
 h = subplot(4,1,2);
 set(h, 'Position', [0.1 .55 0.8 0.2]);
 hold on
 plot(exh_ret(1,1:CAS_end_idx), 'MarkerFaceColor','b↩
    ','MarkerEdgeColor','b','Marker','o',...
'LineStyle','--','color','b','MarkerSize',3);
 plot(int_adv(1,1:CAS_end_idx), 'MarkerFaceColor','k↩
    ','MarkerEdgeColor','k','Marker','o',...
'LineStyle','--','color','k','MarkerSize',3);
 ylabel({'Valve';'Timing (CA)'})
 grid on;
 set(gca,'FontSize',14)
 yyaxis right
 plot(MAP_avg(1,1:CAS_end_idx)/1000, 'MarkerFaceColor↩
    ','r','MarkerEdgeColor','r','Marker','o',...
'LineStyle','--','color','r','MarkerSize',3);
 ylabel('MAP (kPa)')
 xlim([0 zz])
 legend('Exh-Ret','Intake-Adv','MAP')
 set(gca,'XTicklabel',[])
 h = subplot(4,1,3);
 set(h, 'Position', [0.1 .32 0.8 0.2]);
 hold on
 plot(IGN_CAS(1,1:CAS_end_idx), 'MarkerFaceColor','k↩
    ','MarkerEdgeColor','k','Marker','o',...
'LineStyle','--','color','k','MarkerSize',3);
 grid on;
 set(gca,'FontSize',14)
 ylabel({'Ignition','(ATDC)'})
 yyaxis right
 plot(Lam_ATI_cycle(cycle_diff_CAS_ATI+3:CAS_end_idx+↩
    cycle_diff_CAS_ATI-1), 'MarkerFaceColor','r','↩
    MarkerEdgeColor','r','Marker','o',...
'LineStyle','--','color','r','MarkerSize',3)
```

```
 ylabel('Lambda')
 xlim([0 zz])
 set(gca,'XTicklabel',[])
 h = subplot(4,1,4);
 set(h, 'Position', [0.1 .09 0.8 0.2]);
 hold on
 plot(m_air_mg(1,2:end), 'MarkerFaceColor','r','↩
    MarkerEdgeColor','r','Marker','o','LineStyle↩
    ','--','color','r','MarkerSize',3);
 ylabel('Air mass (mg)')
 ylim([0 700])
 yyaxis right
  plot(m_res_trap(1,2:end), 'MarkerFaceColor','k','↩
     MarkerEdgeColor','k','Marker','o',...
'LineStyle','--','color','k','MarkerSize',3);
 plot(m_exh_ov(1,2:end), 'MarkerFaceColor','b','↩
    MarkerEdgeColor','b','Marker','o',...
'LineStyle','--','color','b','MarkerSize',3);
 ylabel('Residula mass (mg)')
 grid on;
 set(gca,'FontSize',14)
 legend('Air Mass','Trapped Residual','Overlap ↩
    Backflow')
 ylim([0 70])
 xlim([0 zz])
 set(gca,'XTicklabel',[])
```

Appendix B

Real-Time In-Cylinder Air Charge, Residual Gas, and Temperature Model

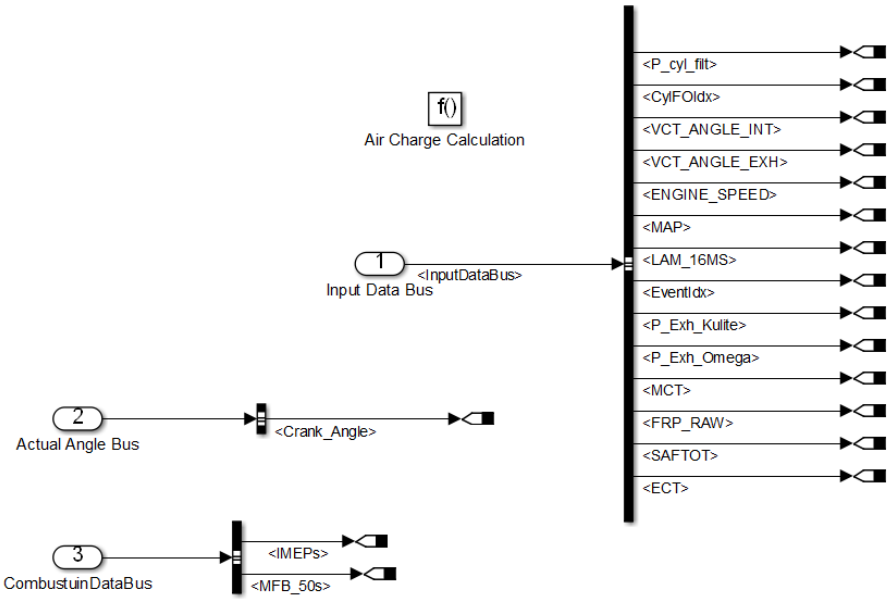
f()
Air Charge Calculation
1
Input Data Bus
<InputDataBus>
2
Actual Angle Bus
<Crank_Angle>
3
CombustuinDataBus
<IMEPs>
<MFB_50s>
<P_cyl_filt>
<CylFOIdx>
<VCT_ANGLE_INT>
<VCT_ANGLE_EXH>
<ENGINE_SPEED>
<MAP>
<LAM_16MS>
<EventIdx>
<P_Exh_Kulite>
<P_Exh_Omega>
<MCT>
<FRP_RAW>
<SAFTOT>
<ECT>

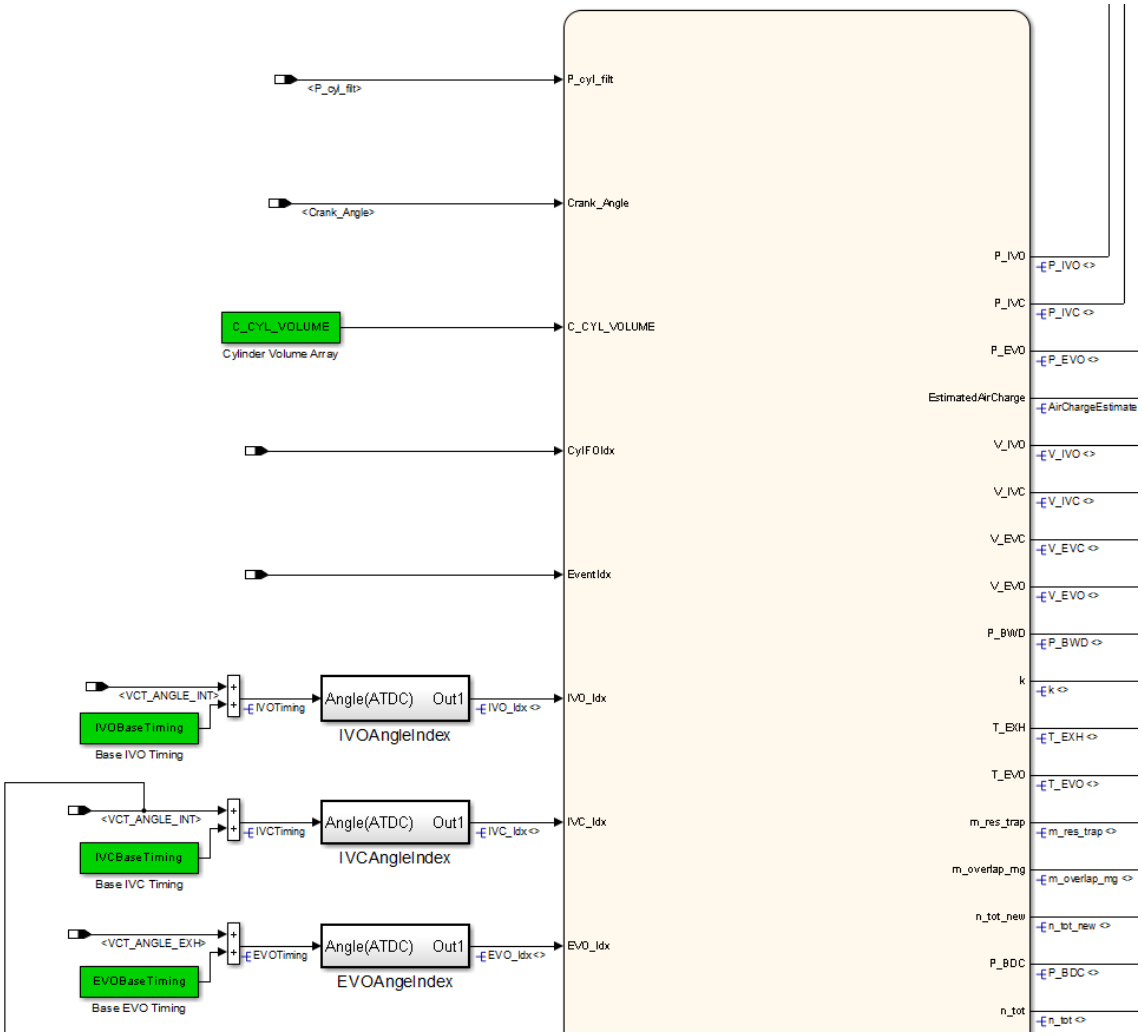
<P_cyl_filt>
P_cyl_filt
<Crank_Angle>
Crank_Angle
C_CYL_VOLUME
Cylinder Volume Array
C_CYL_VOLUME
CylFOIdx
EventIdx
<VCT_ANGLE_INT>
IVOBaseTiming
Base IVO Timing
IVOTiming
Angle(ATDC) Out1
IVOAngleIndex
IVO_Idx <>
IVO_Idx
<VCT_ANGLE_INT>
IVCBaseTiming
Base IVC Timing
IVCTiming
Angle(ATDC) Out1
IVCAngleIndex
IVC_Idx <>
IVC_Idx
<VCT_ANGLE_EXH>
EVOBaseTiming
Base EVO Timing
EVOTiming
Angle(ATDC) Out1
EVOAngleIndex
EVO_Idx <>
EVO_Idx
P_IVO
P_IVO <>
P_IVC
P_IVC <>
P_EVO
P_EVO <>
EstimatedAirCharge
AirChargeEstimate
V_IVO
V_IVO <>
V_IVC
V_IVC <>
V_EVC
V_EVC <>
V_EVO
V_EVO <>
P_BWD
P_BWD <>
k
k <>
T_EXH
T_EXH <>
T_EVO
T_EVO <>
m_res_trap
m_res_trap <>
m_overlap_mg
m_overlap_mg <>
n_tot_new
n_tot_new <>
P_BDC
P_BDC <>
n_tot
n_tot <>

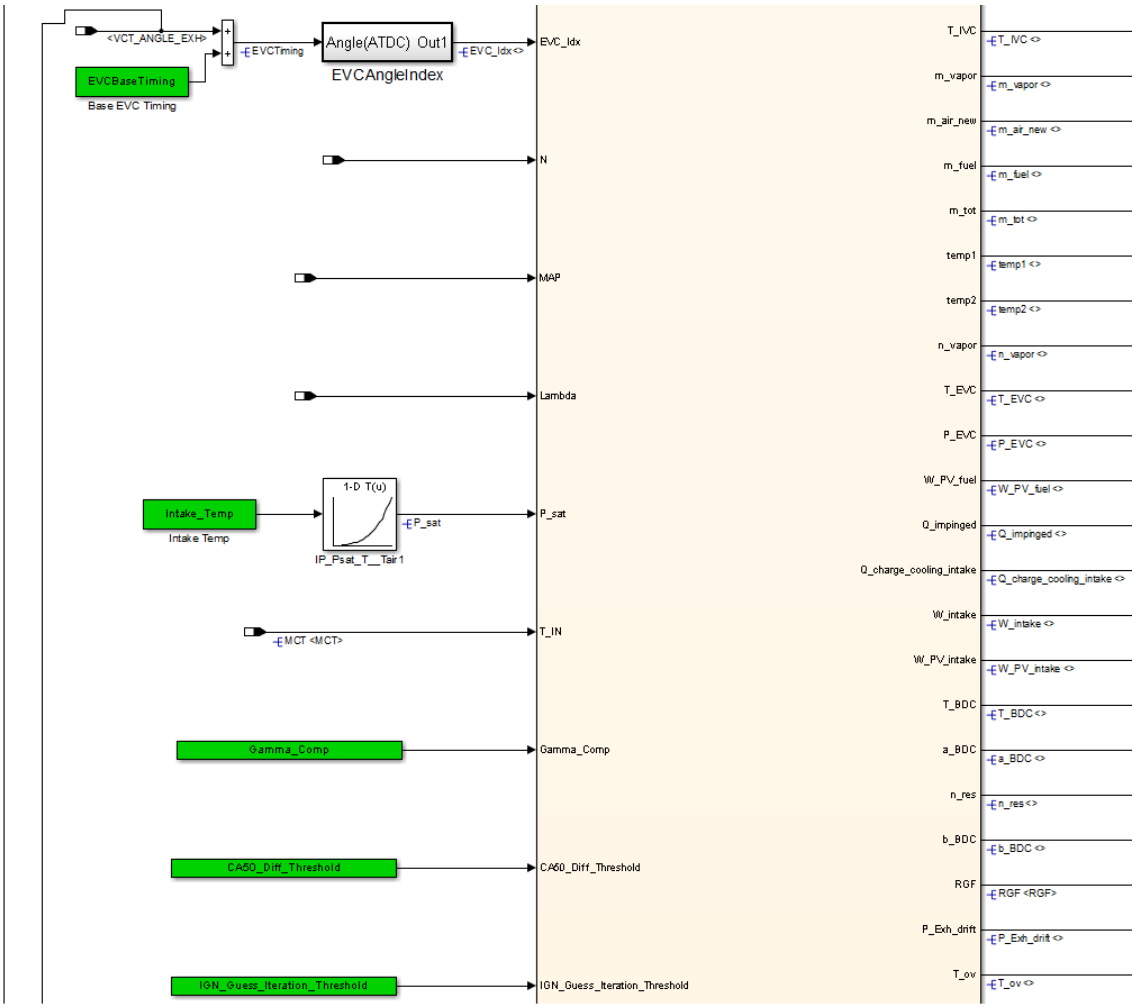
<VCT_ANGLE_EXH>
EVCTiming
Angle(ATDC) Out1
EVC_Idx<>
EVCAngleIndex
EVCBaseTiming
Base EVC Timing
Intake_Temp
Intake Temp
1-D T(u)
P_sat
IP_Psat_T__Tair1
MCT <MCT>
Gamma_Comp
CA50_Diff_Threshold
IGN_Guess_Iteration_Threshold
EVC_Idx
N
MAP
Lambda
P_sat
T_IN
Gamma_Comp
CA50_Diff_Threshold
IGN_Guess_Iteration_Threshold
T_IVC
T_IVC <>
m_vapor
m_vapor <>
m_air_new
m_air_new <>
m_fuel
m_fuel <>
m_tot
m_tot <>
temp1
temp1 <>
temp2
temp2 <>
n_vapor
n_vapor <>
T_EVC
T_EVC <>
P_EVC
P_EVC <>
W_PV_fuel
W_PV_fuel <>
Q_impinged
Q_impinged <>
Q_charge_cooling_intake
Q_charge_cooling_intake <>
W_intake
W_intake <>
W_PV_intake
W_PV_intake <>
T_BDC
T_BDC <>
a_BDC
a_BDC <>
n_res
n_res <>
b_BDC
b_BDC <>
RGF
RGF <RGF>
P_Exh_drift
P_Exh_drift <>
T_ov
T_ov <>

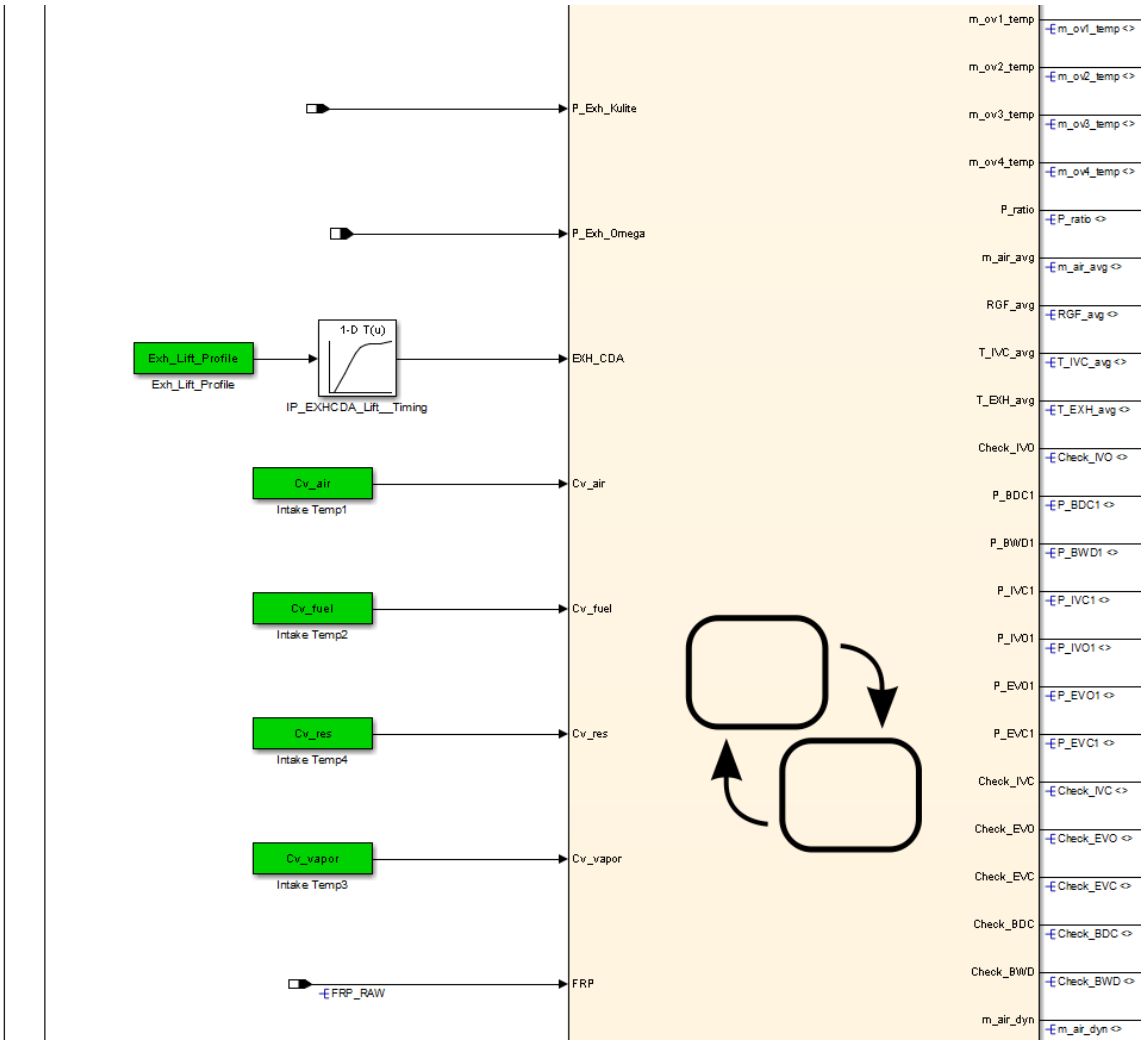
P_Exh_Kulite
P_Exh_Omega
Exh_Lift_Profile
Exh_Lift_Profile
1-D T(u)
IP_EXHCDA_Lift__Timing
EXH_CDA
Cv_air
Intake Temp1
Cv_air
Cv_fuel
Intake Temp2
Cv_fuel
Cv_res
Intake Temp4
Cv_res
Cv_vapor
Intake Temp3
Cv_vapor
FRP_RAW
FRP
m_ov1_temp
m_ov1_temp <>
m_ov2_temp
m_ov2_temp <>
m_ov3_temp
m_ov3_temp <>
m_ov4_temp
m_ov4_temp <>
P_ratio
P_ratio <>
m_air_avg
m_air_avg <>
RGF_avg
RGF_avg <>
T_IVC_avg
T_IVC_avg <>
T_EXH_avg
T_EXH_avg <>
Check_IVO
Check_IVO <>
P_BDC1
P_BDC1 <>
P_BWD1
P_BWD1 <>
P_IVC1
P_IVC1 <>
P_IVO1
P_IVO1 <>
P_EVO1
P_EVO1 <>
P_EVC1
P_EVC1 <>
Check_IVC
Check_IVC <>
Check_EVO
Check_EVO <>
Check_EVC
Check_EVC <>
Check_BDC
Check_BDC <>
Check_BWD
Check_BWD <>
m_air_dyn
m_air_dyn <>

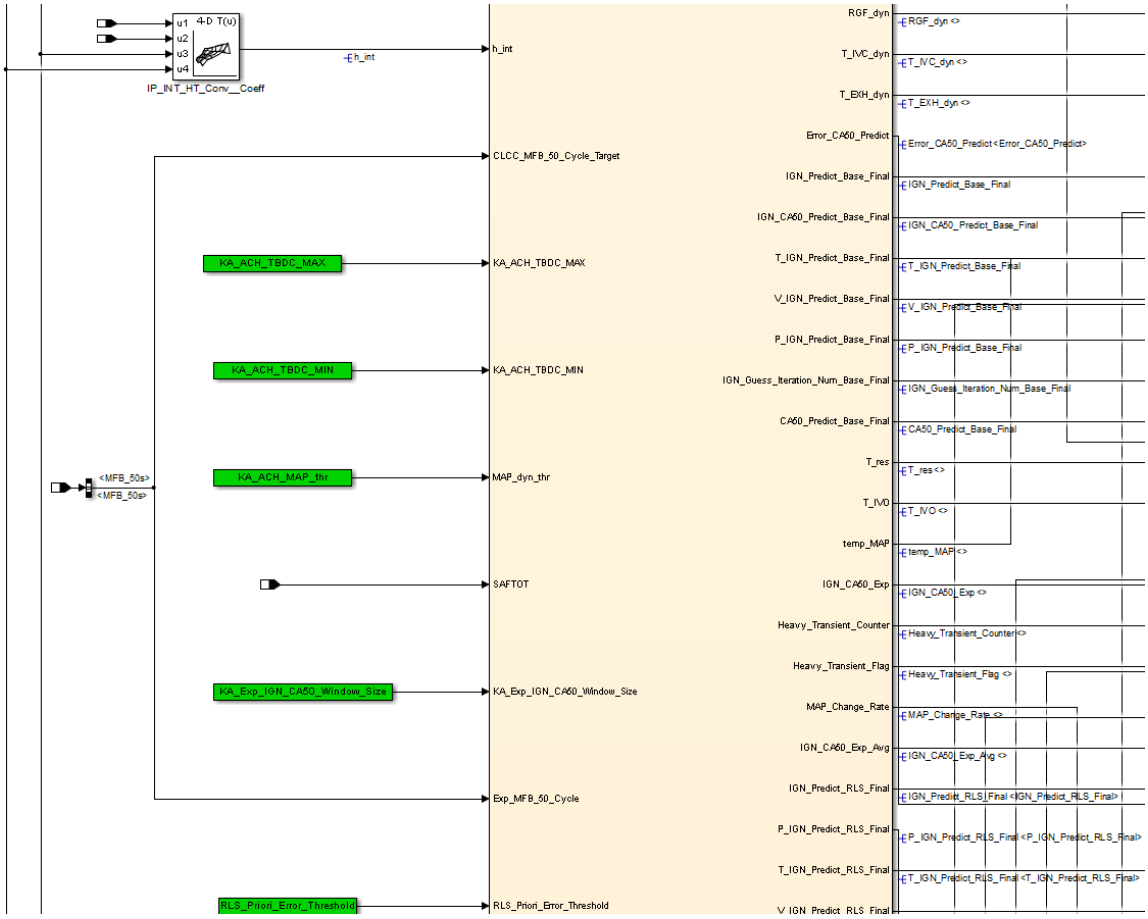
u1
u2
u3
u4
4-D T(u)
IP_INT_HT_Conv__Coeff
h_int
h_int
CLCC_MFB_50_Cycle_Target
KA_ACH_TBDC_MAX
KA_ACH_TBDC_MAX
KA_ACH_TBDC_MIN
KA_ACH_TBDC_MIN
<MFB_50s>
<MFB_50s>
KA_ACH_MAP_thr
MAP_dyn_thr
SAFTOT
KA_Exp_IGN_CA50_Window_Size
KA_Exp_IGN_CA50_Window_Size
Exp_MFB_50_Cycle
RLS_Priori_Error_Threshold
RLS_Priori_Error_Threshold
RGF_dyn
RGF_dyn <>
T_IVC_dyn
T_IVC_dyn <>
T_EXH_dyn
T_EXH_dyn <>
Error_CA50_Predict
Error_CA50_Predict <Error_CA50_Predict>
IGN_Predict_Base_Final
IGN_Predict_Base_Final
IGN_CA50_Predict_Base_Final
IGN_CA50_Predict_Base_Final
T_IGN_Predict_Base_Final
T_IGN_Predict_Base_Final
V_IGN_Predict_Base_Final
V_IGN_Predict_Base_Final
P_IGN_Predict_Base_Final
P_IGN_Predict_Base_Final
IGN_Guess_Iteration_Num_Base_Final
IGN_Guess_Iteration_Num_Base_Final
CA50_Predict_Base_Final
CA50_Predict_Base_Final
T_res
T_res <>
T_IVO
T_IVO <>
temp_MAP
temp_MAP <>
IGN_CA50_Exp
IGN_CA50_Exp <>
Heavy_Transient_Counter
Heavy_Transient_Counter <>
Heavy_Transient_Flag
Heavy_Transient_Flag <>
MAP_Change_Rate
MAP_Change_Rate <>
IGN_CA50_Exp_Avg
IGN_CA50_Exp_Avg <>
IGN_Predict_RLS_Final
IGN_Predict_RLS_Final <IGN_Predict_RLS_Final>
P_IGN_Predict_RLS_Final
P_IGN_Predict_RLS_Final <P_IGN_Predict_RLS_Final>
T_IGN_Predict_RLS_Final
T_IGN_Predict_RLS_Final <T_IGN_Predict_RLS_Final>
V_IGN_Predict_RLS_Final

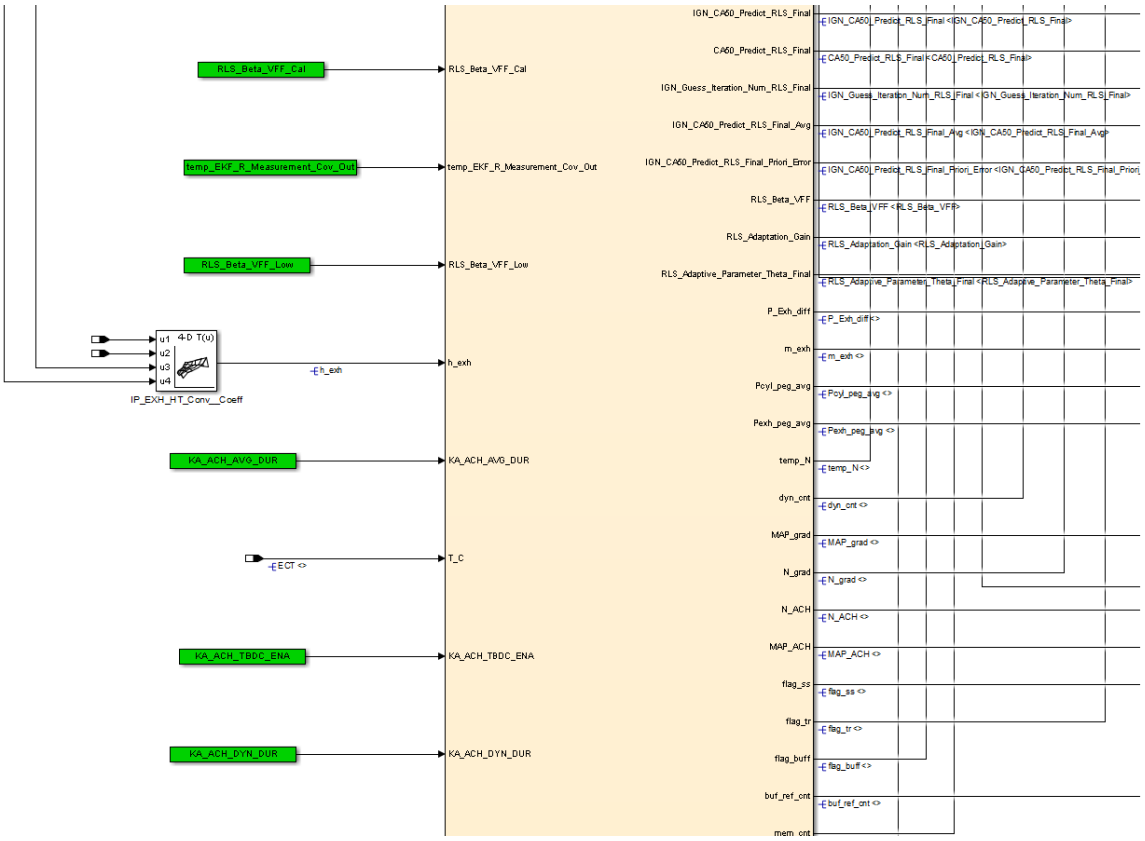
RLS_Beta_VFF_Cal
temp_EKF_R_Measurement_Cov_Out
RLS_Beta_VFF_Low
u1 4-D T(u)
u2
u3
u4
IP_EXH_HT_Conv__Coeff
h_exh
KA_ACH_AVG_DUR
ECT <>
KA_ACH_TBDC_ENA
KA_ACH_DYN_DUR
RLS_Beta_VFF_Cal
temp_EKF_R_Measurement_Cov_Out
RLS_Beta_VFF_Low
h_exh
KA_ACH_AVG_DUR
T_C
KA_ACH_TBDC_ENA
KA_ACH_DYN_DUR
IGN_CA50_Predict_RLS_Final
CA50_Predict_RLS_Final
IGN_Guess_Iteration_Num_RLS_Final
IGN_CA50_Predict_RLS_Final_Avg
IGN_CA50_Predict_RLS_Final_Priori_Error
RLS_Beta_VFF
RLS_Adaptation_Gain
RLS_Adaptive_Parameter_Theta_Final
P_Exh_diff
m_exh
Pcyl_peg_avg
Pexh_peg_avg
temp_N
dyn_cnt
MAP_grad
N_grad
N_ACH
MAP_ACH
flag_ss
flag_tr
flag_buff
buf_ref_cnt
mem_cnt
IGN_CA50_Predict_RLS_Final <IGN_CA50_Predict_RLS_Final>
CA50_Predict_RLS_Final <CA50_Predict_RLS_Final>
IGN_Guess_Iteration_Num_RLS_Final <IGN_Guess_Iteration_Num_RLS_Final>
IGN_CA50_Predict_RLS_Final_Avg <IGN_CA50_Predict_RLS_Final_Avg>
IGN_CA50_Predict_RLS_Final_Priori_Error <IGN_CA50_Predict_RLS_Final_Priori
RLS_Beta_VFF <RLS_Beta_VFF>
RLS_Adaptation_Gain <RLS_Adaptation_Gain>
RLS_Adaptive_Parameter_Theta_Final <RLS_Adaptive_Parameter_Theta_Final>
P_Exh_diff <>
m_exh <>
Pcyl_peg_avg <>
Pexh_peg_avg <>
temp_N <>
dyn_cnt <>
MAP_grad <>
N_grad <>
N_ACH <>
MAP_ACH <>
flag_ss <>
flag_tr <>
flag_buff <>
buf_ref_cnt <>

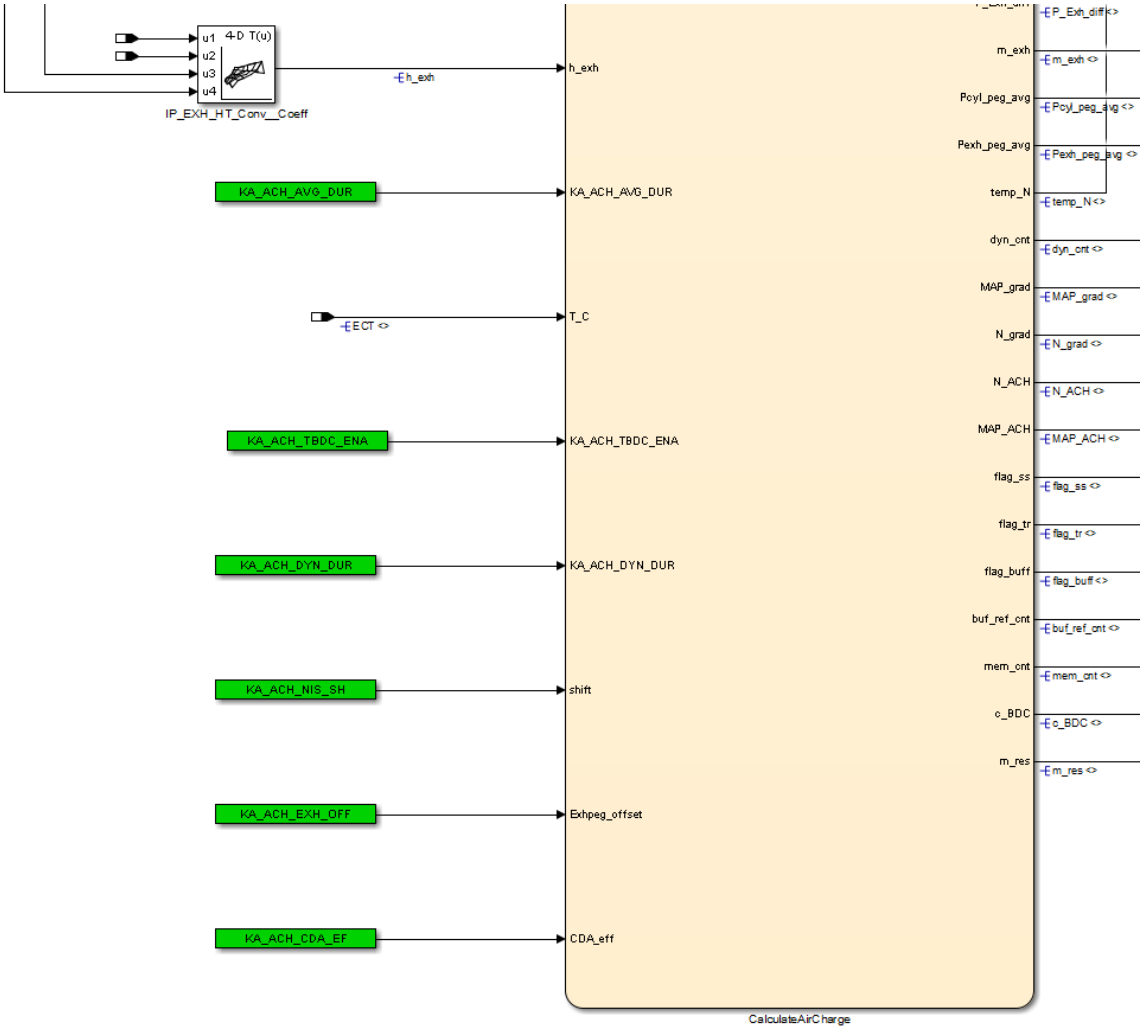
u1
u2
u3
u4
4-D T(u)
IP_EXH_HT_Conv__Coeff
h_exh
KA_ACH_AVG_DUR
ECT <>
KA_ACH_TBDC_ENA
KA_ACH_DYN_DUR
KA_ACH_NIS_SH
KA_ACH_EXH_OFF
KA_ACH_CDA_EF
h_exh
KA_ACH_AVG_DUR
T_C
KA_ACH_TBDC_ENA
KA_ACH_DYN_DUR
shift
Exhpeg_offset
CDA_eff
CalculateAirCharge
P_Exh_diff <>
m_exh
m_exh <>
Pcyl_peg_avg
Pcyl_peg_avg <>
Pexh_peg_avg
Pexh_peg_avg <>
temp_N
temp_N <>
dyn_cnt
dyn_cnt <>
MAP_grad
MAP_grad <>
N_grad
N_grad <>
N_ACH
N_ACH <>
MAP_ACH
MAP_ACH <>
flag_ss
flag_ss <>
flag_tr
flag_tr <>
flag_buff
flag_buff <>
buf_ref_cnt
buf_ref_cnt <>
mem_cnt
mem_cnt <>
c_BDC
c_BDC <>
m_res
m_res <>

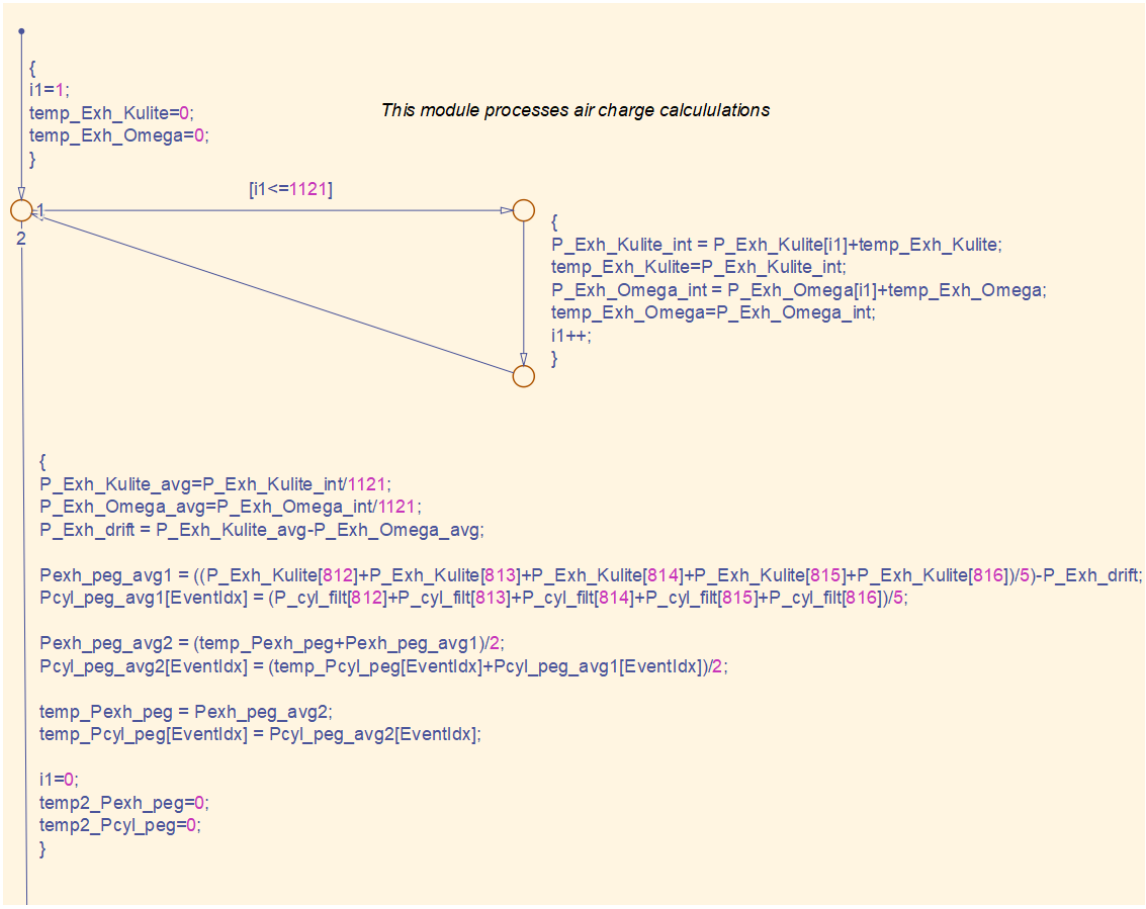
{
i1=1;
temp_Exh_Kulite=0;
temp_Exh_Omega=0;
}
This module processes air charge calcululations
[i1<=1121]
1
2
{
P_Exh_Kulite_int = P_Exh_Kulite[i1]+temp_Exh_Kulite;
temp_Exh_Kulite=P_Exh_Kulite_int;
P_Exh_Omega_int = P_Exh_Omega[i1]+temp_Exh_Omega;
temp_Exh_Omega=P_Exh_Omega_int;
i1++;
}
{
P_Exh_Kulite_avg=P_Exh_Kulite_int/1121;
P_Exh_Omega_avg=P_Exh_Omega_int/1121;
P_Exh_drift = P_Exh_Kulite_avg-P_Exh_Omega_avg;
Pexh_peg_avg1 = ((P_Exh_Kulite[812]+P_Exh_Kulite[813]+P_Exh_Kulite[814]+P_Exh_Kulite[815]+P_Exh_Kulite[816])/5)-P_Exh_drift;
Pcyl_peg_avg1[EventIdx] = (P_cyl_filt[812]+P_cyl_filt[813]+P_cyl_filt[814]+P_cyl_filt[815]+P_cyl_filt[816])/5;
Pexh_peg_avg2 = (temp_Pexh_peg+Pexh_peg_avg1)/2;
Pcyl_peg_avg2[EventIdx] = (temp_Pcyl_peg[EventIdx]+Pcyl_peg_avg1[EventIdx])/2;
temp_Pexh_peg = Pexh_peg_avg2;
temp_Pcyl_peg[EventIdx] = Pcyl_peg_avg2[EventIdx];
i1=0;
temp2_Pexh_peg=0;
temp2_Pcyl_peg=0;
}

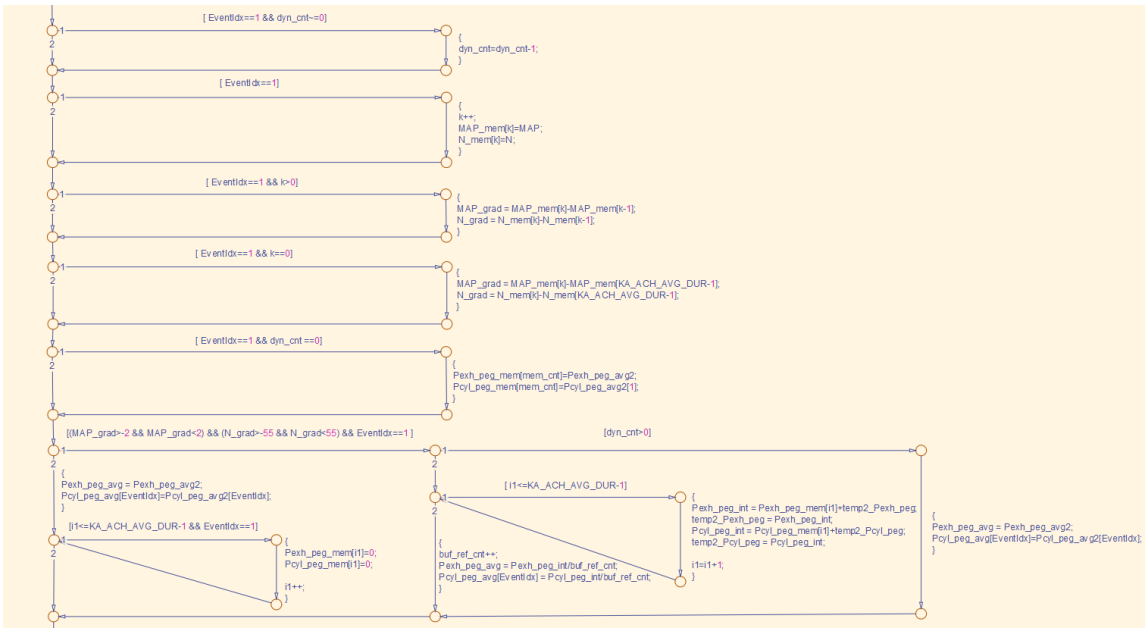
[EventIdx==1 && dyn_cnt~=0]
{
dyn_cnt=dyn_cnt-1;
}
[EventIdx==1]
{
k++;
MAP_mem[k]=MAP;
N_mem[k]=N;
}
[EventIdx==1 && k>0]
{
MAP_grad = MAP_mem[k]-MAP_mem[k-1];
N_grad = N_mem[k]-N_mem[k-1];
}
[EventIdx==1 && k==0]
{
MAP_grad = MAP_mem[k]-MAP_mem[KA_ACH_AVG_DUR-1];
N_grad = N_mem[k]-N_mem[KA_ACH_AVG_DUR-1];
}
[EventIdx==1 && dyn_cnt ==0]
{
Pexh_peg_mem[mem_cnt]=Pexh_peg_avg2;
Pcyl_peg_mem[mem_cnt]=Pcyl_peg_avg2[1];
}
[(MAP_grad>-2 && MAP_grad<2) && (N_grad>-55 && N_grad<55) && EventIdx==1]
{
Pexh_peg_avg = Pexh_peg_avg2;
Pcyl_peg_avg[EventIdx]=Pcyl_peg_avg2[EventIdx];
}
[i1<=KA_ACH_AVG_DUR-1 && EventIdx==1]
{
Pexh_peg_mem[i1]=0;
Pcyl_peg_mem[i1]=0;
i1++;
}
[dyn_cnt>0]
[i1<=KA_ACH_AVG_DUR-1]
{
buf_ref_cnt++;
Pexh_peg_avg = Pexh_peg_int/buf_ref_cnt;
Pcyl_peg_avg[EventIdx] = Pcyl_peg_int/buf_ref_cnt;
}
{
Pexh_peg_int = Pexh_peg_mem[i1]+temp2_Pexh_peg;
temp2_Pexh_peg = Pexh_peg_int;
Pcyl_peg_int = Pcyl_peg_mem[i1]+temp2_Pcyl_peg;
temp2_Pcyl_peg = Pcyl_peg_int;
i1=i1+1;
}
{
Pexh_peg_avg = Pexh_peg_avg2;
Pcyl_peg_avg[EventIdx]=Pcyl_peg_avg2[EventIdx];
}

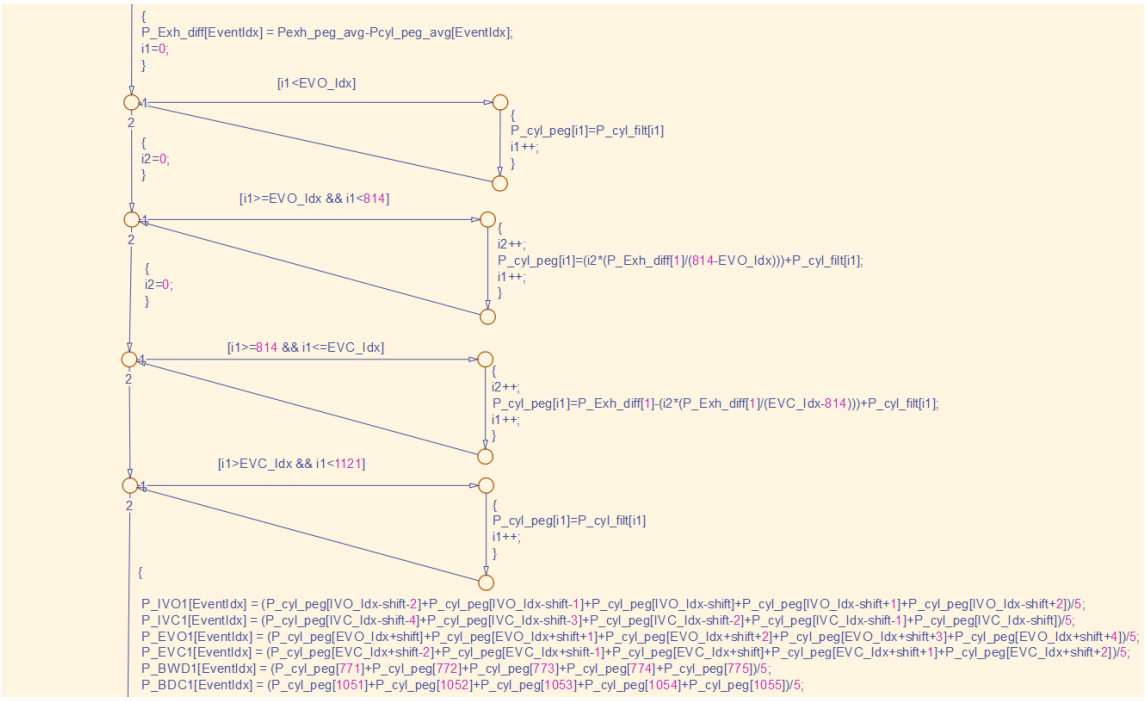
{
P_Exh_diff[EventIdx] = Pexh_peg_avg-Pcyl_peg_avg[EventIdx];
i1=0;
}
[i1<EVO_Idx]
1
2
{
P_cyl_peg[i1]=P_cyl_filt[i1]
i1++;
}
{
i2=0;
}
[i1>=EVO_Idx && i1<814]
1
2
{
i2++;
P_cyl_peg[i1]=(i2*(P_Exh_diff[1]/(814-EVO_Idx)))+P_cyl_filt[i1];
i1++;
}
{
i2=0;
}
[i1>=814 && i1<=EVC_Idx]
1
2
{
i2++;
P_cyl_peg[i1]=P_Exh_diff[1]-(i2*(P_Exh_diff[1]/(EVC_Idx-814)))+P_cyl_filt[i1];
i1++;
}
[i1>EVC_Idx && i1<1121]
1
2
{
P_cyl_peg[i1]=P_cyl_filt[i1]
i1++;
}
{
P_IVO1[EventIdx] = (P_cyl_peg[IVO_Idx-shift-2]+P_cyl_peg[IVO_Idx-shift-1]+P_cyl_peg[IVO_Idx-shift]+P_cyl_peg[IVO_Idx-shift+1]+P_cyl_peg[IVO_Idx-shift+2])/5;
P_IVC1[EventIdx] = (P_cyl_peg[IVC_Idx-shift-4]+P_cyl_peg[IVC_Idx-shift-3]+P_cyl_peg[IVC_Idx-shift-2]+P_cyl_peg[IVC_Idx-shift-1]+P_cyl_peg[IVC_Idx-shift])/5;
P_EVO1[EventIdx] = (P_cyl_peg[EVO_Idx+shift]+P_cyl_peg[EVO_Idx+shift+1]+P_cyl_peg[EVO_Idx+shift+2]+P_cyl_peg[EVO_Idx+shift+3]+P_cyl_peg[EVO_Idx+shift+4])/5;
P_EVC1[EventIdx] = (P_cyl_peg[EVC_Idx+shift-2]+P_cyl_peg[EVC_Idx+shift-1]+P_cyl_peg[EVC_Idx+shift]+P_cyl_peg[EVC_Idx+shift+1]+P_cyl_peg[EVC_Idx+shift+2])/5;
P_BWD1[EventIdx] = (P_cyl_peg[771]+P_cyl_peg[772]+P_cyl_peg[773]+P_cyl_peg[774]+P_cyl_peg[775])/5;
P_BDC1[EventIdx] = (P_cyl_peg[1051]+P_cyl_peg[1052]+P_cyl_peg[1053]+P_cyl_peg[1054]+P_cyl_peg[1055])/5;

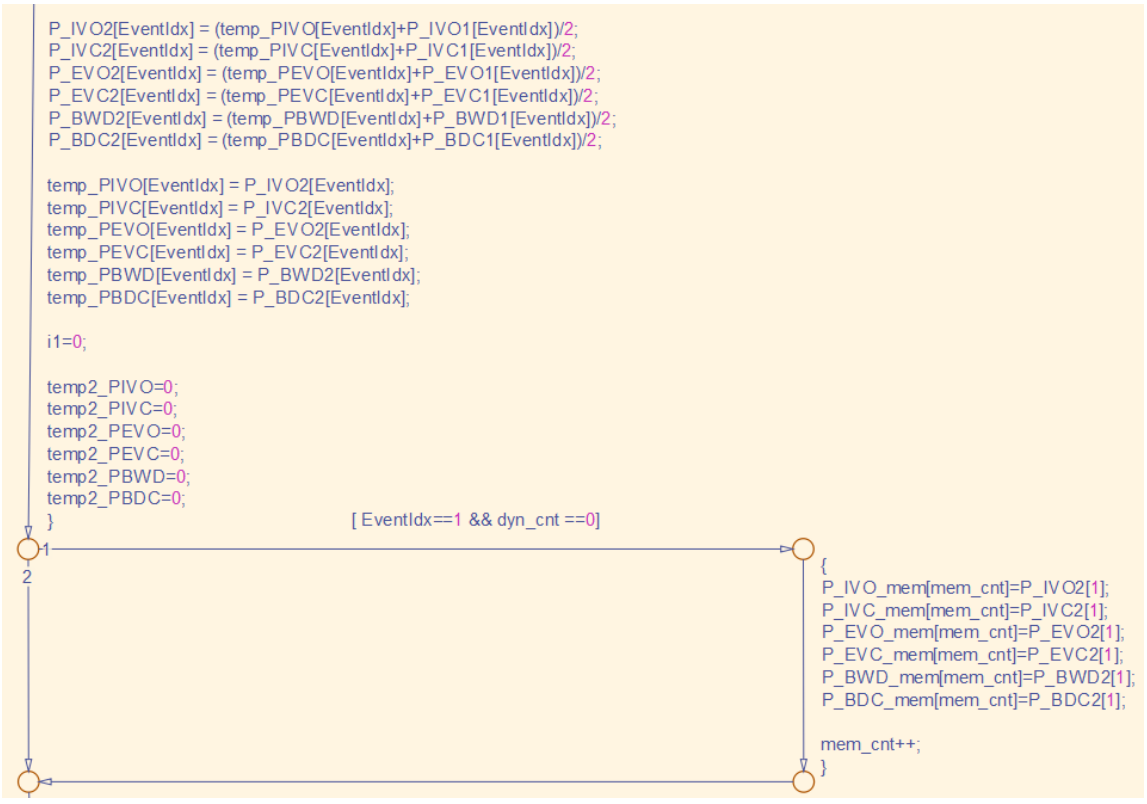
P_IVO2[EventIdx] = (temp_PIVO[EventIdx]+P_IVO1[EventIdx])/2;
P_IVC2[EventIdx] = (temp_PIVC[EventIdx]+P_IVC1[EventIdx])/2;
P_EVO2[EventIdx] = (temp_PEVO[EventIdx]+P_EVO1[EventIdx])/2;
P_EVC2[EventIdx] = (temp_PEVC[EventIdx]+P_EVC1[EventIdx])/2;
P_BWD2[EventIdx] = (temp_PBWD[EventIdx]+P_BWD1[EventIdx])/2;
P_BDC2[EventIdx] = (temp_PBDC[EventIdx]+P_BDC1[EventIdx])/2;
temp_PIVO[EventIdx] = P_IVO2[EventIdx];
temp_PIVC[EventIdx] = P_IVC2[EventIdx];
temp_PEVO[EventIdx] = P_EVO2[EventIdx];
temp_PEVC[EventIdx] = P_EVC2[EventIdx];
temp_PBWD[EventIdx] = P_BWD2[EventIdx];
temp_PBDC[EventIdx] = P_BDC2[EventIdx];
i1=0;
temp2_PIVO=0;
temp2_PIVC=0;
temp2_PEVO=0;
temp2_PEVC=0;
temp2_PBWD=0;
temp2_PBDC=0;
}
[EventIdx==1 && dyn_cnt ==0]
1
2
{
P_IVO_mem[mem_cnt]=P_IVO2[1];
P_IVC_mem[mem_cnt]=P_IVC2[1];
P_EVO_mem[mem_cnt]=P_EVO2[1];
P_EVC_mem[mem_cnt]=P_EVC2[1];
P_BWD_mem[mem_cnt]=P_BWD2[1];
P_BDC_mem[mem_cnt]=P_BDC2[1];
mem_cnt++;
}

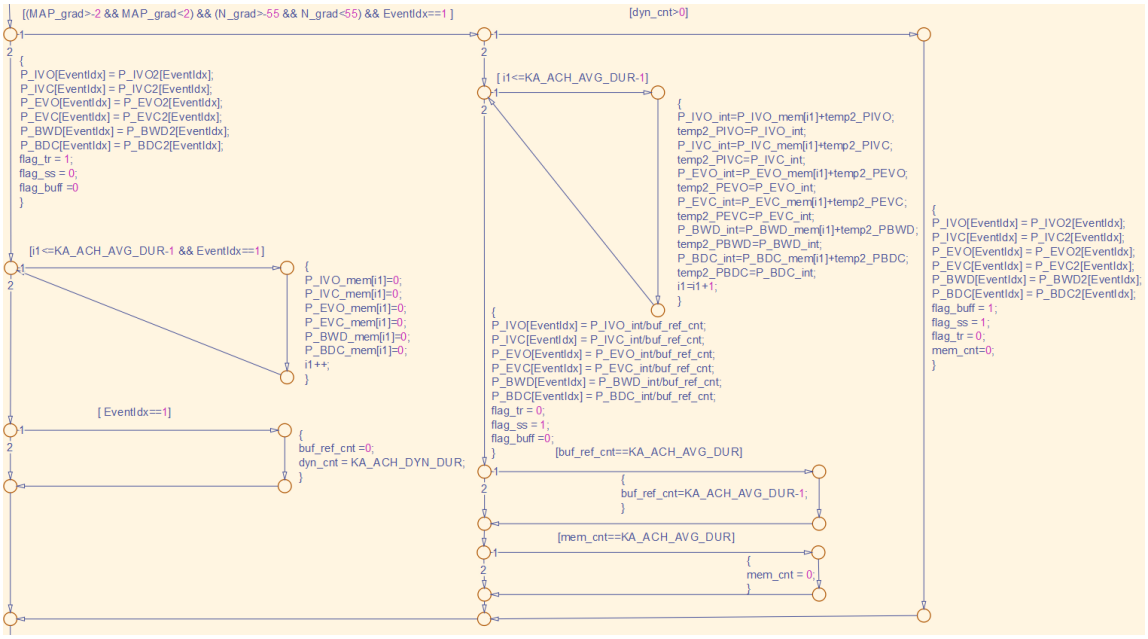
[(MAP_grad>-2 && MAP_grad<2) && (N_grad>-55 && N_grad<55) && EventIdx==1]
{
P_IVO[EventIdx] = P_IVO2[EventIdx];
P_IVC[EventIdx] = P_IVC2[EventIdx];
P_EVO[EventIdx] = P_EVO2[EventIdx];
P_EVC[EventIdx] = P_EVC2[EventIdx];
P_BWD[EventIdx] = P_BWD2[EventIdx];
P_BDC[EventIdx] = P_BDC2[EventIdx];
flag_tr = 1;
flag_ss = 0;
flag_buff =0
}
[i1<=KA_ACH_AVG_DUR-1 && EventIdx==1]
{
P_IVO_mem[i1]=0;
P_IVC_mem[i1]=0;
P_EVO_mem[i1]=0;
P_EVC_mem[i1]=0;
P_BWD_mem[i1]=0;
P_BDC_mem[i1]=0;
i1++;
}
[EventIdx==1]
{
buf_ref_cnt =0;
dyn_cnt = KA_ACH_DYN_DUR;
}
[dyn_cnt>0]
[i1<=KA_ACH_AVG_DUR-1]
{
P_IVO_int=P_IVO_mem[i1]+temp2_PIVO;
temp2_PIVO=P_IVO_int;
P_IVC_int=P_IVC_mem[i1]+temp2_PIVC;
temp2_PIVC=P_IVC_int;
P_EVO_int=P_EVO_mem[i1]+temp2_PEVO;
temp2_PEVO=P_EVO_int;
P_EVC_int=P_EVC_mem[i1]+temp2_PEVC;
temp2_PEVC=P_EVC_int;
P_BWD_int=P_BWD_mem[i1]+temp2_PBWD;
temp2_PBWD=P_BWD_int;
P_BDC_int=P_BDC_mem[i1]+temp2_PBDC;
temp2_PBDC=P_BDC_int;
i1=i1+1;
}
{
P_IVO[EventIdx] = P_IVO_int/buf_ref_cnt;
P_IVC[EventIdx] = P_IVC_int/buf_ref_cnt;
P_EVO[EventIdx] = P_EVO_int/buf_ref_cnt;
P_EVC[EventIdx] = P_EVC_int/buf_ref_cnt;
P_BWD[EventIdx] = P_BWD_int/buf_ref_cnt;
P_BDC[EventIdx] = P_BDC_int/buf_ref_cnt;
flag_tr = 0;
flag_ss = 1;
flag_buff =0;
}
[buf_ref_cnt==KA_ACH_AVG_DUR]
{
buf_ref_cnt=KA_ACH_AVG_DUR-1;
}
[mem_cnt==KA_ACH_AVG_DUR]
{
mem_cnt = 0;
}
{
P_IVO[EventIdx] = P_IVO2[EventIdx];
P_IVC[EventIdx] = P_IVC2[EventIdx];
P_EVO[EventIdx] = P_EVO2[EventIdx];
P_EVC[EventIdx] = P_EVC2[EventIdx];
P_BWD[EventIdx] = P_BWD2[EventIdx];
P_BDC[EventIdx] = P_BDC2[EventIdx];
flag_buff = 1;
flag_ss = 1;
flag_tr = 0;
mem_cnt=0;
}


{
MAP_ACH =MAP*1;
N_ACH =N*1;
temp_MAP = MAP*100;
temp_N = N*100;
current_angle = Crank_Angle[IVO_Idx] + C_TDC_REF_FRAME_CORRECTION;
}
[current_angle<0]
1
2
Convert negative angles to positive by adding 720 degrees.
[Can still break if angle > 720... needs to be fixed. gvr]
{current_angle = current_angle+C_DEGREES_PER_CYCLE;}
[current_angle>=C_DEGREES_PER_CYCLE]
1
2
Convert angles past the end point.
{current_angle=current_angle-C_DEGREES_PER_CYCLE;}
{
angle_index = uint32(current_angle*C_CRANK_ANGLE_ARRAY_RESOLUTION);
V_IVO[EventIdx] = C_CYL_VOLUME[angle_index];
current_angle = Crank_Angle[IVC_Idx] + C_TDC_REF_FRAME_CORRECTION;
}
[current_angle<0]
1
2
Convert negative angles to positive by adding 720 degrees.
[Can still break if angle > 720... needs to be fixed. gvr]
{current_angle = current_angle+C_DEGREES_PER_CYCLE;}
[current_angle>=C_DEGREES_PER_CYCLE]
1
2
Convert angles past the end point.
{current_angle=current_angle-C_DEGREES_PER_CYCLE;}
{
angle_index = uint32(current_angle*C_CRANK_ANGLE_ARRAY_RESOLUTION);
V_IVC[EventIdx] = C_CYL_VOLUME[angle_index];
current_angle = Crank_Angle[EVO_Idx] + C_TDC_REF_FRAME_CORRECTION;
}

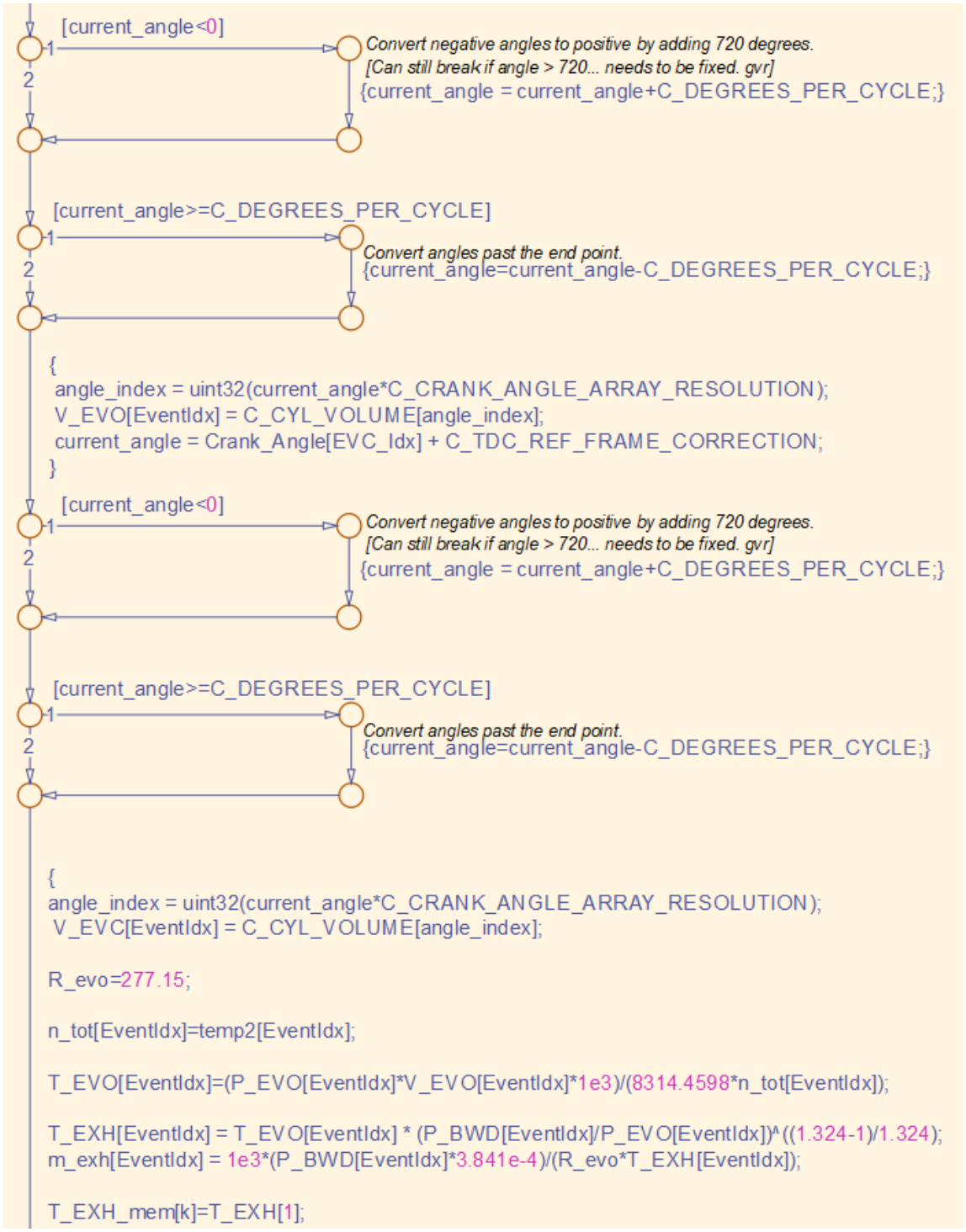
[current_angle<0]
1
2
Convert negative angles to positive by adding 720 degrees.
[Can still break if angle > 720... needs to be fixed. gvr]
{current_angle = current_angle+C_DEGREES_PER_CYCLE;}
[current_angle>=C_DEGREES_PER_CYCLE]
1
2
Convert angles past the end point.
{current_angle=current_angle-C_DEGREES_PER_CYCLE;}
{
angle_index = uint32(current_angle*C_CRANK_ANGLE_ARRAY_RESOLUTION);
V_EVO[EventIdx] = C_CYL_VOLUME[angle_index];
current_angle = Crank_Angle[EVC_Idx] + C_TDC_REF_FRAME_CORRECTION;
}
[current_angle<0]
1
2
Convert negative angles to positive by adding 720 degrees.
[Can still break if angle > 720... needs to be fixed. gvr]
{current_angle = current_angle+C_DEGREES_PER_CYCLE;}
[current_angle>=C_DEGREES_PER_CYCLE]
1
2
Convert angles past the end point.
{current_angle=current_angle-C_DEGREES_PER_CYCLE;}
{
angle_index = uint32(current_angle*C_CRANK_ANGLE_ARRAY_RESOLUTION);
V_EVC[EventIdx] = C_CYL_VOLUME[angle_index];
R_evo=277.15;
n_tot[EventIdx]=temp2[EventIdx];
T_EVO[EventIdx]=(P_EVO[EventIdx]*V_EVO[EventIdx]*1e3)/(8314.4598*n_tot[EventIdx]);
T_EXH[EventIdx] = T_EVO[EventIdx] * (P_BWD[EventIdx]/P_EVO[EventIdx])^((1.324-1)/1.324);
m_exh[EventIdx] = 1e3*(P_BWD[EventIdx]*3.841e-4)/(R_evo*T_EXH[EventIdx]);
T_EXH_mem[k]=T_EXH[1];

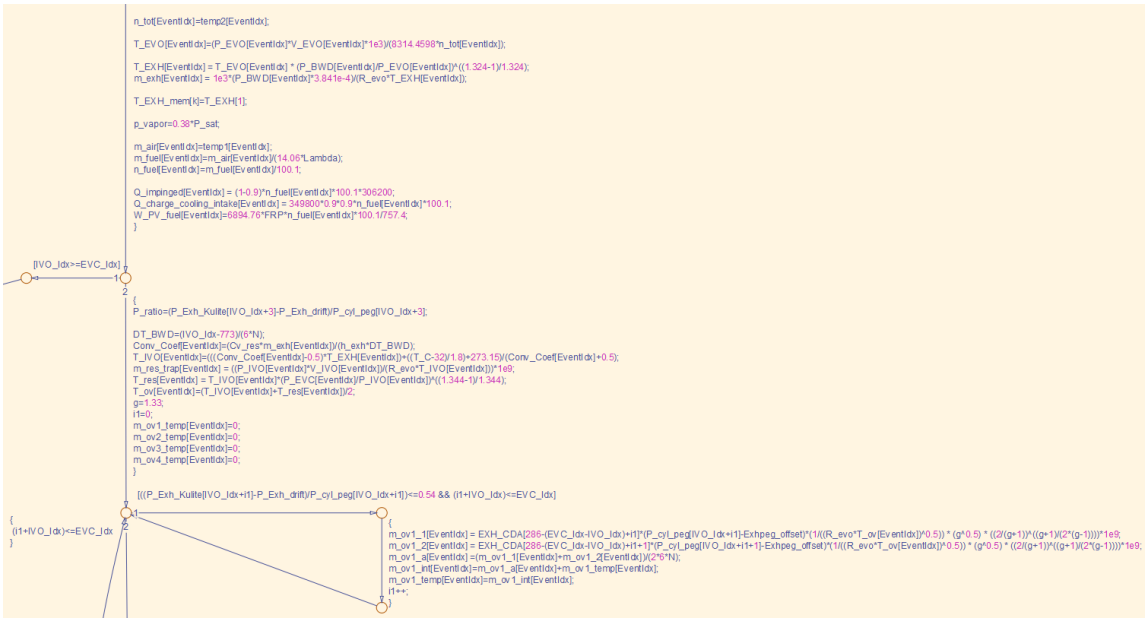
n_tot[EventIdx]=temp2[EventIdx];
T_EVO[EventIdx]=(P_EVO[EventIdx]*V_EVO[EventIdx]*1e3)/(8314.4598*n_tot[EventIdx]);
T_EXH[EventIdx] = T_EVO[EventIdx] * (P_BWD[EventIdx]/P_EVO[EventIdx])^((1.324-1)/1.324);
m_exh[EventIdx] = 1e3*(P_BWD[EventIdx]*3.841e-4)/(R_evo*T_EXH[EventIdx]);
T_EXH_mem[k]=T_EXH[1];
p_vapor=0.38*P_sat;
m_air[EventIdx]=temp1[EventIdx];
m_fuel[EventIdx]=m_air[EventIdx]/(14.06*Lambda);
n_fuel[EventIdx]=m_fuel[EventIdx]/100.1;
Q_impinged[EventIdx] = (1-0.9)*n_fuel[EventIdx]*100.1*306200;
Q_charge_cooling_intake[EventIdx] = 349800*0.9*0.9*n_fuel[EventIdx]*100.1;
W_PV_fuel[EventIdx]=6894.76*FRP*n_fuel[EventIdx]*100.1/757.4;
[IVO_Idx>=EVC_Idx]
P_ratio=(P_Exh_Kulite[IVO_Idx+3]-P_Exh_drift)/P_cyl_peg[IVO_Idx+3];
DT_BWD=(IVO_Idx-773)/(6*N);
Conv_Coef[EventIdx]=(Cv_res*m_exh[EventIdx])/(h_exh*DT_BWD);
T_IVO[EventIdx]=(((Conv_Coef[EventIdx]-0.5)*T_EXH[EventIdx])+((T_C-32)/1.8)+273.15)/(Conv_Coef[EventIdx]+0.5);
m_res_trap[EventIdx] = ((P_IVO[EventIdx]*V_IVO[EventIdx])/(R_evo*T_IVO[EventIdx]))*1e9;
T_res[EventIdx] = T_IVO[EventIdx]*(P_EVC[EventIdx]/P_IVO[EventIdx])^((1.344-1)/1.344);
T_ov[EventIdx]=(T_IVO[EventIdx]+T_res[EventIdx])/2;
g=1.33;
i1=0;
m_ov1_temp[EventIdx]=0;
m_ov2_temp[EventIdx]=0;
m_ov3_temp[EventIdx]=0;
m_ov4_temp[EventIdx]=0;
[((P_Exh_Kulite[IVO_Idx+i1]-P_Exh_drift)/P_cyl_peg[IVO_Idx+i1])<=0.54 && (i1+IVO_Idx)<=EVC_Idx]
{
(i1+IVO_Idx)<=EVC_Idx
}
m_ov1_1[EventIdx] = EXH_CDA[286-(EVC_Idx-IVO_Idx)+i1]*(P_cyl_peg[IVO_Idx+i1]-Exhpeg_offset)^(1/((R_evo*T_ov[EventIdx])^0.5)) * (g^0.5) * ((2/(g+1))^((g+1)/(2*(g-1))))*1e9;
m_ov1_2[EventIdx] = EXH_CDA[286-(EVC_Idx-IVO_Idx)+i1+1]*(P_cyl_peg[IVO_Idx+i1+1]-Exhpeg_offset)^(1/((R_evo*T_ov[EventIdx])^0.5)) * (g^0.5) * ((2/(g+1))^((g+1)/(2*(g-1))))*1e9;
m_ov1_a[EventIdx] =(m_ov1_1[EventIdx]+m_ov1_2[EventIdx])/(2*6*N);
m_ov1_int[EventIdx]=m_ov1_a[EventIdx]+m_ov1_temp[EventIdx];
m_ov1_temp[EventIdx]=m_ov1_int[EventIdx];
i1++;


[((P_Exh_Kulite[IVO_Idx+i1]-P_Exh_drift)/P_cyl_peg[IVO_Idx+i1])>0.54 && ((P_Exh_Kulite[IVO_Idx+i1]-P_Exh_drift)/P_cyl_peg[IVO_Idx+i1])<1 && (i1+IVO_Idx)<=EVC_Idx]
m_ov2_1[EventIdx] = EXH_CDA[286-(EVC_Idx-IVO_Idx)+i1]*(P_cyl_peg[IVO_Idx+i1]-Exhpeg_offset)^(1/((R_evo*T_ov[EventIdx])^0.5))*
((2*g/(g-1))^0.5)*(((P_Exh_Kulite[IVO_Idx+i1]-P_Exh_drift)/(P_cyl_peg[IVO_Idx+i1]-Exhpeg_offset))^(1/g))*((1-(((P_Exh_Kulite[IVO_Idx+i1]-P_Exh_drift)/(P_cyl_peg[IVO_Idx+i1]-Exhpeg_offset))^((g-1)/g)))^0.5)*1e9;
m_ov2_2[EventIdx] = EXH_CDA[286-(EVC_Idx-IVO_Idx)+i1+1]*(P_cyl_peg[IVO_Idx+i1+1]-Exhpeg_offset)^(1/((R_evo*T_ov[EventIdx])^0.5))*
((2*g/(g-1))^0.5)*(((P_Exh_Kulite[IVO_Idx+i1+1]-P_Exh_drift)/(P_cyl_peg[IVO_Idx+i1+1]-Exhpeg_offset))^(1/g))*((1-(((P_Exh_Kulite[IVO_Idx+i1+1]-P_Exh_drift)/(P_cyl_peg[IVO_Idx+i1+1]
-Exhpeg_offset))^((g-1)/g)))^0.5)*1e9;
m_ov2_a[EventIdx] =(m_ov2_1[EventIdx]+m_ov2_2[EventIdx])/(2*6*N);
m_ov2_int[EventIdx]=m_ov2_a[EventIdx]+m_ov2_temp[EventIdx];
m_ov2_temp[EventIdx]=m_ov2_int[EventIdx];
i1++;
[((P_Exh_Kulite[IVO_Idx+i1]-P_Exh_drift)/P_cyl_peg[IVO_Idx+i1])>=1 && ((P_Exh_Kulite[IVO_Idx+i1]-P_Exh_drift)/P_cyl_peg[IVO_Idx+i1])<1.852 && (i1+IVO_Idx)<=EVC_Idx]
m_ov3_1[EventIdx] = EXH_CDA[286-(EVC_Idx-IVO_Idx)+i1]*(P_Exh_Kulite[IVO_Idx+i1]-P_Exh_drift)^(1/((R_evo*830)^0.5))*
((2*g/(g-1))^0.5)*(((P_cyl_peg[IVO_Idx+i1]-Exhpeg_offset)/(P_Exh_Kulite[IVO_Idx+i1]-P_Exh_drift))^(1/g))*((1-(((P_cyl_peg[IVO_Idx+i1]-Exhpeg_offset)/(P_Exh_Kulite[IVO_Idx+i1]-P_Exh_drift))^((g-1)/g)))^0.5)*1e9;
m_ov3_2[EventIdx] = EXH_CDA[286-(EVC_Idx-IVO_Idx)+i1+1]*(P_Exh_Kulite[IVO_Idx+i1+1]-P_Exh_drift)^(1/((R_evo*830)^0.5))*
((2*g/(g-1))^0.5)*(((P_cyl_peg[IVO_Idx+i1+1]-Exhpeg_offset)/(P_Exh_Kulite[IVO_Idx+i1+1]-P_Exh_drift))^(1/g))*((1-(((P_cyl_peg[IVO_Idx+i1+1]-Exhpeg_offset)/(P_Exh_Kulite[IVO_Idx+i1+1]-P_Exh_drift))^((g-1)/g)))^0.5)*1e9;
m_ov3_a[EventIdx] =(m_ov3_1[EventIdx]+m_ov3_2[EventIdx])/(2*6*N);
m_ov3_int[EventIdx]=m_ov3_a[EventIdx]+m_ov3_temp[EventIdx];
m_ov3_temp[EventIdx]=m_ov3_int[EventIdx];
i1++;
[((P_Exh_Kulite[IVO_Idx+i1]-P_Exh_drift)/P_cyl_peg[IVO_Idx+i1])>=1.852 && (i1+IVO_Idx)<=EVC_Idx]
m_ov4_1[EventIdx] = EXH_CDA[286-(EVC_Idx-IVO_Idx)+i1]*((P_Exh_Kulite[IVO_Idx+i1]-P_Exh_drift))*(1/((R_evo*830)^0.5)) * (g^0.5) * ((2/(g+1))^((g+1)/(2*(g-1))))*1e9;
m_ov4_2[EventIdx] = EXH_CDA[286-(EVC_Idx-IVO_Idx)+i1+1]*((P_Exh_Kulite[IVO_Idx+i1+1]-P_Exh_drift))*(1/((R_evo*830)^0.5)) * (g^0.5) * ((2/(g+1))^((g+1)/(2*(g-1))))*1e9;
m_ov4_a[EventIdx] =(m_ov4_1[EventIdx]+m_ov4_2[EventIdx])/(2*6*N);
m_ov4_int[EventIdx]=m_ov4_a[EventIdx]+m_ov4_temp[EventIdx];
m_ov4_temp[EventIdx]=m_ov4_int[EventIdx];
i1++;
m_overlap_mg2[EventIdx]=CDA_eff*(m_ov3_temp[EventIdx]+m_ov4_temp[EventIdx]-m_ov1_temp[EventIdx]-m_ov2_temp[EventIdx]);
[flag_nov == 1]
temp_m_overlap[EventIdx] = m_overlap_mg2[EventIdx];
m_overlap_mg1[EventIdx] = (temp_m_overlap[EventIdx]+m_overlap_mg2[EventIdx])/2;
temp_m_overlap[EventIdx] = m_overlap_mg1[EventIdx];
i1=0;
temp2_m_overlap=0;
[EventIdx==1 && dyn_cnt ==0]
{m_overlap_mem[mov_cnt]=m_overlap_mg1[1];
mov_cnt++;}

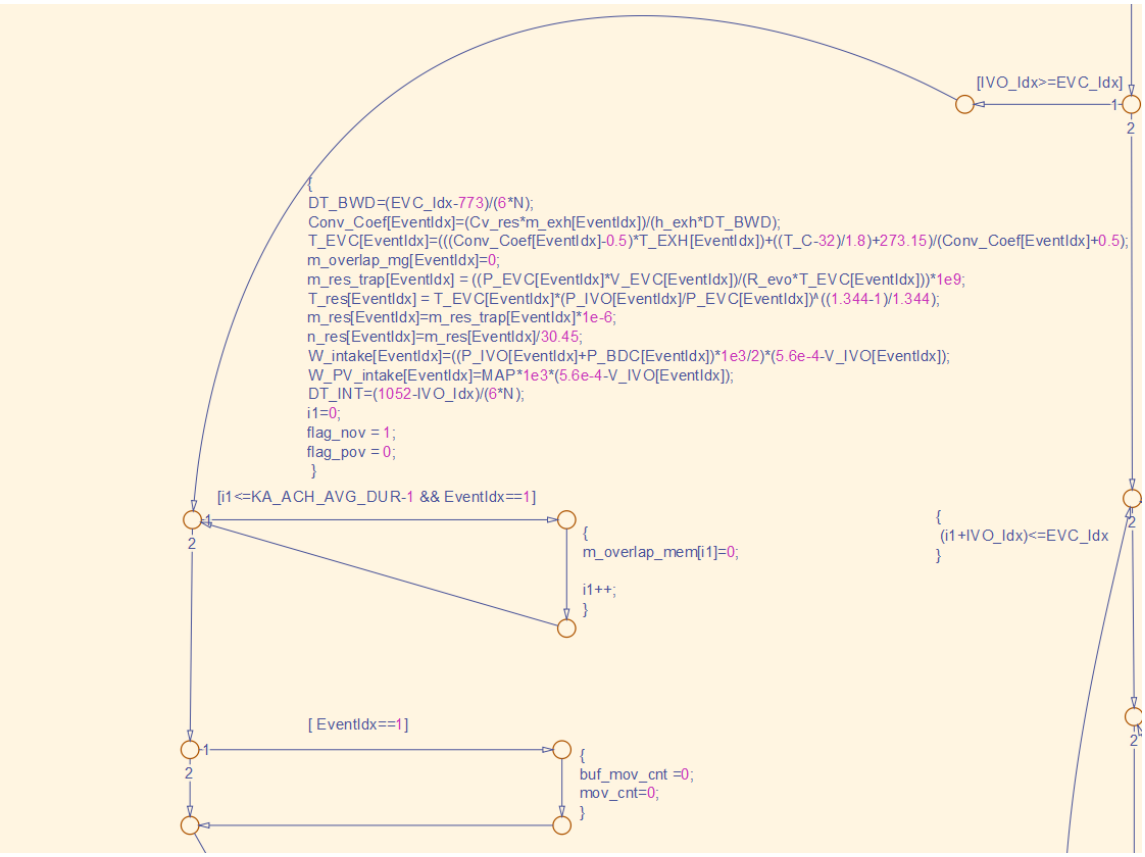
[IVO_Idx>=EVC_Idx]
1
2
{
DT_BWD=(EVC_Idx-773)/(6*N);
Conv_Coef[EventIdx]=(Cv_res*m_exh[EventIdx])/(h_exh*DT_BWD);
T_EVC[EventIdx]=(((Conv_Coef[EventIdx]-0.5)*T_EXH[EventIdx])+((T_C-32)/1.8)+273.15)/(Conv_Coef[EventIdx]+0.5);
m_overlap_mg[EventIdx]=0;
m_res_trap[EventIdx] = ((P_EVC[EventIdx]*V_EVC[EventIdx])/(R_evo*T_EVC[EventIdx]))*1e9;
T_res[EventIdx] = T_EVC[EventIdx]*(P_IVO[EventIdx]/P_EVC[EventIdx])^((1.344-1)/1.344);
m_res[EventIdx]=m_res_trap[EventIdx]*1e-6;
n_res[EventIdx]=m_res[EventIdx]/30.45;
W_intake[EventIdx]=((P_IVO[EventIdx]+P_BDC[EventIdx])*1e3/2)*(5.6e-4-V_IVO[EventIdx]);
W_PV_intake[EventIdx]=MAP*1e3*(5.6e-4-V_IVO[EventIdx]);
DT_INT=(1052-IVO_Idx)/(6*N);
i1=0;
flag_nov = 1;
flag_pov = 0;
}
[i1<=KA_ACH_AVG_DUR-1 && EventIdx==1]
1
2
{
m_overlap_mem[i1]=0;
i1++;
}
{
(i1+IVO_Idx)<=EVC_Idx
}
[EventIdx==1]
1
2
{
buf_mov_cnt =0;
mov_cnt=0;
}

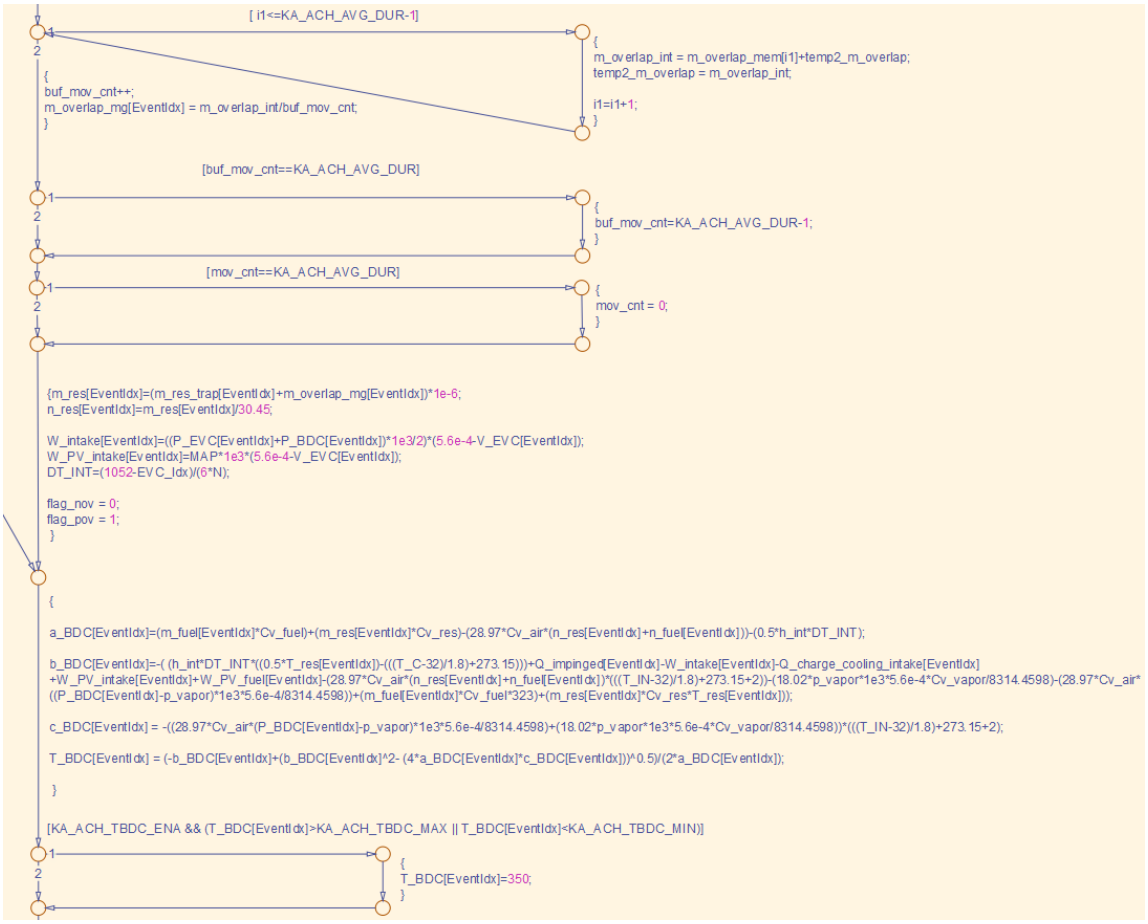
[i1<=KA_ACH_AVG_DUR-1]
1
2
{
buf_mov_cnt++;
m_overlap_mg[EventIdx] = m_overlap_int/buf_mov_cnt;
}
{
m_overlap_int = m_overlap_mem[i1]+temp2_m_overlap;
temp2_m_overlap = m_overlap_int;
i1=i1+1;
}
[buf_mov_cnt==KA_ACH_AVG_DUR]
1
2
{
buf_mov_cnt=KA_ACH_AVG_DUR-1;
}
[mov_cnt==KA_ACH_AVG_DUR]
1
2
{
mov_cnt = 0;
}
{m_res[EventIdx]=(m_res_trap[EventIdx]+m_overlap_mg[EventIdx])*1e-6;
n_res[EventIdx]=m_res[EventIdx]/30.45;
W_intake[EventIdx]=((P_EVC[EventIdx]+P_BDC[EventIdx])*1e3/2)*(5.6e-4-V_EVC[EventIdx]);
W_PV_intake[EventIdx]=MAP*1e3*(5.6e-4-V_EVC[EventIdx]);
DT_INT=(1052-EVC_Idx)/(6*N);
flag_nov = 0;
flag_pov = 1;
}
{
a_BDC[EventIdx]=(m_fuel[EventIdx]*Cv_fuel)+(m_res[EventIdx]*Cv_res)-(28.97*Cv_air*(n_res[EventIdx]+n_fuel[EventIdx]))-(0.5*h_int*DT_INT);
b_BDC[EventIdx]=-((h_int*DT_INT*((0.5*T_res[EventIdx])-(((T_C-32)/1.8)+273.15)))+Q_impinged[EventIdx]-W_intake[EventIdx]-Q_charge_cooling_intake[EventIdx]
+W_PV_intake[EventIdx]+W_PV_fuel[EventIdx]-(28.97*Cv_air*(n_res[EventIdx]+n_fuel[EventIdx]))*((((T_IN-32)/1.8)+273.15+2))-(18.02*p_vapor*1e3*5.6e-4*Cv_vapor/8314.4598)-(28.97*Cv_air*
((P_BDC[EventIdx]-p_vapor)*1e3*5.6e-4/8314.4598))+(m_fuel[EventIdx]*Cv_fuel*323)+(m_res[EventIdx]*Cv_res*T_res[EventIdx]));
c_BDC[EventIdx] = -((28.97*Cv_air*(P_BDC[EventIdx]-p_vapor)*1e3*5.6e-4/8314.4598)+(18.02*p_vapor*1e3*5.6e-4*Cv_vapor/8314.4598))*((((T_IN-32)/1.8)+273.15+2);
T_BDC[EventIdx] = (-b_BDC[EventIdx]+(b_BDC[EventIdx]^2- (4*a_BDC[EventIdx]*c_BDC[EventIdx]))^0.5)/(2*a_BDC[EventIdx]);
}
[KA_ACH_TBDC_ENA && (T_BDC[EventIdx]>KA_ACH_TBDC_MAX || T_BDC[EventIdx]<KA_ACH_TBDC_MIN)]
1
2
{
T_BDC[EventIdx]=350;
}

```
{
T_IVC[EventIdx]=T_BDC[EventIdx]*(P_IVC[EventIdx]/P_BDC[EventIdx])^((1.3-1)/1.3);

T_IVC_mem[k]=T_IVC[1];

n_tot_new[EventIdx]=((P_IVC[EventIdx]*1e3*V_IVC[EventIdx])/(8314.4598*T_IVC[EventIdx]));
temp2[EventIdx]=n_tot_new[EventIdx];


m_vapor[EventIdx]=(p_vapor*1e3*V_IVC[EventIdx]*1e6)/(461.5*T_IVC[EventIdx]);
n_vapor[EventIdx]=m_vapor[EventIdx]*1e-6/18.02;

n_air[EventIdx]=n_tot_new[EventIdx]-n_res[EventIdx]-n_vapor[EventIdx]-n_fuel[EventIdx];
m_air_new[EventIdx]=n_air[EventIdx]*28.97;
m_air_mem[k]=m_air_new[1];
temp1[EventIdx]=m_air_new[EventIdx];

m_tot[EventIdx]=(n_fuel[EventIdx]*100.1)+(n_vapor[EventIdx]*18.02)+m_air_new[EventIdx]+(n_res[EventIdx]*30.45);


EstimatedAirCharge[EventIdx] = m_air_new[EventIdx];
RGF[EventIdx]=m_res[EventIdx]/(m_air_new[EventIdx]+m_res[EventIdx]);

RGF_mem[k]=RGF[1];

i1=0;
temp_air=0;
temp_RGF=0;
temp_T_IVC=0;
temp_T_EXH=0;
}
```

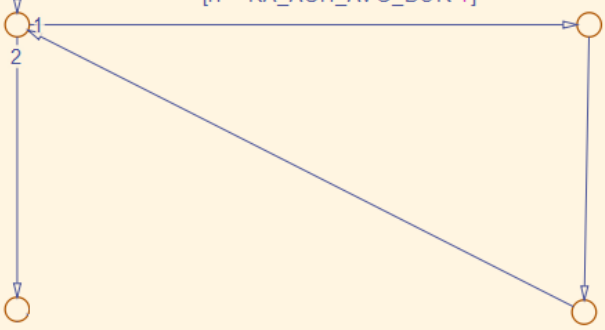


```
{
m_air_int=m_air_mem[i1]+temp_air;
temp_air=m_air_int;
RGF_int=RGF_mem[i1]+temp_RGF;
temp_RGF=RGF_int;
T_IVC_int=T_IVC_mem[i1]+temp_T_IVC;
temp_T_IVC=T_IVC_int;
T_EXH_int=T_EXH_mem[i1]+temp_T_EXH;
temp_T_EXH=T_EXH_int;
i1++;
}
```

Appendix C

Letters of Permission

Beth Darchi Jul 30, 2021, 12:27 PM (6 days ago)

to me

Dear Mr. Khameneian,

It is our pleasure to grant you permission to use **all or any part of** the ASME paper "Model-Based Dynamic In-Cylinder Air Charge, Residual Gas and Temperature Estimation for a GDI Spark Ignition Engine Using Cylinder, Intake and Exhaust Pressures," **by** Amir Khameneian, Xin Wang, Paul Dice, Mahdi Shahbakhti, Jefferey D. Naber, Chad Archer, Peter Moilanen, Chris Glugla, Garlan Huberts, Paper No: DSCC2020-3280, cited in your letter for inclusion in a Ph.D. dissertation entitled Dynamic Engine-Out Emissions Analysis for a Gasoline Turbocharged Direct - Injection Engine During the Cold Crank-Start Conditions in Elevated HEV Cranking Speed to be published Michigan Technological University.

Permission is granted for the specific use as stated herein and does not permit further use of the materials without proper authorization. Proper attribution must be made to the author(s) of the materials. **Please note**: if any or all of the figures and/or Tables are of another source, permission should be granted from that outside source or include the reference of the original source. ASME does not grant permission for outside source material that may be referenced in the ASME works.

As is customary, we request that you ensure full acknowledgment of this material, the author(s), source and ASME as original publisher.

Many thanks for your interest in ASME publications.

Sincerely,

Beth Darchi
Publishing Administrator
ASME
2 Park Avenue
New York, NY 10016-5990